Enhancing the Delivery of Therapeutic Cargo to Cancer Cells Using Cell Penetrating Peptides

A Thesis Submitted for the Degree of
Philosophiae Doctor in Cardiff University

by

Noura Gamal Mohamed AbdAllah Eissa

December 2015

Cardiff School of Pharmacy and Pharmaceutical Sciences

Cardiff University

Abstract

Cell penetrating peptides (CPPs) have received considerable attention as cellular delivery vectors for small-molecule and macromolecular therapeutics. Hundreds of CPP sequences have now been described including bioportides that serve as single entity modifiers of cell physiology. Translation of promising CPP pre-clinical studies have however been disappointing as few identified delivery-systems have progressed to clinical trials. This project aimed to extend on studies using CPPs for delivering peptides influencing NF-κB signalling and to search for novel membrane active peptides that could be classed as CPPs or bioportides.

In-house methods measuring IκB-α degradation and luciferase expression assays were developed to study the capacity of penetratin to influence NF-κB activity via delivery of the NBD peptide (Pen-NBD: DRQIKIWFQNRRMKWKKTALDWSWLQTE). Results from these studies highlighted how two methods investigating the same signalling pathway could give very different results. Pen-NBD did not reduce TNF-α-induced IκB-α degradation but induced reduction in TNF-α-induced luciferase activity. This effect was also observed in cells treated with penetratin alone or DMSO-diluent.

EJP-18 (LFMRRRHIVRKRTLRRLL) represents a novel peptide from the EGFR juxtamembrane region and was found to be membrane active and internalised into cells. This thesis further characterised this peptide including two other sequences from this region of EGFR (EJP-21-

LFMRRRHIVRKRTLRRLLQER and E-64562- RRRHIVRKRTLRRLLQER). In studied cancer cell lines, EJP-18 was toxic in an EGFR-dependant manner and aside from being a potential bioportide, also effectively delivered protein (BSA) and siRNA into cells. EJP-18/BSA was delivered to the lysosome and it remains to be determined whether it could be utilised to deliver siRNA to the cytosol. Cytotoxicity and protein delivery studies with EJP-21 and E-64562 highlighted the critical importance of terminal hydrophobicity in the EJP-18 sequence; this may extend to other studies involving CPPs.

This thesis provides new information on *in vitro* activity of CPPs and CPP-chimeras. Additionally, new peptides were discovered that could potentially be classed as bioportides and CPPs.

For my family,

Love you all

Acknowledgements

List of Contents

List of Figures

xiv

xv

List of Tables

List of Abstracts and Publications

Abstracts:

1) Sayers, E.J., He, L., Moody, P., <u>Eissa, N.G.</u>, Cleal, K., Borri, P., Watson, P., and Jones, A.T. (2014) Scrutinising Endocytic Pathways for Cellular Uptake and Delivery of Therapeutic Macromolecules. 13th European Symposium on Controlled Drug Delivery, Egmond aan Zee, The Netherlands. ISBN 978-90-902-8211-4 P40-41

2) <u>Eissa, N.G.</u>, Sayers, E.J., Brennan, P., Pepper, C., Taggart, M. and Jones, A.T. (2014) Influence of peptide cargo sequence on delivery capacity of cell penetrating peptides. 13th European Symposium on Controlled Drug Delivery, Egmond aan Zee, The Netherlands. ISBN 978-90-902-8211-4 P100-101.

3) Alexandre, R., <u>Eissa, N.G.</u>, Sayers, E.J., Fegan, C., Jones, A. T., Pepper C. and Brennan, P. (2013) Developing novel CPPs for targeting NF-κB in chronic lymphocytic leukaemia cells. Protein-Protein Interactions (PPI) International conference: Emerging Science and Therapeutic Potential, Royal Society, London.

Publications:

1) Sayers E.J., Cleal, K., <u>Eissa, N.G.</u>, Watson, P., and Jones, A.T (2014). Distal phenylalanine modification for enhancing cellular delivery of fluorophores, proteins and quantum dots by cell penetrating peptides. *Journal of Controlled Release,* 195**,** 55-62.

List of Abbreviations

AAVs	Adeno-associated viruses
ABC-DLBCL	Activated B-cell like DLBCL
ATCC	American type culture collection
BCA	Bicinchoninic acid assay
BSA	Bovine serum albumin
Cav-1	Caveolin-1
CCK	Cholecystokinin octapeptide
CK2	Casein kinase 2
CLIO	Cross linked superparamagnetic iron oxide
CM	Complete medium
CPP	Cell penetrating peptide
DLBCL	Diffuse large B-cell lymphoma
DMD	Duchenne muscular dystrophy
DMEM	Dulbecco's modified eagle medium
DMSO	Dimethyl sulphoxide
DNA	Deoxyribonucleic acid
DOPE	1,2-dioleoyl-sn-glycero-3-phosphoethanolamine
DOTAP	1,2-dioleoyl-3-trimethylammonium propane
DOTMA	N-[1-(2,3-dioleyloxy)propyl]-N,N,Ntrimethylammonium chloride
DTH	Delayed-type hypersensitivity
DTT	Dithiothreitol
ECL	Enhanced chemiluminescence
EDTA	Ethylenediaminetetraacetic acid
EGF	Epidermal growth factor
EGFR	Epidermal growth factor receptor
EGFP	Enhanced green fluorescent protein
EPR	Enhanced permeability and retention
FADD	FAS-associated death domain

FAM	5-carboxy fluorescein
FITC	Fluorescein isothiocyanate
GAGs	Glycosaminoglycans
GFP	Green fluorescent protein
HSPG	Heparin sulphate proteoglycans
HSV-1s	Herpes simplex-1 viruses
IAPs	Inhibitors of apoptosis
ICs	Immunoconjugates
IP	Intraperitoneal
JM	Juxtamembrane
LPS	Lipopolysaccharide
LSDs	Lysosomal storage diseases
MDR	Multidrug resistance
MEFs	Mouse embryonic fibroblasts
MLV	Multilamellar vesicles
MRI	Magnetic resonance imaging
NBD	NEMO Binding Domain
NF-κB	Nuclear factor-kappa B
NIK	NF-κB inducing kinase
NLS	Nuclear localisation sequence
NMR	Nuclear magnetic resonance
NPCs	nuclear pore complexes
OSCC	Oral squamous cell carcinoma
PAGE	Polyacrylamide gel electrophoresis
PAK-1	p-21 activated kinase-1
PAMAM	Polyamidoamine
PBS	Phosphate buffered saline
PBST	PBS containing 0.025% Tween20
PCNA	Proliferation cell nuclear antigen
pDNA	Plasmid DNA
PEI	Polyethylenimine
PLL	Poly L-lysine

PNA	Peptide nucleic acid
PTDs	Protein transduction domains
PVDF	Polyvinylidene fluoride
QDs	Quantum dots
QSAR	Quantitative structure activity relationship
RIP	Receptor interacting protein
RISC	RNA-induced silencing complex
RPMI	Roswell park memorial institute medium
SFM	Serum free medium
siRNA	Short interfering ribonucleic acid
Smac	Second mitochondria derived activator of caspases
SODD	Silencer of death domain
TACE	TNF-α-converting enzyme
TBE	Tris-Borate/EDTA
TNFR-1	TNF receptor1
TNFR-2	TNF receptor2
TNF-α	Tumour necrosis factor alpha
TRADD	TNFR-associated domain
TRAF-2	TNFR-associated factor 2
TRAIL	Tumor necrosis factor–related apoptosis-inducing ligand
β-gal	β-galactosidase

Chapter 1: General Introduction

1.1 Introduction

Recent decades have witnessed significant efforts to develop new, more efficient, less toxic and more cost effective therapeutics for lethal and chronic diseases. As an example, cancer can be listed as a chronic and lethal disease and despite extensive efforts several cancers remain a major challenge to treat. Existing therapeutic approaches such as surgery, chemotherapy and radiotherapy often show undesired side effects, including damage to healthy cells (Luo *et al*., 2015). The effectiveness of chemotherapeutics can also be limited by the multidrug resistance (MDR) phenomenon in which cells, once become resistant to one anticancer drug, develop resistance to structurally and mechanistically unrelated compounds (Gottesman *et al*., 2002, Baguley, 2010).

In genetic disorders such as cystic fibrosis, where there is a mutation in a certain gene, small molecules can generally only be used to deal with the symptoms and complications associated with the disease rather than providing a real cure for the condition. In theory, the most effective treatment for such diseases would involve targeted intracellular delivery of the corrected gene sequence. In reality, therapeutic gene delivery is difficult to achieve and as a result, there is an urgent need to develop better or alternative approaches (Ratjen and Döring, 2003). For both cancer and inherited diseases, there is a major opportunity to design drugs that are based on biological molecules and a variety of these macromolecular therapeutics have been studied, ranging from peptides, proteins, oligonucleotides and whole genes. Their site of action lies

inside cells, however, their size, polarity and net negative charge hinder their penetration through the plasma membrane (Yin *et al.*, 2014). There is therefore great demand for, and potential benefit from, developing effective delivery vectors for macromolecular therapeutics.

1.1.1 Diseases

Several diseases such as cancer and other genetic disorders have been, and still remain, major threats to human life and alternatives to conventional treatment regimes is required. The information below summarises some of the major disease challenges facing modern day society and how macromolecular drugs could provide cures.

1.1.1.1 Cancer

Cancer is a major social burden affecting people of all ages and is also a leading cause of global mortality. GLOBOCAN figure reveals that 14.1 million people were newly diagnosed with cancer in 2012 and 8.2 million died because of cancer in the same year (WHO 2012). Cancer develops as a result of cumulative and irreparable DNA damage in normal cells that causes those cells to undergo uncontrolled proliferation and division. Normally, healthy cells have their own repair mechanisms for such damage. However, in some cases, errors occur leading to permanent DNA mutations and consequently alterations in the genes/proteins expressed (Bertram, 2000). Once formed, cancer cells can invade local tissues and if they enter the blood or lymph system, the cancer can metastasise to different organs (Nishida *et al*., 2006). The fact that people now live longer will result in cancer becoming an increasing burden unless new

effective therapies are discovered. We have now an unprecedented level of understanding of cancer at the molecular level and this opens door to the design of molecules that could silence proteins that regulate cell growth and division (siRNA) or interfere with their activity by inhibiting their interaction with binding partners. Therapeutic peptides acting at the intracellular level have huge therapeutic potential to do this with high specificity (Raucher *et al.*, 2009, J Boohaker *et al.*, 2012).

1.1.1.2   Genetic Diseases

Genetic disorders are caused by one or more gene abnormalities which may be inherited from maternal or paternal DNA or by mutations acquired due to new DNA damage. Different types of genetic disorders such as cystic fibrosis, Huntington's disease and severe combined immunodeficiency are well described in literature in terms of their epidemiology, cause and symptoms.

A simple approach for treatment of these diseases and also acquired diseases, such as cancer, that has proven very difficult to develop, is based on gene therapy i.e. replacement of the faulty gene with the correct version.

1.2   Macromolecules: Peptides and DNA-based Drugs

Sequencing of the human genome, in addition to data demonstrating the genetic and proteomic basis of many diseases provides a major impetus for the development of macromolecular therapeutics such as peptides, proteins and genes (Jones, 2008).

1.2.1 Therapeutic peptides

Despite their huge potential, peptides directly interfering with intracellular events have yet to materialise to viable therapeutic products. Currently there are few clinically approved peptide that functions directly inside cells. Of note is that the distinction between therapeutic peptides and therapeutic proteins can be vague and unclear.

Peptides as therapeutic entities offer several advantages over other types of therapies. These include their high specificity owing to their high levels of chemical and biological diversity. They also, as a result of high specificity and biological nature, are relatively non toxic. In addition, small peptides fall below the immunogenic threshold and generally do not induce a strong immune response (Mason, 2010). Another important consideration is the fact that they can be rationally designed to interfere with a known protein-protein interaction.

Today, more than 60 therapeutic peptides and proteins are marketed worldwide. Nearly 270 peptides are still under clinical investigation and almost 400 are in an advanced preclinical stage. Examples of naturally occurring therapeutic peptides and proteins are insulin, oxytocin and cyclosporine but few of them act directly on intracellular targets. There is also an active research field specifically focusing on delivering more peptides and proteins that have intracellular targets. They are, however, unlikely to be membrane permeable in their own right and will require some kind of vector system to deliver them to the insides of cells. A major focus of work has centred on the use of cell penetrating peptides (CPPs) to perform this.

1.2.2   Nucleotide-based Drugs

The genetic basis of many diseases highlights the potential benefit of DNA-based therapies to cure the problem at its root. The approach is based on the introduction of nucleotides intended to functionally replace missing or mutated genes or silence the expression of disease causing proteins. Examples of nucleotide-based drugs are plasmids, antisense and antigene oligonucleotides and short interfering RNA (siRNA).

Plasmids are double-stranded self replicating DNA constructs that contain genes encoding specific proteins (Uherek and Wels, 2000, Patil *et al.*, 2005). Plasmids also contain promoter and enhancer sequences to upregulate transgene expression (Fitzsimons *et al.*, 2002). Oligonucleotides, either antisense or antigene, are short single-stranded DNA segments that are designed to selectively inhibit the expression of a single protein. Antisense oligonucleotides function in the cytosol where they interact with mRNA and inhibit its translation or processing thereby inhibiting protein synthesis (Crooke, 1999). Antigene nucleotides are those targeted to genomic DNA so, like plasmids, nuclear entry is a key for them to exert their effect (Stull and Szoka Jr, 1995).

Short interfering RNA (siRNA) is a class of short, double-stranded RNA molecules consisting of 21-23 nucleotide bases designed to be complementary to the mRNA sequence responsible for the transcription of a specific protein. siRNA incorporates into the RNA-induced silencing complex (RISC) where the siRNA duplex is unwound. The sense strand is degraded and the antisense

strand binds to RISC which then allows the RISC to recognise and degrade complementary mRNA. This ultimately leads to loss of protein translation and depletion or "silencing" of the corresponding gene (Bhindi *et al.*, 2007).

1.3   Drug Delivery Vectors

Today, despite extensive research, the delivery of therapeutic macromolecules such as peptides and nucleotides to the insides of cells remains a major challenge due to the effectiveness of biological barriers that lie between route of administration and site of action. Added to this is the fact that biological therapeutics are sensitive to proteases and nucleases. They are fragile to the hostile environment of the gastrointestinal tract thus limiting our ability to deliver them orally and would also be susceptible to hydrolysis in serum. This means they need to be protected until they reach their intracellular targets. The plasma membrane functions as a protective and regulatory structure allowing the passage of essential small molecules such as sugars, ions and amino acids through membrane protein pumps or channels. It acts as an important barrier for the passage of macromolecules into the inside of the cell (Conner and Schmid, 2003). Biological membranes can also be found inside the cell and good examples are endosomal membranes for delivery to the cytosol (e.g. siRNA) and if this is overcome then the nuclear membrane poses a challenge if gene delivery (e.g. plasmid) is the therapeutic goal. Thus, the delivery vectors need to be designed for extracellular protection and for overcoming biological barriers (Mintzer and Simanek, 2008, Yin *et al.*, 2014). Alternatively, physical methods have also been used for gene delivery.

Physical transfection of macromolecules can be achieved by mechanical methods (microinjection, pressure-mediated transfection and particle bombardment), electrical methods (electroporation) or magnetic field-enhanced transfection (Magnetofection). *In vitro*, these are effective methods but *in vivo* they have significant drawbacks (Luo and Saltzman, 2000, Mehier-Humbert and Guy, 2005, Al-Dosari and Gao, 2009, Mellott *et al.*, 2013).

An ideal drug delivery vector would be cheap to produce, ineffective at eliciting an immune response but effective at interacting with its cargo, protecting it from degradation, delivering it to its site of action at tissue, cell and intracellular level (Crystal, 1995). Given the diversity of the targeted diseases and cargo, it is unlikely that a single vector could be designed that would suit all applications (Thomas *et al.*, 2003, Gardlík *et al.*, 2005, Nayerossadat *et al.*, 2012).

Vector-assisted delivery techniques can utilise either viral or nonviral systems (Wiethoff and Middaugh, 2003, Nayerossadat *et al.*, 2012). In case of peptide or nucleotide-based therapeutics, efficient delivery using either systems involves a number of steps: (1) complexation and/or entrapment with the vector, (2) interaction with the plasma membrane and internalisation via endocytosis (3) endosomal disruption and the release of the therapeutic to the site of action either in the cytosol or further to the nucleus (Patil *et al.*, 2005).

1.3.1 *Viral Vectors*

Viral vector based gene therapy, was first used in the treatment of hereditary single-gene defects. Nowadays, their use in the treatment of cancer and other

diseases is the subject of much research. A major reasoning supporting the usage of viral delivery vectors lies in the fact that viruses have evolved highly efficient strategies for gaining access to host cells and for directing the cellular machinery to express their own genetic information (Crystal, 1995, Thomas *et al.*, 2003, Vannucci *et al.*, 2013). Five main classes of viral vectors derived from oncoretroviruses, lentiviruses, adenoviruses, adeno-associated viruses (AAVs) and herpes simplex-1 viruses (HSV-1s) are recognized (Thomas *et al.*, 2003, Mali, 2013, Vannucci *et al.*, 2013).

Viral vectors provide high delivery and transfection efficiency in a variety of human cells (Hendrie and Russell, 2005). Despite their efficiency, safety issues due to possible generation of toxicity and immunogenicity as well as mutagenesis at critical regions of DNA are still a concern as is their inability to deliver large DNA sequences (Patil *et al.*, 2005, Glover *et al.*, 2005, Al-Dosari and Gao, 2009, Yin *et al.*, 2014).

1.3.2   *Nonviral vectors*

Nonviral vectors provide safety advantages over viral vectors in terms of reduced pathogenicity and possible mutagenesis in addition to their easier formulation and lower cost of production (Glover *et al.*, 2005, Yin *et al.*, 2014). Traditionally, vectors for delivering nucleotides have been cationic in nature and are able to associate with negative charges to form complexes. These vectors include polymers forming polyplexes and liposomes forming lipoplexes that need to interact with the plasma membrane and be internalised into the inside of the cell (El-Aneed, 2004, Guo and Huang, 2011). There is

then most often a need to endosomal escape to release the cargo into the cytosol. Stabilization and targeting of polyplexes and lipoplexes to specific cell types can be achieved by utilizing the interactions between surface receptors and ligands attached to the vector. These ligands can be small molecules such as galactose and folate, or peptides and proteins such as transferrin and antibodies (Davis, 2002, Pathak *et al*., 2009).

1.3.2.1 Cationic polymers

Cationic polymers are synthetic cationic compounds that complex DNA, forming polyplexes. These include the widely studied polymers; polyethylenimine (PEI) and poly L-lysine (PLL), in addition to chitosan and dendrimers (Figure 1-1).
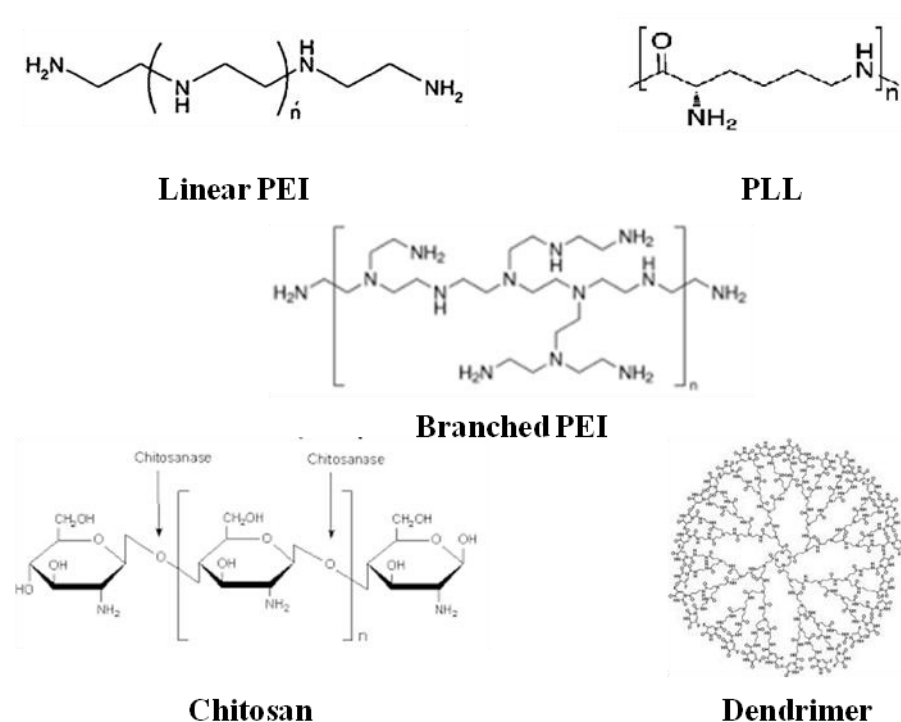
Figure 1-1: Structures of cationic polymers used in delivery.

PEI is one of the most widely studied examples of cationic polyamines. PEI can be synthesized in different lengths as a branched or linear polymer. It possesses a high charge density at reduced pH values due to the presence of a nitrogen atom at every third position along the polymer that can be protonated. This is responsible for the buffering effect, also named proton sponge effect, of PEI. The buffering capacity of PEI is thought to aid in rapid endosomal escape resulting in high transfection efficiency (Mintzer and Simanek, 2008).

PLL polymers are one of the early studied cationic polymers for gene transfer that are also biodegradable once administered into the body. PLL are linear homopolypeptides of the basic amino acid lysine as the repeat unit. At physiological pH, the amine group in PLL structure is positively charged and therefore lacks the buffering capacity required for endosomal escape. For the enhancement of transfection efficiency, a lysosomotropic agent such as chloroquine is often added (El-Sayed *et al*., 2009, Yin *et al*., 2014). Alternatively, PLL can be substituted by histidine groups which become protonated at pH <6 (Midoux and Monsigny, 1999). Relatively stable DNA complexes with better DNA condensation and transfection efficiency were obtained with high molecular weight PLL, however, this was also associated with increased cytotoxicity (Wolfert *et al*., 1999, Lv *et al*., 2006).

Chitosan is a natural biodegradable and biocompatible linear aminopolysaccaride. It is obtained by deacetylation of chitin; a polysaccharide found in the exoskeleton of crusteans and insects, to form a polymer of N-acetyl-D-glucosamine and D-glucosamine (Mansouri *et al.*, 2004). Chitosan's

cationic nature enhances electrostatic interaction with mucus and negatively charged mucosal surfaces. Chitosan is also able to form electrostatic interactions with other macromolecules such as DNA which has the benefit of protecting DNA form degradation by nucleases (Morille *et al.*, 2008, Mao *et al.*, 2010).

Dendrimers are spherical, highly branched polymers with tree-like three dimensional structures. They are synthetic macromolecules composed of three specific domains: (1) a central core, (2) repetitive branch units in a geometrical radiated organization forming successive generations, and (3) a large number of terminals on the outer surface. Several types of dendrimers are used such as polyamines, polyamides and polyesters. Polyamidoamine (PAMAM) is the most commonly encountered dendrimer for its high transfection efficiency. The primary amine groups on the dendrimer surface are responsible for charged molecules (DNA or siRNA) binding and condensation into nanoscale particles and promotes its cellular uptake. Moreover, the tertiary amines buried in the interior of the dendrimers promote endosomal escape of the DNA or siRNA through the proton-sponge effect (Morille *et al*., 2008, Liu *et al*., 2012).

1.3.2.2 Cationic lipids (cationic liposomes)

Cationic lipids have emerged as one of the most versatile tools for gene delivery. Liposomes are vesicles comprised of a phospholipid bilayer enclosing an aqueous compartment. Multilamellar vesicles (MLV) are formed when multiple bilayers of lipid are formed around the central core in a concentric fashion. Unilamellar vesicles can be obtained by sonication of MLV.

Liposomes can complex both hydrophilic and hydrophobic drugs. DNA-based therapeutics can be either entrapped in the aqueous core of the liposome or complexed with the phospholipid lamellae. A cationic liposomal formulation usually consists of a mixture of cationic and zwitterionic lipids. Cationic lipids such as 1,2-dioleoyl-3-trimethylammonium propane (DOTAP) and N-[1-(2,3-dioleyloxy)propyl]-*N,N,N*trimethylammonium chloride (DOTMA), help in DNA complexation and condensation as well as cellular binding. Zwitterionic lipids, also referred to as helper lipids, such as 1,2-dioleoyl-sn-glycero-3-phosphoethanolamine (DOPE) and cholesterol work by promoting membrane perturbation and fusion (Patil *et al*., 2005, Pathak *et al*., 2009). Several commercial formulations of cationic lipids have emerged such as Lipofectamine (Invitrogen, Carlsbad, CA), Tranfectam (promega, Madison, WI) and others; however their application is restricted to *in vitro* studies. Liposomes offer several advantages in drug delivery. Opposing viruses, liposomes are generally nonimmunogenic due to the absence of proteinaceous contents and they can be synthesized to have a variety of properties in terms of size, composition and surface charge. Liposomes also have the advantage of being biodegradable and can be formulated for controlled and targeted delivery (Patil *et al*., 2005, Slingerland *et al*., 2012). Despite these advantages, toxicity and instability of cationic lipids is still a concern in drug delivery (Patil *et al*., 2005, Yin *et al*., 2014, Severino *et al*., 2015).

It is clear that viral vectors can provide superior transfection efficiency but immunogenicity and possible oncogenic effects limit their application. On the other hand, non-viral vectors such as cationic polymers and lipids are less

immunogenic than viral counterparts but this is at the expense of reduced transfection efficiency and increased cytotoxic side effects. Thus, for therapeutic cargos to be delivered intracellularly, there is a need for the design of alternative vectors to efficiently cross the plasma membrane and allow their cargo to reach their desired target site.

1.4 Cell Penetrating Peptides (CPPs)

The term cell penetrating peptide (CPP) is now over 20 years old and describes short peptide sequences that have the capacity to deliver themselves and cargo of various forms from the outside to the inside of cells. A major discovery in CPP history was made in 1988 by Frankel and Pabo while developing an assay for measuring the activity of Tat protein from the Human immune-deficiency virus-1. Unexpectedly the purified Tat, when added to the culture medium of HL3T1 cells, was able to enter cells and translocate into the nucleus (Frankel and Pabo, 1988). Another observation was made by the group of Prochiantz in 1991 who showed that a 60 amino acid polypeptide from the sequence of the *Drosophila Antennapedia* homeodomain protein (pAntp, penetratin) could be internalized by neurons, reach the nucleus and cause significant morphological changes in the cultured cells (Joliot *et al*., 1991). This was followed by the discovery of the first what we would now term as a CPP; derived from the third helix of Antennapedia homeodomain and named penetratin. Penetratin is a 16 amino acid peptide with the sequence RQIKIWFQNRRMKWKK (Derossi *et al*., 1994). Since the discovery of penetratin, major efforts have been made to develop other peptide sequences to deliver covalently or non-covalently attached cargos into cells and the number of CPP sequences has increased

dramatically. Interestingly, some CPPs have nuclear localisation sequences (NLS) that allow for their nuclear translocation across nuclear pores either alone or with conjugated cargos. Molecules are transported into the nucleus generally across the nuclear pore complexes (NPCs). The inner diameter of NPCs is only $\approx$ 9 nM which allows the free diffusion of small molecules, however, macromolecules such as DNA cannot diffuse through the pores (Morille *et al*., 2008). NLS are sequences rich in basic amino acids and are thought to be transported into the nucleus through binding to cytoplasmic receptors known as importins; α/β or both, followed by translocation through nuclear pores. NLS can be monopartite with one cluster of basic amino acids such as in the sequence from simian virus (SV40) large tumour antigen (PKKKRKV), bipartite with two clusters of basic amino acids such as in p53 protein (KRALPNNTSSSPQPKKK) (Bolhassani, 2011) or tripartite such as the NLS in epidermal growth factor receptor (EGFR) (RRRHIVRKRTLRRLL) (Hsu and Hung, 2007).

The term CPP is now widely used to describe a class of short sequence peptides, usually less than 30 amino acid residues, that have been found to successfully internalise into many different mammalian cells (Stewart *et al*., 2008) and non-mammalian cell types (Nekhotiaeva *et al*., 2004) including yeast (Holm *et al*., 2005) and plant protoplasts (Mae *et al*., 2005). A unified term for peptide sequences with penetrating properties has not yet been agreed upon and alternative terminologies include protein transduction domains (PTDs), and membrane translocation sequences (Jarver and Langel, 2004, Milletti, 2012). In this thesis, the term CPP will be used to describe a peptide

that can enter cells via one or more mechanism and can at the very least deliver a small payload such as a fluorophore.

Today, CPPs have been shown to have the capacity to not only gain access to cells but to also deliver a range of cargos of widely different sizes and composition. These include siRNA (Eguchi and Dowdy, 2009), small molecules such as fluorophores (Jones and Sayers, 2012), proteins, peptides (Milletti, 2012), plasmid DNA, PNA (peptide nucleic acid) and liposome nanoparticles (Morris *et al*., 2008, Nakamura *et al*., 2013). The sequences of a range of studied CPPs are listed in Table 1-1. There are many other sequences in the literature that have been shown to have similar effects in cells and also not included are D-isoforms that are designed to have the same cell penetrating function but reduced sensitivity to degradation. Also not included are details of the nature of the N- and C-terminus (e.g. acyl, amide) and the various modifications that are placed on them for conjugation (e.g. cysteine). Any modification of peptides used in this thesis is highlighted when the peptide sequence is described in the Materials and Methods.

Table 1-1: In alphabetical order, amino acid sequences of studied CPPs; adapted from (Jones and Sayers, 2012).

Peptides	Sequence	References
8K	KKKKKKKK	(Davé et al., 2007)
CADY	GLWRALWRLLRSLWRLLWRA	(Crombez et al., 2009)
EB1	LIRLWSHLIHIWFQNRRLKWKKK	(Lundberg et al., 2007)
GALA	WEAALAEALAEALAEHLAEALAEALEALAA	(Subbarao et al., 1987)
HIV-1 Rev	TRQARRNRRRRWRERQR	(Sugita et al., 2008)
KALA	WEAKLAKALAKALAKHLAKALAKALKACEA	(Wyman et al., 1997)
Kaposi FGF derived	AAVALLPAVLLALLAP	(Lin et al., 1995)
MAP	KLALKLALKALKAALKLA	(Oehlke et al., 1998)
Mastoparan	INLKALAALAKKIL	(Konno et al., 2000)
Maurocalcine	GDCLPHLKLCKENKDCCSKKCKRRGTNIEKRCR	(Estève et al., 2005)
mellittin	GIGAVLKVLTTGLPALISWIKRKRQQ	(Dempsey, 1990)
MPG	GALFLGFLGAAGSTMGAWSQPKKKRKV	(Simeoni et al., 2003)
PasR8	FFLIPKGRRRRRRRR	(Takayama et al., 2009)
Penetratin	RQIKIWFQNRRMKWKK	(Derossi et al., 1994)
Pep-1	KETWWETWWTEWSQPKKKRKV	(Deshayes et al., 2004)
PepFect 14	Stearyl-AGYLLGKLLOOLAAAALOOLL [c]	(Ezzat et al., 2011)
PFVYLI	PFVYLI	(Rhee and Davis, 2006)
pHLIP	AEQNPIYWARYADWLFTTPLLLLDLALLVDADEGT	(Reshetnyak et al., 2008)
PTD-5	RRQRRTSKLMKRGG	(Rehman et al., 2003)
pVec	LLIILRRRIRKQAHAHSK	(Elmquist et al., 2001)
R7W	RRRRRRRW	(Maiolo et al., 2005)
R8	RRRRRRRR	(Fretz et al., 2007)

R9F2	RRRRRRRRRFFC	(Nelson *et al.*, 2005)
SAP(E)	VELPPPVELPPPVELPPP	(Martín *et al.*, 2011)
Tat	GRKKRRQRRRQ	(Vives *et al.*, 1997)
TP10	AGYLLGKINLKALAALAKKIL	(Soomets *et al.*, 2000)
Transportan	GWTLNSAGYLLGKINLKALAALAKKIL	(Pooga *et al.*, 1998)
YTA2	YTAIAWVKAFIRKLRK	(Lindgren *et al.*, 2006)

^c O represents ornithine

1.4.1 *Classification of CPPs*

CPPs can be categorised into three major classes: (i) cationic such as Tat, and polyarginines (Milletti, 2012), (ii) amphipathic, whereby alterations between cationic and hydrophobic residues give rise to α-helical structures (Fernández-Carneado *et al.*, 2004)- MAP and transportan, and (iii) hydrophobic such as the sequence PFVYLI (Watkins *et al.*, 2009b) and Kaposi Fibroblast Growth Factor (Lin *et al.*, 1995). There is no specific class for anionic peptides; however, SAP(E) is a recently described anionic CPP shown to deliver fluorophores into a range of cell lines (Martín *et al.*, 2011, Jones and Sayers, 2012).

CPPs can also be classified based on their origin: (i) Protein derived CPPs, which refers to those peptides derived from the sequence of a parent translocation protein such as Tat and penetratin. (ii) Designed such as R8 or "chimeric" CPPs which refers to sequences obtained by the covalent attachment of a hydrophilic and a hydrophobic domain of different origin separated by a linker. For example, MPG in Table 1-1 is derived from the

fusion of the HIV glycoprotein 41 peptide and the NLS sequence of SV40 T-antigen. Another example is transportan which was derived from the coupling of the minimal active part of the neuropeptide galanin and mastoparan. (iii) Model CPPs such as MAP, represent sequences synthetically designed to produce amphipathic α-helical structures or simulating structures of known CPPs (Zorko and Langel, 2005).

1.4.2 Internalisation Mechanisms of CPPs

As more and more CPPs sequences are described, it is becoming increasingly more difficult to suggest that a single mechanism is responsible for the translocating property of all of them. Added to this is (1) the fact that they have been tested in many different model systems from synthetic to *in vitro* to *in vivo*, (2) some CPPs have been extensively studied (Tat, Penetratin and R8) while others have received less attention, (3) that mechanism of action will undoubtedly be influenced by choice of cargo. In this section, fragments of the literature have been selected to highlight different types of uptake mechanisms for the few selected CPPs that have been extensively studied. This ranges from direct translocation across the plasma membrane into the cytosol through to the use of defined endocytic pathways to initially gain entry in the cytoplasm. These studies initially and generally look at CPPs attached to small cargo such as fluorophores.

Initially, it was thought that the uptake of CPPs occurred by direct translocation through the lipid bilayer cell membrane in a receptor- and energy-independent process (Derossi *et al*., 1994, Vives *et al*., 1997). This commonly

accepted mechanism of internalisation was re-evaluated when in 2002, Lundberg and Johansson provided evidence that herpes simplex virus VP22 protein adhered to the cell membrane of living cells and nuclear import only occurred after cell fixation (Lundberg and Johansson, 2002). Later, Richard *et al.* compared the distribution of Tat and $(Arg)_9$ between fixed and unfixed cells. The live cell imaging revealed a punctate cytoplasmic distribution characteristic of endocytosis and there was overlap between the peptides and endocytic markers. Fixed cells showed nuclear localisation suggesting this localisation was an artefact induced by fixation (Richard *et al.*, 2003). In another study, the internalization of unconjugated Tat was found to involve clathrin dependent endocytosis as well as heparan sulphate receptors (Richard *et al.*, 2005). As a result, endocytosis gained greater prominence as an uptake mechanism, however it should be noted that uptake of CPPs still occurs at low temperatures which suggests the involvement of alternative energy-independent internalization mechanisms (Patel *et al.*, 2007). The study of Fretz *et al.* showed that in leukaemic KG1a cells, R8 peptides attached to the fluorophore Alexa488 were particularly prone to allowing the internalisation of these CPPs when they were placed on ice and thus when endocytosis was inhibited (Fretz *et al.*, 2007). The reason for this has yet to be determined and this direct translocation mechanism is further described in the next section. Different internalisation mechanisms of CPPs are presented in Figure 1-2.
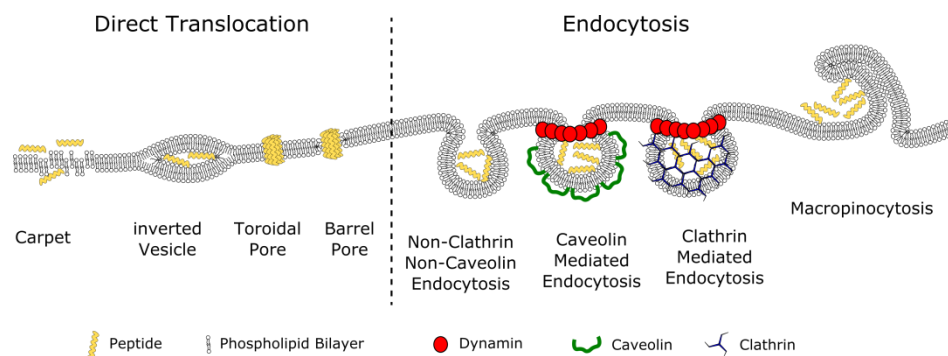
Figure 1-2: Different internalization mechanisms of CPPs; adapted from (Trabulo *et al.*, 2010).

1.4.2.1 Direct Translocation

Direct translocation of CPPs across membranes has been observed using several different biological and synthetic systems. The proposed models for this event to occur include the "inverted micelle model", the "carpet model" and those that induce pores in the membrane. In 1996, Derossi *et al.* outlined the "inverted micelle model" to explain the translocation of penetratin (Figure 1-2). This model suggests that the interaction of CPPs with cell membranes results in a disturbance of the lipid bilayer which leads to the formation of inverted hexagonal structures called inverted micelles. Peptides would then be entrapped within the hydrophilic medium in the core of the formed micelle up to the point at which they interact with the biological membrane leading to an inverse process. This would then cause destabilization of the inverted micelles and allow the release of the entrapped peptides into the cell interior (Derossi *et al.*, 1996).

In the "carpet model", the extensive association between the peptide and the surface of the cell membrane causes a temporary destabilization of the

membrane as well as phospholipid reorganization. As a result, the peptides and their conjugates can cross through the membrane (Pouny *et al*., 1992, Shai, 1999, Copolovici *et al*., 2014).

The membrane pore formation models involve two types of pore: barrel stave pores and toroidal pores. In the barrel stave model, peptides form an amphipathic alpha-helix structure when introduced into the membrane. This allows for an interaction between the hydrophobic face of the amphipathic helix and the aliphatic chains of the phospholipids bilayer while the hydrophilic face would line the inside of the pore (Madani *et al*., 2011). Toroidal pores differ from barrel stave pores in that the peptides interact entirely with the polar groups of the phospholipids of the membrane causing an obvious rearrangement of the lipid bilayer (Yang *et al*., 2001, Trabulo *et al*., 2010).

1.4.2.2 CPP Cell Uptake via Endocytosis

Endocytosis is a term that describes the process by which a cell internalises a portion of its plasma membrane into the cytoplasm in the form of a vesicle that also contains extracellular fluid. It can be broadly divided into two forms classically termed as phagocytosis and pinocytosis. Phagocytosis only occurs in specialized cells (macrophages, monocytes and neutrophils) that function to clear large pathogens such as yeast or bacteria, apoptotic cells and cell debris (Conner and Schmid, 2003, Doherty and McMahon, 2009). Pinocytosis, on the other hand, is used by all cells for the uptake of fluids and solutes (Patel *et al*., 2007). This occurs via different pathways such as macropinocytosis, clathrin-

mediated endocytosis, caveolae-mediated endocytosis and other less known pathways (Cleal *et al*., 2013).

Macropinocytosis is an actin-dependent form of endocytosis and may be a constitutive event or occurs via stimulation with growth factors such as epidermal growth factor (EGF) or phorbol esters (Swanson, 1989, Jones, 2007, Kerr and Teasdale, 2009). Macropinocytosis involves membrane ruffling with the inward folding of the outer surface of the plasma membrane. The formed protrusions collapse and fuse with the ruffled membrane to form large vesicles named macropinosomes. Macropinocytosis is a means for cells to engulf significant volumes of extracellular fluid and macropinocytosis may be the major route for the internalization of cationic CPPs such as Tat (Kaplan *et al*., 2005, Jones, 2007, Cleal *et al*., 2013).

Clathrin and caveolae-mediated endocytosis are the most studied forms of pinocytosis and these pathways have also been suggested to be involved in the uptake of CPPs. Clathrin-mediated endocytosis is a well characterised endocytic pathway by which materials are internalised through clathrin-coated vesicles. These vesicles are formed by the sequestration of clathrin proteins to form clathrin cage invaginations at the plasma membrane and they enclose the extracellular molecule after binding to the membrane. Once internalised, the clathrin-coated vesicles lose its coat to enable fusion with early endocytic compartments that direct traffic to other cellular compartments including recycling endosomes (McMahon and Boucrot, 2011). Caveolae are described as flask-shaped, non-coated plasma membrane invaginations that are localized

in domains called lipid rafts. They are enriched in cholesterol and glycosphingolipids (Reeves *et al*., 2012). Unlike macropinocytosis that is known to engulf material into large vesicles, caveolae are approximately 50 nm in diameter while clathrin coated vesicles are slightly bigger, 80-100 nm (Conner and Schmid, 2003, Madani *et al*., 2011).

To assess the involvement of different endocytotic internalization pathways in CPP uptake, several experiments may be performed based on changing the experimental conditions: (i) investigating uptake at low temperature (approximately 4ºC), (ii) evaluating the colocalisation of peptides with either endocytic probes that are known to utilise specific endocytotic internalization pathways such as transferrin for clathrin-mediated endocytosis or protein markers such as Caveolin-1 expressed in cells as GFP-tagged variants to label caveolae, (iii) overexpression of dominant negative mutants of proteins such as Dynamin that are involved in defined endocytotic processes (iv) use of pharmacological inhibitors that are deemed to inhibit defined pathways and (v) siRNA depletion of proteins known to regulate specific endocytic pathways (Mundy *et al*., 2002, Trabulo *et al*., 2010, Al Soraj *et al*., 2012, Cleal *et al*., 2013).

1.4.2.3   Factors affecting Translocation Efficiency

The cellular uptake mechanism of CPPs can be affected by several factors including the nature and secondary structure of the CPP (Heitz *et al*., 2009, Copolovici *et al*., 2014). In order to understand important peptide features required for membrane translocation, one can compare physico-chemical

characteristics from different CPPs. Generally, CPPs contain a high content of basic amino acids resulting in a net positive charge (Lundberg and Langel, 2003, Jones and Sayers, 2012). Arginine is the most basic amino acid with a pKa of 12.5 due to the presence of the guanidine moiety which is positively charged at physiological pH. This residue is thought to confer many advantages to CPPs regarding interaction with the cell and entry into the cell interior. Structurally, the guanidinium group is characterized by a planar Y-shape which allows the delocalization of its cationic charge. The molecule is stabilized by resonance of the positive charge evenly on the three nitrogen atoms as shown in Figure 1-3A. As a result of its unique shape and multiple hydrogen bonding, a guanidinium group can form both electrostatic and hydrogen bonding with anionic and polar molecules (Schug and Lindner, 2005). The guanidinium group forms bi- or multi-dentate hydrogen bonds with the phosphates of more than one lipid head groups. Lysine (pKa $\approx$ 10.5) lacks a guanidinium moiety and instead has an amino group (Figure 1-3B), which forms a mono-dentate hydrogen bond with the phosphate on a single lipid head group. This indicates that the guanidinium group of arginine is more efficient in interacting with bulky lipid head groups of the cell membrane than the amino group of lysine (Rothbard *et al.*, 2004, Schmidt *et al.*, 2010).
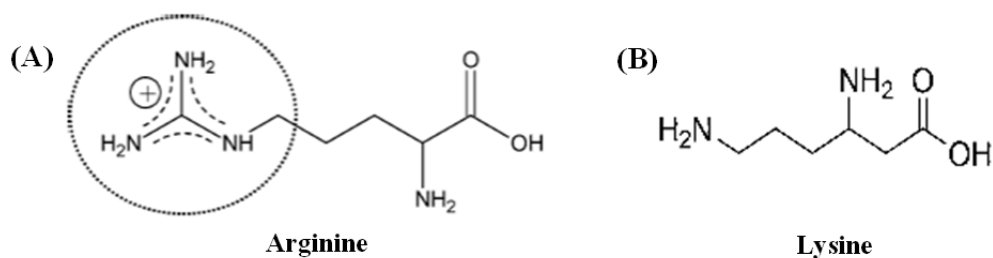
Figure 1-3: Structures of arginine, lysine. (A) structure of arginine and the guanidinium moiety highlighted and (B) structure of lysine with the amino group instead of the guanidinium moiety.

The properties of arginine and to a lesser extent lysine allow the peptides to not only interact with lipids on the cell surface or possibly the inner surface of the endosomal membrane but also with heparan sulphate proteoglycans (HSPG) that protrude from the cell surface. These are negatively charged sugars attached to surface proteins that are thought to have major influence on the way cationic CPPs interact with cells and enter cells (Futaki *et al*., 2001, Belting, 2003, Schmidt *et al*., 2010). It has been also shown that HSPG acts as a surface receptor for Tat, which is rich in arginine. HIV-1 Tat protein internalisation is impaired in cells lacking all types of glycosaminoglycans (GAGs) or those specifically lacking HSPG or cells that were pre-treated with HSPG-degrading enzymes (Tyagi *et al*., 2001).

Non-electrostatic effects such as hydrophobicity and peptide structural transitions can also have a role in the binding affinity of amphipathic CPPs to cell membranes (Ziegler, 2008). For example, penetratin adopts a random coil structure when in aqueous solution that transforms to an α-helical structure at high lipid to peptide molar ratios. A higher degree of β-sheet conformation of penetratin is induced by reducing the lipid to peptide ratio (Magzoub *et al*.,

2002). These amphipathic secondary structures that penetratin adopts allow the hydrophobic peptide residues to directly interact with the non-polar interior of the lipid membrane. This causes membrane destabilization and enhances CPP internalization (Binder and Lindblom, 2003, Schmidt *et al.*, 2010)

The nature of the cargo also plays a role in the internalisation mechanism of CPPs (Heitz *et al.*, 2009, Koren and Torchilin, 2012, Copolovici *et al.*, 2014). Studies on Tat provide a good example of this. When unconjugated, it is thought to enter cells mainly by clathrin-mediated endocytosis (Richard *et al.*, 2005). However, the fusion protein GST-Tat-GFP, is primarily internalised via the caveolin-mediated pathway (Fittipaldi *et al.*, 2003), while the Tat-HA2 fusion peptide is internalized via lipid raft-dependent macropinocytosis (Wadia *et al.*, 2004). It should be noted that all these studies predominantly used chemical inhibitors of endocytosis to define uptake mechanism and all of these suffer from lack of specificity (Ivanov, 2008).

1.5 CPPs and Cargo Delivery for Therapeutic Applications

The discovery of CPPs and their ability to cross the plasma membrane provided hope that they could be used as drug delivery vectors. CPPs offer potential to improve the delivery of therapeutic cargos such as oligonucleotides and peptides that were previously of limited therapeutic value due to their poor permeability and rapid degradation (Lindgren *et al.*, 2000, Chugh *et al.*, 2010). Examples of cargos delivered by CPPs are described in sections 1.5.1 to 1.5.4, and elsewhere in the thesis.

1.5.1   Delivery of small molecules

A good example of small molecular entities that have been delivered into cells by CPPs are the numerous fluorophores that have been used to analyse CPP uptake. These include fluorescein dyes such as fluorescein isothiocyanate (FITC) (Okamura *et al*., 2005), rhodamine dyes (Fretz *et al*., 2007) and Alexa dyes such as Alexa488 (Kosuge *et al*., 2008). These dyes all have their unique properties (Jones and Sayers, 2012, Bechara and Sagan, 2013) but very few studies have been performed to specifically study what effect the fluorophore has on cell entry.

CPPs have also been studies for the delivery of anticancer agents such as taxol and doxorubicin. Taxol; a widely used chemotherapeutic agent, when conjugated with octaarginine (r8), was delivered in both *in vitro* and *in vivo* models of taxol-resistant ovarian cancer. The conjugate produced enhanced anticancer effect over taxol alone in ovarian-tumour-bearing mouse models (Dubikovskaya *et al*., 2008). In another study, the administration of r8-doxorubicin conjugates effectively suppressed tumour proliferation to the same extent as doxorubicin without causing the significant weight loss associated with the unconjugated drug (Nakase *et al*., 2012). Coupling of doxorubicin with D-penetratin has been shown to enhance its uptake and increased its cytotoxicity by 20 fold compared to free doxorubicin in human erythroleukemic (k562/ADR) resistant cells (Mazel *et al*., 2001). Conjugating octaarginine with a vinblastine derivative showed an antiproliferative effect against sensitive and resistant leukemia HL-60 cells as well as HeLa cells (Bánóczi *et al*., 2010).

1.5.2   Nucleic acid delivery

The delivery of DNA- and RNA-based therapeutics to mediate a physiological response represents a major challenge. Several studies have been performed using CPPs to deliver DNA cargo for controlling gene expression or for silencing the activity of certain proteins. Oligomers of Tat have demonstrated the ability to complex plasmid DNA and mediate gene delivery to cultured cells (Tat$_2$ and Tat$_3$ > Tat$_4$). The transfection efficiency of Tat$_2$ was enhanced by 40 fold in presence of chloroquine (Rudolph *et al*., 2003). Tat$_2$, Tat$_3$ and Tat$_4$ are dimer, trimer and tetramers of Tat repeats [C(YGRKKRRQRRRG)$_{2-4}$] respectively with an intervening glycine. Penetratin and transportan covalently attached to thiol-containing siRNAs, targeting luciferase or green fluorescent gene (GFP), efficiently reduced transient and stable expression of these proteins in different cell lines. Penetratin-siRNA and transportan-siRNA conjugates were able to enter the cell and decrease luciferase levels and this decrease remained stable for up to 3 days. The conjugates also caused knockdown of GFP expression which was shown to persist for up to seven days (Muratovska and Eccles, 2004). Further examples of the successful delivery of nucleic acids using CPPs will be described in chapter 5.

1.5.3   Metallic nanoparticle delivery

CPPs have been successfully used to mediate the delivery of nanoparticles for diagnostic, therapeutic and imaging purposes. Superparamagnetic iron oxide nanoparticles have been used as powerful non-invasive tools for biomedical imaging, clinical diagnosis and therapy (Jin *et al*., 2014). Iron oxide

nanoparticles showed efficient labelling of cells when conjugated with Tat. Moreover, increasing the number of Tat per cross linked superparamagnetic iron oxide (CLIO) particle (above 10 per CLIO) facilitated their cellular uptake and enhanced their intracellular accumulation by 100 fold (Zhao *et al.*, 2002). This allows the intracellular magnetic labelling and detection by magnetic resonance imaging (MRI). Studies performed by Lewin *et al.* showed that tracking of labelled cells *in vivo* using MRI was possible using functionalized CLIO-Tat (Lewin *et al.*, 2000, Sawant and Torchilin, 2010). In another study, gold nanoparticles functionalized with Tat were able to cross the plasma membrane and enter the nucleus in human fibroblasts while unconjugated particles were only detected in the cytoplasm in vacuoles or around the mitochondria and failed to enter the nucleus (de la Fuente and Berry, 2005).

Quantum dots (QDs) are semiconductor nanoparticles that are used as fluorescence probes due to a number of favourable photoproperties such as high luminescence efficiency and photostability in addition to broad absorption and narrow emission profiles (Gao *et al.*, 2004). In a number of studies, CPPs have been used to enhance the cellular uptake of QDs (Xue *et al.*, 2007, Ruan *et al.*, 2007, Stewart *et al.*, 2008).

1.5.4 *Peptide and Protein delivery*

CPPs have also been used to deliver a range of peptides and whole proteins. An *in vivo* study that raised significant interest in CPP research emanated from the Dowdy lab in 1999 (Schwarze *et al.*, 1999). They studied delivery of β-galactosidase (β-gal) conjugated with Tat after intraperitoneal injection into

mice. Enzyme activity was found to be distributed in all tissues. Cai *et al.* also showed successful delivery of β-gal using Tat after portal vein, intravenous, intraperitoneal and oral administration in mice (Cai *et al*., 2006). These studies opened new opportunities for using this sequence and newly discovered CPPs to deliver proteins and peptides to cells.

It is beyond the scope of this thesis to describe all the attempts now made to use CPPs to deliver protein and peptides to cells. Focus will be given to studies that have used CPPs to deliver peptide and protein cargo targeting either cancer or the NF-κB pathway.

1.6   CPPs and Cancer

The ideal cancer therapy targets only cancer cells with the aim of eliminating all of them from the body. For several types of cancer, with current approved approaches, this remains a major challenge. The understanding we now have of cancer allows us to think of new types of drugs including peptides and proteins that in most cases need a delivery vector to enter cells.

As cancer cells proliferate and a solid tumour expands, the demand for oxygen and nutrition increases (Iyer *et al*., 2006). The tumour vasculature differs from the normal vasculature: in a solid tumour the blood vessels are disorganised, irregular in shape, dilated, leaky and of greater density (Skinner *et al*., 1990, Baluk *et al*., 2005). Tumour endothelial cells have large fenestrations which results in the leakage of serum components such as macromolecules and nanoparticles into the tumour cells. Tumour cells also show poor lymphatic drainage which reduces the clearance of macromolecules from the tumour and

leads to their intratumoural accumulation. This phenomenon is termed the enhanced permeability and retention (EPR) effect and has been used for the targeting of macromolecules to solid tumour cells using nanoparticle formulations (Iyer *et al.*, 2006).

CPPs have been studied as delivery vectors for peptides and proteins in formulations that do and do not rely on the EPR effect to gain access to tumour cells and a few examples will be given here specifically for protein delivery and peptide delivery is covered in later sections in this introduction covering NF-κB and EGFR and also in introduction to chapters 3, 4 and 6.

The CPPs are designed to facilitate the targeting and delivery of tumour suppressor or proapoptotic proteins to tumour cells. Second mitochondria derived activator of caspases (Smac) is a mitochondrial protein that is released into the cytosol in response to apoptotic stimuli and is capable of inactivating inhibitor of apoptosis (IAP) proteins such as XIAP, c-IAP-1, and c-IAP-2 and prevents them from inhibiting caspases (Vucic *et al.*, 2002). Several groups have demonstrated that the N-terminus of the Smac protein can be linked to CPPs such as penetratin and Tat to increase cellular uptake (Snyder and Dowdy, 2004). Smac/penetratin fusion peptide was able to cross the plasma membrane of various cell lines and bind to endogenous IAPs, decrease caspases-3 aggregation in the cytoplasm and enhance drug-induced caspases action. The fusion peptide increased the induced apoptosis and antiproliferative effects of a variety of chemotherapeutic agents such as doxorubicin and paclitaxel (Arnt *et al.*, 2002). In another study, an intracranial glioblastoma

xenograft model was used to test the effect of Smac-Tat peptide *in vivo*. Initially, the effect of tumor necrosis factor–related apoptosis-inducing ligand (TRAIL) alone was examined. TRAIL caused reduced tumor volume and moderately extended the life of nude mice bearing established intracranial U87MG tumors. Smac/Tat alone had no effect on tumor growth but when combined with TRAIL strongly enhanced its antitumor activity in a human glioma xenograft model *in vivo*. Moreover, a synergistic effect was observed in case of Smac/Tat and TRAIL combinations and mice treated with the combination had complete eradication of established intracranially growing glioma and showed better survival (Fulda *et al*., 2002).

Intraperitoneal (IP) delivery of penetratin-conjugated p16 peptide (an inhibitor of cell cycle progression) suppressed the growth of pancreatic cancer cells in peritoneal and subcutaneous tumours in nude mice (Hosotani *et al*., 2002). No systemic toxicity was reported in the above study which suggests that cancer cells may be more sensitive to the effects of tumour suppressor peptides than normal cells. This demonstrates potential for the use of CPP vectors for specific, targeted delivery of cytotoxic agents in cancer treatment (Snyder and Dowdy, 2004). In a study by Roeder *et al.,* Herpes Simplex Virus VP22 protein was used to deliver E2 protein which triggers growth arrest and/or apoptosis when overexpressed in cells. VP22-E2 fusion protein was found to induce apoptosis in transiently-transfected, human papillomavirus (HPV)-transformed cervical carcinoma cell lines (Roeder *et al*., 2004).

Anti-p21 antibodies when conjugated to 17-mer peptides derived from HIV-1 Tat protein (<u>GRKKRR</u>QRRRPPQGYGC, NLS underlined) sensitized breast cancer cells, MDA-MB-468 and MCF-7, to the antiproliferative effects of cytotoxic agents depending on the different ability of these agents to induce p21 expression in cells. p21 is a cyclin-dependent kinase inhibitor that plays a role in protecting cells against lethal DNA damage through cell cycle arrest to allow for DNA repair or promote apoptosis in case of DNA repair failure. The ability of Tat-anti-p21 immunoconjugates (ICs) to sensitize cancer cells to cytotoxic agents offers promising approaches towards more effective anticancer treatment (Hu *et al*., 2006).

1.7 CPPs and Nuclear factor-kappa B (NF-κB)

1.7.1 *Introduction to NF-κB*

NF-κB is a protein complex first described in 1986 by Sen and Baltimore (Sen and Baltimore, 1986). It plays a major role in cell inflammation, differentiation, growth and cell survival (Bharti and Aggarwal, 2002, Baltimore, 2011). It was so named because it was found bound to an enhancer element of the immunoglobulin kappa light chain gene in the nucleus of B cells (Ghosh *et al*., 1995, Sethi *et al*., 2008). NF-κB regulates the expression of several genes in response to infection and stress (Müller *et al*., 1995, Baltimore, 2011). In unstimulated cells, NF-κB is sequestered in a latent form in the cytosol via the formation of a complex with an inhibitory protein known as IκB (O'Neill and Kaltschmidt, 1997, Wan and Lenardo, 2010).

The vertebrate NF-κB family includes five cellular proteins: RelA (p65), c-Rel, RelB, p50/ NF-κB1 and p52/ NF-κB2. These protein homo- or heterodimerize to generate diverse combinations of dimeric complexes. These complexes bind to DNA target sites known as κB sites where they directly regulate gene expression (Gilmore, 2006). The heterodimer consisting of p50 and p65 is considered the main activated variants of the NF-κB pathway that translocate to the nucleus to mediate transcription and protein expression (Tas *et al*., 2005).

The NF-κB pathway has been shown to be activated via three different processes (Figure 1-4) (Viatour *et al*., 2005). The first pathway, also named classical pathway, is enhanced by pro-inflammatory cytokines such as tumour necrosis factor (TNF). TNF, through TNF receptor, acts on different adaptor proteins including TNF-receptor-associated death domain protein (TRADD), receptor-interacting protein (RIP) and TNF-receptor-associated factor 2 (TRAF2). This leads to the activation of IκB-kinase (IKK) complex (Lin *et al*., 2010). This complex consists of two catalytic subunits named IKK-α and IKK-β as well as a regulatory subunit known as IKK-γ/NEMO (Ghosh and Karin, 2002). The activated IKK complex phosphorylates IκB-α which is then ubiquitinated and degraded by the proteosome (Viatour *et al*., 2005). The free NF-κB dimmers can then migrate to the nucleus where they regulate the transcriptional activation of multiple target genes (Li and Verma, 2002). The second pathway, also named the non-canonical pathway, is activated by cytokines such as B-cell activating factor (BAFF) (Claudio *et al*., 2002),

lymphotoxin β (Dejardin *et al*., 2002) or CD40 ligand (Coope *et al*., 2002). This pathway can also be activated by viruses such as human T-cell leukaemia virus (Xiao *et al*., 2001) and Epstein-Barr virus (Eliopoulos *et al*., 2003). In this pathway, NF-κB-inducing kinase (NIK) activates an IKKα homodimer (ankyrin-containing and inhibitory molecule p100 is its substrate). Upon phosphorylation by IKKα, p100 is ubiquitinated and cleaved allowing NF-κB protein p52 to move as a heterodimer with RelB into the nucleus (Prasad *et al*., 2010). Activation of the noncanonical pathway has a major role in the regulation of B cell survival and maturation, and in the formation of secondary lymphoid organs (Senftleben *et al*., 2001). The third NF-κB pathway is triggered by DNA damage induced by mutagenic stimuli such as UV radiation or doxorubicin. This pathway is considered atypical as it is independent of IKK activation and instead is based on activation of casein kinase 2 (CK2). CK2 enhances IκB-α degradation via the proteosome (Lin *et al*., 2010). Although this pathway has a minor role in normal activation of NF-κB, it is thought that the pathway may be involved in skin carcinogenesis induced by UV exposure (Karin, 2006).
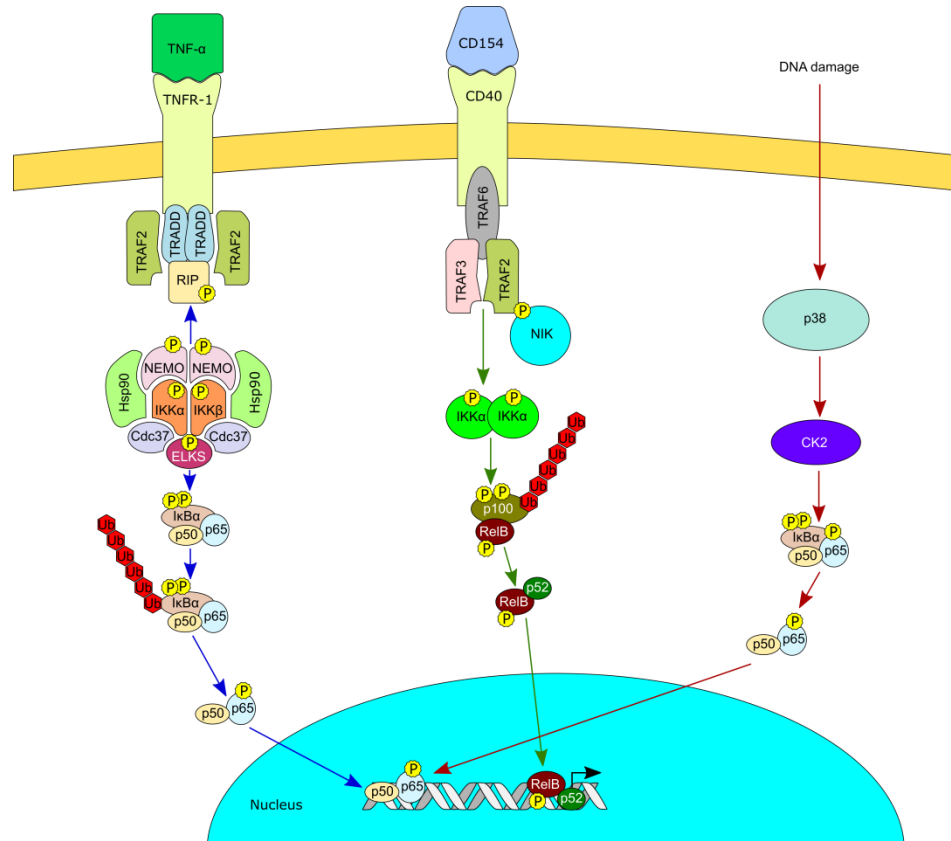
Figure 1-4: Different NF-κB activation pathways; adapted from (Viatour *et al*., 2005).

Constitutive IKK activity and high levels of nuclear p65 have been observed in inflammatory diseases as well as different solid tumours. This illustrates the contribution of NF-κB activation in the development of cancer and chronic inflammatory diseases. Inhibition of NF-κB activity has therapeutic potential in the treatment of cancer and inflammatory disorders (Sumitomo *et al*., 1999, Chaturvedi *et al*., 2011).

1.7.2   *CPPS and delivery of Therapeutic Peptides Targeting NF-κB*

As described, aberrant NF-κB activity has been associated with the development of several diseases as chronic inflammation, auto-immune

diseases and certain types of cancer (Orange and May, 2008). This highlights this pathway as an exciting target for therapeutic intervention. The identification of the components of the pathway and how they interact with each other has led to the design of small molecule drugs and macromolecular therapeutics that specifically interfere with NF-κB activation. This includes several approaches aimed at delivering NF-κB targeting peptide sequences attached to CPPs (Figure 1-5). The strategy is based on using a sequence derived from an NF-κB protein that inside the cytosol of cells interferes with a specific protein-protein interaction regulating the pathway.
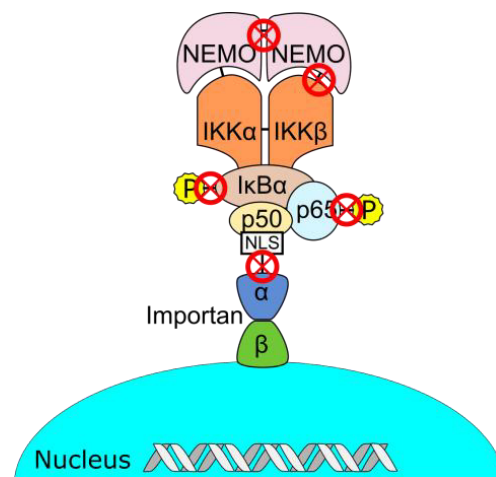
Figure 1-5: CPPs-and associated peptide cargos that disrupt the classical NF-κB pathway; adapted from (Orange and May, 2008). CPPs-cargos targeting the classical NF-κB pathway are indicated by the circled red "x". Some are discussed in more detail in the text.

Jacek Hawiger and colleagues were the first to design a peptide to interfere with NF-κB activation. The peptide, SN50, contained the NLS of p50 (N50: VQRKRQKLMP) attached to a CPP derived from Kaposi fibroblast growth factor (K-FGF). SN50 was found, in cultured monocytic and endothelial cell to

block the nuclear translocation of p50/p65 in a dose dependent manner after the activation of NF-κB pathway with TNF or lipopolysaccharide (LPS) (Lin *et al.*, 1995). Nuclear entry of p50/p65 was inhibited due to SN50 binding to the importin complex and thereby competitively inhibiting the binding of p50 (Torgerson *et al.*, 1998).

Peptides delivered from p65 subunit of NF-κB, p65-P1 and p65-P6, have also been reported to interfere with the NF-κB pathway. Penetratin-p65-P1 and penetratin-p65-P6 inhibited cytoplasmic p65 phosphorylation and nuclear translocation but had no effect on IκB-α phosphorylation and degradation in TNF-activated-KBM-5 chronic myeloid leukaemia cells. Penetratin-p65-P1 (100 μM) suppressed TNF-α-induced NF-κB activation by 25% and the activation was totally abolished at 150 μM. Penetratin-p65-P1 also inhibited NF-κB activation induced by different activators such as LPS, interleukin-1 (IL-1) and others (Takada *et al.*, 2004). Here, penetratin-p65-P1 also suppressed NF-κB-dependent reporter gene expression induced by TNF-α.

NEMO Binding Domain peptide (NBD) is a short peptide derived from the NBD region of IKKβ corresponding to amino acids 735-745 that disrupts NEMO-association with IKKs *in vitro* and blocks TNF-induced NF-κB activation *in vivo* when successfully delivered into cells. The underlined sequence in IKKβ (F<u>TALDWSWLQTE</u>EEEHSCLEQAS) is the (NBD). CPPs have been used to deliver the NBD peptide *in vitro* and *in vivo*. NBD peptide (TALD<u>WS</u>W<u>L</u>QTE) fused with penetratin blocked the TNF-α-induced NF-κB activation in HeLa cells at 100 and 200μM. The inhibitory effect of the NBD

peptide was abolished in a mutant peptide where the two tryptophan residues (underlined) were replaced with alanine residues (TALD<u>A</u>S<u>A</u>LQTE) (May *et al*., 2000).

Tat has also been used to deliver NBD peptide into human polymorphonuclear neutrophils (PMNs). Tat-NBD, at 50 and 100μM, showed a high capability to block LPS induced NF-κB activation thus accelerating apoptosis. This was not observed with the W-A mutant peptide (Choi *et al*., 2003).

PTD-5-NBD (RRQRRTSKLMKRGG<u>TALDWSWLQTE</u>) was investigated for *in situ* delivery to mouse pancreatic islets where improved islet function was observed and IL-1β induced cell death was prevented. As a result, islet viability was improved after isolation (Rehman *et al*., 2003). A cationic CPP consisting of eight lysines was also able to transduce NBD peptide into cells and tissues (Davé *et al*., 2007). In a NF-κB reporter system, the peptide termed 8K-NBD inhibited TNF-induced NF-κB activation in a dose dependent manner. Moreover, it also inhibited the nuclear translocation of NF-κB. More examples for CPP mediated-NBD delivery will be discussed in section 3.1.

It should be noted and emphasised here that for all studies using CPPs to deliver peptides targeting NF-κB, relatively high concentrations (> 50 μM) were needed to reach the desired effects. This is much higher than that shown to allow CPPs to enter cells and in many cases, this concentration leads to direct translocation across the plasma membrane rather than having to depend on an endocytic mechanism (Duchardt *et al*., 2007, Fretz *et al*., 2007, Watkins *et al*., 2009a).

1.8 Epidermal growth factor receptor (EGFR), cancer and CPPs

1.8.1 Introduction to EGFR

The EGFR family (also known as type I receptor tyrosine kinases or ErbB tyrosine kinase receptors) is composed of four homologous receptors: the epidermal growth factor receptor (ErbB1/ EGFR/ HER1), ErbB2 (HER2/neu), ErbB3 (HER3), and ErbB4 (HER4). Each receptor is composed of an extracellular ligand-binding domain, a transmembrane lipophilic region and (bar ErbB3) a cytoplasmic protein tyrosine kinase domain (Olayioye *et al*., 2000, Mendelsohn and Baselga, 2000, Riese and Stern, 1998). A group of growth factor ligands such as epidermal growth factor (EGF), transforming growth factor alpha (TGF-α) and others, bind the extracellular domain of the EGF receptor, leading to receptor activation with the exception of HER2 which has no known ligands (Olayioye *et al*., 2000, Nicholson *et al*., 2001). The receptor becomes activated by dimerization of two similar receptors; homodimerization, or two different members of the same receptor family; heterodimerization (Lemmon and Schlessinger, 1994). Dimerization activates the intrinsic kinase activity of the receptors and tyrosine transautophosphorylation occurs. This leads to the downstream phosphorylation of several intracellular substrates involved in the regulation of several signalling cascades (Mendelsohn and Baselga, 2000). ErbB receptors are more highly expressed in different tissues of epithelial, mesenchymal and neuronal origin and are involved in cellular development, proliferation and differentiation. Deregulated expression of ErbB receptors accompanies numerous types of human cancer (Olayioye *et al*., 2000).

The overexpression of EGFR can convert a normal cell into a malignant one through sustained signals for cell proliferation, angiogenesis, anti-apoptosis and metastasis. The extracellular ligand binding domain and the intracellular tyrosine kinase have been shown important for EGFR activation. EGFR homo- or hetero-dimerization is initiated by the binding of one of the EGF-related growth factors (ligands) to the extracellular binding domain. Subsequently, autophosphorylation by its kinase domain as well as phosphorylation of other cytoplasmic substrates occurs, signalling different cascades of cellular responses including proliferation and anti-apoptosis (Sebastian *et al.*, 2006). Two major approved potential strategies targeting EGFR family include monoclonal antibodies directed towards the extracellular domain of HER2 such as Trastuzumab (Herceptin) and small molecule tyrosine kinase inhibitors such as gefitinib and erlotinib (Hynes and MacDonald, 2009).

CPPs have been used to deliver therapeutic cargos targeting EGFR for anticancer purposes. A Tat-based Y211 cell penetrating PCNA peptide (Y211F;YGRKKRRQRRRGTFALRFLNFFTK) was able to block Y211 phosphorylation and inhibit the growth of triple-negative and EGFR tyrosine kinase inhibitor-resistant breast cancer cells (Yu *et al.*, 2013). Tyrosine 211 phosphorylation of proliferation cell nuclear antigen (PCNA) coincides with pronounced cancer cell proliferation and correlates with poor survival of breast cancer patients. RF6 which represents an active motif of the cell penetrating PCNA peptide, as a Tat conjugate (YGRKKRRQRRRGRFLNFF), and its D-isomer were also toxic in two breast cancer cell lines. The three peptides were also active *in vivo* where they caused a significant reduction in tumour

volume in a murine model. In another study, a Tat-derived peptide (P3; YGRKKRRQR) was conjugated to an ErbB2-extracellular domain binding peptide (AHNP) to specifically target ErbB2-overexpressing breast cancer cells. P3-AHNP delivered signal transducers and activators of transcription-STAT3BP, a peptide known to inhibit STAT3 signalling that contributes to tumour progression, into ErbB2-overexpressing breast cancer cells and inhibit tumour growth *in vitro* and *in vivo* (Tan *et al*., 2006).

1.8.2 EJP-18: A sequence from Juxtamembrane domain with cell penetrating properties

The role of the transmembrane region of EGFR (corresponding to amino acids 622-644) was initially thought to be a passive anchor of the receptor to the membrane. However, it has been found that this region is important in receptor association and that EGF-induced dimerization is significantly more efficient (at least 10,000 fold higher) for a fragment of EGFR that contains both the extracellular and transmembrane domains than it is for a fragment that lacks the transmembrane domain (Tanner and Kyte, 1999, Bennasroune *et al*., 2004). This was also supported by the work of Bennasroune *et al.* who constructed expression vectors encoding short fusion peptides encompassing transmembrane domains of EGFR, ErbB2 and insulin receptors. In their study, the membrane expression of the fusion peptides in human cell lines overexpressing EGFR or ErbB2 specifically inhibited the autophosphorylation and subsequent signalling of their respective receptor. The juxtamembrane (JM) region of EGFR (corresponding to amino acids 645-689) harbours a tripartite NLS (**RRR**HIV**RKR**TL**RR,** amino acids 645-657); an NLS

containing three clusters (bold) of basic amino acids. A study by Hsu and Hung revealed that the tripartite NLS in the EGFR juxtamembrane region is capable of mediating nuclear localization of EGFR as well as cytoplasmic proteins such as pyruvate kinase tagged with a green fluorescent protein (GFP) (Hsu and Hung, 2007).

From all of the above, an interesting sequence from the JM domain region was investigated in the lab for possible therapeutic and delivery purposes. The 18 amino acid sequence was given the name EJP-18 (LFMRRRHIVRKRTLRRLL) and corresponds to EGFR amino acids 642-659. This peptide, and derivatives of, were studied in detail in this thesis, focusing on their interaction with cells and capacity to deliver associated cargo (Chapters 4-6).

1.8.3   Bioportides

To exert a biological action, CPPs are conjugated either covalently or non-covalently with bioactive cargos including peptides, proteins, and nucleotides. However, the term bioportide has been introduced to describe peptides that in their own right are able to enter cells and mediate a biological response. This is significantly different from the normal strategy of attaching a CPP to a peptide cargo to enhance delivery (Howl and Jones, 2008). In 2005, Hallbrink *et al*., proposed a quantitative structure activity relationship (QSAR) to predict polycationic CPP motifs from the primary sequences of proteins (Hällbrink *et al*., 2005). The QSAR prediction algorithm was subsequently employed to predict CPPs and also bioportides within the human cytochrome *c* protein. Two

bioportides; Cyt $c^{77\text{-}101}$ (*H*-GTKMIFVGIKKKEERADLIAYLKKA-NH$_2$) and Cyt $c^{86\text{-}101}$ (*H*-KKKEERADLIAYLKKA-NH$_2$) were shown to enter cells and induce apoptosis through DNA fragmentation (Howl and Jones, 2008). Camptide and nosangiotide are two bioportides derived respectively from the human type 1 calcitonin receptor (hCTR-1) and the calmodulin binding domain of endothelial nitric oxide synthase (eNOS). Camptide was able to modulate hepatitis C infectivity in hepatoma cells and insulin secretion from isolated rat pancreatic islets. Nosangiotide was found to be a potent anti-angiogenic agent (Howl *et al*., 2012). Bioportides clearly are interesting alternatives to conventional CPP-peptide chimeras and are discussed later in chapters 4 and 7 in conjunction with studies involving EJP-18.

1.9   Hypothesis underlying this thesis

Understanding the mechanism by which CPPs associate with cells and enter cells is fundamental to their transition from the *in vitro* to the *in vivo* setting. New CPP sequences need to be investigated as alternatives to identified variants that to date have not fulfilled their promise.

The hypothesis for this study is:

Identifying new peptide sequences with cell penetrating properties or modifying existing CPP sequences can be used to more effectively deliver therapeutic entities or act as bioactive components or bioportides.

1.10 Aim of thesis

The overall aim of this thesis is to expand our knowledge on CPPs and their cargo delivery capacity as well as identifying new sequences with cell penetrating capacities. This will be achieved through the following:

- Characterisation of the capacity of penetratin to deliver a therapeutic peptide targeting NF-κB signalling pathway. This will include developing *in vitro* protocols for analysing NK-κB activation and inhibition.

- Characterising new peptide sequences derived from the JM domain of EGFR for cell penetrating capacity and assessing their toxicity in a panel of cancer cell lines.

- Assessing the effectiveness of these EGFR derived sequences as delivery vectors for small molecular weight cargo, proteins and nucleotides.

1.11 References

AL SORAJ, M., HE, L., PEYNSHAERT, K., COUSAERT, J., VERCAUTEREN, D., BRAECKMANS, K., DE SMEDT, S. C. & JONES, A. T. 2012. siRNA and pharmacological inhibition of endocytic pathways to characterize the differential role of macropinocytosis and the actin cytoskeleton on cellular uptake of dextran and cationic cell penetrating peptides octaarginine (R8) and HIV-Tat. *J Control Release,* 161**,** 132-141.

AL-DOSARI, M. S. & GAO, X. 2009. Nonviral gene delivery: principle, limitations, and recent progress. *The AAPS journal,* 11**,** 671-681.

ARNT, C. R., CHIOREAN, M. V., HELDEBRANT, M. P., GORES, G. J. & KAUFMANN, S. H. 2002. Synthetic Smac/DIABLO peptides enhance the effects of chemotherapeutic agents by binding XIAP and cIAP1 in situ. *Journal of Biological Chemistry,* 277**,** 44236-44243.

BAGULEY, B. C. 2010. Multidrug resistance in cancer. *In:* ZHOU, J. (ed.) *Multi-drug resistance in cancer.* Springer, 596, 1-14.

BALTIMORE, D. 2011. NF-[kappa] B is 25. *Nature immunology,* 12**,** 683-685.

BALUK, P., HASHIZUME, H. & MCDONALD, D. M. 2005. Cellular abnormalities of blood vessels as targets in cancer. *Current Opinion in Genetics & Development,* 15**,** 102-111.

BECHARA, C. & SAGAN, S. 2013. Cell-penetrating peptides: 20years later, where do we stand? *FEBS letters,* 587**,** 1693-1702.

BELTING, M. 2003. Heparan sulfate proteoglycan as a plasma membrane carrier. *Trends Biochem Sci,* 28**,** 145-151.

BENNASROUNE, A., FICKOVA, M., GARDIN, A., DIRRIG-GROSCH, S., AUNIS, D., CRÉMEL, G. & HUBERT, P. 2004. Transmembrane peptides as inhibitors of ErbB receptor signaling. *Molecular biology of the cell,* 15**,** 3464-3474.

BERTRAM, J. S. 2000. The molecular biology of cancer. *Molecular aspects of medicine,* 21**,** 167-223.

BHARTI, A. C. & AGGARWAL, B. B. 2002. Nuclear factor-kappa B and cancer: its role in prevention and therapy. *Biochem Pharmacol,* 64**,** 883-888.

BHINDI, R., FAHMY, R. G., LOWE, H. C., CHESTERMAN, C. N., DASS, C. R., CAIRNS, M. J., SARAVOLAC, E. G., SUN, L.-Q. & KHACHIGIAN, L. M. 2007. Brothers in arms: DNA enzymes, short interfering RNA, and the emerging wave of small-molecule nucleic acid-based gene-silencing strategies. *The American journal of pathology,* 171**,** 1079-1088.

BINDER, H. & LINDBLOM, G. 2003. Charge-dependent translocation of the Trojan peptide penetratin across lipid membranes. *Biophysical journal,* 85**,** 982-995.

BOLHASSANI, A. 2011. Potential efficacy of cell-penetrating peptides for nucleic acid and drug delivery in cancer. *Biochim Biophys Acta,* 1816**,** 232-246.

BÁNÓCZI, Z., GORKA-KERESKÉNYI, A. L., REMÉNYI, J., ORBÁN, E., HAZAI, L., TŐKÉSI, N. L., OLÁH, J., OVÁDI, J., BÉNI, Z. & HÁDA, V. 2010. Synthesis and in vitro antitumor effect of vinblastine derivative− oligoarginine conjugates. *Bioconjugate chemistry,* 21**,** 1948-1955.

CAI, S. R., XU, G., BECKER-HAPAK, M., MA, M., DOWDY, S. F. & MCLEOD, H. L. 2006. The kinetics and tissue distribution of protein transduction in mice. *Eur J Pharm Sci,* 27**,** 311-319.

CHATURVEDI, M., SUNG, B., YADAV, V., KANNAPPAN, R. & AGGARWAL, B. 2011. NF-κB addiction and its role in cancer:'one size does not fit all'. *Oncogene,* 30**,** 1615-1630.

CHOI, M., ROLLE, S., WELLNER, M., CARDOSO, M. C., SCHEIDEREIT, C., LUFT, F. C. & KETTRITZ, R. 2003. Inhibition of NF-kappaB by a TAT-NEMO-binding domain peptide accelerates constitutive apoptosis and abrogates LPS-delayed neutrophil apoptosis. *Blood,* 102**,** 2259-2267.

CHUGH, A., EUDES, F. & SHIM, Y. S. 2010. Cell-penetrating peptides: Nanocarrier for macromolecule delivery in living cells. *IUBMB Life,* 62**,** 183-193.

CLAUDIO, E., BROWN, K., PARK, S., WANG, H. & SIEBENLIST, U. 2002. BAFF-induced NEMO-independent processing of NF-kappa B2 in maturing B cells. *Nat Immunol,* 3**,** 958-965.

CLEAL, K., HE, L., D WATSON, P. & T JONES, A. 2013. Endocytosis, intracellular traffic and fate of cell penetrating peptide based conjugates and nanoparticles. *Current pharmaceutical design,* 19**,** 2878-2894.

CONNER, S. D. & SCHMID, S. L. 2003. Regulated portals of entry into the cell. *Nature,* 422**,** 37-44.

COOPE, H. J., ATKINSON, P. G., HUHSE, B., BELICH, M., JANZEN, J., HOLMAN, M. J., KLAUS, G. G., JOHNSTON, L. H. & LEY, S. C. 2002. CD40 regulates the processing of NF-kappaB2 p100 to p52. *EMBO J,* 21**,** 5375-5385.

COPOLOVICI, D. M., LANGEL, K., ERISTE, E. & LANGEL, U. 2014. Cell-penetrating peptides: design, synthesis, and applications. ACS nano, 8, 1972-1994.

CROMBEZ, L., ALDRIAN-HERRADA, G., KONATE, K., NGUYEN, Q. N., MCMASTER, G. K., BRASSEUR, R., HEITZ, F. & DIVITA, G. 2009. A new potent secondary amphipathic cell–penetrating peptide for siRNA delivery into mammalian cells. Molecular therapy, 17, 95-103.

CROOKE, S. T. 1999. Molecular mechanisms of action of antisense drugs. *Biochimica et Biophysica Acta (BBA)-Gene Structure and Expression,* 1489**,** 31-43.

CRYSTAL, R. G. 1995. Transfer of genes to humans: early lessons and obstacles to success. *Science,* 270**,** 404-410.

DAVIS, M. E. 2002. Non-viral gene delivery systems. *Current opinion in biotechnology,* 13**,** 128-131.

DAVÉ, S. H., TILSTRA, J. S., MATSUOKA, K., LI, F., KARRASCH, T., UNO, J. K., SEPULVEDA, A. R., JOBIN, C., BALDWIN, A. S. & ROBBINS, P. D. 2007. Amelioration of chronic murine colitis by peptide-mediated transduction of the IκB kinase inhibitor NEMO binding domain peptide. *The Journal of Immunology,* 179**,** 7852-7859.

DE LA FUENTE, J. M. & BERRY, C. C. 2005. Tat peptide as an efficient molecule to translocate gold nanoparticles into the cell nucleus. *Bioconjugate chemistry,* 16**,** 1176-1180.

DEJARDIN, E., DROIN, N. M., DELHASE, M., HAAS, E., CAO, Y., MAKRIS, C., LI, Z. W., KARIN, M., WARE, C. F. & GREEN, D. R. 2002. The lymphotoxin-beta receptor induces different patterns of gene expression via two NF-kappaB pathways. *Immunity,* 17**,** 525-535.

DEMPSEY, C. E. 1990. The actions of melittin on membranes. *Biochimica et Biophysica Acta (BBA)-Reviews on Biomembranes,* 1031**,** 143-161.

DEROSSI, D., CALVET, S., TREMBLEAU, A., BRUNISSEN, A., CHASSAING, G. & PROCHIANTZ, A. 1996. Cell internalization of the third helix of the Antennapedia homeodomain is receptor-independent. *Journal of Biological Chemistry,* 271**,** 18188-18193.

DEROSSI, D., JOLIOT, A. H., CHASSAING, G. & PROCHIANTZ, A. 1994. The third helix of the Antennapedia homeodomain translocates through biological membranes. *Journal of Biological Chemistry,* 269**,** 10444-10450.

DESHAYES, S., HEITZ, A., MORRIS, M. C., CHARNET, P., DIVITA, G. & HEITZ, F. 2004. Insight into the mechanism of internalization of the cell-penetrating carrier peptide Pep-1 through conformational analysis. *Biochemistry,* 43**,** 1449-1457.

DOHERTY, G. J. & MCMAHON, H. T. 2009. Mechanisms of endocytosis. *Annual review of biochemistry,* 78**,** 857-902.

DUBIKOVSKAYA, E. A., THORNE, S. H., PILLOW, T. H., CONTAG, C. H. & WENDER, P. A. 2008. Overcoming multidrug resistance of small-molecule therapeutics through conjugation with releasable octaarginine transporters. *Proceedings of the National Academy of Sciences,* 105**,** 12128-12133.

DUCHARDT, F., FOTIN-MLECZEK, M., SCHWARZ, H., FISCHER, R. & BROCK, R. 2007. A comprehensive model for the cellular uptake of cationic cell-penetrating peptides. *Traffic,* 8**,** 848-866.

48

EGUCHI, A. & DOWDY, S. F. 2009. siRNA delivery using peptide transduction domains. *Trends in Pharmacological Sciences,* 30**,** 341-345.

EL-ANEED, A. 2004. An overview of current delivery systems in cancer gene therapy. *Journal of Controlled Release,* 94**,** 1-14.

EL-SAYED, A., FUTAKI, S. & HARASHIMA, H. 2009. Delivery of macromolecules using arginine-rich cell-penetrating peptides: ways to overcome endosomal entrapment. *AAPS J,* 11**,** 13-22.

ELIOPOULOS, A. G., CAAMANO, J. H., FLAVELL, J., REYNOLDS, G. M., MURRAY, P. G., POYET, J.-L. & YOUNG, L. S. 2003. Epstein–Barr virus-encoded latent infection membrane protein 1 regulates the processing of p100 NF-κB2 to p52 via an IKKγ/NEMO-independent signalling pathway. *Oncogene,* 22**,** 7557-7569.

ELMQUIST, A., LINDGREN, M., BARTFAI, T. & LANGEL, Ü. 2001. VE-cadherin-derived cell-penetrating peptide, pVEC, with carrier functions. *Experimental cell research,* 269**,** 237-244.

ESTÈVE, E., MABROUK, K., DUPUIS, A., SMIDA-REZGUI, S., ALTAFAJ, X., GRUNWALD, D., PLATEL, J.-C., ANDREOTTI, N., MARTY, I. & SABATIER, J.-M. 2005. Transduction of the Scorpion Toxin Maurocalcine into Cells EVIDENCE THAT THE TOXIN CROSSES THE PLASMA MEMBRANE. *Journal of Biological Chemistry,* 280**,** 12833-12839.

EZZAT, K., ANDALOUSSI, S. E., ZAGHLOUL, E. M., LEHTO, T., LINDBERG, S., MORENO, P. M., VIOLA, J. R., MAGDY, T., ABDO, R. & GUTERSTAM, P. 2011. PepFect 14, a novel cell-penetrating peptide for oligonucleotide delivery in solution and as solid formulation. *Nucleic acids research,* 39**,** 5284-5298.

FERNÁNDEZ-CARNEADO, J., KOGAN, M. J., PUJALS, S. & GIRALT, E. 2004. Amphipathic peptides and drug delivery. *Biopolymers,* 76**,** 196-203.

FITTIPALDI, A., FERRARI, A., ZOPPÉ, M., ARCANGELI, C., PELLEGRINI, V., BELTRAM, F. & GIACCA, M. 2003. Cell membrane lipid rafts mediate caveolar endocytosis of HIV-1 Tat fusion proteins. *J Biol Chem,* 278**,** 34141-34149.

FITZSIMONS, H. L., BLAND, R. J. & DURING, M. J. 2002. Promoters and regulatory elements that improve adeno-associated virus transgene expression in the brain. *Methods,* 28**,** 227-236.

FRANKEL, A. D. & PABO, C. O. 1988. Cellular uptake of the tat protein from human immunodeficiency virus. *Cell,* 55**,** 1189-1193.

FRETZ, M. M., PENNING, N. A., AL-TAEI, S., FUTAKI, S., TAKEUCHI, T., NAKASE, I., STORM, G. & JONES, A. T. 2007. Temperature-, concentration- and cholesterol-dependent translocation of L- and D-octa-arginine across the plasma and nuclear membrane of CD34+ leukaemia cells. *Biochem J,* 403**,** 335-342.

FULDA, S., WICK, W., WELLER, M. & DEBATIN, K.-M. 2002. Smac agonists sensitize for Apo2L/TRAIL-or anticancer drug-induced apoptosis and induce regression of malignant glioma in vivo. *Nature medicine,* 8**,** 808-815.

FUTAKI, S., SUZUKI, T., OHASHI, W., YAGAMI, T., TANAKA, S., UEDA, K. & SUGIURA, Y. 2001. Arginine-rich peptides. An abundant source of membrane-permeable peptides having potential as carriers for intracellular protein delivery. *J Biol Chem,* 276**,** 5836-5840.

GAO, X., CUI, Y., LEVENSON, R. M., CHUNG, L. W. & NIE, S. 2004. In vivo cancer targeting and imaging with semiconductor quantum dots. *Nature biotechnology,* 22**,** 969-976.

GARDLÍK, R., PÁLFFY, R., HODOSY, J., LUKÁCS, J., TURNA, J. & CELEC, P. 2005. Vectors and delivery systems in gene therapy. *Medical Science Monitor Basic Research,* 11**,** RA110-RA121.

GHOSH, G., VAN DUYNE, G., GHOSH, S. & SIGLER, P. B. 1995. Structure of NF-kappa B p50 homodimer bound to a kappa B site. *Nature,* 373**,** 303-310.

GHOSH, S. & KARIN, M. 2002. Missing pieces in the NF-kappaB puzzle. *Cell,* 109 Suppl**,** S81-96.

GILMORE, T. D. 2006. Introduction to NF-κB: players, pathways, perspectives. *Oncogene,* 25**,** 6680-6684.

GLOVER, D. J., LIPPS, H. J. & JANS, D. A. 2005. Towards safe, non-viral therapeutic gene expression in humans. *Nature Reviews Genetics,* 6**,** 299-310.

GOTTESMAN, M. M., FOJO, T. & BATES, S. E. 2002. Multidrug resistance in cancer: role of ATP-dependent transporters. *Nat Rev Cancer,* 2**,** 48-58.

GUO, X. & HUANG, L. 2011. Recent advances in nonviral vectors for gene delivery. *Accounts of chemical research,* 45**,** 971-979.

HEITZ, F., MORRIS, M. C. & DIVITA, G. 2009. Twenty years of cell-penetrating peptides: from molecular mechanisms to therapeutics. *Br J Pharmacol,* 157**,** 195-206.

HENDRIE, P. C. & RUSSELL, D. W. 2005. Gene targeting with viral vectors. *Molecular Therapy,* 12**,** 9-17.

HOLM, T., NETZEREAB, S., HANSEN, M., LANGEL, U. & HALLBRINK, M. 2005. Uptake of cell-penetrating peptides in yeasts. *FEBS Lett,* 579**,** 5217-5222.

HOSOTANI, R., MIYAMOTO, Y., FUJIMOTO, K., DOI, R., OTAKA, A., FUJII, N. & IMAMURA, M. 2002. Trojan p16 peptide suppresses pancreatic cancer growth and prolongs survival in mice. *Clinical cancer research,* 8**,** 1271-1276.

HOWL, J. & JONES, S. 2008. Proteomimetic cell penetrating peptides. *International Journal of Peptide Research and Therapeutics,* 14**,** 359-366.

HOWL, J., MATOU-NASRI, S., WEST, D. C., FARQUHAR, M., SLANINOVA, J., OSTENSON, C. G., ZORKO, M., OSTLUND, P., KUMAR, S., LANGEL, U., MCKEATING, J. & JONES, S. 2012. Bioportide: an emergent concept of bioactive cell-penetrating peptides. *Cell Mol Life Sci,* 69**,** 2951-2966.

HSU, S.-C. & HUNG, M.-C. 2007. Characterization of a novel tripartite nuclear localization sequence in the EGFR family. *Journal of Biological Chemistry,* 282**,** 10432-10440.

HU, M., WANG, J., CHEN, P. & REILLY, R. M. 2006. HIV-1 Tat peptide immunoconjugates differentially sensitize breast cancer cells to selected antiproliferative agents that induce the cyclin-dependent kinase inhibitor p21WAF-1/CIP-1. *Bioconjugate chemistry,* 17**,** 1280-1287.

HYNES, N. E. & MACDONALD, G. 2009. ErbB receptors and signaling pathways in cancer. *Current opinion in cell biology,* 21**,** 177-184.

HÄLLBRINK, M., KILK, K., ELMQUIST, A., LUNDBERG, P., LINDGREN, M., JIANG, Y., POOGA, M., SOOMETS, U. & LANGEL, Ü. 2005. Prediction of cell-penetrating peptides. *International Journal of Peptide Research and Therapeutics,* 11**,** 249-259.

IVANOV, A. I. 2008. Pharmacological inhibition of endocytic pathways: is it specific enough to be useful? *Exocytosis and Endocytosis.* Springer, 440, 15-33

IYER, A. K., KHALED, G., FANG, J. & MAEDA, H. 2006. Exploiting the enhanced permeability and retention effect for tumor targeting. *Drug Discov Today,* 11**,** 812-818.

J BOOHAKER, R., W LEE, M., VISHNUBHOTLA, P., LM PEREZ, J. & R KHALED, A. 2012. The use of therapeutic peptides to target and to kill cancer cells. *Current medicinal chemistry,* 19**,** 3794-3804.

JARVER, P. & LANGEL, U. 2004. The use of cell-penetrating peptides as a tool for gene regulation. *Drug Discov Today,* 9**,** 395-402.

JIN, R., LIN, B., LI, D. & AI, H. 2014. Superparamagnetic iron oxide nanoparticles for MR imaging and therapy: design considerations and clinical applications. *Current opinion in pharmacology,* 18**,** 18-27.

JOLIOT, A., PERNELLE, C., DEAGOSTINI-BAZIN, H. & PROCHIANTZ, A. 1991. Antennapedia homeobox peptide regulates neural morphogenesis. *Proc Natl Acad Sci U S A,* 88**,** 1864-1868.

JONES, A. T. 2007. Macropinocytosis: searching for an endocytic identity and role in the uptake of cell penetrating peptides. *J Cell Mol Med,* 11**,** 670-684.

JONES, A. T. 2008. Gateways and tools for drug delivery: endocytic pathways and the cellular dynamics of cell penetrating peptides. *Int J Pharm,* 354**,** 34-38.

JONES, A. T. & SAYERS, E. J. 2012. Cell entry of cell penetrating peptides: tales of tails wagging dogs. *Journal of Controlled Release,* 161**,** 582-591.

KAPLAN, I. M., WADIA, J. S. & DOWDY, S. F. 2005. Cationic TAT peptide transduction domain enters cells by macropinocytosis. *J Control Release,* 102**,** 247-253.

KARIN, M. 2006. Nuclear factor-kappaB in cancer development and progression. *Nature,* 441**,** 431-436.

KERR, M. C. & TEASDALE, R. D. 2009. Defining macropinocytosis. *Traffic,* 10**,** 364-371.

KIANG, T., WEN, J., LIM, H. W. & LEONG, K. W. 2004. The effect of the degree of chitosan deacetylation on the efficiency of gene transfection. *Biomaterials,* 25**,** 5293-5301.

KONNO, K., HISADA, M., NAOKI, H., ITAGAKI, Y., KAWAI, N., MIWA, A., YASUHARA, T., MORIMOTO, Y. & NAKATA, Y. 2000. Structure and biological activities of eumenine mastoparan-AF (EMP-AF), a new mast cell degranulating peptide in the venom of the solitary wasp (Anterhynchium flavomarginatum micado). *Toxicon,* 38**,** 1505-1515.

KOREN, E. & TORCHILIN, V. P. 2012. Cell-penetrating peptides: breaking through to the other side. *Trends in molecular medicine,* 18**,** 385-393.

KOSUGE, M., TAKEUCHI, T., NAKASE, I., JONES, A. T. & FUTAKI, S. 2008. Cellular internalization and distribution of arginine-rich peptides as a function of extracellular peptide concentration, serum, and plasma membrane associated proteoglycans. *Bioconjugate chemistry,* 19**,** 656-664.

LEMMON, M. A. & SCHLESSINGER, J. 1994. Regulation of signal transduction and signal diversity by receptor oligomerization. *Trends Biochem Sci,* 19**,** 459-463.

LEWIN, M., CARLESSO, N., TUNG, C.-H., TANG, X.-W., CORY, D., SCADDEN, D. T. & WEISSLEDER, R. 2000. Tat peptide-derivatized magnetic nanoparticles allow in vivo tracking and recovery of progenitor cells. *Nature biotechnology,* 18**,** 410-414.

LI, Q. & VERMA, I. M. 2002. NF-kappaB regulation in the immune system. *Nat Rev Immunol,* 2**,** 725-734.

LIN, Y., BAI, L., CHEN, W. & XU, S. 2010. The NF-κB activation pathways, emerging molecular targets for cancer prevention and therapy. *Expert opinion on therapeutic targets,* 14**,** 45-55.

LIN, Y. Z., YAO, S. Y., VEACH, R. A., TORGERSON, T. R. & HAWIGER, J. 1995. Inhibition of nuclear translocation of transcription factor NF-kappa B by a synthetic peptide containing a cell membrane-permeable motif and nuclear localization sequence. *J Biol Chem,* 270**,** 14255-14258.

LINDGREN, M., HALLBRINK, M., PROCHIANTZ, A. & LANGEL, U. 2000. Cell-penetrating peptides. *Trends Pharmacol Sci,* 21**,** 99-103.

LINDGREN, M., ROSENTHAL-AIZMAN, K., SAAR, K., EIRÍKSDÓTTIR, E., JIANG, Y., SASSIAN, M., ÖSTLUND, P., HÄLLBRINK, M. & LANGEL, Ü. 2006. Overcoming methotrexate resistance in breast cancer tumour cells by the use of a new cell-penetrating peptide. *Biochemical pharmacology,* 71**,** 416-425.

LIU, X., ROCCHI, P. & PENG, L. 2012. Dendrimers as non-viral vectors for siRNA delivery. *New Journal of Chemistry,* 36**,** 256-263.

LUNDBERG, M. & JOHANSSON, M. 2002. Positively charged DNA-binding proteins cause apparent cell membrane translocation. *Biochemical and biophysical research communications,* 291**,** 367-371.

LUNDBERG, P., EL-ANDALOUSSI, S., SUTLU, T., JOHANSSON, H. & LANGEL, U. 2007. Delivery of short interfering RNA using endosomolytic cell-penetrating peptides. *FASEB J,* 21**,** 2664-71.

LUNDBERG, P. & LANGEL, U. 2003. A brief introduction to cell-penetrating peptides. *J Mol Recognit,* 16**,** 227-233.

LUO, D. & SALTZMAN, W. M. 2000. Synthetic DNA delivery systems. *Nat Biotechnol,* 18**,** 33-37.

LUO, J., LUO, Y., SUN, J., ZHOU, Y., ZHANG, Y. & YANG, X. 2015. Adeno-associated virus-mediated cancer gene therapy: Current status. *Cancer letters,* 356**,** 347-356.

LV, H., ZHANG, S., WANG, B., CUI, S. & YAN, J. 2006. Toxicity of cationic lipids and cationic polymers in gene delivery. *Journal of Controlled Release,* 114**,** 100-109.

MADANI, F., LINDBERG, S., LANGEL, U., FUTAKI, S. & GRASLUND, A. 2011. Mechanisms of cellular uptake of cell-penetrating peptides. *J Biophys,* 2011**,** 414729.

MAE, M., MYRBERG, H., JIANG, Y., PAVES, H., VALKNA, A. & LANGEL, U. 2005. Internalisation of cell-penetrating peptides into tobacco protoplasts. *Biochim Biophys Acta,* 1669**,** 101-107.

MAGZOUB, M., ERIKSSON, L. G. & GRÄSLUND, A. 2002. Conformational states of the cell-penetrating peptide penetratin when interacting with phospholipid vesicles: effects of surface charge and peptide concentration. *Biochimica Et Biophysica Acta (BBA)-Biomembranes,* 1563**,** 53-63.

MAIOLO, J. R., FERRER, M. & OTTINGER, E. A. 2005. Effects of cargo molecules on the cellular uptake of arginine-rich cell-penetrating peptides. *Biochimica et Biophysica Acta (BBA)-Biomembranes,* 1712**,** 161-172.

MALI, S. 2013. Delivery systems for gene therapy. *Indian journal of human genetics,* 19**,** 3-8.

MANSOURI, S., LAVIGNE, P., CORSI, K., BENDERDOUR, M., BEAUMONT, E. & FERNANDES, J. C. 2004. Chitosan-DNA nanoparticles as non-viral vectors in gene therapy: strategies to improve transfection efficacy. *European Journal of Pharmaceutics and Biopharmaceutics,* 57**,** 1-8.

MAO, S., SUN, W. & KISSEL, T. 2010. Chitosan-based formulations for delivery of DNA and siRNA. *Advanced drug delivery reviews,* 62**,** 12-27.

MARTÍN, I., TEIXIDÓ, M. & GIRALT, E. 2011. Design, Synthesis and Characterization of a New Anionic Cell-Penetrating Peptide: SAP (E). *ChemBioChem,* 12**,** 896-903.

MASON, J. M. 2010. Design and development of peptides and peptide mimetics as antagonists for therapeutic intervention. *Future Med Chem,* 2**,** 1813-1822.

MAY, M. J., D'ACQUISTO, F., MADGE, L. A., GLÖCKNER, J., POBER, J. S. & GHOSH, S. 2000. Selective inhibition of NF-kappaB activation by a peptide that blocks the interaction of NEMO with the IkappaB kinase complex. *Science,* 289**,** 1550-1554.

MAZEL, M., CLAIR, P., ROUSSELLE, C., VIDAL, P., SCHERRMANN, J.-M., MATHIEU, D. & TEMSAMANI, J. 2001. Doxorubicin-peptide conjugates overcome multidrug resistance. *Anti-cancer drugs,* 12**,** 107-116.

MCMAHON, H. T. & BOUCROT, E. 2011. Molecular mechanism and physiological functions of clathrin-mediated endocytosis. *Nature reviews Molecular cell biology,* 12**,** 517-533.

MEHIER-HUMBERT, S. & GUY, R. H. 2005. Physical methods for gene transfer: improving the kinetics of gene delivery into cells. *Advanced drug delivery reviews,* 57**,** 733-753.

MELLOTT, A. J., FORREST, M. L. & DETAMORE, M. S. 2013. Physical non-viral gene delivery methods for tissue engineering. *Annals of biomedical engineering,* 41**,** 446-468.

MENDELSOHN, J. & BASELGA, J. 2000. The EGF receptor family as targets for cancer therapy. *Oncogene,* 19**,** 6550-6565.

MIDOUX, P. & MONSIGNY, M. 1999. Efficient gene transfer by histidylated polylysine/pDNA complexes. *Bioconjugate chemistry,* 10**,** 406-411.

MILLETTI, F. 2012. Cell-penetrating peptides: classes, origin, and current landscape. *Drug Discov Today,* 17**,** 850-860.

MINTZER, M. A. & SIMANEK, E. E. 2008. Nonviral vectors for gene delivery. *Chemical reviews,* 109**,** 259-302.

MORILLE, M., PASSIRANI, C., VONARBOURG, A., CLAVREUL, A. & BENOIT, J.-P. 2008. Progress in developing cationic vectors for non-viral systemic gene therapy against cancer. *Biomaterials,* 29**,** 3477-3496.

MORRIS, M. C., DESHAYES, S., HEITZ, F. & DIVITA, G. 2008. Cell-penetrating peptides: from molecular mechanisms to therapeutics. *Biol Cell,* 100**,** 201-217.

MUNDY, D. I., MACHLEIDT, T., YING, Y.-S., ANDERSON, R. G. & BLOOM, G. S. 2002. Dual control of caveolar membrane traffic by microtubules and the actin cytoskeleton. *Journal of cell science,* 115**,** 4327-4339.

MURATOVSKA, A. & ECCLES, M. R. 2004. Conjugate for efficient delivery of short interfering RNA (siRNA) into mammalian cells. *FEBS letters,* 558**,** 63-68.

MÜLLER, C. W., REY, F. A., SODEOKA, M., VERDINE, G. L. & HARRISON, S. C. 1995. Structure of the NF-kappa B p50 homodimer bound to DNA. *Nature,* 373**,** 311-317.

NAKAMURA, T., YAMAZAKI, D., YAMAUCHI, J. & HARASHIMA, H. 2013. The nanoparticulation by octaarginine-modified liposome improves α-galactosylceramide-mediated antitumor therapy via systemic administration. *Journal of Controlled Release,* 171**,** 216-224.

NAKASE, I., KONISHI, Y., UEDA, M., SAJI, H. & FUTAKI, S. 2012. Accumulation of arginine-rich cell-penetrating peptides in tumors and the potential for anticancer drug delivery in vivo. *J Control Release,* 159**,** 181-188.

NAYEROSSADAT, N., MAEDEH, T. & ALI, P. A. 2012. Viral and nonviral delivery systems for gene delivery. *Advanced biomedical research,* 1-27.

NEKHOTIAEVA, N., ELMQUIST, A., RAJARAO, G. K., HALLBRINK, M., LANGEL, U. & GOOD, L. 2004. Cell entry and antimicrobial properties of eukaryotic cell-penetrating peptides. *FASEB J,* 18**,** 394-396.

NELSON, M. H., STEIN, D. A., KROEKER, A. D., HATLEVIG, S. A., IVERSEN, P. L. & MOULTON, H. M. 2005. Arginine-rich peptide conjugation to morpholino oligomers: effects on antisense activity and specificity. *Bioconjugate chemistry,* 16**,** 959-966.

NICHOLSON, R., GEE, J. & HARPER, M. 2001. EGFR and cancer prognosis. *European Journal of Cancer,* 37**,** 9-15.

NISHIDA, N., YANO, H., NISHIDA, T., KAMURA, T. & KOJIRO, M. 2006. Angiogenesis in cancer. *Vasc Health Risk Manag,* 2**,** 213-219.

O'NEILL, L. A. & KALTSCHMIDT, C. 1997. NF-kappa B: a crucial transcription factor for glial and neuronal cell function. *Trends Neurosci,* 20**,** 252-258.

OEHLKE, J., SCHELLER, A., WIESNER, B., KRAUSE, E., BEYERMANN, M., KLAUSCHENZ, E., MELZIG, M. & BIENERT, M. 1998. Cellular uptake of an α-helical amphipathic model peptide with the potential to deliver polar compounds into the cell interior non-endocytically. *Biochimica et Biophysica Acta (BBA)-Biomembranes,* 1414**,** 127-139.

OKAMURA, E., NINOMIYA, K., FUTAKI, S., NAGAI, Y., KIMURA, T., WAKAI, C., MATUBAYASI, N., SUGIURA, Y. & NAKAHARA, M. 2005. Real-time in-cell 19F NMR study on uptake of fluorescent and nonfluorescent 19F-octaarginines into human Jurkat cells. *Chemistry Letters,* 34**,** 1064-1065.

OLAYIOYE, M. A., NEVE, R. M., LANE, H. A. & HYNES, N. E. 2000. The ErbB signaling network: receptor heterodimerization in development and cancer. *EMBO J,* 19**,** 3159-3167.

ORANGE, J. S. & MAY, M. J. 2008. Cell penetrating peptide inhibitors of nuclear factor-kappa B. *Cell Mol Life Sci,* 65**,** 3564-3591.

PATEL, L. N., ZARO, J. L. & SHEN, W. C. 2007. Cell penetrating peptides: intracellular pathways and pharmaceutical perspectives. *Pharm Res,* 24**,** 1977-1992.

PATHAK, A., PATNAIK, S. & GUPTA, K. C. 2009. Recent trends in non-viral vector-mediated gene delivery. *Biotechnology journal,* 4**,** 1559-1572.

PATIL, S. D., RHODES, D. G. & BURGESS, D. J. 2005. DNA-based therapeutics and DNA delivery systems: a comprehensive review. *The AAPS journal,* 7**,** E61-E77.

POOGA, M., HÄLLBRINK, M. & ZORKO, M. 1998. Cell penetration by transportan. *The FASEB journal,* 12**,** 67-77.

POUNY, Y., RAPAPORT, D., MOR, A., NICOLAS, P. & SHAI, Y. 1992. Interaction of antimicrobial dermaseptin and its fluorescently labeled analogs with phospholipid membranes. *Biochemistry,* 31**,** 12416-12423.

PRASAD, S., RAVINDRAN, J. & AGGARWAL, B. B. 2010. NF-κB and cancer: how intimate is this relationship. *Molecular and cellular biochemistry,* 336**,** 25-37.

RATJEN, F. & DÖRING, G. 2003. Cystic fibrosis. *Lancet,* 361**,** 681-689.

RAUCHER, D., MOKTAN, S., MASSODI, I. & BIDWELL, G. L., 3RD 2009. Therapeutic peptides for cancer therapy. Part II - cell cycle inhibitory peptides and apoptosis-inducing peptides. *Expert Opin Drug Deliv,* 6**,** 1049-1064.

REEVES, V. L., THOMAS, C. M. & SMART, E. J. 2012. Lipid rafts, caveolae and GPI-linked proteins. *Caveolins and Caveolae.* Springer, 729, 3-13

REHMAN, K. K., BERTERA, S., BOTTINO, R., BALAMURUGAN, A. N., MAI, J. C., MI, Z., TRUCCO, M. & ROBBINS, P. D. 2003. Protection of islets by in situ peptide-mediated transduction of the Ikappa B kinase inhibitor Nemo-binding domain peptide. *J Biol Chem,* 278**,** 9862-9868.

RESHETNYAK, Y. K., ANDREEV, O. A., SEGALA, M., MARKIN, V. S. & ENGELMAN, D. M. 2008. Energetics of peptide (pHLIP) binding to and folding across a lipid bilayer membrane. *Proceedings of the National Academy of Sciences,* 105**,** 15340-15345.

RHEE, M. & DAVIS, P. 2006. Mechanism of uptake of C105Y, a novel cell-penetrating peptide. *Journal of Biological Chemistry,* 281**,** 1233-1240.

RICHARD, J. P., MELIKOV, K., BROOKS, H., PREVOT, P., LEBLEU, B. & CHERNOMORDIK, L. V. 2005. Cellular uptake of unconjugated TAT peptide involves clathrin-dependent endocytosis and heparan sulfate receptors. *J Biol Chem,* 280**,** 15300-15306.

RICHARD, J. P., MELIKOV, K., VIVES, E., RAMOS, C., VERBEURE, B., GAIT, M. J., CHERNOMORDIK, L. V. & LEBLEU, B. 2003. Cell-penetrating peptides. A reevaluation of the mechanism of cellular uptake. *J Biol Chem,* 278**,** 585-590.

RIESE, D. J. & STERN, D. F. 1998. Specificity within the EGF family/ErbB receptor family signaling network. *Bioessays,* 20**,** 41-48.

ROEDER, G. E., PARISH, J. L., STERN, P. L. & GASTON, K. 2004. Herpes simplex virus VP22-human papillomavirus E2 fusion proteins produced in mammalian or bacterial cells enter mammalian cells and induce apoptotic cell death. *Biotechnol Appl Biochem,* 40**,** 157-165.

ROTHBARD, J. B., JESSOP, T. C., LEWIS, R. S., MURRAY, B. A. & WENDER, P. A. 2004. Role of membrane potential and hydrogen bonding in the mechanism of translocation of guanidinium-rich peptides into cells. *Journal of the American Chemical Society,* 126**,** 9506-9507.

RUAN, G., AGRAWAL, A., MARCUS, A. I. & NIE, S. 2007. Imaging and tracking of tat peptide-conjugated quantum dots in living cells: new insights into nanoparticle uptake, intracellular transport, and vesicle

shedding. *Journal of the American Chemical Society,* 129**,** 14759-14766.

RUDOLPH, C., PLANK, C., LAUSIER, J., SCHILLINGER, U., MÜLLER, R. H. & ROSENECKER, J. 2003. Oligomers of the arginine-rich motif of the HIV-1 TAT protein are capable of transferring plasmid DNA into cells. *Journal of Biological Chemistry,* 278**,** 11411-11418.

SAWANT, R. & TORCHILIN, V. 2010. Intracellular transduction using cell-penetrating peptides. *Mol Biosyst,* 6**,** 628-640.

SCHMIDT, N., MISHRA, A., LAI, G. H. & WONG, G. C. 2010. Arginine-rich cell-penetrating peptides. *FEBS Lett,* 584**,** 1806-1813.

SCHUG, K. A. & LINDNER, W. 2005. Noncovalent binding between guanidinium and anionic groups: focus on biological- and synthetic-based arginine/guanidinium interactions with phosph[on]ate and sulf[on]ate residues. *Chem Rev,* 105**,** 67-114.

SCHWARZE, S. R., HO, A., VOCERO-AKBANI, A. & DOWDY, S. F. 1999. In vivo protein transduction: delivery of a biologically active protein into the mouse. *Science,* 285**,** 1569-1572.

SEBASTIAN, S., SETTLEMAN, J., RESHKIN, S. J., AZZARITI, A., BELLIZZI, A. & PARADISO, A. 2006. The complexity of targeting EGFR signalling in cancer: from expression to turnover. *Biochimica et Biophysica Acta (BBA)-Reviews on Cancer,* 1766**,** 120-139.

SEN, R. & BALTIMORE, D. 1986. Inducibility of κ immunoglobulin enhancer-binding protein NF-κB by a posttranslational mechanism. *Cell,* 47**,** 921-928.

SENFTLEBEN, U., CAO, Y., XIAO, G., GRETEN, F. R., KRÄHN, G., BONIZZI, G., CHEN, Y., HU, Y., FONG, A., SUN, S. C. & KARIN, M. 2001. Activation by IKKalpha of a second, evolutionary conserved, NF-kappa B signaling pathway. *Science,* 293**,** 1495-1499.

SETHI, G., SUNG, B. & AGGARWAL, B. B. 2008. Nuclear factor-κB activation: from bench to bedside. *Experimental Biology and Medicine,* 233**,** 21-31.

SEVERINO, P., SZYMANSKI, M., FAVARO, M., AZZONI, A. R., CHAUD, M. V., SANTANA, M. H. A., SILVA, A. M. & SOUTO, E. B. 2015. Development and characterization of a cationic lipid nanocarrier as non-viral vector for gene therapy. *European Journal of Pharmaceutical Sciences,* 66**,** 78-82.

SHAI, Y. 1999. Mechanism of the binding, insertion and destabilization of phospholipid bilayer membranes by α-helical antimicrobial and cell

non-selective membrane-lytic peptides. *Biochimica et Biophysica Acta (BBA)-Biomembranes,* 1462**,** 55-70.

SIMEONI, F., MORRIS, M. C., HEITZ, F. & DIVITA, G. 2003. Insight into the mechanism of the peptide-based gene delivery system MPG: implications for delivery of siRNA into mammalian cells. *Nucleic acids research,* 31**,** 2717-2724.

SKINNER, S. A., TUTTON, P. J. & O'BRIEN, P. E. 1990. Microvascular architecture of experimental colon tumors in the rat. *Cancer Res,* 50**,** 2411-2417.

SLINGERLAND, M., GUCHELAAR, H.-J. & GELDERBLOM, H. 2012. Liposomal drug formulations in cancer therapy: 15 years along the road. *Drug discovery today,* 17**,** 160-166.

SNYDER, E. L. & DOWDY, S. F. 2004. Cell penetrating peptides in drug delivery. *Pharm Res,* 21**,** 389-393.

SOOMETS, U., LINDGREN, M., GALLET, X., HÄLLBRINK, M., ELMQUIST, A., BALASPIRI, L., ZORKO, M., POOGA, M., BRASSEUR, R. & LANGEL, Ü. 2000. Deletion analogues of transportan. *Biochim. Biophys. Acta,* 1467, 165-176.

STEWART, K. M., HORTON, K. L. & KELLEY, S. O. 2008. Cell-penetrating peptides as delivery vehicles for biology and medicine. *Org Biomol Chem,* 6**,** 2242-2255.

STULL, R. A. & SZOKA JR, F. C. 1995. Antigene, ribozyme and aptamer nucleic acid drugs: progress and prospects. *Pharmaceutical research,* 12**,** 465-483.

SUBBARAO, N. K., PARENTE, R. A., SZOKA JR, F. C., NADASDI, L. & PONGRACZ, K. 1987. The pH-dependent bilayer destabilization by an amphipathic peptide. *Biochemistry,* 26**,** 2964-2972.

SUGITA, T., YOSHIKAWA, T., MUKAI, Y., YAMANADA, N., IMAI, S., NAGANO, K., YOSHIDA, Y., SHIBATA, H., YOSHIOKA, Y. & NAKAGAWA, S. 2008. Comparative study on transduction and toxicity of protein transduction domains. *British journal of pharmacology,* 153**,** 1143-1152.

SUMITOMO, M., TACHIBANA, M., NAKASHIMA, J., MURAI, M., MIYAJIMA, A., KIMURA, F., HAYAKAWA, M. & NAKAMURA, H. 1999. An essential role for nuclear factor kappa B in preventing TNF-alpha-induced cell death in prostate cancer cells. *J Urol,* 161**,** 674-679.

SWANSON, J. A. 1989. Phorbol esters stimulate macropinocytosis and solute flow through macrophages. *Journal of cell science,* 94**,** 135-142.

TAKADA, Y., SINGH, S. & AGGARWAL, B. B. 2004. Identification of a p65 peptide that selectively inhibits NF-κ B activation induced by various inflammatory stimuli and its role in down-regulation of NF-κB-mediated gene expression and up-regulation of apoptosis. *Journal of Biological Chemistry,* 279**,** 15096-15104.

TAKAYAMA, K., NAKASE, I., MICHIUE, H., TAKEUCHI, T., TOMIZAWA, K., MATSUI, H. & FUTAKI, S. 2009. Enhanced intracellular delivery using arginine-rich peptides by the addition of penetration accelerating sequences (Pas). *Journal of Controlled Release,* 138**,** 128-133.

TAN, M., LAN, K.-H., YAO, J., LU, C.-H., SUN, M., NEAL, C. L., LU, J. & YU, D. 2006. Selective inhibition of ErbB2-overexpressing breast cancer in vivo by a novel TAT-based ErbB2-targeting signal transducers and activators of transcription 3–blocking peptide. *Cancer research,* 66**,** 3764-3772.

TANNER, K. G. & KYTE, J. 1999. Dimerization of the extracellular domain of the receptor for epidermal growth factor containing the membrane-spanning segment in response to treatment with epidermal growth factor. *Journal of Biological Chemistry,* 274**,** 35985-35990.

TAS, S. W., DE JONG, E. C., HAJJI, N., MAY, M. J., GHOSH, S., VERVOORDELDONK, M. J. & TAK, P. P. 2005. Selective inhibition of NF-kappaB in dendritic cells by the NEMO-binding domain peptide blocks maturation and prevents T cell proliferation and polarization. *Eur J Immunol,* 35**,** 1164-1174.

THOMAS, C. E., EHRHARDT, A. & KAY, M. A. 2003. Progress and problems with the use of viral vectors for gene therapy. *Nat Rev Genet,* 4**,** 346-358.

TORGERSON, T. R., COLOSIA, A. D., DONAHUE, J. P., LIN, Y. Z. & HAWIGER, J. 1998. Regulation of NF-kappa B, AP-1, NFAT, and STAT1 nuclear import in T lymphocytes by noninvasive delivery of peptide carrying the nuclear localization sequence of NF-kappa B p50. *J Immunol,* 161**,** 6084-6092.

TRABULO, S., CARDOSO, A. L., MANO, M. & DE LIMA, M. C. P. 2010. Cell-Penetrating Peptides—Mechanisms of Cellular Uptake and Generation of Delivery Systems. *Pharmaceuticals,* 3**,** 961-993.

TYAGI, M., RUSNATI, M., PRESTA, M. & GIACCA, M. 2001. Internalization of HIV-1 tat requires cell surface heparan sulfate proteoglycans. *J Biol Chem,* 276**,** 3254-3261.

UHEREK, C. & WELS, W. 2000. DNA-carrier proteins for targeted gene delivery. *Advanced drug delivery reviews,* 44**,** 153-166.

VANNUCCI, L., LAI, M., CHIUPPESI, F., CECCHERINI-NELLI, L. & PISTELLO, M. 2013. Viral vectors: a look back and ahead on gene transfer technology. *New Microbiol,* 36**,** 1-22.

VIATOUR, P., MERVILLE, M. P., BOURS, V. & CHARIOT, A. 2005. Phosphorylation of NF-kappaB and IkappaB proteins: implications in cancer and inflammation. *Trends Biochem Sci,* 30**,** 43-52.

VIVES, E., BRODIN, P. & LEBLEU, B. 1997. A truncated HIV-1 Tat protein basic domain rapidly translocates through the plasma membrane and accumulates in the cell nucleus. *Journal of Biological Chemistry,* 272**,** 16010-16017.

VUCIC, D., DESHAYES, K., ACKERLY, H., PISABARRO, M. T., KADKHODAYAN, S., FAIRBROTHER, W. J. & DIXIT, V. M. 2002. SMAC negatively regulates the anti-apoptotic activity of melanoma inhibitor of apoptosis (ML-IAP). *Journal of Biological Chemistry,* 277**,** 12275-12279.

WADIA, J. S., STAN, R. V. & DOWDY, S. F. 2004. Transducible TAT-HA fusogenic peptide enhances escape of TAT-fusion proteins after lipid raft macropinocytosis. *Nat Med,* 10**,** 310-315.

WAN, F. & LENARDO, M. J. 2010. The nuclear signaling of NF-κB: current knowledge, new insights, and future perspectives. *Cell research,* 20**,** 24-33.

WATKINS, C., SCHMALJOHANN, D., FUTAKI, S. & JONES, A. 2009a. Low concentration thresholds of plasma membranes for rapid energy-independent translocation of a cell-penetrating peptide. *Biochem. J,* 420**,** 179-189.

WATKINS, C. L., BRENNAN, P., FEGAN, C., TAKAYAMA, K., NAKASE, I., FUTAKI, S. & JONES, A. T. 2009b. Cellular uptake, distribution and cytotoxicity of the hydrophobic cell penetrating peptide sequence PFVYLI linked to the proapoptotic domain peptide PAD. *Journal of Controlled Release,* 140**,** 237-244.

WIETHOFF, C. M. & MIDDAUGH, C. R. 2003. Barriers to nonviral gene delivery. *Journal of pharmaceutical sciences,* 92**,** 203-217.

WOLFERT, M. A., DASH, P. R., NAZAROVA, O., OUPICKY, D., SEYMOUR, L. W., SMART, S., STROHALM, J. & ULBRICH, K. 1999. Polyelectrolyte vectors for gene delivery: influence of cationic polymer on biophysical properties of complexes formed with DNA. *Bioconjugate chemistry,* 10**,** 993-1004.

WYMAN, T. B., NICOL, F., ZELPHATI, O., SCARIA, P., PLANK, C. & SZOKA, F. C. 1997. Design, synthesis, and characterization of a cationic peptide that binds to nucleic acids and permeabilizes bilayers. *Biochemistry,* 36**,** 3008-3017.

XIAO, G., CVIJIC, M. E., FONG, A., HARHAJ, E. W., UHLIK, M. T., WATERFIELD, M. & SUN, S. C. 2001. Retroviral oncoprotein Tax induces processing of NF-κB2/p100 in T cells: evidence for the involvement of IKKα. *The EMBO Journal,* 20**,** 6805-6815.

XUE, F., CHEN, J., GUO, J., WANG, C., YANG, W., WANG, P. & LU, D. 2007. Enhancement of intracellular delivery of CdTe quantum dots (QDs) to living cells by Tat conjugation. *Journal of fluorescence,* 17**,** 149-154.

YANG, L., HARROUN, T. A., WEISS, T. M., DING, L. & HUANG, H. W. 2001. Barrel-stave model or toroidal model? A case study on melittin pores. *Biophysical journal,* 81**,** 1475-1485.

YIN, H., KANASTY, R. L., ELTOUKHY, A. A., VEGAS, A. J., DORKIN, J. R. & ANDERSON, D. G. 2014. Non-viral vectors for gene-based therapy. *Nature Reviews Genetics,* 15**,** 541-555.

YU, Y.-L., CHOU, R.-H., LIANG, J.-H., CHANG, W.-J., SU, K.-J., TSENG, Y.-J., HUANG, W.-C., WANG, S.-C. & HUNG, M.-C. 2013. Targeting the EGFR/PCNA signaling suppresses tumor growth of triple-negative breast cancer cells with cell-penetrating PCNA peptides. *PloS one,* 8**,** e61362.

ZHAO, M., KIRCHER, M. F., JOSEPHSON, L. & WEISSLEDER, R. 2002. Differential conjugation of tat peptide to superparamagnetic nanoparticles and its effect on cellular uptake. *Bioconjugate chemistry,* 13**,** 840-844.

ZIEGLER, A. 2008. Thermodynamic studies and binding mechanisms of cell-penetrating peptides with lipids and glycosaminoglycans. *Adv Drug Deliv Rev,* 60**,** 580-597.

ZORKO, M. & LANGEL, U. 2005. Cell-penetrating peptides: mechanism and kinetics of cargo delivery. *Adv Drug Deliv Rev,* 57**,** 529-545.

Chapter 2: Materials and Methods

2.1 Materials

Tissue culture plasticware was manufactured by Corning® and supplied by Fisher Scientific (Loughborough, UK). Laboratory disposables and organic solvents were also purchased from Fisher Scientific. Details of experimental materials, associated suppliers and relevant catalogue numbers are provided in Appendix A and therefore are omitted from this Chapter. General usage chemicals and reagents were supplied by Sigma-Aldrich (Poole, UK) unless otherwise mentioned in Appendix A. Cell lines and plasmids that were gifts to the laboratory are stated in the text, along with the source. The peptides used throughout this thesis are listed in Table 2-1.

Table 2-1: List of peptides used in this thesis.

Peptide	Origin	Sequence	Mass unlabelled	Mass Rhodamine labelled
Penetratin	1	NH_2-DRQIKIWFQNRRMKWKK-COOH	2361	-
Penetratin-NBD	1	NH_2-DRQIKIWFQNRRMKWKKTALDWSWLQTE-COOH	3692	-
EJP-18	2	Ac-LFMRRRHIVRKRTLRRLL-NH_2	2462.13	2832.55
EJP-21	2	Ac-LFMRRRHIVRKRTLRRLLQER-NH_2	2875.56	3245.97
E-64562	2	Ac-RRRHIVRKRTLRRLLQER-NH_2	2484.03	2854.44
R8	2	Ac-RRRRRRRR-NH_2	1308.58	1678.99
R8-GC	3	NH_2-RRRRRRRRGC-COOH	1427.7	-

(1) Imgenex, (2) EZ-biolab and (3) American peptide company

(2) NBD, NEMO binding domain

2.2   *In vitro* procedures

2.2.1   *General cell culture*

All tissue culture procedures were carried out in a class II laminar flow hood after decontamination of all sterilised consumables with 70% ethanol solution. All cells were maintained at 37ºC with 5% CO_2 in a humidified incubator. Routinely (3 months), all cell lines in the laboratory were tested for mycoplasma using a LookOut® Mycoplasma PCR Detection Kit (Sigma) (Wymant, 2014).

2.2.2   *Cell lines*

A number of suspension and adherent cell lines were studied during this project. These are cell lines routinely used in the laboratory for CPP and other studies. HeLa and KG1a cell lines have been extensively used as cell models for CPP research in the Jones laboratory.

2.2.2.1   Suspension cells (non-adherent cells)

KG1a; acute myeloid leukaemia (AML), cells were obtained from European Collection of Authenticated Cell Cultures (ECACC).

2.2.2.2   Adherent cells

HeLa cervical cancer cells from two sources were used in this thesis. HeLa used in Chapter 3 were obtained from the European Molecular Biology Laboratory (Simpson *et al*., 2004). In subsequent chapters, HeLa cells used were purchased from the American Type Culture Collection (ATCC).

NF-kB Luciferase Reporter HeLa stable cell line was a kind gift from Professor Michael Taggart (Newcastle University) and originally obtained from Signosis (California, USA, # SL-0001).

Low passage (P9) MCF-7 and MDA-MB-231 breast cancer cells were a kind gift from the Breast Cancer Molecular Pharmacology Group (BCMPG) at the Cardiff School of Pharmacy and Pharmaceutical Sciences. The authenticated cells were donated to the group by AstraZeneca or purchased from the ATCC.

A431 epidermal cancer cells were a kind gift from Dr Elaine Ferguson, School of Dentistry, Cardiff University.

2.2.3   Media

KG1a, MCF-7 and MDA-MB-231 cells were cultured in Roswell Park Memorial Institute medium (RPMI) supplemented with 10% Foetal Bovine Serum (FBS), 100 U/mL penicillin and 100 µg/mL streptomycin. HeLa and A431 cells were maintained in Dulbecco's Modified Eagle Medium (DMEM) supplemented with 10% FBS, 100 U/mL penicillin and 100 µg/mL streptomycin. HeLa NF-κB Luciferase Reporter HeLa stable cells were maintained in the same medium used for HeLa but with the addition of 100 µg/mL hygromycin.

2.2.4   Maintenance

2.2.4.1   Routine maintenance

The cells were passaged every 3-5 days. For adherent cells: cells were washed with phosphate buffered saline (PBS) then incubated for 3 min with 0.05%

trypsin/ethylenediaminetetraacetic acid (EDTA) to detach the cells. A431 required longer incubation with trypsin ($\approx$ 10 min) for complete detachment. After trypsinisation, the cells were collected in 10 mL of culture medium then centrifuged at 900 x g for 3 min. For non-adherent cell line, cells were directly centrifuged at 900 x g for 3 min.

For both adherent and non-adherent cell lines, the supernatant was then aspirated and the pellet was resuspended in 5 mL fresh, pre-warmed medium. 1-2 mL of cells was then transferred to a new T-75 flask.

All experiments were carried at passage number below 30 and in antibiotic free medium, other than HeLa NF-κB Luciferase Reporter HeLa stable cell line that is cultured in hygromycin.

2.2.4.2   Cryogenic freezing of cells

Stocks of cells were produced by freezing down 70% confluent cells in freezing medium. Freezing medium for all cell lines contained 20% FBS and 5% dimethyl sulphoxide (DMSO) except for KG1a: 32% FBS and 8% DMSO. Before freezing, cells were centrifuged, the supernatant was removed and cells were resuspended in the appropriate volume of freezing medium to yield a cell density of 1 x 10^6 viable cells/mL. One mL aliquots of cell suspension were then transferred to sterile cryogenic vials. The cryovials were frozen in a Mr. Frosty^{TM} freezing container filled with isopropanol at -20ºC for 5 h then at -80ºC overnight before being transferred to liquid nitrogen for long-term storage.

2.2.4.3 Cell recovery from cryogenically frozen stocks

Cryogenic vials were thawed in the water bath at 37ºC and were then immediately transferred into a sterile centrifuge tube containing 9 mL pre-warmed culture medium and centrifuged at 900 x g for 3 min. The supernatant was aspirated and the pellet resuspended in 5 mL culture medium and transferred into T-25 flask with the medium being changed every 2 days. The cells were then seeded into T-75 flasks.

2.2.4.4 Determination of cell number and viability

To determine viable cell numbers prior to seeding for *in vitro* experiments, trypan blue exclusion assay and haemocytometer counting were used. Trypan blue is membrane-impermeable in viable cells and can therefore only penetrate and stain dead cells. During cell counting, blue-stained (dead) cells were therefore excluded from counting. To determine the number of viable cells, 20 µL of cell suspension was mixed with an equal volume of Trypan blue (0.2% v/v in PBS). A coverslip was mounted onto the haemocytometer and approximately 10 µL was applied under the edge of the coverslip. The slide was placed under an inverted light microscope and viable cells were counted in each quadrant. The average of 4 quadrants was determined and the cell density (number of cells/mL) was calculated using the following equation:

Cell density = mean number of cells per quadrant x dilution factor x 10^4

2.3   Cell viability assay

Cell viabilities were determined using the CellTiter-Blue® assay in accordance with manufacturer's instructions (section 2.3.1 and 2.3.2). The assay depends on the fact that viable cells have the ability to convert the nonfluorescent redox dye named resazurin into a fluorescent end product, resorufin. Resazurin acts as an intermediate electron acceptor in the electron transport chain that takes place between the final reduction of oxygen and cytochrome oxidase through the exchange of molecular oxygen. Table 2-2 shows the tested compounds, range of concentrations and cell lines used in each case. The diluent control of all tested compounds was distilled water unless otherwise stated.

Table 2-2: List of tested compounds for cell viability, range of concentrations evaluated and cell lines used for each compound.

Tested Compounds	Concentrations	Cell lines tested
D-Nu-BCP-9-r8 and r8	0.005-20 µM	MCF-7 and KG1a
*Penetratin-NBD and penetratin	0.2-50 µM	HeLa**, MCF-7 and KG1a
TNF	0.1-20 ng/mL	HeLa, MCF-7, MDA-MB-231 and KG1a
EJP-18, EJP-21, E-64562, R8 and their rhodamine conjugates***	0.1-100 µM	HeLa, MCF-7, MDA-MB-231, A431 and KG1a
peptides/labelled bovine serum albumin (BSA-Alexa 647) complexes	10 µM peptide/10 µg/mL BSA-Alexa 647	HeLa

* The diluent control was DMSO
** 100 µM was also tested for HeLa cells
*** R8 and rhodamine conjugates of R8, EJP-21 and E-64562 were only tested in HeLa cells

2.3.1   CellTiter-Blue assay in non-adherent cells

KG1a cells (1.5×10^4 cells/well in a total volume of 100 µL) were seeded in black 96-well plates in complete medium (media supplemented with 10% FBS). A number of different compounds were tested across a range of concentrations (listed in Table 2-2). Cells were incubated under tissue culture conditions (37°C, 5% CO_2) with the compounds, or diluent controls, diluted in complete medium for a total period of 24 h. After 20 h incubation, 20 µL of CellTiter-Blue reagent was added per well and the plates were returned to the incubator for 4 h. Fluorescence ($544_{Ex}/590_{Em}$) was measured using a Fluostar Optima Fluorescent plate reader. The percent of cell viability was then calculated using the following equation:

$$Cell\ Viability = \frac{F_{590nm}(\text{treated cells}) - F_{590nm}(\text{background})}{F_{590nm}(\text{positive control}) - F_{590nm}(\text{background})} \times 100\%$$

Where:

F = fluorescence

Background = fluorescence of medium alone

Positive control= fluorescence of untreated cells

2.3.2   CellTiter-Blue assay in adherent cells

Cells were seeded at suitable density (listed in Table 2-3) in black 96-well plates in complete medium and were incubated overnight at 37°C, 5% CO_2. The following day, cells were treated with a range of concentrations of tested compounds. Cells were incubated with the compounds for 24 h (37°C, 5% CO_2). In case of peptide/BSA-Alexa647 complexes, cell viability was also evaluated after 72 h incubation. The following day, 20 µL of CellTiter-Blue

reagent was added to each well and the plates were returned to the incubator. Fluorescence intensity was measured and cell viability was calculated as described in section 2.3.1.

Table 2-3: Seeding density of different cell lines in 96-well plate for Cell-Titer Blue assay

Cell Line	Cell Density (cells/well)
HeLa	8×10^3
MCF-7	2.5×10^3
MDA-MB-231	2×10^3
A431	2×10^4

2.4   Microscopy

2.4.1   Confocal microscopy

Confocal fluorescence microscopy analysis was performed on a Leica SP5 inverted confocal laser scanning microscope. The microscope was equipped with a 63x, 1.4 NA oil-immersion objective and 405, 488, 543 and 633 nm lasers. Gain and offset settings were optimised for each fluorescent channel within a single experiment but kept consistent throughout each experiment. Sequential scanning mode was used to record images to prevent channel crosstalk/bleedthrough. Images were scanned at 400 or 700 Hz with a line average of three to reduce noise. Live cell imaging was performed to exclude any fixation artefacts and maximal projection images were taken through z-axis. For single section images, the midpoint was identified by initial scanning of the cells through the z-axis and identifying the central section. Where Hoechst is employed as a nuclear marker, the midpoint most often

represents the section that contains the largest nuclear area. Complete microscope and image acquisition settings can be found in Appendix B (Table B-1). For live cell imaging experiments performed at 37˚C, the imaging dishes were housed on the microscope temperature control stage set to 37˚C. The maximum excitation and emission wavelengths of the fluorophores used are listed in Table 2-4.

After acquisition, images were analysed in ImageJ software to create single sections or max projections, for adding scale bars and performing colocalisation analysis based on Pearson's coefficient (Moody *et al*., 2015). Brightness and contrast were adjusted consistently within an experiment (where required) so that images can be compared directly.

Table 2-4: List of fluorophores used with their maximum excitation and emission wavelengths.

Fluorophore	Maximum Excitation (nm)	Maximum Emission (nm)
Tetramethylrhodamine*	554	578
Alexa 488	494	519
Alexa 647	651	671
Indodicarbocyanine (Cy5)	650	670
DRAQ7	599/646	678/694
Hoechst 33342	350	450

*From here on in tetramethylrhodamine is referred to as Rhodamine or Rh.

All confocal microscopy studies were performed in HeLa cells as a well characterised CPP-*in vitro* model in our laboratory. Rhodamine labelled peptides were used for peptide uptake and colocalisation studies. In some cases, unlabelled peptides were mixed with cargo (siRNA, Protein) labelled

with one of the fluorophores listed in Table 2-4. Information on these is presented in subsequent sections.

All experiments were performed three times, unless otherwise stated in the figure legends, and representative images from one experiment is shown.

2.4.1.1 Cellular uptake of Rh-labelled peptides

Cells (2.5×10^5) were seeded into 35 mm MatTek dishes and incubated overnight in complete medium at 37ºC, 5% CO_2. The following day, the medium was aspirated and the cells were washed three times with serum free medium (SFM) or complete medium according to experiment type. A range of concentrations (1-20 µM) of Rh-peptides were added to the cells in a total volume of 200 µl in the imaging region of the dish. The dishes were then returned to tissue culture conditions for 1 h. The medium was then aspirated and the cells were washed three times with imaging medium (phenol red free DMEM supplemented with 20 mM HEPES pH 7.4 and 10% FBS). Imaging medium (500 µL) was added to the cells and live cells were immediately visualised by confocal microscopy. When nuclei were needed to be visualised during the experiment, imaging medium (500 µL) was supplemented with 0.5 µL of 10 mg/mL Hoechst before and during imaging. To test membrane integrity of cells, 2.5 µL of DRAQ7 (0.3mM) (instead of Hoechst) was added to the imaging medium.

2.4.1.2 Uptake of 10 µM Rh-peptides at different temperatures

Cells (2.5×10^5) were seeded and incubated as described in section 2.4.1.1. The following day, they were incubated with 10 µM Rh-peptides in 200 µL of SFM

at either 4ºC (on ice) or 37ºC in the tissue culture incubator. After 1 h incubation, the medium was aspirated and the cells were washed as previously described. Imaging medium (500 µL) containing 0.5 µL Hoechst (10 mg/mL stock) was added and live cells were visualised immediately by confocal microscopy.

2.4.1.3 Uptake of BSA-Alexa488/647 alone or complexed with peptides

Cells (2.5×10^5) were seeded and incubated as described in section 2.4.1.1. The following day, BSA-Alexa488/647 were incubated with cells alone or complexed with peptides. Peptide/BSA-Alexa488/647 complexes were formed by incubating 2, 5 or 10 µM peptide with 10 µg/mL BSA-Alexa488/647 for 30 min at 37ºC in distilled water (total volume 50 µL). Complexes were then diluted 1 in 4 in SFM or complete medium and incubated with cells for 1 h at 37ºC. Cells were then washed and imaging medium was added as previously described in section 2.4.1.1. Live cells were visualised immediately by confocal microscopy. For all experiments, BSA-Alexa488/647 treated as above with diluent (distilled water) was incubated with cells to determine the effect of peptide on cell uptake.

2.4.1.4 Uptake of EJP-18/Cy5-Cav-1 siRNA and oligofecatmine/Cy5-Cav-1 siRNA complexes

Cells (2.5×10^5) were seeded and incubated as described in section 2.4.1.1. The following day, cells were treated with EJP-18 complexed with Cy5-siRNA targeting caveolin-1 (Cav-1) or oligofectamine/Cy5-siRNA complexes in 200 µL Opti-MEM at 37ºC for 3 h. EJP-18/Cy5-siRNA complexes were formed by

mixing a fixed concentration of Cy5-siRNA, 50 nM or 100 nM, with increasing concentrations of peptide to achieve different molar ratios (peptide/cargo) in Opti-MEM (total volume = 50 μL). Molar ratios and volumes for 50 nM and 100 nM Cy5-siRNA are listed in Appendix C (Tables C-1 and C-2 respectively). Complexes were diluted 1 in 4 in Opti-MEM and incubated with cells for 3 h at 37ºC before being washed and imaged as live cells as described in section 2.4.1.1. For oligofectamine/50 nM Cy5-siRNA complexes, 1 μL of 10 μM stock Cy5-siRNA was diluted in 99 μL Opti-MEM and 0.8 μL oligofectamine was diluted in 99.2 μL Opti-MEM in two separate eppendorfs. The diluted Cy5-siRNA and diluted oligofectamine were then combined and mixed gently and incubated at room temperature for 30 min and then incubated with cells as described earlier. Double the amounts of both Cy5-siRNA and oligofectamine were used for 100 nM Cy5-siRNA complexes.

5′-Cy5-Caveolin-1 siRNA sequence (MWG sequence)

Sense sequence 5′ Cy5-AGACGAGCUGAGCGAGAAG-3′

2.4.1.5   Colocalisation studies of Rh-peptides with Dextran-Alexa488

Cells (2.25×10^5) were seeded into 35 mm MatTek imaging dishes and incubated in complete medium at 37ºC, 5% CO_2. After 4-6 h, 150 μL of 0.1 mg/mL dextran-Alexa488 were added to the cells that were returned to the incubator for 2 h. The cells were then washed 3-4 times with complete medium to remove any traces of dextran-Alexa488 and the cells were then incubated with 1.5 mL complete medium overnight at 37ºC and 5% CO_2. Following this overnight chase of dextran-Alexa488 through the endocytic system to terminal

lysosomes, 40 µL of 50 µM stock Rh-peptides were added to 160 µL SFM (the final concentration of the peptide is 10 µM) and incubated with the cells for 1 h. Cells were then washed three times with imaging medium and visualised immediately by confocal microscopy using the 488 and 543 lasers. Rhodamine-Alexa488 colocalisation was also measured after the Rh-peptides were similarly incubated with the cells for 1 h and then chased for a further hour in peptide free medium. Images were processed using ImageJ as described in section 2.4.1. and colocalisation values were obtained using Pearson Coefficient analysis as described in Moody *et al.* (Moody *et al.*, 2015).

2.4.1.6 Colocalisation studies of peptides/BSA-Alexa647 complexes with Dextran-Alexa488

Cells (2.25 x 10^5) were seeded and treated with dextran-Alexa488 as described in section 2.4.1.5. Following the overnight dextran-Alexa488 chase, complexes of peptides/BSA-Alexa647 were prepared and diluted as described in section 2.4.1.3. The complexes were added to the cells and incubated for 1 h. Cells were then washed three times with imaging medium and visualised by confocal microscopy using the 488 and 633 lasers. Colocalisation was also measured after the complexes were similarly incubated with the cells for 1 h and then chased for a further hour in complex free medium. Images were processed and colocalisation values were obtained as described in section 2.4.1.5.

2.4.2 *Wide field system microscopy (for eGFP expression in HeLa cells)*

Wide field microscopy analysis was performed using a Leica DMIRB inverted microscope equipped with a 10 x 0.25 NA objective. Microscope settings can

be found in Appendix B (Table B-2). The system operates on Openlab 5.5.0 software and captured samples were processed using ImageJ.

2.5   Western blotting

2.5.1   Cell culture

HeLa cells were seeded in 6 or 12-well plates and grown in complete medium overnight at 37ºC and 5% CO_2. Cells were then subjected to one of several different experimental procedures as described in the next section and section 2.9.1. Seeding densities (per well) in 6-well plates for different treatments (experiments) were as follows:

TNF-α stimulation (in absence and presence of peptides): 250,000 cells

siRNA transfection: 180,000 cells.

For all experiments the cells were 70-80% confluent at the point of lysate collection. Seeding densities were adjusted accordingly when 12 well plates were used.

2.5.1.1   TNF-α treatment in the absence and presence of peptides

HeLa cells were plated overnight in CM. The following day, they were serum starved by overnight incubation in DMEM supplemented with 0.1% FBS (low serum medium) or incubated in complete medium. The cells were then incubated with TNF-α as described in Chapter 3. In the case of peptide (penetratin and penetratin-NBD) treatments, cells were incubated overnight in CM then preincubated with peptides for 3 h in medium containing 0.1% FBS

prior to addition of TNF-α. Lysates were then collected and prepared for analysis of IκB-α degradation as described in sections 2.5.2 - 2.5.7. In this section, data presented as N=1 describe experiments performed to confirm information provided in the literature.

2.5.1.2 Determination of EGFR levels in cancer cell lines

For adherent cell lines (HeLa, A431, MCF-7 and MDA-MB-231), cells were grown to 70% confluency in T-75. The medium was aspirated and the cells were washed three times with PBS. Lysis buffer 0.5 mL (plus protease inhibitors) was added on ice and the cells were scraped from the flask surface. The flask content was transferred to an eppendorf tube and kept on ice for 5-15 minutes then centrifuged (13,800 x g 4ºC) for 15 minutes. The supernatant was then transferred to a clean eppendorf. For non-adherent KG1a cells, the total volume of a T-75 flask was transferred to a 15 mL centrifuge tube, centrifuged at 900 x g and then resuspended in 5 mL fresh medium. A volume containing 1 x 10^6 cells was then centrifuged and resuspended in 1.5 mL medium and transferred into an eppendorf. This was centrifuged (900 x g) then the supernatant was discarded and the pellet was resuspended in PBS, re-centrifuged and resuspended in PBS one more time before resuspending the pellet in lysis buffer (620 μL). After 5-15 minutes, the eppendorf was centrifuged (13,800 x g 4ºC) and the supernatant was collected. Following lysate collection and protein quantification, 20 μg of protein was loaded on 10% precast gel. Proteins were then transferred to polyvinylidene fluoride (PVDF) membranes and EGFR was detected via immunoblotting and ECL as described in sections 2.5.5-2.5.7.

2.5.2   *Lysate collection and preparation*

2.5.2.1   Lysate collection

According to each experiment, the cell culture plates were placed on ice and the medium was aspirated from the wells. The cells were then washed twice with ice-cold PBS. Lysis buffer (150 mM NaCl, 50 mM Tris base pH 8.0, dH$_2$0 and 1% Triton X-100 including protease inhibitor) was added to each well (60-80 μL) and the plates were placed on ice on a lateral, circular shaker for 5 min. The cells were then scraped off the wells and the cell suspension was pipetted into pre-cooled eppendorfs. Samples were then centrifuged (13,800 x g 4ºC) for 10 min. The eppendorfs were then returned to ice and the supernatant was transferred to fresh, pre-cooled eppendorfs.

2.5.2.2   Bicinchoninic acid assay (BCA assay)

The protein concentration of each sample was determined by BCA assay. BSA protein standards were prepared in lysis buffer in concentrations 0, 0.2, 0.4, 0.6, 0.8 and 1 mg/mL. Cell lysates were diluted 1:6 for the sample absorbance measurement to fit in the linear range of the assay. The BCA working solution was prepared by mixing 49 parts of biochoninic acid with 1 part copper sulphate pentahydrate. This working solution (200 μL) was pipetted into a flat-bottomed 96 well plate and 10 μL of the standards/samples were added per well. The standards were added in duplicates and the samples in triplicates. The plate was incubated at 37º for 30 min before the absorbance was measured at 562 nm on a plate reader.

A calibration curve was constructed by plotting the absorbance measurements against the known BSA standard concentrations. The equation of the line that best fits the calibration graph was then used to calculate unknown sample concentrations (allowing for the dilution factor).

2.5.2.3 Lysate preparation for polyacrylamide gel electrophoresis (PAGE)

Sample concentrations from BCA assays were equalised using lysis buffer. Four times strength (4 x) loading buffer (8% sodium dodecyl sulphate (SDS), 40% glycerol, 0.008% bromophenol blue, 0.25 M Tris-HCL and newly prepared 2M dithiothreitol (DTT to give a concentration of 400 mM) were added in the ratio of 3 parts sample: 1 part buffer. The samples were then denatured by heating on a heating block at $\geq$ 95ºC for 5 min. Samples were returned to ice to cool then centrifuged at 13,800 x g for 30 s at 4ºC to pellet debris. Samples were stored at -20ºC.

2.5.3 *Standard SDS-PAGE gel preparation*

Precast Mini-PROTEAN TGX^{TM} gels were used for SDS-PAGE for the experiments in this thesis except for chapter 3 in which the gels were freshly prepared on the day of experiment according to the recipes in Tables 2-5 and 2-6.

The gels were cast and run using a BioRad Mini-Protean II SDS-PAGE assembly system. The front and back plates were assembled in the clamp frame and secured into the casting stand. The resolving gel was prepared according to the following recipe table (TEMED was added last):

Table 2-5: Resolving gel recipes for 10% and 12% acrylamide gels

Contents	10% gel		12% gel	
40% acrylamide/Bis	2.5 mL	5 mL	3 mL	6 mL
3M Tris pH 8.8	1.25 mL	2.5 mL	1.25 mL	2.5 mL
10% SDS	100 µL	200 µL	100 µL	200 µL
dH$_2$O	6.10 mL	12.2 mL	5.6 mL	11.2 mL
10% APS (freshly prepared)	75 µL	150 µL	75 µL	150 µL
TEMED	7.5 µL	15 µL	7.5 µL	15 µL
Total volume of gel	10 mL	20 mL	10 mL	20 mL

Once TEMED has been added, the resolving gel contents were quickly mixed by inverting the capped universal tube. The mixture was then poured into the casting mould leaving a 2.5 cm gap at the top which was then filled with 100% isopropanol.

The resolving gel was allowed to set for 45 min. Once the gel had solidified, isopropanol was discarded and the gap at the top was gently washed eight times with dH$_2$O. Meanwhile, the stacking gel was then prepared using the following recipe table:

Table 2-6: Stacking gel recipes for 2 gels

Contents	4% gel
40% acrylamide/Bis	1 mL
3M Tris pH 6.8	1.3 mL
10% SDS	100 µL
dH$_2$O	7.22 mL
0.1% Bromophenol blue	300 µL
10% APS (freshly prepared)	75 µL
TEMED	10 µL
Total volume of gel	10 mL

The gel contents were mixed by inversion and the mixture was added on top of the set resolving gel and the well comb was positioned at the top of the stacking gel. The stacking gel was allowed to polymerise for 30 min before the comb was removed. The gels (in their casting plates and clamps) were transferred to the running tank and immersed in running buffer (385 mM glycine, 250 mM Tris base and 0.5% SDS) ready for sample loading.

2.5.4 Sample loading and SDS-PAGE

Protein (15-20 μg) from each sample was loaded onto a 4% acrylamide stacking gel using gel loading tips. Protein standard molecular weight marker (8-10 μL) was loaded in most cases onto the outermost wells. The gels were run at 100V for 85 min or until the sample was visible at the end of the gel. The glass plate was pulled apart and the gel was carefully removed and placed into a container and rinsed with dH_2O.

2.5.5 Protein transfer and Ponceau staining

Proteins were transferred to a PVDF membrane at 100 V for 1 h at 4ºC.

Initially the gel was equilibrated for 5 min in transfer buffer (150mM glycine, 20 mM Tris-base and 20% methanol) cooled to 4ºC. The transfer cassette was placed into a container filled with cold transfer buffer. An ice unit was placed in the tank to cool down the transfer system to ensure efficient transfer. The transfer sandwich was assembled in order of sponge, blotting paper, gel, PVDF membrane, blotting paper and sponge. Prior to assembly, the PVDF membrane was soaked in 100% methanol for 1 min before immersion in transfer buffer for 10 min and all other components were equilibrated in cold transfer buffer

for 10 min. The tank containing the electroblotting apparatus was filled with pre-cooled transfer buffer and a magnetic stirrer was placed at the bottom of the tank to evenly circulate any heat generated during transfer. Following transfer, the PVDF membrane was removed and rinsed with dH_2O before being immersed in ponceau S solution to visualise transferred protein. The membrane was returned to dH_2O and the staining was checked to ensure even transfer and sample loading. The membrane was cut into strips to separate light and heavy weight proteins. The positioning of the cut was dependent on the molecular weight of the protein analysed versus the loading control. The Ponceau solution was recycled and the membrane was washed 4 x 5 min in PBS until the red Ponceau stain had been removed.

2.5.6   *Protein detection by immunoblotting*

The membrane strips were incubated for 1 h at room temperature with 5% milk in PBS containing 0.025% Tween20 (PBST) to block non-specific binding sites. The milk was then discarded and the strips were incubated for 1 h with primary antibodies, listed in Table 2-7, diluted in 2% milk in PBST overnight at 4°C.

The following day, membrane strips were washed 3 x 5 min in PBST prior to 1 h incubation at room temperature on an orbital rotator with the appropriate secondary antibody (listed in Table 2-7), diluted in 2% PBST. Secondary antibody incubation was performed at room temperature on the rotator. The membranes strips were washed 3 x 5 min in PBST before development (section 2.5.7).

Table 2-7: Primary and secondary antibodies and dilutions for Western blotting

Primary antibodies	Dilution	Secondary antibodies (all Pierce)	Dilution
Mouse anti-Tubulin (#T9026, Sigma) (Al Soraj *et al.*, 2012)	1:2000	Goat anti-mouse HRP (#32430, Thermoscientific)	1:2000
Rabbit anti-IKB-α (#sc-847, Santa Cruz Biotechnology) (Aldieri *et al.*, 2003)	1:200	Goat anti-rabbit HRP (#32460, Thermoscientific)	1:10,000
Rabbit anti-GADPH(#2118S, Cell Signalling) (Hou *et al.*, 2011)	1:1000	Goat anti-rabbit HRP	1:2000
Rabbit anti-EGFR (#HPA018530, Sigma) (Arabi *et al.*, 2012)	1:1000	Goat anti-rabbit HRP	1:2000
Rabbit anti-Caveolin-1 (#3238S, Cell Signalling) (Al Soraj *et al.*, 2012)	1:1000	Goat anti-rabbit HRP	1:2000
Rabbit anti-PAK-1 (#2602S, Cell Signalling) (Williamson and Bass, 2015)	1:200	Goat anti-rabbit HRP	1:2000
Mouse anti-β-tubulin HRP conjugated (# AB21058, Abcam) (Castro-Diaz *et al.*, 2014)	1:50,000	-	

2.5.7 *Enhanced chemiluminescence detection of transferred proteins*

Equal volumes of enhanced chemiluminescence (ECL) reagents were mixed together then added to the PVDF membrane strips and left for 5 min. Clarity^{TM} Western ECL was used for the majority of Western blotting procedures but SuperSignal West Femto was used for low level expression (where indicated). The PVDF membrane strips were gently shaken to remove excess solution and

wrapped in cling film. The membranes were then either imaged using a BioRad ChemiDoc system or were placed inside a developer cassette and transferred to the dark room for imaging with ECL hyperfilm that was then processed in an x-ray developer.

2.5.8   *Band intensity quantification using ImageJ*

Band intensities were quantified using the gel analyzing tool in ImageJ to obtain the average intensity of each band. The values were exported to excel where they were normalised against the loading control. For full experimental procedure see (Wymant, 2014).

2.6   Native PAGE under non-reducing conditions

These gels were used to investigate the electrophoretic migration of peptide/protein complexes. They were prepared as described in section 2.5.3 with some modifications. Here, DTT was removed from the sample buffer only and SDS was excluded from the sample buffer, reagents used to make the resolving and stacking gels and also the running buffer. The heat denaturing step following the addition of the sample buffer was also omitted. Gel running also was performed as described in section 2.5.4.

2.7   Agarose gel electrophoresis

2.7.1   *Gel preparation*

A gel casting tray was cleaned with dH_2O and autoclave tape was fixed at both ends. Agarose gels (0.8, 1or 2%) were prepared according to the molecular weight of the studied components. To prepare a 1% gel, 1 g of agarose was

dissolved in 100 mL 0.5 x Tris-Borate/EDTA (TBE) from a 10 x TBE stock solution composed of 54 g Tris Base, 27.5 g boric acid, 40 mL of 0.25 M EDTA made up to 1 L with dH_2O. The agarose-TBE mixture was microwaved for 6 x 30 s on full power to dissolve the agarose and destroy any nucleases. The mixture was gently swirled between each heating interval to ensure even heat distribution and mixing. The solution was allowed to cool for 3 min before 50 μL of 5 mg/mL ethidium bromide was added and the solution was poured into the gel casting tray. The ethidium bromide was omitted when the gels were analysed for protein visualisation only. A well comb was placed into the liquid agarose and the gel was left to set in the electrophoresis tank for 40 min. Once solidified, the comb and autoclave tape were removed and the electrophoresis tank was filled with 0.5 x TBE running buffer ensuring complete coverage of the gel.

2.7.2 *Peptide/cargo complex preparation*

EJP-18 was complexed with different cargos including BSA-Alexa647, two different siRNA sequences targeting Caveolin-1 and p21-activated kinase-1 (PAK-1) (sequences below), and also a pEGFP-N1 plasmid. pEGFP-N1 was a kind gift from Dr. Pete Watson, School of Bioscience, Cardiff University (Wakana *et al*., 2008).

Caveolin-1 siRNA was described in 1.4.1.4 and PAK-1 siRNA had sense sequence 5′ -AUAACGGCCUAGACAUUCA-3′. Both, obtained from MWG, had previously been validated for silencing their respective targets using Oligofectamine as a transfecting reagent (Al Soraj *et al*., 2012).

2.7.2.1 EJP-18/protein complex preparation

The EJP-18/BSA-Alexa647 complexes were prepared by mixing increasing concentrations of EJP-18 with 1 µg BSA-Alexa647 (1mg/mL stock) giving peptide/protein molar ratios ranging from 1 to 100 (the final complexing volume was always 10 µL). The solutions were mixed by gently pipetting up and down and incubated at 37ºC for 30 min before being loaded onto a 0.8% agarose gel.

2.7.2.2 EJP-18/siRNA complex preparation

To prepare the complexes, 0.5 µg siRNA was mixed with increasing concentrations of EJP-18 giving rise to peptide/siRNA molar ratios ranging from 1 to 200. The mixture was prepared by incubating increasing concentrations of EJP-18 with 3.8 µL of Cav-1 or PAK-1 siRNA respectively (10 µM stock solution) in nuclease free water (the final complexing volume = 12 µL) at room temperature for 30 min. The commercial siRNA transfection reagent Oligofectamine is routinely used in the laboratory for silencing proteins and was also mixed (5.6 µL), as a complexing control, with 3.8 µL siRNA.

2.7.2.3 EJP-18/plasmid complex preparation

p-EGFP-N1 plasmid (1 µg from 1 mg/mL stock) was mixed with increasing concentrations of EJP-18 to give a peptide/plasmid charge ratio up to 50:1 positive charges on EJP-18 to negative charges on pEGFP-N1. This is based on the fact that pEGFP-N1 has a molecular weight of 2.82×10^6 and 4700 base pairs (thus 9400 negative charges) while EJP-18 has a molecular weight of 2462.13 and 8 positive charges. The complex was formed as described in

section 2.7.2.2. As a positive control for complexation, the commercial transfection reagent FuGENE 6 (3 μL) was mixed with 1 μL p-EGFP-N1 and the mixture was also incubated at room temperature for 30 min before loading on to gels.

2.7.3   Agarose gel electrophoresis

EJP-18/cargo complexes were mixed with 5 x sample loading buffer (30% glycerol, 0.2% bromophenol blue in dH_2O) at a ratio of 5:1. Samples were loaded onto the agarose gel and molecular weight markers were loaded to the first lane of the gel. The gel was run at 80 V for 2 h before the gel was imaged on the BioRad Chemidoc imaging system. The gel used for EJP-18/BSA-Alexa647 complexes was imaged using the Typhoon 9410 Variable Mode Imager (GE Healthcare) using filter: 670 BP 30 Cy5, (Red laser – 633nm), focal plane (+ 3 mm for agarose gels and platen for native gels).

2.8   Coomassie Brilliant Blue staining of native gels

Native gels were prepared as described in section 2.6 and EJP-18/BSA-Alexa647 complexes were prepared as described earlier in section 2.7.2.1. The complexes were loaded onto the gel and were separated by electrophoresis as described in section 2.5.4. The gel was then rinsed gently in dH_2O before being immersed in coomassie blue staining solution (1 g coomassie blue dye, 50% (v/v) methanol, 10% (v/v) glacial acetic acid and 40% (v/v) dH_2O). The gel was incubated with the staining solution for 1 h. The gel was then washed several times with the destaining solution (50% methanol, 10% glacial acetic

acid and 40% dH$_2$O) until the dye was removed and the background is clear. The gel was imaged on the BioRad Chemidoc imaging system.

2.9   Transfection experiments

2.9.1   siRNA transfection

The following method describes volumes and quantities per well of a 6-well plate and is based on a previous publication (Al Soraj *et al*., 2012).

HeLa (1.8 x 10^5 cells/well) were seeded in 6-well plates and cultured to 60% confluence in DMEM supplemented with 10% FBS. Cells were transfected with siRNA (sequences below) 24 h after plating. The transfection reagent consisted of oligofectamine/siRNA complexes or EJP-18/siRNA complexes. To prepare oligofectamine/siRNA complexes, 4.8 μL of oligofectamine was gently mixed with Opti-MEM to a final volume of 24 μL. A volume (1.2 μL) from a 50 μM siRNA stock solution was diluted in 214.8 μL of Opti-MEM. The diluted siRNA and oligofectamine solutions were then combined and mixed gently and incubated at room temperature for 30 min. EJP-18/siRNA transfection mixture was prepared by incubating for 30 min at room temperature in sterile eppendorfs 1.2 μL of 50 μM stock siRNA with 12 μL of 1 mM EJP-18 stock solution in Opti-MEM to a final volume of 50 μL. Then 190 μL Opti-MEM was added to give a final volume of 240 μL. For each well, the medium was aspirated and the cells were washed twice with Opti-MEM and replaced with 960 μL Opti-MEM. The complete oligofectamine/siRNA and EJP-18/siRNA complexes (240μl) were then added dropwise to the cells. These were incubated at 37ºC, 5% CO$_2$ for 4 h before 600 μL of Opti-MEM

medium containing 30% (v/v) serum was added to the culture medium. The cells were then incubated under tissue culture conditions for 48 h prior to further experimentation.

In the above experiments, the final siRNA concentration was 50nM and where indicated in the results chapters, was increased to 100 nM. In this case, 2.4 μL of 50 μM stock siRNA and 9.6 μL oligofectamine were used to prepare the transfection reagent. The concentration of EJP-18 was unchanged.

siRNA sequences

GFP siRNA (Al Soraj *et al.*, 2012)

Sense sequence 5′-GGCUACGUCCAGGAGCGCAdTdT-3′

siRNA sequences targeting Caveolin-1 and PAK-1 have previously been stated in sections 2.4.1.4 and 2.7.2.

2.9.2 *DNA plasmid transfection*

Hela cells (6.7×10^4) were seeded into 12-well plate on coverslips (No. 1.5, ϕ 16 mm, 0.13-0.17 mm thick) and cultured for 24 h in complete medium at 37ºC, 5% CO_2. After 24 h, the cells were $\approx$ 60% confluent. FuGENE 6 transfection mixture was prepared by mixing 3 μL of FuGENE 6 with 97 μL of SFM and incubating at room temperature for 5 min. The diluted FuGENE 6 was then added to 1 μg of plasmid DNA (1 μg/μL stock) in 99 μL of SFM. The mixture was incubated at room temperature for 30 min. EJP-18/plasmid DNA complexes were prepared by mixing in sterile eppendorfs 1 μL of plasmid DNA (1 μg/μL stock) with increasing amounts of peptide to give peptide:

plasmid charge ratios up to 50:1 (the final complexing volume was always 25 μL). The eppendorfs were then incubated at room temperature for 30 min before adding 175 μL SFM. The medium in the wells was replaced with 800 μL SFM then 200 μL of the complexes was added dropwise to the cells. These were then incubated for 4 h at 37ºC, 5% CO_2. The medium was changed for fresh complete medium after 4 h and the cells were then returned to the incubator. Post-transfection (24 h), the cells were fixed with 3% paraformaldehyde as described in the following section.

2.10 Fixation protocol: paraformaldehyde

The medium was aspirated and the cells were washed three times in PBS then fixed in 3% paraformaldehyde for 15 min. The cells were then washed with PBS three times before blocking the free aldehyde groups with 50 mM ammonium chloride for 10 min. The cells were washed again three times with PBS and Hoechst in PBS (1:10,000 from 10 mg/mL stock solution) was added for 10 min to stain the nuclei. The cells were washed with PBS and the coverslips were lifted from the wells, dipped once in PBS then into water and mounted on glass slides with 12 μL Dako oil. The slides were then placed in a dark cupboard for 30 min before imaging and then sealed with clear nail varnish. Images from this experiment were acquired on the Leica Wide Field system as described in section 2.4.2.

2.11 Luciferase assay

The method was developed following initial consultation with the Signosis and Promega luciferase assay protocol and then the method was optimised as

described below. The NF-κB Luciferase Reporter HeLa stable cell line was used for all these experiments.

2.11.1 Measuring luciferase expression in NF-κB Luciferase Reporter HeLa Cells

This below describes the final assay used to test a variety of reagents and was based on optimisation that is summarised below. Cells (8×10^3 per well) were seeded in black 96-well plates in complete medium and incubated overnight at 37°C, 5% CO_2. The following day, cells were incubated with a range of concentrations of tested compounds (penetratin-NBD, penetratin, R8) for 2 h. TNF-α (20 ng/mL in SFM) was then added into each well and the plate was returned to the incubator for 8 h. The plate was then removed from the incubator and the medium was aspirated. Lysis buffer (20 μL) (Promega) was added to the cells and the plate was placed on an orbital shaker for 15 min. The plate was then subjected to a freeze-thaw cycle by incubating at -80°C for 15 min then at room temperature for 15 min. Luciferase substrate (100 μL) was added to each well with gentle pipetting and the luminescence intensity was immediately analysed using a Fluostar Optima luminescent plate reader.

2.11.2 Optimisation of the cell-based luciferase assay

2.11.2.1 Number of cells required

Cells (1×10^3 to 5×10^4 cells/ well) were seeded in 96-glass well plate and were incubated at 37°C, 5% CO_2 for 24 h. The confluency of the cells was checked 24 h later to determine the seeding density required to achieve 80-90% confluency at 24 h.

2.11.2.2 Concentration of TNF-α

The cells were seeded as described in section 2.11.1. and on the following day, were incubated with TNF-α (0-100 ng/mL) for 8 h. After TNF-α incubation, the medium was aspirated and the cells were treated as described in section 2.11.1.

2.11.2.3 Freezing-thawing cycle

The cells were seeded in two black 96-well plates as described in section 2.11.1. On the following day, the cells were incubated with TNF-α (20 ng/mL) for 8 h followed by medium aspiration and addition of 20 μL lysis buffer. One plate was frozen at -80°C for 15 min then thawed at room temperature for 15 min. This process was omitted for the second plate. The experiment was further continued as described in section 2.11.1.

2.12 Statistical methods

Statistical analysis was performed using one-way ANOVA followed by Tukey post-hoc test to reveal significance between groups. Data were analysed using GraphPad Prism 5 software.

2.13 References

AL SORAJ, M., HE, L., PEYNSHAERT, K., COUSAERT, J., VERCAUTEREN, D., BRAECKMANS, K., DE SMEDT, S. C. & JONES, A. T. 2012. siRNA and pharmacological inhibition of endocytic pathways to characterize the differential role of macropinocytosis and the actin cytoskeleton on cellular uptake of dextran and cationic cell penetrating peptides octaarginine (R8) and HIV-Tat. *J Control Release,* 161**,** 132-141.

ALDIERI, E., ATRAGENE, D., BERGANDI, L., RIGANTI, C., COSTAMAGNA, C., BOSIA, A. & GHIGO, D. 2003. Artemisinin

inhibits inducible nitric oxide synthase and nuclear factor NF-kB activation. *FEBS letters,* 552**,** 141-144.

ARABI, A., ULLAH, K., BRANCA, R. M., JOHANSSON, J., BANDARRA, D., HANEKLAUS, M., FU, J., ARIËS, I., NILSSON, P. & DEN BOER, M. L. 2012. Proteomic screen reveals Fbw7 as a modulator of the NF-κB pathway. *Nature communications,* 3**,** 976.

CASTRO-DIAZ, N., ECCO, G., COLUCCIO, A., KAPOPOULOU, A., YAZDANPANAH, B., FRIEDLI, M., DUC, J., JANG, S. M., TURELLI, P. & TRONO, D. 2014. Evolutionally dynamic L1 regulation in embryonic stem cells. *Genes & development,* 28**,** 1397-1409.

HOU, Y.-J., DONG, L.-W., TAN, Y.-X., YANG, G.-Z., PAN, Y.-F., LI, Z., TANG, L., WANG, M., WANG, Q. & WANG, H.-Y. 2011. Inhibition of active autophagy induces apoptosis and increases chemosensitivity in cholangiocarcinoma. *Laboratory investigation,* 91**,** 1146-1157.

MOODY, P. R., SAYERS, E. J., MAGNUSSON, J. P., ALEXANDER, C., BORRI, P., WATSON, P. & JONES, A. T. 2015. Receptor Crosslinking: A General Method to Trigger Internalization and Lysosomal Targeting of Therapeutic Receptor: Ligand Complexes. *Molecular Therapy*, doi: 10.1038/mt.2015.178.

SIMPSON, J. C., GRIFFITHS, G., WESSLING-RESNICK, M., FRANSEN, J. A., BENNETT, H. & JONES, A. T. 2004. A role for the small GTPase Rab21 in the early endocytic pathway. *Journal of cell science,* 117**,** 6297-6311.

WAKANA, Y., TAKAI, S., NAKAJIMA, K.-I., TANI, K., YAMAMOTO, A., WATSON, P., STEPHENS, D. J., HAURI, H.-P. & TAGAYA, M. 2008. Bap31 is an itinerant protein that moves between the peripheral endoplasmic reticulum (ER) and a juxtanuclear compartment related to ER-associated degradation. *Molecular biology of the cell,* 19**,** 1825-1836.

WILLIAMSON, R. C. & BASS, M. D. 2015. Comparing the Affinity of GTPase-binding Proteins using Competition Assays. *JoVE (Journal of Visualized Experiments)***,** e53254-e53254.

WYMANT, J. 2014. The role of BCA2 in receptor tyrosine kinase endocytosis and breast cancer. Cardiff University.

Chapter 3: Experimental analysis of CPP-NBD chimeras designed to target canonical NF-κB signalling

3.1 Introduction

NF-κB is a ubiquitous and essential transcription factor for genes involved in inflammation, cell proliferation, survival, adhesion, and differentiation. Dysregulation of NF-κB has been linked to numerous diseases including cancer and inflammatory conditions such as rheumatoid arthritis (Strickland and Ghosh, 2006). Activation of NF-κB promotes cell survival and suppresses apoptosis in tumour cells (Naugler and Karin, 2008). Various genes that are involved in tumour cell invasion and angiogenesis have also been found to be regulated by NF-κB (Bharti and Aggarwal, 2002). These include cell adhesion molecules, COX-2, VEGF, chemokines and inflammatory cytokines. Owing to its regulatory role in the expression of oncogenic and inflammatory genes, NF-κB is an attractive therapeutic target in a number of diseases.

In unstimulated cells, NF-κB protein complexes in the cytosol are sequestered by a family of inhibitors termed inhibitory IκBs. Cellular stimulation leads to phosphorylation and activation of Ikk complex which in turn phosphorylates IκB-α and targets it for ubiquitination and proteosomal degradation as shown in Figure 1-4. Removal of the inhibitory IκB-α then allows NF-κB dimers to translocate to the nucleus to activate transcription (Karin *et al*., 2002, Hayden and Ghosh, 2008).

As previously described in section 1.7.2, the classical (canonical) NF-κB pathway has been targeted by therapeutic peptides, such as the NBD peptide,

that have been delivered to their cellular targets by CPPs (Orange and May, 2008).

The NBD peptide is a chimera of a selective IKK inhibitor sequence fused with penetratin to mediate membrane translocation- from herein it is termed Pen-NBD. The IKK inhibitor sequence consists of 11 amino acids that correspond to a domain located at the carboxy terminus of the catalytic IKK-β subunit that binds to the scaffold protein NEMO (May *et al.*, 2000). Examples of CPP mediated delivery of NBD inhibitory peptides were listed in section 1.7.2 and more specific examples are described below.

A variety of CPPs (penetratin, K-FGF, PTD-5, Tat, 6R and 8K; listed in Table 1-1) have in fact been studied as delivery vectors for IKK inhibitor sequence and to produce biological effects *in vitro* and *in vivo* (Kahja and Robbins 2010). *In vitro*, pretreatment of HeLa luciferase reporter cells with the described CPPs-NBD peptides at high concentrations of 100 μM, resulted in reduced IL-1β-induced NF-κB transcriptional activity. At this concentration, cytotoxicity was, however, reported with both penetratin- and K-FGF-NBD peptide treatments. *In vivo*, from the several studied CPP-NBD peptides, 8K- and 6R-NBD peptides were the most effective in blocking footpad swelling in a KLH-induced delayed-type hypersensitivity (DTH) murine model of inflammatory arthritis (Khaja and Robbins, 2010).

NBD peptide, as a delivered sequence, has also been shown to inhibit constitutive NF-κB activity in different cancer cell lines resulting in increased sensitization to chemotherapeutic agents and increased apoptosis. For example,

cotreatment of BT-474 breast cancer cells with Pen-NBD peptide and doxorubicin prevented doxorubicin-induced NF-κB activation and sensitised BT-474 cells to doxorubicin antitumor activity (Tapia *et al*., 2007). In an *in vitro* melanoma study, Pen-NBD peptide treatment resulted in concentration-dependent inhibition of cell proliferation through direct inhibition of constitutive NF-κB DNA-binding activity. The peptide was shown to induce apoptosis in the A375 human melanoma cells via activation of caspase-3 (Ianaro *et al*., 2009). In a separate study, Pen-NBD peptide inhibited both TNF-α-induced and constitutive NF-κB activation in both *in vitro* and *in vivo* models of mouse oral squamous cell carcinoma (OSCC) (Furuta *et al*., 2012). OSCC is a malignant tumour of the oral cavity, head and neck (Haddad and Shin, 2008). OSCC invade the maxilla and mandibular bone and bone invasion is a common problem associated with OSCC; bone destruction is thought to be mediated by osteoclasts (Jimi *et al*., 2011). Pen-NBD peptide treatment reduced the number of osteoclasts, induced apoptosis and reduced cancer cell proliferation (Furuta *et al*., 2012). The most aggressive and least chemoresponsive subtype of diffuse large B-cell lymphoma (DLBCL), called spontaneous activated B-cell like DLBCL (ABC-DLBCL), is characterized by constitutive canonical NF-κB activity (Lenz *et al*., 2008). In a canine model of ABC-DLBCL, the Pen-NBD peptide (100 μM) inhibited this constitutive NF-κB activity and rapidly induced apoptosis in primary malignant B-cells *in vitro*. Reduced expression of NF-κB target genes (e.g. Bcl-2, cyclin-D1 and IκB-α) and reduced tumour burden have also been reported following intratumoral injections of Pen-NBD peptide in dogs with relapsed DLBCL

(Gaurnier-Hausser *et al*., 2011). It has also been shown that inhibition of NF-κB activity through retroviral transduction of super-repressor form of IκB-α that cannot be phosphorylated was toxic to ABC-DLBCL which established the NF-κB pathway as a molecular target for drug development of this aggressive subtype (Davis *et al*., 2001). These publications led to a phase 1 clinical trial in which Pen-NBD peptide was systemically administered to dogs with ABC-DLBCL. The overall results from the trial illustrated that intravenous administration of Pen-NBD peptide to dogs was safe and could effectively block constitutive canonical NF-κB activity, promote apoptosis, decrease malignant B cell proliferation and reduce tumour burden in a subset of dogs with ABC-DLBCL. A single dose of Pen-NBD peptide was not able to reverse chemoresistance and further studies are required to decide if multiple administration of Pen-NBD peptide can reverse this chemoresistance and improve clinical response (Ndikuyeze *et al*., 2014).

In addition to inhibiting canonical NF-κB activation in different cancer cell lines, systemic administration of Pen-NBD has been reported to reduce acute and chronic inflammation in multiple murine models without altering basal NF-κB activity. In a murine model of cerulein-induced pancreatitis, a single IP injection of Pen-NBD immediately before the first cerulein injection attenuated some of the inflammatory responses associated with acute pancreatitis. Treatment with Pen-NBD reduced pancreatic inflammation and lung haemorrhage but had no effect on oedema of either the pancreas or the lung (Ethridge *et al*., 2002). In an experimental model of inflammation in mice,

carrageenan-induced paw oedema and NF-κB activation in inflamed paw tissue, IP injection of Pen-NBD significantly inhibited oedema formation in a dose-dependent manner. Cellular infiltration in the inflamed mice paws through suppression of NF-κB activity was also reported and was associated with reduced COX-2 and TNF-α mRNA levels (di Meglio *et al*., 2005). Pen-NBD peptide also effectively reduced inflammation and enhanced regeneration in the muscles of mdx mice; a widely used mouse model for Duchenne muscular dystrophy (DMD) (Peterson *et al*., 2011). DMD is a severe genetic disorder characterised by progressive skeletal muscle weakness and causing high mortality rates as a result of diaphragm and/or cardiac muscle failure (Blake *et al*., 2002). Pen-NBD effectively improved diaphragm muscle contractile dysfunction in mdx mice, the murine animal model (Peterson *et al*., 2011).

For several Pen-NBD studies, the inhibitory effect of the Pen-NBD peptide was abolished when the NBD sequence was mutated in which the two tryptophan residues (T<u>W</u>LD<u>W</u>SALQTE) were replaced with alanine residues (T<u>A</u>LD<u>A</u>SALQTE) (di Meglio *et al*., 2005, Ianaro *et al*., 2009, Khaja and Robbins, 2010, Gaurnier-Hausser *et al*., 2011, Furuta *et al*., 2012). It remains to be determined whether this is an appropriate control for these kinds of studies as a 2x W-A switch could also influence the interaction of the peptide with cells.

In this thesis, Tumour necrosis factor-alpha (TNF-α) was used for stimulation of the classical NF-κB pathway. TNF-α is a potent pro-inflammatory,

multifunctional cytokine and has roles in inflammation and immunity in addition to cell survival and apoptosis. TNF-α is produced primarily by activated macrophages, though a variety of other TNF-α-producing cell types have also been described including lymphocytes, fibroblasts, smooth muscle cells, tumour cells and natural killer cells (van Horssen *et al.*, 2006). Despite being named for its ability to promote tumour necrosis, there are many studies which show that TNF-α can also act as a tumour promoter in numerous cancer cell models (Karin, 2006).

TNF-α is present in two forms: precursor and soluble. TNF-α precursor is a 26 kDa transmembrane protein homotrimer comprised of three polypeptides, 233 amino acids in length. The soluble form of TNF-α is released upon cleavage of the precursor protein by metalloproteinases such as TNF-α-converting enzyme (TACE). Soluble TNF-α is a 17 kDa homotrimer of 157 amino acid residues (Horiuchi *et al.*, 2010).

TNF-α exerts its main effects through two receptors: TNF receptor1 and 2 (TNFR-1, TNFR-2) (Li *et al.*, 2002). These have regulatory roles in apoptosis, the immune response, organ development and metabolism (Costelli *et al.*, 1993, Takada *et al.*, 2003, Popa *et al.*, 2007). The majority of the biological responses induced by TNF-α are triggered by TNFR-1 despite the cytokine having greater affinity for TNFR-2 (Tartaglia and Goeddel, 1992). TNFR-1 and TNFR-2 have a number of key differences in structure and function: TNFR-1 is expressed on all cell types while TNFR-2 is expressed mainly on immune cells (van Horssen *et al.*, 2006).

Figure 3-1 highlights the signalling response to TNF-α by TNFR1. Upon TNF-α binding, the receptor forms a trimmer that is then associated with the release of the silencer of death domain (SODD) protein from the intracellular domain. TNFR-associated domain (TRADD) is then able to bind to the freed death domain of TNFR-1 and this in turn activates one of the adaptor proteins: receptor interacting protein (RIP), TNFR-associated factor 2 (TRAF-2) and FAS-associated death domain (FADD) (Wajant *et al.*, 2003, van Horssen *et al.*, 2006). Adaptor protein activation initiates several intracellular signalling cascades that ultimately either induce or inhibit apoptosis (Horiuchi *et al.*, 2010). The pro-apoptotic pathway is initiated when activated (TNFR-1 associated) FADD binds pro-caspase-8 that instigates a protease cascade leading to activation of endonucleases and consequently DNA fragmentation and apoptosis.

Activation of NF-κB transcription factor is responsible for inhibition of the TNF-α-induced apoptosis. This anti-apoptotic pathway occurs when TNFR-1 signals cell survival via activation of the adaptor proteins TRAF-2 and RIP (instead of FADD). Activation of these adaptors causes downstream activation of the NF-κB transcription factor via NIK. Active NF-κB mediates transcription of different proteins which promote cell proliferation and survival and proteins involved in inflammatory responses and cell protection via anti-apoptotic factors. Usually activation of TNFR-1 is accompanied by the activation of the NF-κB pathway and therefore by the promotion of cell growth and survival. Apoptosis occurs when new protein synthesis is blocked or when

the NF-κB activation is hindered before TNF-α stimulation (van Horssen *et al*.,
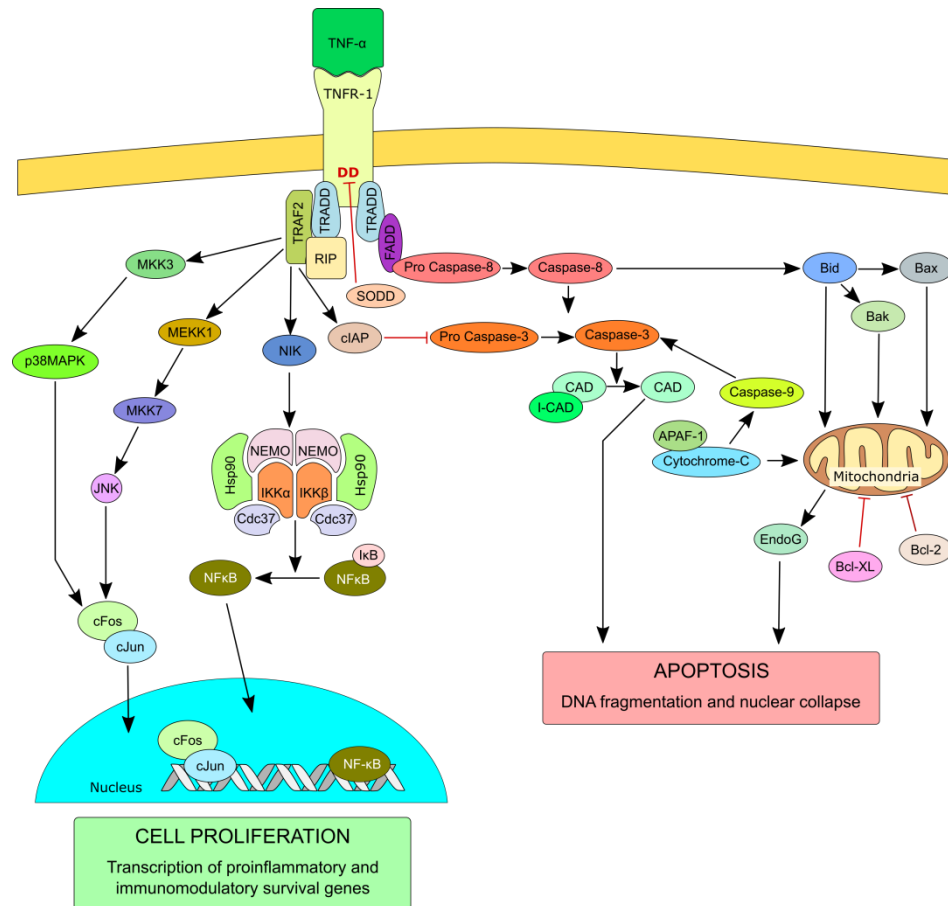
2006).

Figure 3-1: The different signalling pathway of TNF-α; adapted from (van Horssen *et al*., 2006).

3.2   Summary, Aims and Objectives

There is extensive documentation to suggest Pen-NBD peptide inhibits NF-κB

signalling but only at relatively high concentrations of between 100 and 200

μM in many studies. This is much higher than that required to show cell uptake

of penetratin attached to fluorophores suggesting the cargo sequence (NBD

sequence) is having strong effects either in cell uptake or that there is

inefficient targeting of the peptide cargo to the desired site. The aims of this

chapter were to perform more studies to further investigate these effects with a view to lowering the amount of peptide to give the same or, ideally, enhanced physiological effects.

The objectives of this chapter were to:

1. Analyse the viability using the CellTiter-Blue assay of cancer cell lines treated with TNF-α.

2. Develop in-house *in vitro* protocols for analysing NF-κB activation and inhibition using degradation of IκB-α or expression of luciferase expression.

3. Further characterise the ability of Pen-NBD peptide to interfere with NF-κB signalling via inhibition of TNF-α-induced NF-κB activation.

4. Design and study new peptide sequences containing modifications in the NBD peptide sequence or the arrangement with CPP to enhance the efficiency of NF-κB inhibition via a CPP based delivery approach.

3.3   Results

3.3.1   *Evaluating the suitability of the CellTiter-Blue assay for measuring cell viability*

A variety of methods can be used to assess cell viability and upon initiation of this project, the CellTiter-Blue assay had very recently been introduced into the lab as an alternative to the MTT assay. This was found to give more reproducible results and was easier to perform (Helen Wiggins, PhD thesis submitted). Initially, the assay was tested in cell lines treated with the chimeric cytotoxic peptide, D-NuBCP-9-r8 that had been previously characterised as a

membrane active cytotoxic peptide in the laboratory using the MTT assay (Watkins *et al.*, 2011). This then served as a positive cytotoxic peptide control. D-NuBCP-9-r8 is comprised of two key functional sequences: a Nur-77 derived D-isoform sequence (fsrslhll) attached to r8 for intracellular delivery. For this thesis, the viability of KG1a cells treated with increasing concentrations (0.1 - 20 μM) of r8 alone or D-NuBCP-9-r8 was initially investigated and the results in Figure 3-2A highlights the cytotoxicity of this peptide as opposed to r8 that was non-toxic at these concentrations.

These results were in general agreement with those obtained by MTT assay in the Watkins *et al.* study (Watkins *et al.*, 2011). Similar results with a very steep loss of viability at > 2 μM were obtained in MCF-7 breast cancer cells that had not previously been tested (Figure 3-2B). It should be noted that a major finding of the Watkins *et al.* study was that this peptide was in fact inducing Bcl-2 independent necrosis rather than Bcl-2 dependent apoptosis. D-NuBCP9-r8 did however serve as a good positive cytotoxic peptide marker for viability assays.
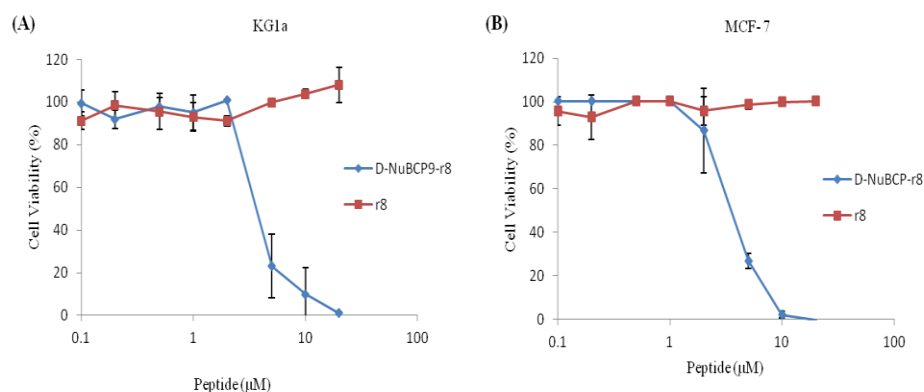
Figure 3-2: Viability of (A) KG1a leukaemia and (B) MCF-7 cells incubated with D-NuBCP9-r8. Viability of cells were evaluated using CellTiter-Blue assay following 24 h incubation with 0.1-20 μM r8 alone or D-NuBCP9-r8. Results represent means ± SD for three independent experiments performed in triplicate.

3.3.2 Cell Viability assays of Penetratin, Pen-NBD and TNF-α

3.3.2.1 Penetratin and Pen-NBD peptide

Initially, cell viability assays were performed in cells treated with increasing concentration of the commercial Imgenex Pen-NBD peptide or Penetratin (# IMG-2000). This was initially performed in three routinely cultured cell lines- KG1a, MCF-7 and HeLa. Cells were incubated with the peptides (0.1-50 μM) under tissue culture conditions for 24 h. Diluent/vehicle controls were performed by incubating cells with various concentrations of DMSO, equivalent to those used in the peptide treatments. The results of three independent assays, shown in Figure 3-3 (A & B), showed that neither penetratin nor Pen-NBD caused cytotoxicity up to 20 μM but toxic effects were noted in KG1a cells at 50 μM. In HeLa cells that were the subject of further studies with this peptide, the peptide concentration was increased to 100 μM and some toxicity was noted at this value (Figure 3-3C). However, this same extent of cytotoxicity was also observed in the diluent control samples showing a DMSO contribution to loss of cell viability.
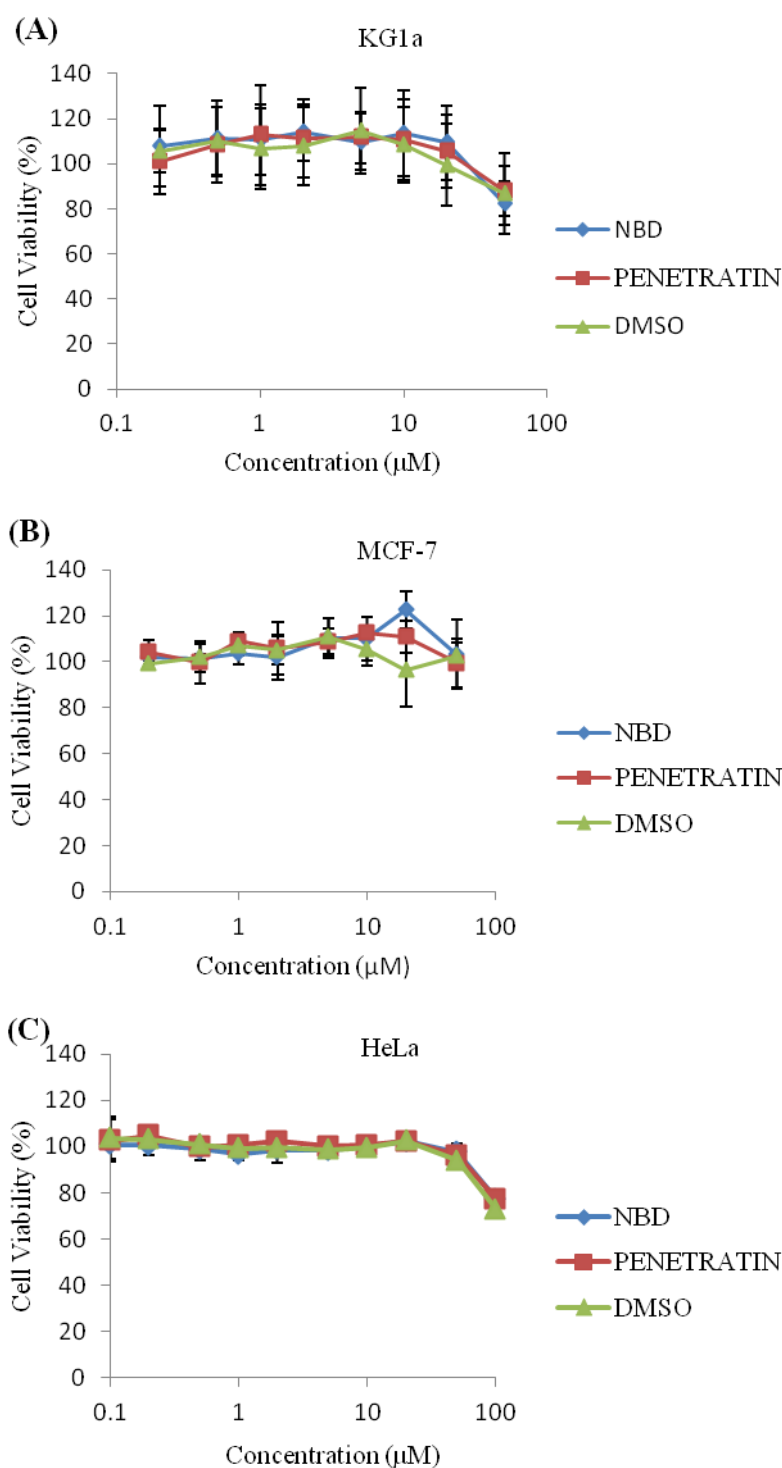
Figure 3-3: Viability of different cell lines incubated with penetratin or Pen-NBD (NBD) peptide. Viability of cells was evaluated using CellTiter-Blue assay following 24 h incubation with 0.2-50 μM penetratin alone or Pen-NBD peptide in KG1a and MCF-7 cells and 0.1-100 μM in HeLa cells. Control cells were treated with peptide diluent control; DMSO. Results for (A & B) represent means ± SD for three independent experiments performed in triplicate and results for (C) represent means ± SD for three independent experiments performed in duplicate.

3.3.2.2 Effects of TNF-α on cell viability

The effects of TNF-α on NF-κB activation has been described in section 3.1 and this was the chosen ligand for investigating the putative effects of the Pen-NBD peptide and variants on NF-κB signalling. As the name suggests, this protein can also have cytotoxic effects and therefore the same panel of three cell lines including a further breast cancer cell line MDA-MB-231 were investigated to determine whether TNF-α induced cytotoxicity. These data were needed as later experiments would involve the use of this protein as an NF-κB activator.

Cell viability assays were performed following 24 h exposure to increasing concentrations of TNF-α (0.1-20 ng/mL) and control cells were incubated with TNF-α diluent. Figure 3-4 highlights that TNF-α treatment did not alter cell viability across all the studied concentrations and that HeLa cells gave very consistent data. This cell line was chosen for future experiments in this chapter for this reason and the fact that the NF-κB luciferase reporter stable cell line became available to us via collaboration with Professor Michael Taggart at Newcastle University.
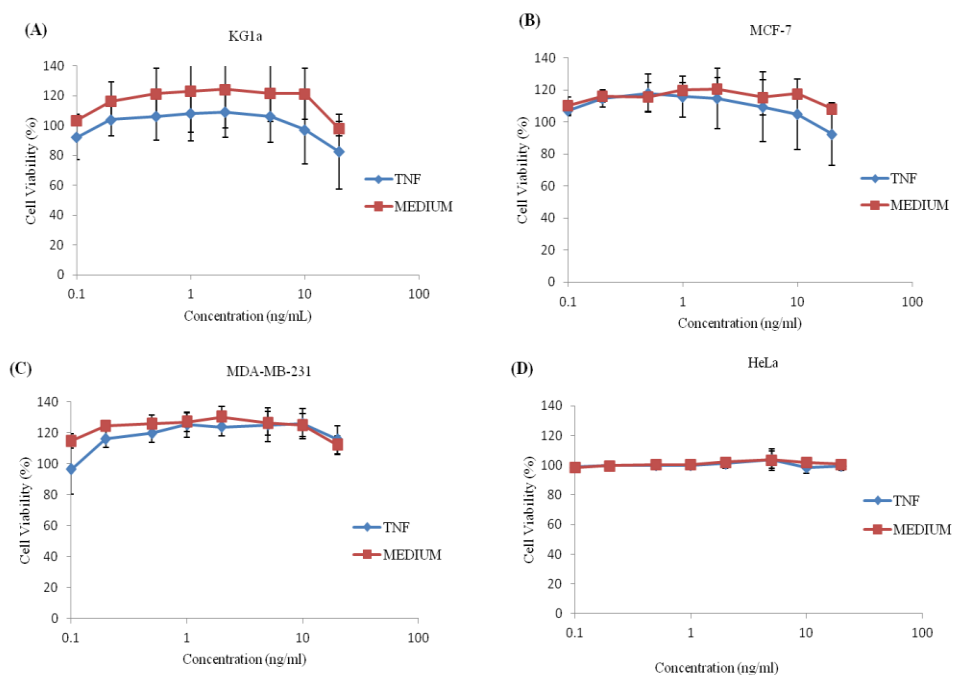
Figure 3-4: Viability of different cell lines incubated with TNF-α. Viability of cells was evaluated using CellTiter-Blue assay following 24 h incubation with 0.1-20 ng/mL TNF-α. Control cells were treated only with medium. Results for (A & D) represent means ± SD for three independent experiments performed in triplicate and results for (B & C) represent means for two independent experiments performed in triplicate.

3.3.3 Analysing the effect of TNF-α on NF-κB signalling

To measure any potential inhibitory effects of NBD peptides on NF-κB signalling, it was important to have a robust assay showing NF-κB activation. IκB-α is rapidly ubiquitinylated and degraded in response to TNF-α (Machleidt *et al.*, 1994, Traenckner *et al.*, 1994, Moon *et al.*, 2006) and this can be measured in cell lysates using Western Blotting. Through collaboration with the University of Newcastle that provided a general method, HeLa cells were serum starved by overnight incubation in DMEM supplemented with 0.1% FBS (low serum medium). Serum starvation is commonly employed to sensitise cells to the effects of this ligand on signalling (Ozes *et al.*, 1999). In the case of cationic CPPs, serum can also significantly alter cellular uptake and

potentially the capacity to reach the cytosol (Jones and Sayers, 2012). The following day, the cells were treated for 0-240 min with 20 ng/mL TNF-α (diluted in low serum medium) or with low serum medium alone (diluent control). Lysates were then collected and Western blotting for IκB-α was performed to measure its degradation versus α-tubulin as a housekeeping loading control. The data in Figure 3-5 show that 10 min incubation with 20 ng/mL TNF-α caused a considerable reduction in IκB-α. Almost complete disappearance of IκB-α band was observed after 30 min incubation and points thereafter up to 240 min when a faint IκB-α band reappeared as newly synthesised material. Based on these data, it was decided that for further experiments, the degradation of IκB-α would be determined after 60 min TNF-α incubation.
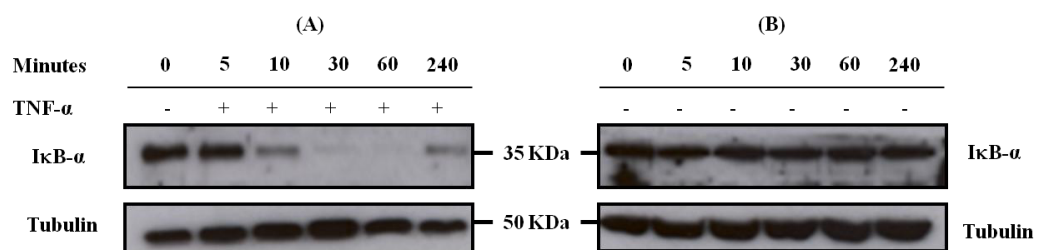
Figure 3-5: TNF-α -induced IκB-α degradation in HeLa cells. (A) Cells were treated with 20 ng/mL TNF-α for the indicated time periods, (B) Control cells were treated with medium alone. Lysates were collected and Western blotting was performed for IκB-α and tubulin. Three independent experiments were performed and a representative blot is shown.

3.3.4 Analysing the effect of serum starvation on TNF-α-dependent degradation of IκB-α

To exclude any potential effects of overnight serum starvation on the cells treated with TNF-α, the TNF-α stimulation experiment was repeated with cells serum starved overnight or incubated in CM. The next day, the cells were

treated with 20 ng/mL TNF-α in medium containing 0.1% FBS for 0-240 min before measuring IκB-α degradation. Figure 3-6 reveals that the effect of TNF-α on IκB-α degradation was not affected by serum starvation. In both cases, the IκB-α band disappeared after 30 minutes and reappeared by 240 min. Based on these findings, subsequent experiments were performed in the absence of serum starvation, TNF-α (in absence or presence of peptides) was added in medium containing 0.1% FBS to minimise the possible interaction between cationic CPPs and serum contents.
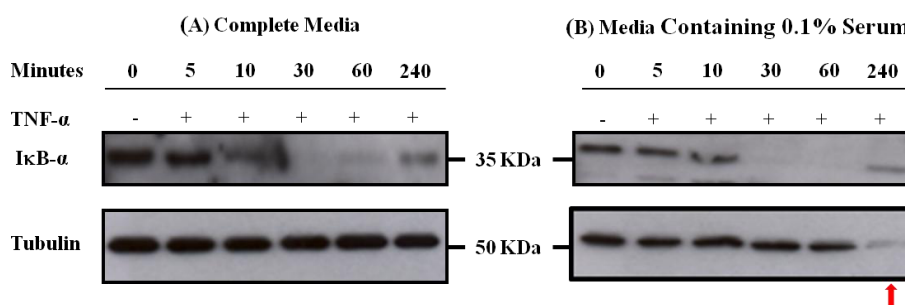
Figure 3-6: TNF-α dependent degradation of IκB-α in HeLa cells in different starvation conditions. Cells were incubated overnight in either (A) complete medium or (B) medium containing 0.1% FBS (serum starved) then treated with 20 ng/mL TNF-α in medium containing 0.1% FBS. Lysates were collected and Western blotting was performed for IκB-α and tubulin. *Red arrow denotes an underloaded lane.* (N=1)

3.3.5 Assessing the effect of TNF-α concentration on the degradation of IκB-α

Typical concentrations of TNF-α used in *in vitro* studies of NF-κB activation range between 10 ng/mL (May *et al.*, 2000, Tas *et al.*, 2005) and 20 ng/mL (Choi *et al.*, 2003). To investigate the response of NF-κB to different TNF-α doses, HeLa cells were incubated with different concentrations of TNF-α for 1 h in medium containing 0.1% serum before performing Western blotting analysis for IκB-α degradation. Interestingly, NF-κB activation manifested as

degradation of IκB-α occurred at the lowest TNF-α dose of 1 ng/mL (Figure 3-7).
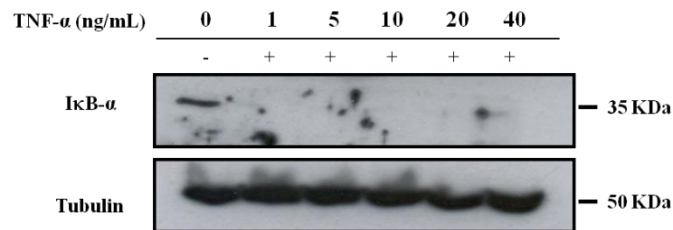
Figure 3-7: Effect of TNF-α concentration on degradation of IκB-α in HeLa cells. Cells were treated with 0-40 ng/mL TNF-α in medium containing 0.1% FBS for 1 h. Lysates were collected and Western blotting was performed for IκB-α and tubulin. (N=1)

3.3.6 Analysing the effect of Pen-NBD and penetratin on IκB-α degradation

Investigations were then performed to explore the effect of penetratin and Pen-NBD on IκB-α levels after TNF-α stimulation (IκB-α degradation). HeLa cells were treated with 100 μM of penetratin, Pen-NBD or DMSO (as peptide diluent) in medium containing 0.1% FBS for 3 h prior to treatment with 20 ng/mL TNF-α. Figure 3-8 demonstrates that 100 μM Pen-NBD and penetratin had no effect on the degradation of IκB-α induced by TNF-α.

Penetratin (µM)	-	-	100	-
NBD (µM)	-	-	-	100
DMSO	+	+	-	-
TNF-α	-	+	+	+

IκB-α — 35 KDa

Tubulin — 50 KDa
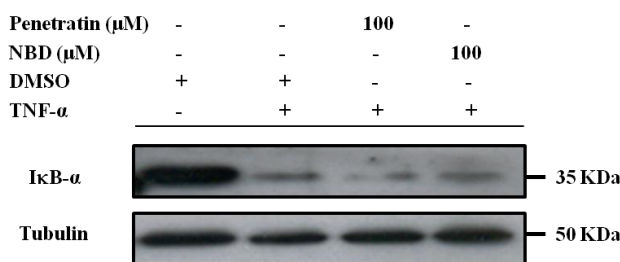
Figure 3-8: Effect of penetratin and Pen-NBD on the degradation of IκB-α in HeLa cells in response to TNF-α. Cells were treated with 100 µM Pen-NBD (NBD) or penetratin for 3 h in medium containing 0.1% FBS. DMSO was used as a diluent control. Where shown, TNF-α (20 ng/mL) was then added for 1 h. Lysates were collected and Western blotting was performed for IκB-α and tubulin. Three independent experiments were performed and a representative blot is shown.

The data above suggested that even at these high concentrations, Pen-NBD was unable to inhibit TNF-α-induced degradation of IκB-α and suggested that it could therefore not inhibit the downstream effects of NF-κB activation. To further investigate this, use was made of the Luciferase reporter stable cell line that expresses luciferase in a NF-κB dependant manner. The assay is described in section 2.11.1 whose optimisation is described below.

3.3.7 Luciferase expression in NF-κB Luciferase Reporter HeLa stable cell line

Signosis has established an NF-κB luciferase reporter stable cell line by transfection of NF-κB luciferase reporter vector containing a hygromycin resistance gene followed by hygromycin selection. The luciferase activity of this reporter cell line is proportional to activity of NF-κB, and so luminescence can be measured as a reporter of NF-κB activation.

3.3.7.1   Optimisation of the luciferase assay

3.3.7.1.1 Number of cells required for luciferase activity measurements

For viability assays, HeLa cells were seeded as 8×10^3 cells/well in 96 black well plates. To determine the seeding density of NF-κB luciferase reporter stable cells, different number of cells (ranging from 1×10^3 to 5×10^4 cells/ well) were seeded in a 96 glass well plate in DMEM supplemented with 10% FBS, 100 U/mL penicillin, 100 μg/mL streptomycin and 100 μg/mL hygromycin according to manufacturer's protocol and incubated overnight at 37ºC, 5% CO_2. The following day, the cells confluency was observed by microscopy and to reach 70-90 % confluency, 8×10^3 cells/well were required and this seeding density was used for all further experiments.

3.3.7.1.2 Optimising   TNF-α   concentration   for   luciferase   activity measurements

Investigations were performed to determine the concentration of TNF-α required to activate the NF-κB pathway in the reporter cell line. For this, cells were seeded and incubated for 8 h with TNF-α concentrations ranging from 0-100 ng/mL. The medium was aspirated and the cells were treated for measuring luciferase activity. The data in Figure 3-9 demonstrated that TNF-α addition was accompanied by the stimulation of NF-κB as illustrated by a dose dependent increase in luciferase activity compared to unstimulated cells. Statistical significance was evaluated by one-way ANOVA which indicated that the difference between groups were statistically significant $F_{(12, 26)} = 15.01$, $p < 0.0001$. Tukey post-hoc tests revealed that the luciferase activity

increased significantly between cells treated with and without TNF-α at concentrations ≥ 5 μM.
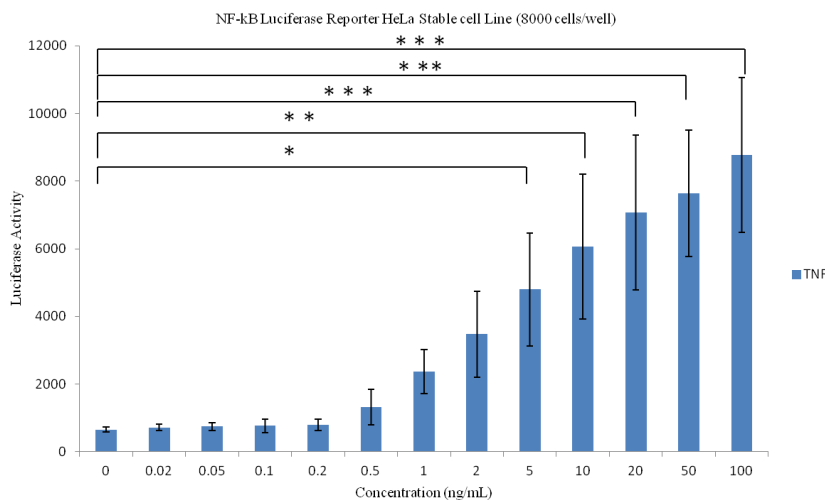
Figure 3-9: TNF-α induced a dose dependent NF-κB activation. NF-κB luciferase reporter HeLa stable cells were stimulated for 8 h with 0-100 ng/mL TNF-α prior to lysis and analysis of luciferase activity. Results represent means ± SD for three separate experiments performed in triplicate. *Statistical Significance *** p ≤ 0.001, ** p ≤ 0.01 and * p ≤ 0.05.*

3.3.7.1.3   The Effect of Freezing and Thawing

A freezing and thawing step is described in the Signosis protocol for the luciferase assay; the reason for this is not explained. This step follows the addition of lysis buffer to cells as described in section 2.11.1. It involves 15 min freezing at -80ºC then thawing at room temperature for another 15 min before adding the luciferase substrate. However, the Promega luciferase assay reagent protocol did not include a freezing-thawing step. To evaluate the effect of this step on relative luciferase activity, cells were seeded in two plates and treated as described in section 2.11.2.3. As shown in Figure 3-10, TNF-α induced NF-κB activation in both conditions, however, the luciferase activity was of higher intensity when freeze-thaw step was utilised. For this reason, this step was used for all subsequent experiments.
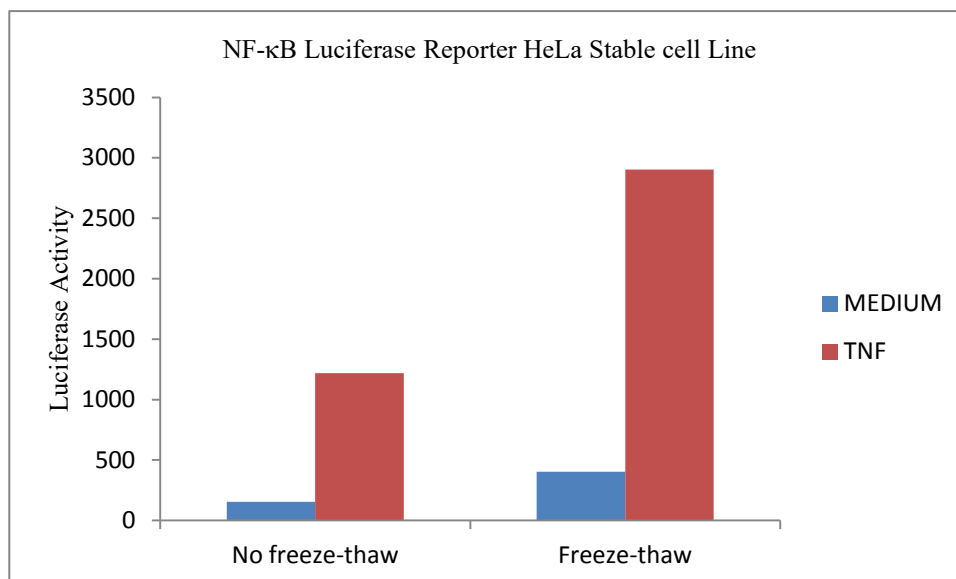
Figure 3-10: Effect of freeze-thaw cycle of TNF-α-induced NF-κB activation. NF-κB luciferase reporter HeLa stable cells were stimulated for 8 h with 20 ng/mL TNF-α prior to lysis and analysis of luciferase activity without or with a freeze-thaw step. (N=1)

3.3.7.2   Penetratin and Pen-NBD inhibit TNF-α-induced NF-κB activation

Western blotting showed that incubation of HeLa cells with TNF-α was accompanied by NF-κB activation, assessed by the degradation of IκB-α (Figure 3-5). However, using this assay, pre-incubation with Pen-NBD at 100 μM was unable to prevent TNF-α-induced degradation of IκB-α. To evaluate the ability of this chimera to interfere with the TNF-α-induced activation of NF-κB, luciferase activity was assessed using the reporter cell line as described in section 2.11.1. Cells were incubated with various concentrations of Pen-NBD chimera, penetratin and serial dilutions of DMSO were also included as controls. From three independent experiments, pretreatment of the cells with Pen-NBD, as well as with penetratin, induced inhibition in TNF-α-stimulated NF-κB activity that was clearly identified at 100 μM (Figure 3-11D). This suggests that the reduced luciferase activity in TNF-α-stimulated cells is not specific to the NBD-inhibitory cargo and that penetratin alone can decrease the

transcriptional activity of NF-κB in TNF-α-stimulated cells. Surprisingly, the data also showed inhibition of TNF-α-stimulated NF-κB activity in cells pretreated with 2% DMSO (the concentration of DMSO present in 100 μM peptides). The difference between groups was statistically significant by one-way ANOVA $F(12, 26) = 5.634$, $p = 0.0001$. Tukey post-hoc tests revealed that the reduction in luciferase activity was statistically significant in cells pretreated with 100 μM penetratin, 100 μM Pen-NBD or 2% DMSO compared to those treated with TNF-α alone ($p < 0.01$).

(A)

NF-κB Luciferase Reporter HeLa Stable Cell Line

(B)

NF-κB Luciferase Reporter HeLa Stable Cell Line

(C)

NF-κB Luciferase Reporter HeLa Stable Cell Line

(D)
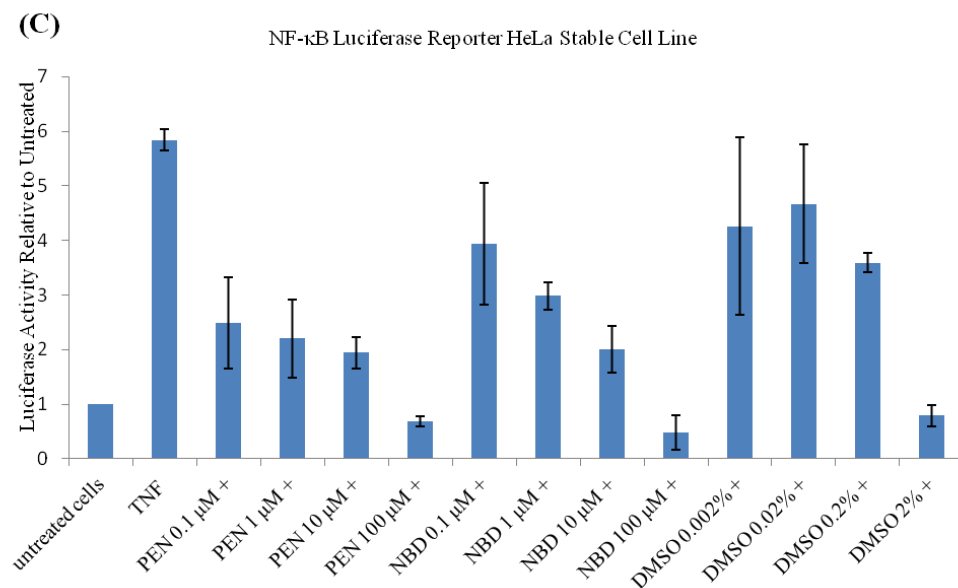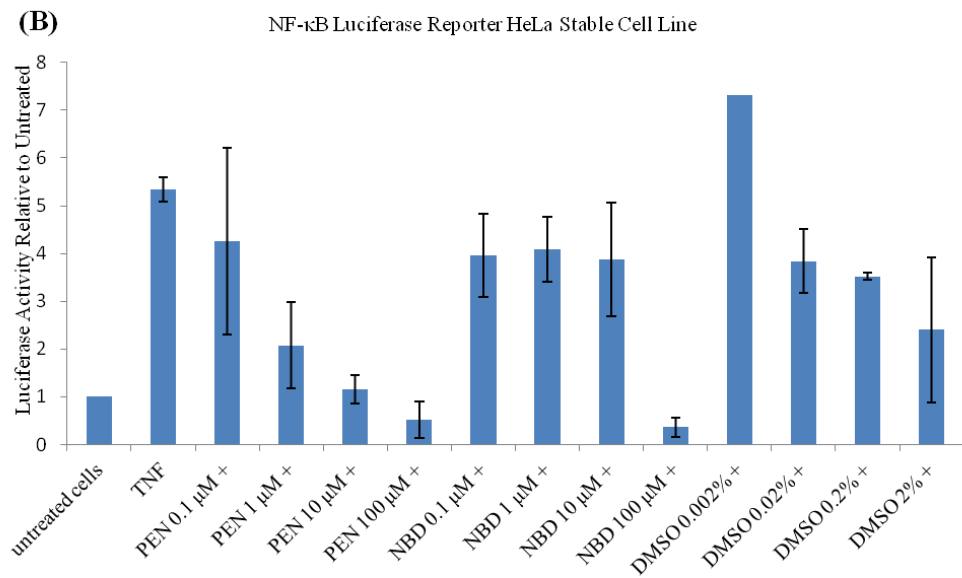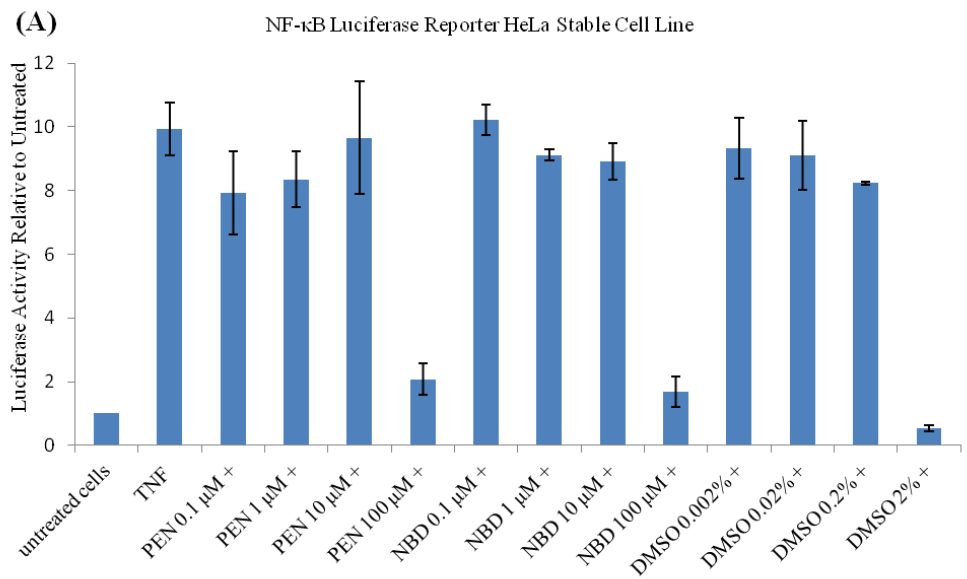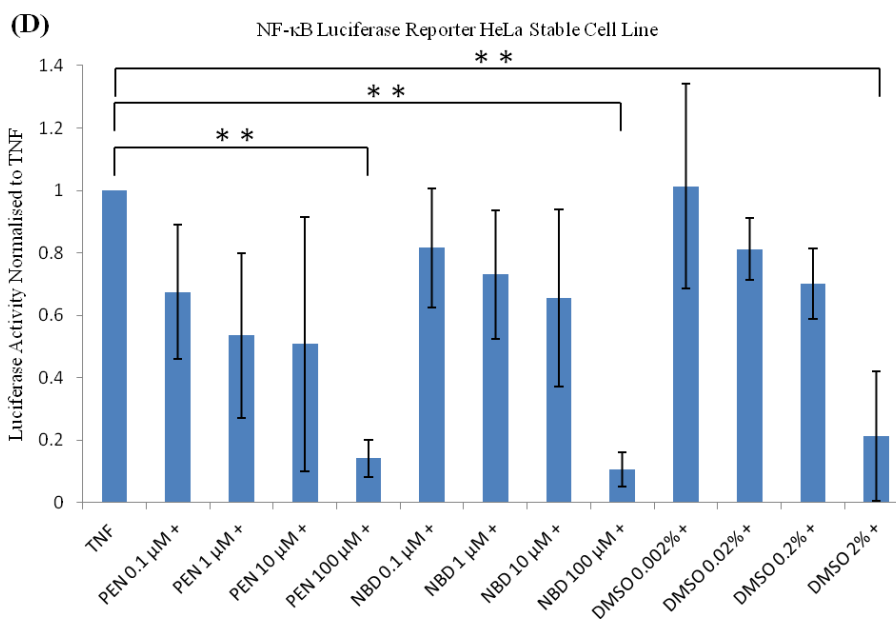
Figure 3-11: TNF-α-induced NF-κB activation is inhibited by Pen-NBD chimera (NBD) and penetratin. Peptide-treated cells were incubated with various concentrations of Pen-NBD (NBD), penetratin (PEN) or DMSO (diluent control) for 2 h before TNF-α (20 ng/mL) was added. Luciferase activity was measured 8 h later. (A, B & C) single experiments performed in triplicate and (D) are means ± SD for the three separate experiments, A-C. *Statistical Significance ** p ≤ 0.01.*

3.3.7.3   Effect of penetratin and R8 on NF-κB activity

The results from the previous section suggest a role for penetratin and also the peptide diluent (DMSO) in inhibiting NF-κB activity in the NF-κB Luciferase Reporter HeLa stable cell line. A study by Fotin-Mleczek *et al.* showed that three cationic CPPs- penetratin, Tat and nona-arginine interfered with TNF-α-mediated signal transduction (Fotin-Mleczek *et al.*, 2005). To examine the effect of an alternative and very cationic CPP on NF-κB activity *in vitro*, the experiments described in section 3.3.7.2 were repeated using R8. Cells were exposed to various concentrations of R8 (0.1-100 µM) for 2 h. Cells were also treated with 100 µM penetratin or 2% DMSO. Figure 3-12D confirms that 100 µM penetratin and 2% DMSO inhibited TNF-α induced NF-κB transcriptional

activity. This suggests that the diminished NF-κB activity can be due to a diluent effect rather than the peptides used here. The difference between cells pretreated with various concentrations of R8 (dissolved in dH_2O) and cells treated with TNF-α was not statistically significant as confirmed using one-way ANOVA analysis ($p < 0.05$).

.
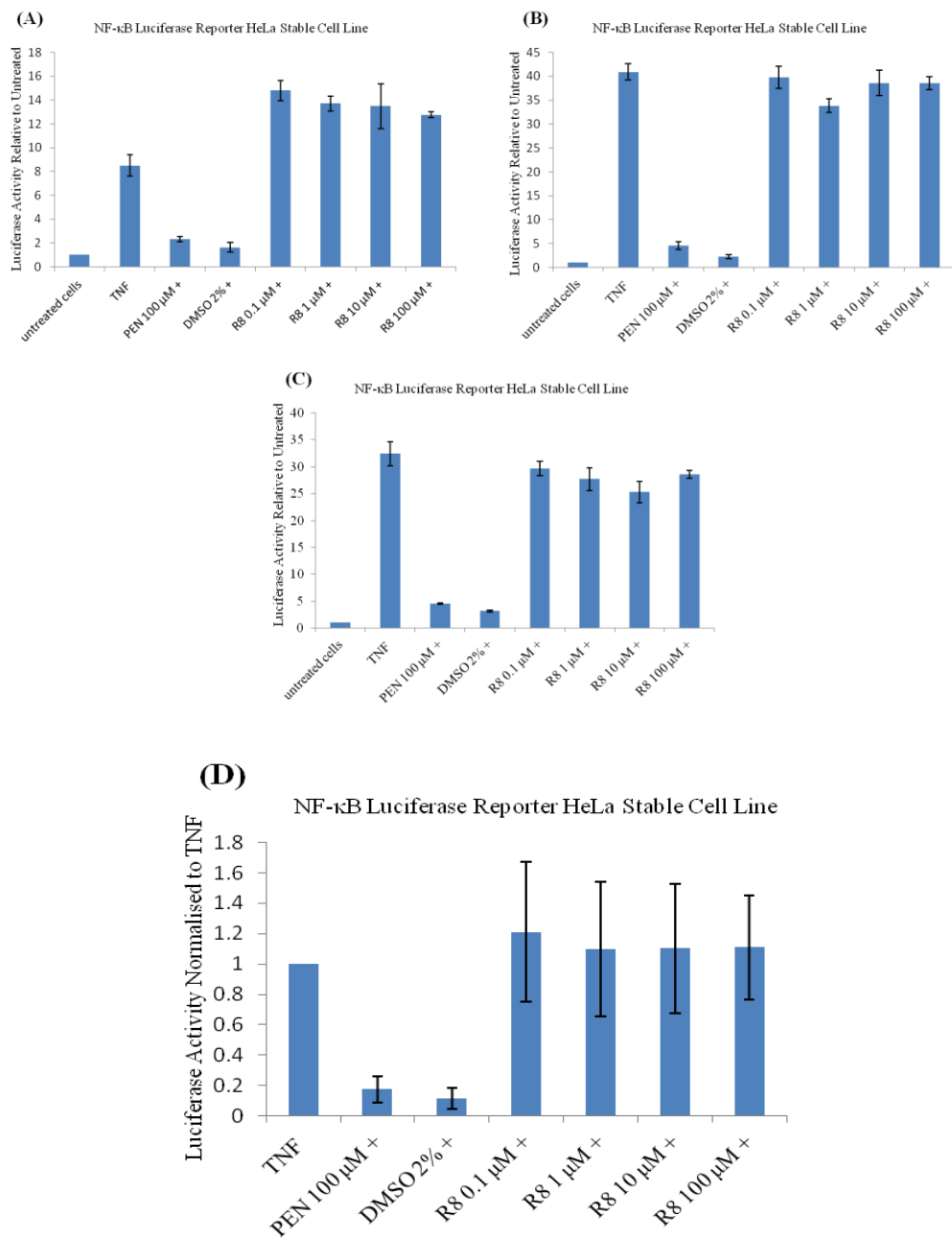
Figure 3-12: Effect of cationic CPPs (penetratin and R8) on TNF-α-induced NF-κB activation. Peptide-treated cells were incubated with various concentrations of R8, penetratin (100 μM) or DMSO (diluent control of penetratin) for 2 h before TNF-α (20 ng/mL) was added. Luciferase activity was measured 8 h later. (A, B & C) single experiments performed in triplicate and (D) are means ± SD for the three separate experiments, A-C.

3.3.8   F-NBD-Pen sequence

One of the aims of this study was to investigate the possibility of designing new CPP chimeras to target NF-κB signalling. The data shown in this chapter together with the fact that the pen-NBD peptide was insoluble in aqueous solutions was a major concern and only one more peptide sequence was investigated with sequence Ac-**F**TALDWSWLQTERQIKIWFQNRRMKWKK-amide and termed F-NBD-Pen. The sequence was chosen based on the fact that the Jones laboratory had discovered that phenylalanine on the N-terminus of a short peptide cargo had pronounced positive effects on cell uptake (Watkins *et al*., 2011). The NBD sequence lies at the N-terminus of F-NBD-Pen and additionally a phenylalanine residue that sits naturally at the N-terminus of the IKKγ NEMO binding domain occurring before the NBD sequence was included to see if this could influence cell uptake and allow us to perform experiments at much lower concentrations- thus reducing the DMSO effect.

Unfortunately, F-NBD-Pen precipitated out of solution immediately upon addition to aqueous medium from a DMSO stock and no further experiments were performed with it.

3.4   Discussion

Elevated NF-κB activity can lead to inflammatory diseases and cancer (Baltimore, 2011) and CPPs have been widely studied as delivery vectors for a variety of macromolecules including therapeutic peptides (Milletti, 2012). For this reason, a range of CPPs have been used to deliver NF-κB targeting

peptides including the NBD inhibitory peptide used here (sections 1.7.2 and 3.1). The initial goal of this study was to assess the inhibitory effect of Pen-NBD peptide in TNF-α-stimulated (NF-κB activated) cells. The work also allowed for analyses of the effects of penetratin alone and another cationic CPP (R8) on NF-κB activity in a TNF-α-stimulated NF-κB luciferase reporter cell line.

TNF-α was used to activate the canonical NF-κB pathway measured initially using Western blotting for the IκB-α protein whose degradation was rapid and clearly visible after 10 minutes of TNF-α addition. Complete loss of the band, indicative of extensive proteasomal degradation, was observed after 30 and 60 min incubation. The IκB-α band reappeared after 4 h incubation due to resynthesis. This occurs because NF-κB activation is transient and the IκB-α gene is inducible by NF-κB which produces an inhibitory feedback loop (Baltimore, 2011). The fact that TNF-α mediates rapid NF-κB activation and a strong negative feedback regulation resulted in an oscillatory NF-κB activation profile. This leads to the alternating regulation of IκB-α expression seen in Figure 3-5 and in the literature (Smale, 2011).

The effect of TNF-α on IκB-α degradation was not affected by overnight serum starvation. To our knowledge the effect of serum starvation on TNF-α-induced IκB-α degradation has not been previously explored in NBD literature and with this knowledge, it is easier to compare the results from other TNF-α studies carried out in the presence or absence of serum or where serum information is not provided.

Serum is also known to affect CPP performance; especially cationic variants (Kosuge *et al*., 2008, Jones and Sayers, 2012). For example internalisation of CPPs can be reduced in the presence of serum due to non specific binding of the CPP to serum proteins such as albumin thus reducing the amount of peptide that can interact with the cell. The effects of serum on CPP or CPP-cargo internalisation will be further discussed in chapters 4 and 5.

In HeLa cells, TNF-α activated the NF-κB classical signalling pathway at 1 ng/mL, approximately 10 fold lower than commonly used concentration of this cytokine. This is in line with data showing strong NF-κB activity even at 0.1 ng/mL in immortalized 3T3 mouse embryonic fibroblasts (MEFs) (Cheong *et al*., 2006). Thus, with an assay available to measure NF-κB activation, the NBD peptide was selected as a targeting entity for this activity and penetratin as the CPP. Pen-NBD peptide is commercially available and well described in the literature to influence NF-κB activity, albeit at high concentrations (May *et al*., 2000). The ability of Pen-NBD peptide to prevent the degradation of IκB-α in TNF-α-stimulated cells was initially assessed by Western blotting and surprisingly the data showed no effect in TNF-α-stimulated cells. This is in contrast to claims that pretreatment of SCCVII cells with Pen-NBD for 30 min prior to TNF-α stimulation for 15 min inhibited TNF-α-induced p65 phosphorylation and IκB-α degradation (Furuta *et al*., 2012). Another study used an immune-complex kinase assay to show that high, 100 and 200 μM, concentrations of Pen-NBD peptide reduced TNF-α-induced IKK activity (May *et al*., 2000). It has also been reported that pretreatment of dendritic cells

with 50 μM Pen-NBD peptide inhibited the phosphorylation of IκB-α and reduced the level of phospho-IκB-α in LPS-stimulated cells. Surprisingly, the data showed that although LPS stimulation reduced total IκB-α protein, the Pen-NBD peptide appeared to be unable to rescue IκB-α levels, despite inhibiting its phosphorylation (Tas *et al.*, 2005). The difference in results from these studies and those produced in this thesis could be due to several factors including cell types but even at 100 μM, Pen-NBD was unable to rescue IκB-α degradation when HeLa cells were treated with TNF-α. Interestingly, and conversely, the results for the NF-κB reporter HeLa cell line showed a significant reduction in TNF-α-induced luciferase activity when cells were pre-treated with the peptide at 100 μM. These findings support published findings of SCCVII cells transiently transfected with PBII x luciferase reporter plasmid that were pre-treated with Pen-NBD prior to TNF-α stimulation. In these cells, Pen-NBD (40 μM) suppressed TNF-α-induced transcriptional activity (Furuta *et al.*, 2012). Another study showed that Pen-NBD (10 μM and 100 μM) could inhibit luciferase activity in IL-1β-stimulated HeLa cells transiently transfected with NF-κB luciferase reporter plasmid, however, cytotoxicity was observed at 100 μM (Khaja and Robbins, 2010). In this study, pretreatment of the same reporter HeLa cells with NBD peptides conjugated with Tat, 8K, 6R, PTD-5 and K-FGF (100 μM) for 3 h significantly inhibited luciferase activity after IL-1β stimulation.

A reduction in luciferase activity was also observed in our stable HeLa cells pre-treated with penetratin alone. These findings are in agreement with the

results of Letoha *et al*., who in 2006 demonstrated that penetratin could inhibit NF-κB transcriptional activity in mouse L929 fibroblasts and RAW 264.7 macrophages transformed with pNF-kB-luc4. Pretreating these cells with 25 μM penetratin for 30 min before TNF-α or LPS stimulation caused a significant reduction in NF-κB transcriptional activity. The penetratin studies were also extended in a rat model of cholecystokinin octapeptide (CCK) induced-acute pancreatitis in which activation and nuclear translocation of NF-κB peaks at 30 min after CCK administration. Western blotting of pancreas samples were performed and showed that penetratin pre-treatment prevented degradation of IκB-α whereas, a glycine mutant analogue of penetratin devoid of positive charges did not have any effect on NF-κB activity (Letoha *et al*., 2006). According to these results and earlier results by Bolton *et al.* (2000), penetratin could be considered to have intrinsic biological activity rather than just being an inert delivery vector. They reported that direct injection of penetratin into rat brain induced neurotoxic effects in a dose-dependent pattern (Bolton *et al*., 2000). Fotin-Mleczek *et al*., (2005) also demonstrated that penetratin and nona-arginine could inhibit the TNF-α-mediated signal transduction. Preincubation of HeLa cells with penetratin reduced the TNF-α/cycloheximide-induced caspase activity and protected cells against apoptosis. Penetratin and nona-arginine also inhibited TNF-α-induced IL-8 secretion in TNF-α-stimulated HeLa cells and in absence of cycloheximide. Both peptides were able to inhibit the translocation of p65 from the cytoplasm into the nucleus in TNF-α-stimulated cells. They concluded that penetratin was found to induce the endocytosis of TNF-α receptors through a dynamin-dependent manner without

the activation of the receptor (Fotin-Mleczek *et al.*, 2005). These separate findings could explain the reduced luciferase activity in cells preincubated with penetratin before TNF-α stimulation seen in Figure 3-11. Penetratin alone could have potentiated the effect of the NBD inhibitory peptide cargo, by inducing receptor internalization and inhibiting TNF-α-dependent signal transduction. Alternatively, penetratin-induced receptor internalization (without receptor activation) could cause reduced NF-kB transcriptional activity measured by the luciferase assay i.e. the penetratin exerts an inhibitory effect independent of the NBD cargo. Using a mutant NBD sequence would provide more information about the different contributing effects of the CPP and the cargo and previously used is the NBD sequence where the tryptophans are replaced with alanines- TALD<u>W</u>S<u>W</u>LQTE to TALD<u>A</u>S<u>A</u>LQTE (di Meglio *et al.*, 2005, Ianaro *et al.*, 2009, Khaja and Robbins, 2010, Gaurnier-Hausser *et al.*, 2011, Furuta *et al.*, 2012). This was not tested in this study but it is questionable whether this represents a true control bearing in mind that a W-A mutation twice in the same short sequence, could very easily influence cell binding and uptake rather than just binding with NEMO once internalised into the cytosol. In support of this is that tryptophan residues have previously been shown to influence CPP interactions with artificial membranes and also cells (Mishra *et al.*, 2011, Jones and Sayers, 2012).

Davé *et al.* (2007) showed that a CPP consisting of eight lysine residues (8K) was able to transduce the NBD inhibitory peptide into cells and tissues. In HEK293 cells stably transfected with a multimerized NF-κB DNA binding element-luciferase reporter gene, pretreatment with 8K-NBD for 1 h before

TNF-α stimulation caused a dose-dependent inhibition of NF-κB activity. It should, however, be noted that no effect were seen below 50 μM and 400 μM of peptide was needed to show maximal effects. The effect of the 8K CPP alone on TNF-α-stimulated NF-κB reporter cells was not examined.

One unanticipated finding was that DMSO alone caused a reduction in luciferase activity in TNF-α-stimulated NF-κB reporter cells. Pen-NBD and penetratin were dissolved in DMSO to a final stock concentration of 5 mM according to the manufacturer's instructions. In other published studies, higher stock solutions of Pen-NBD were prepared in DMSO: 20 mM (May *et al.*, 2000) and 50 mM (Tas *et al.*, 2005). Pen-NBD has also been solubilised in saline but to what concentration was not noted (Dasgupta *et al.*, 2004). In previous studies evaluating the effect of Pen-NBD or other CPPs-NBD chimeras, there was little mention of any DMSO effects. This may have been due to the use of lower DMSO concentrations in these studies. However, in this chapter, the effect of DMSO was consistently evaluated as a peptide diluent, in volumes equal to the volumes used for different peptides concentrations. DMSO is one of the most common solvents used to dissolve hydrophobic compounds for *in vitro* and *in vivo* experimental studies (Santos *et al.*, 2003) and previous studies have shown that DMSO can exert a wide range of pharmacological effects in experimental animal models. This includes nociception and inflammation depending on route of administration. Oral administration of DMSO produced reduced inflammation in zymosan-induced oedema in the mouse paw, whereas local administration of DMSO alongside zymosan enhanced the inflammatory response in the same mouse model. This

provides evidence that the anti-inflammatory effect of DMSO can be masked by its ability to transport drugs and chemicals across tissue membranes and facilitate the drug diffusion in cellular tissues (Colucci *et al*., 2008). A study by Kelly *et al.* in histiocytic lymphoma cell line, J774, demonstrated that pretreating cells with 2% DMSO 15 min prior to LPS exposure reduced the level of NF-κB activation. DMSO alone had no stimulatory effect on NF-κB activation (Kelly *et al*., 1994). This could be a possible explanation for our results in which 2% DMSO (equivalent to the volume in 100 μM Pen-NBD and penetratin) reduced the TNF-α-induced NF-κB activation (Figure 3-11). Time of exposure to DMSO may also be an important variable. In the earlier noted study by Kelly *et al.*, the cells were treated with DMSO for 15 min, however, in the experiments for Figures 3-11 and 3-12, the cells were pretreated with DMSO for 2 h prior to TNF-α stimulation. DMSO (10%) has also been used as a penetration enhancer in cellular uptake of Tat and was found to increase the uptake of FITC-labelled Tat and Tat-GFP fusion protein (Wang *et al*., 2010). Although the concentration of DMSO in the Tat study is higher than the highest DMSO concentration in experiments used in this thesis (2%), it suggests that the presence of DMSO may enhance the uptake of penetratin and Pen-NBD peptides, and consequently, increases their non-specific and possibly specific effects.

R8 effects on TNF-α-induced NF-κB activation in the reporter cells were assessed in this thesis but no reduction in luciferase activity was observed up to 100 μM. From this, it can be inferred that not all commonly used CPPs affect

NF-κB activity and that the effects observed in Figure 3-11 are mainly due to the influence of DMSO.

3.5   Conclusions

The initial aims of this chapter were to develop models for analysing activation of NF-κB and to then look at CPP mediated delivery of peptides that inhibit NF-κB inhibition. Present in the literature are sequences that have been shown to have effects but only at high concentrations. Two assays were successfully developed and are now available in the laboratory for subsequent studies. As a control peptide, the commercial Pen-NBD sequence was used and data from the few studies that were conducted raise important questions regarding a number of factors that could influence the data including: the influence of the CPP alone, the specifics of the assays with respects to when and how long the reagents are included with cells, the choice of cell lines, the solubility of the peptides and the influence of diluents. All in all this makes data interpretation very difficult and also results in a significant challenge for those comparing similar work in the literature. Further work with NF-κB targeting peptides was not performed.

3.6   References

BALTIMORE, D. 2011. NF-[kappa] B is 25. *Nature immunology,* 12**,** 683-685.

BHARTI, A. C. & AGGARWAL, B. B. 2002. Nuclear factor-kappa B and cancer: its role in prevention and therapy. *Biochem Pharmacol,* 64**,** 883-888.

BLAKE, D. J., WEIR, A., NEWEY, S. E. & DAVIES, K. E. 2002. Function and genetics of dystrophin and dystrophin-related proteins in muscle. *Physiological reviews,* 82**,** 291-329.

BOLTON, S. J., JONES, D. N., DARKER, J. G., EGGLESTON, D. S., HUNTER, A. J. & WALSH, F. S. 2000. Cellular uptake and spread of the cell-permeable peptide penetratin in adult rat brain. *European Journal of Neuroscience,* 12**,** 2847-2855.

CHEONG, R., BERGMANN, A., WERNER, S. L., REGAL, J., HOFFMANN, A. & LEVCHENKO, A. 2006. Transient IκB kinase activity mediates temporal NF-κB dynamics in response to a wide range of tumor necrosis factor-α doses. *Journal of Biological Chemistry,* 281**,** 2945-2950.

CHOI, M., ROLLE, S., WELLNER, M., CARDOSO, M. C., SCHEIDEREIT, C., LUFT, F. C. & KETTRITZ, R. 2003. Inhibition of NF-kappaB by a TAT-NEMO-binding domain peptide accelerates constitutive apoptosis and abrogates LPS-delayed neutrophil apoptosis. *Blood,* 102**,** 2259-2267.

COLUCCI, M., MAIONE, F., BONITO, M. C., PISCOPO, A., DI GIANNUARIO, A. & PIERETTI, S. 2008. New insights of dimethyl sulphoxide effects (DMSO) on experimental in vivo models of nociception and inflammation. *Pharmacological Research,* 57**,** 419-425.

COSTELLI, P., CARBO, N., TESSITORE, L., BAGBY, G. J., LÓPEZ-SORIANO, F. J., ARGILES, J. & BACCINO, F. M. 1993. Tumor necrosis factor-alpha mediates changes in tissue protein turnover in a rat cancer cachexia model. *Journal of Clinical Investigation,* 92**,** 2783-2789.

DASGUPTA, S., JANA, M., ZHOU, Y., FUNG, Y. K., GHOSH, S. & PAHAN, K. 2004. Antineuroinflammatory effect of NF-κB essential modifier-binding domain peptides in the adoptive transfer model of experimental allergic encephalomyelitis. *The Journal of Immunology,* 173**,** 1344-1354.

DAVIS, R. E., BROWN, K. D., SIEBENLIST, U. & STAUDT, L. M. 2001. Constitutive nuclear factor κB activity is required for survival of activated B cell–like diffuse large B cell lymphoma cells. *The Journal of experimental medicine,* 194**,** 1861-1874.

DAVÉ, S. H., TILSTRA, J. S., MATSUOKA, K., LI, F., KARRASCH, T., UNO, J. K., SEPULVEDA, A. R., JOBIN, C., BALDWIN, A. S. & ROBBINS, P. D. 2007. Amelioration of chronic murine colitis by peptide-mediated transduction of the IκB kinase inhibitor NEMO binding domain peptide. *The Journal of Immunology,* 179**,** 7852-7859.

DI MEGLIO, P., IANARO, A. & GHOSH, S. 2005. Amelioration of acute inflammation by systemic administration of a cell-permeable peptide inhibitor of NF-κB activation. *Arthritis & Rheumatism,* 52**,** 951-958.

ETHRIDGE, R. T., HASHIMOTO, K., CHUNG, D. H., EHLERS, R. A., RAJARAMAN, S. & EVERS, B. M. 2002. Selective inhibition of NF-κB attenuates the severity of cerulein-induced acute pancreatitis. *Journal of the American College of Surgeons,* 195**,** 497-505.

FOTIN-MLECZEK, M., WELTE, S., MADER, O., DUCHARDT, F., FISCHER, R., HUFNAGEL, H., SCHEURICH, P. & BROCK, R. 2005. Cationic cell-penetrating peptides interfere with TNF signalling by induction of TNF receptor internalization. *J Cell Sci,* 118**,** 3339-3351.

FURUTA, H., OSAWA, K., SHIN, M., ISHIKAWA, A., MATSUO, K., KHAN, M., AOKI, K., OHYA, K., OKAMOTO, M. & TOMINAGA, K. 2012. Selective inhibition of NF-κB suppresses bone invasion by oral squamous cell carcinoma in vivo. *International Journal of Cancer,* 131**,** E625-E635.

GAURNIER-HAUSSER, A., PATEL, R., BALDWIN, A. S., MAY, M. J. & MASON, N. J. 2011. NEMO-binding domain peptide inhibits constitutive NF-κB activity and reduces tumor burden in a canine model of relapsed, refractory diffuse large B-cell lymphoma. *Clinical Cancer Research,* 17**,** 4661-4671.

HADDAD, R. I. & SHIN, D. M. 2008. Recent advances in head and neck cancer. *New England Journal of Medicine,* 359**,** 1143-1154.

HAYDEN, M. S. & GHOSH, S. 2008. Shared principles in NF-kappaB signaling. *Cell,* 132**,** 344-362.

HORIUCHI, T., MITOMA, H., HARASHIMA, S., TSUKAMOTO, H. & SHIMODA, T. 2010. Transmembrane TNF-alpha: structure, function and interaction with anti-TNF agents. *Rheumatology (Oxford),* 49**,** 1215-1228.

IANARO, A., TERSIGNI, M., BELARDO, G., DI MARTINO, S., NAPOLITANO, M., PALMIERI, G., SINI, M., DE MAIO, A., OMBRA, M. & GENTILCORE, G. 2009. NEMO-binding domain peptide inhibits proliferation of human melanoma cells. *Cancer letters,* 274**,** 331-336.

JIMI, E., FURUTA, H., MATSUO, K., TOMINAGA, K., TAKAHASHI, T. & NAKANISHI, O. 2011. The cellular and molecular mechanisms of bone invasion by oral squamous cell carcinoma. *Oral diseases,* 17**,** 462-468.

JONES, A. T. & SAYERS, E. J. 2012. Cell entry of cell penetrating peptides: tales of tails wagging dogs. *Journal of Controlled Release,* 161**,** 582-591.

KARIN, M. 2006. Nuclear factor-kappaB in cancer development and progression. *Nature,* 441**,** 431-436.

KARIN, M., CAO, Y., GRETEN, F. R. & LI, Z.-W. 2002. NF-κB in cancer: from innocent bystander to major culprit. *Nature reviews cancer,* 2**,** 301-310.

KELLY, K. A., HILL, M. R., YOUKHANA, K., WANKER, F. & GIMBLE, J. M. 1994. Dimethyl sulfoxide modulates NF-kappa B and cytokine activation in lipopolysaccharide-treated murine macrophages. *Infection and immunity,* 62**,** 3122-3128.

KHAJA, K. & ROBBINS, P. 2010. Comparison of functional protein transduction domains using the NEMO binding domain peptide. *Pharmaceuticals,* 3**,** 110-124.

KOSUGE, M., TAKEUCHI, T., NAKASE, I., JONES, A. T. & FUTAKI, S. 2008. Cellular internalization and distribution of arginine-rich peptides as a function of extracellular peptide concentration, serum, and plasma membrane associated proteoglycans. *Bioconjug Chem,* 19**,** 656-664.

LENZ, G., DAVIS, R. E., NGO, V. N., LAM, L., GEORGE, T. C., WRIGHT, G. W., DAVE, S. S., ZHAO, H., XU, W. & ROSENWALD, A. 2008. Oncogenic CARD11 mutations in human diffuse large B cell lymphoma. *Science,* 319**,** 1676-1679.

LETOHA, T., KUSZ, E., PAPAI, G., SZABOLCS, A., KASZAKI, J., VARGA, I., TAKACS, T., PENKE, B. & DUDA, E. 2006. In vitro and in vivo nuclear factor-κB inhibitory effects of the cell-penetrating penetratin peptide. *Molecular pharmacology,* 69**,** 2027-2036.

LI, X., YANG, Y. & ASHWELL, J. D. 2002. TNF-RII and c-IAP1 mediate ubiquitination and degradation of TRAF2. *Nature,* 416**,** 345-347.

MACHLEIDT, T., WIEGMANN, K., HENKEL, T., SCHÜTZE, S., BAEUERLE, P. & KRÖNKE, M. 1994. Sphingomyelinase activates proteolytic I kappa B-alpha degradation in a cell-free system. *Journal of Biological Chemistry,* 269**,** 13760-13765.

MAY, M. J., D'ACQUISTO, F., MADGE, L. A., GLÖCKNER, J., POBER, J. S. & GHOSH, S. 2000. Selective inhibition of NF-kappaB activation by a peptide that blocks the interaction of NEMO with the IkappaB kinase complex. *Science,* 289**,** 1550-1554.

MILLETTI, F. 2012. Cell-penetrating peptides: classes, origin, and current landscape. *Drug Discov Today,* 17**,** 850-860.

MISHRA, A., LAI, G. H., SCHMIDT, N. W., SUN, V. Z., RODRIGUEZ, A. R., TONG, R., TANG, L., CHENG, J., DEMING, T. J. & KAMEI, D. T. 2011. Translocation of HIV TAT peptide and analogues induced by

multiplexed membrane and cytoskeletal interactions. *Proceedings of the National Academy of Sciences,* 108**,** 16883-16888.

MOON, D.-O., JIN, C.-Y., LEE, J.-D., CHOI, Y. H., AHN, S.-C., LEE, C.-M., JEONG, S.-C., PARK, Y.-M. & KIM, G.-Y. 2006. Curcumin Decreases Binding of Shiga-Like Toxin-1B on Human Intestinal Epithelial Cell Line HT29 Stimulated with TNF-. ALPHA. and IL-1. BETA.: Suppression of p38, JNK and NF-. KAPPA. B p65 as Potential Targets. *Biological and Pharmaceutical Bulletin,* 29**,** 1470-1475.

NAUGLER, W. E. & KARIN, M. 2008. NF-κB and cancer—identifying targets and mechanisms. *Current opinion in genetics & development,* 18**,** 19-26.

NDIKUYEZE, G. H., GAURNIER-HAUSSER, A., PATEL, R., BALDWIN, A. S., MAY, M. J., FLOOD, P., KRICK, E., PROPERT, K. J. & MASON, N. J. 2014. A phase I clinical trial of systemically delivered NEMO binding domain peptide in dogs with spontaneous activated B-cell like diffuse large B-cell lymphoma. *PloS one,* 9**,** e95404.

ORANGE, J. S. & MAY, M. J. 2008. Cell penetrating peptide inhibitors of nuclear factor-kappa B. *Cell Mol Life Sci,* 65**,** 3564-3591.

OZES, O. N., MAYO, L. D., GUSTIN, J. A., PFEFFER, S. R., PFEFFER, L. M. & DONNER, D. B. 1999. NF-κB activation by tumour necrosis factor requires the Akt serine–threonine kinase. *Nature,* 401**,** 82-85.

PETERSON, J. M., KLINE, W., CANAN, B. D., RICCA, D. J., KASPAR, B., DELFÍN, D. A., DIRIENZO, K., CLEMENS, P. R., ROBBINS, P. D. & BALDWIN, A. S. 2011. Peptide-based inhibition of NF-κB rescues diaphragm muscle contractile dysfunction in a murine model of Duchenne muscular dystrophy. *Molecular Medicine,* 17**,** 508-515.

POPA, C., NETEA, M. G., VAN RIEL, P. L., VAN DER MEER, J. W. & STALENHOEF, A. F. 2007. The role of TNF-α in chronic inflammatory conditions, intermediary metabolism, and cardiovascular risk. *Journal of lipid research,* 48**,** 751-762.

SANTOS, N. C., FIGUEIRA-COELHO, J., MARTINS-SILVA, J. & SALDANHA, C. 2003. Multidisciplinary utilization of dimethyl sulfoxide: pharmacological, cellular, and molecular aspects. *Biochemical pharmacology,* 65**,** 1035-1041.

SMALE, S. T. 2011. Hierarchies of NF-κB target-gene regulation. *Nat Immunol,* 12**,** 689-694.

STRICKLAND, I. & GHOSH, S. 2006. Use of cell permeable NBD peptides for suppression of inflammation. *Annals of the rheumatic diseases,* 65**,** iii75-iii82.

TAKADA, H., CHEN, N. J., MIRTSOS, C., SUZUKI, S., SUZUKI, N., WAKEHAM, A., MAK, T. W. & YEH, W. C. 2003. Role of SODD in regulation of tumor necrosis factor responses. *Mol Cell Biol,* 23**,** 4026-4033.

TAPIA, M. A., GONZÁLEZ-NAVARRETE, I., DALMASES, A., BOSCH, M., RODRIGUEZ-FANJUL, V., ROLFE, M., ROSS, J. S., MEZQUITA, J., MEZQUITA, C. & BACHS, O. 2007. Inhibition of the canonical IKK/NFκB pathway sensitizes human cancer cells to doxorubicin. *Cell Cycle,* 6**,** 2284-2292.

TARTAGLIA, L. A. & GOEDDEL, D. V. 1992. Two TNF receptors. *Immunol Today,* 13**,** 151-153.

TAS, S. W., DE JONG, E. C., HAJJI, N., MAY, M. J., GHOSH, S., VERVOORDELDONK, M. J. & TAK, P. P. 2005. Selective inhibition of NF-kappaB in dendritic cells by the NEMO-binding domain peptide blocks maturation and prevents T cell proliferation and polarization. *Eur J Immunol,* 35**,** 1164-1174.

TRAENCKNER, E., WILK, S. & BAEUERLE, P. 1994. A proteasome inhibitor prevents activation of NF-kappa B and stabilizes a newly phosphorylated form of I kappa B-alpha that is still bound to NF-kappa B. *The EMBO journal,* 13**,** 5433-5441.

VAN HORSSEN, R., TEN HAGEN, T. L. & EGGERMONT, A. M. 2006. TNF-alpha in cancer treatment: molecular insights, antitumor effects, and clinical utility. *Oncologist,* 11**,** 397-408.

WAJANT, H., PFIZENMAIER, K. & SCHEURICH, P. 2003. Tumor necrosis factor signaling. *Cell Death & Differentiation,* 10**,** 45-65.

WANG, H., ZHONG, C.-Y., WU, J.-F., HUANG, Y.-B. & LIU, C.-B. 2010. Enhancement of TAT cell membrane penetration efficiency by dimethyl sulphoxide. *Journal of Controlled Release,* 143**,** 64-70.

WATKINS, C. L., SAYERS, E. J., ALLENDER, C., BARROW, D., FEGAN, C., BRENNAN, P. & JONES, A. T. 2011. Co-operative membrane disruption between cell-penetrating peptide and cargo: implications for the therapeutic use of the Bcl-2 converter peptide D-NuBCP-9-r8. *Mol Ther,* 19**,** 2124-2132.

Chapter 4: Cellular Uptake and Viability assays of the EGFR-Derived Peptide- EJP-18

4.1 Introduction

Cancer cells which overexpress EGFR (ERbB1) have increased activation of downstream signalling pathways driving cell proliferation, survival, angiogenesis, and metastasis. Because of this, it is a very well studied member of the ErbB family of receptor tyrosine kinases and the target for several different therapeutic strategies based on small molecule drugs and biopharmaceuticals, including peptides. Though these, in some cases, have proved to be effective, there is still a need for better systems to target this receptor as anti-cancer therapy. For example, the development of drug resistance to small molecule drugs remains a major problem (Chen and Fu, 2011, Tartarone *et al.*, 2013).

EGFRs' extracellular ligand binding, dimerisation and intracellular tyrosine kinase domains are critical for receptor activation. This process begins when EGFR homo- or hetero-dimerisation is initiated by the binding of one of several ligands including EGF to the receptor extracellular binding domain. Subsequently, autophosphorylation by the kinase domain occurs leading to phosphorylation of other cytoplasmic substrates and activation of oncogenic signalling cascades (Sebastian *et al.*, 2006). Clinically approved strategies targeting EGFR include monoclonal antibodies directed towards its extracellular domain such as trastuzumab (Herceptin) and small molecule

tyrosine kinase inhibitors gefitinib and erlotinib (Hynes and MacDonald, 2009).

The role of the EGFR transmembrane region (corresponding to amino acids 622-644) was initially thought to be a passive anchor of the receptor to the membrane. However, it has been found that this region plays an important role in mediating EGF effects (Tanner and Kyte, 1999, Bennasroune *et al.*, 2004). Interestingly, studies based on construction of expression vectors encoding short fusion peptides encompassing the transmembrane domain of EGFR and ErbB2 (HER2) showed they could inhibit the autophosphorylation and subsequent signalling of these target receptors. Identical results were obtained using chemically synthesized shorter peptides corresponding to the hydrophobic core of their transmembrane domains (Bennasroune *et al.*, 2004).

The juxtamembrane (JM) region of EGFR (corresponding to amino acids 645-682   (**RRR**HIV**RKR**TL**RRLLQERELVEPLTPSGEAPNQALLRI**))   lies immediately downstream of the transmembrane region and harbours a tripartite nuclear localisation sequence (NLS) (**RRR**HIV**RKR**TL**RR,** amino acids 645-657); containing three clusters of basic amino acids, in bold. The NLS in the EGFR JM region is capable of mediating nuclear localization of EGFR (Hsu and Hung, 2007) and the JM region itself has functions relating to receptor dimerization, signalling and endocytosis (Hubbard, 2009, Jura *et al.*, 2009). Upstream of the JM region in the transmembrane domain lies the triplet LFM which when added to residues 645-59 of the JM region gives the peptide sequence 642-LFMRRRHIVRKRTLRRLL-659. As an unmodified peptide, it

would have a mass of 2421.0, and isoelectric point of 12.88 and net charge of 8.1 at pH 7.0 (pepcalc.com). Interestingly, the cationic (hydrophilic residues) are spaced between hydrophobic residues and based on other CPP sequences and findings that terminal hydrophobicity of CPPs influences peptide-cell interactions (Watkins *et al.*, 2011), it was hypothesised that this peptide, termed EJP-18, could have interesting properties including membrane binding ability and that it may be able to internalise into cells. If it gained access to the cell cytosol, it could potentially interfere with EGFR signalling and the NLS within the sequence may drive it to the nucleus. Of interest is that Thr654 of EGFR (residue 13 of EJP-18) is phosphorylated and this was found to be required for nuclear localisation of the receptor that occurs following irradiation (Dittmann *et al.*, 2010). The same study demonstrated that a short peptide termed T654 from this region of EGFR (RKRTLRRLK) entered cells as a fluorescein labelled conjugate and when added as a Threonine phosphorylated entity, it could also inhibit nuclear localization of EGFR following irradiation. Confocal microscopy data were rather inconclusive with respects to subcellular localisation of the labelled peptide. Microscopy experiments were performed 16 h after peptide addition and there was no information as to whether they were fixed or imaged as live cells. It should also be noticed that the C-terminal lysine in T654 was added solely for labelling with fluorescein and in EGFR this residue is hydrophobic (L). In conclusion, it appeared that T654 was internalising into cells and acting as a short bioportide.

As described in section 1.8.3, bioportides are peptide sequences that have intrinsic cell penetration capacity and bioactivity when located in the

cytoplasm. Attempts have been made to deliver other EGFR cytosolic domain sequences to influence EGFR signalling (Kuroda *et al*., 2013). In another study, a short peptide sequence SVDNPHVC from the cytosolic domain of EGFR that is involved in dimerization was shown as a Tat-chimera to enhance EGFR degradation (Ahsan *et al*., 2013). It should be noted that the peptide, termed Disruptin, was added at a final concentration of 125 µM to show maximum effect that was first noted at 12.5 µM.

Immediately prior to my period in the laboratory, EJP-18 had been purchased as a Rhodamine-labelled peptide and very preliminary live cell confocal microscopy studies were performed in HeLa and KG1a cells by Dr Edward Sayers. These two cell lines are routinely used in the laboratory for CPP studies. It was immediately apparent that this peptide was very effectively internalised into cells but at concentrations of 20 µM in KG1a cells, there was also evidence for the occurrence of plasma membrane perturbation (Figure 4-1).
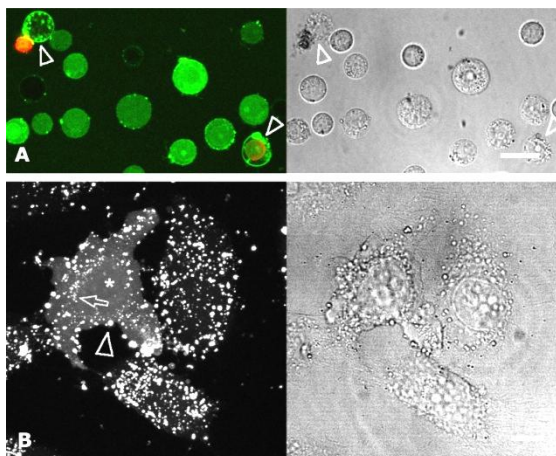
Figure 4-1: Uptake of Rh-EJP-18 peptide into cells after 1 h incubation in CM. (A) KG1a cells were incubated with 20 µM Rh-EJP-18 (pseudocoloured green) for 1 h in CM containing the cell permeable dye DRAQ7 (red). The cells were then analysed by live cell imaging confocal microscopy. All the cells contained cytoplasmic peptide labelling and some (arrowheads) had gross morphological damage and thus DRAQ7 positive. The DRAQ7$^+$ nucleus has been expelled from the cell at the top left of the image. *Scale Bars = 20 µm.* (B) HeLa cells were treated with 10 µM peptide in SFM for 1 h, washed and imaged in imaging medium containing DRAQ7 by confocal microscopy. Large punctate structures were observed inside the cells (arrows), on the plasma membrane (arrowheads) and in the cytosol of the cell labelled with an asterisk. *Scale bars = 10 µm.* Figure kindly supplied by Dr Edward Sayers.

4.2 Summary, Aims and Objectives

The search for new membrane active peptides that could then be termed as CPPs for delivering therapeutics or as bioportides is an ongoing process. EJP-18 (Table 2-1) represented a novel peptide with interesting physical characteristics beyond that afforded by T654 and was clearly entering cancer cells and labelling intracellular vesicles. The aims of this chapter were to further characterise the cellular uptake and toxicity of the new sequence-EJP-18.

The objectives of this chapter were to:

1- Analyse the effect of EJP-18 and its rhodamine conjugate on cancer cell viability using CellTiter-Blue assay.

2- Analyse using live cell confocal microscopy the cellular uptake and subcellular distribution of EJP-18 under different experimental conditions and in comparison with a well characterised CPP- R8.

4.3   Results

4.3.1   Cell Viability assays for EJP-18 and Rh-EJP-18

4.3.1.1   Effect of EJP-18 on the cell viability in a panel of cancer cell lines

In order to assess the cytotoxicity of EJP-18, cell viability was examined in a panel of cancer cells that are routinely cultured in the laboratory for CPP and other work. Briefly, cells were seeded in 96-well plates and incubated with 0-100 μM EJP-18 for 24 h under full tissue culture conditions. Cell viability was then determined via CellTiter-Blue assay as previously described in sections 2.3.1 and 2.3.2. Figure 4-2 shows that up to concentrations of 10 μM, EJP-18 had no effect on viability in any of the tested cell lines. However, varying degrees of cytotoxicity was then seen when different cells were treated with 20 μM peptide for 24 h; KG1a being the most sensitive followed by HeLa and MCF-7 cells. At 100 μM, EJP-18 reduced cell viability of the three cell lines by > 85%. A431 and MDA-MB-231 were the most resistant to toxicity as only 23% and 45% loss in cell viability was respectively observed with 100 μM peptide.
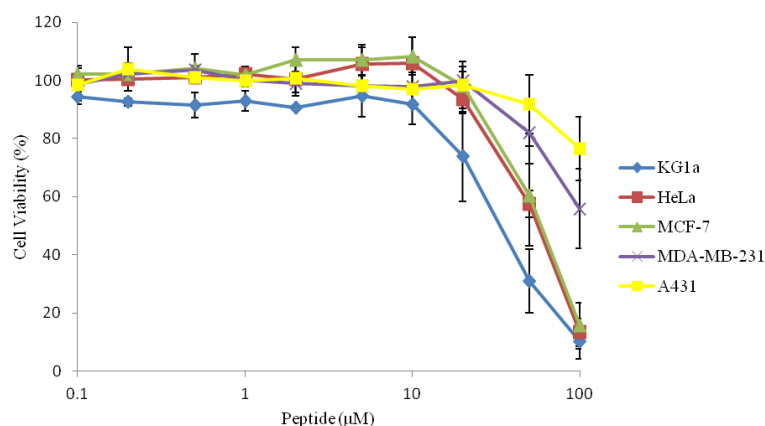
Figure 4-2: Viability of different cell lines incubated with EJP-18. Viability of cells was evaluated using CellTitre-Blue assay following 24 h incubation with 0-100 μM EJP-18 and is expressed as the percentage of viable cells relative to untreated controls. Results represent means ± SD for three independent experiments performed in duplicate.

4.3.1.2 Effect of Rh-EJP-18 on the cell viability in a panel of cancer cell lines

Cell viability experiments were also performed on the rhodamine labelled peptide (Rh-EJP18) at 0-50 μM. Since CellTiter-Blue is a fluorescence based assay, steps were taken to exclude possible interference of rhodamine fluorescence ($554_{Ex}/578_{Em}$) with the resorufin fluorescence produced by the conversion of resazurin in viable cells at ($544_{Ex}/590_{Em}$). Rhodamine correction was performed by performing parallel cell-free experiments i.e. by adding the same serial dilutions of Rh-EJP-18 in medium alone. The fluorescence readings of the Rh-EJP-18 and medium-only controls were then subtracted from the readings of the Rh-EJP-18 treated cells. Figure 4-3 shows that up to 10 μM, Rh-EJP-18 had no effect on viability in any of the cell lines tested. As with EJP-18, concentrations above 20 μM showed varying degree of toxicity according to the cell line; MDA-MB-231 and A431 being the most resistant.

Rh-EJP-18 was very toxic to KG1a, HeLa and MCF-7 at 50 µM but A431 and

MDA-MB-231 cells were unaffected even at this higher concentration.
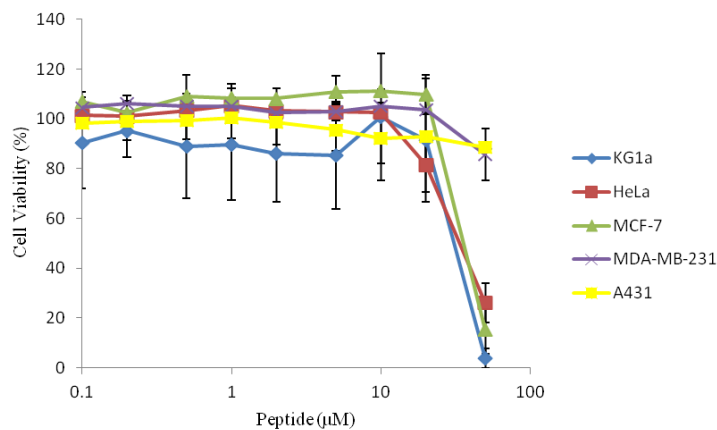
Figure 4-3: Viability of different cell lines incubated with Rh-EJP-18. Rhodamine corrected viability of cells was evaluated using CellTitre-Blue assay following 24 h incubation with 0-50 µM Rh-EJP-18. Cell viability is expressed as the percentage of viable cells relative to untreated controls. Results represent means ± SD for three independent experiments performed in duplicate.

4.3.1.3   Effect of R8 and Rh-R8 on the viability of HeLa cells

R8 is a very well characterised cationic CPP and was used during this study as

a comparative CPP to EJP-18 for cell uptake and delivery. Cell viability of R8

and Rh-R8 were also examined in HeLa cells seeded in 96-well plates and

incubated as above with 0-100 µM peptides for 24 h prior to performing cell

viability assay. R8 was non toxic to HeLa cells at all studied concentrations but

the rhodamine conjugate was toxic at concentrations above 20 µM (Figure

4-4).

.
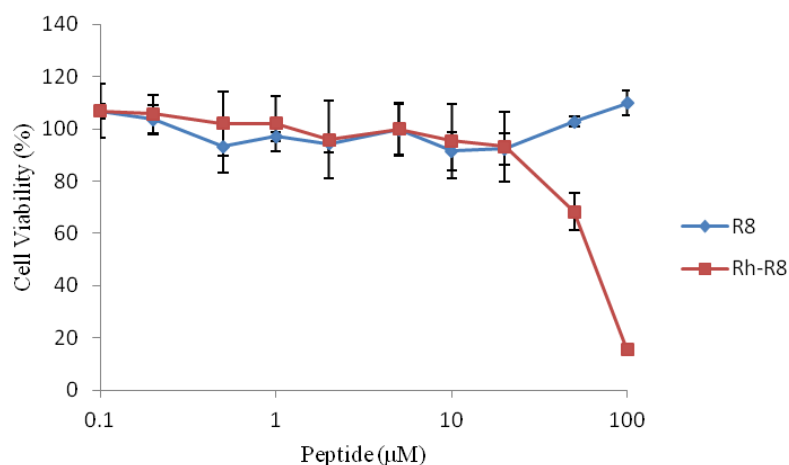
Figure 4-4: Viability of HeLa cells incubated with R8 and Rh-R8. Viability of cells was evaluated using CellTitre-Blue assay following 24 h incubation with 0-100 μM R8 or Rh-R8 and is expressed as the percentage of viable cells relative to untreated controls. Rhodamine correction was considered. Results represent means ± SD for three independent experiments performed in duplicate.

4.3.2 Detecting EGFR levels in different cell lines

Viability studies revealed that both A431 and MDA-MB-231 cells were the most resistant to the toxicity of EJP-18 and its rhodamine conjugate. As EJP-18 is derived from the JM region of EGFR, it was hypothesised that the differences in the toxicity profiles of the cells may be related to their EGFR levels. Relative EGFR expression in the cells was then determined in each of these cell lines. Cells were cultured and lysed with detergents as described in section 1.5.1.2 and proteins were separated using SDS-PAGE. Following protein transfer, membranes were probed with antibodies recognising EGFR and α-tubulin as protein loading control. A431 and MDA-MB-231 are well characterised high EGFR expressing cells (www.proteinatlas.org) (DeFazio *et al.*, 2000, Araki *et al.*, 2007, Al Soraj *et al.*, 2012, Boran *et al.*, 2012) and Figure 4-5 confirms this. A faint band was observed in HeLa cells but EGFR

expression could not be detected in KG1a or MCF-7 cells. This also confirms

proteinatlas information for MCF-7/EGFR but no documentation was available

regarding expression of this protein in KG1a cells. Overall the viability data

suggested that high EGFR expressing cells were protected from the effects of

EJP-18 compared with low or non expressing lines.
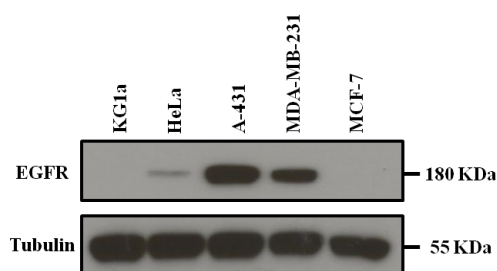
Figure 4-5: EGFR expression in different cell lines. Cell lysates were collected and Western blotting was performed for detection of EGFR and tubulin.

4.3.3 Cellular uptake (subcellular distribution) of Rh-EJP-18 and Rh-R8 in HeLa cells in presence or absence of serum

Preliminary investigation showed that EJP-18 could rapidly enter cells and

label internal vesicles suggesting it was being internalised by endocytosis.

Further analysis was then performed on this peptide in comparison with R8 that

was similarly labelled with rhodamine. HeLa cells have been widely used in

our laboratory for CPP studies with R8 and were the chosen cell line for these

studies. Cells grown in glass bottomed imaging dishes were incubated for 1 h

with serum free medium or complete medium containing 1-20 μM Rh-EJP-18

or 5-20 μM Rh-R8. The cells were washed then imaged as live cells by

confocal microscopy as described in section 2.4.1.1. The cell permeable dye

Hoechst 33342 was added at the end of the experiment to label the nucleus.

Figure 4-6 shows that in the absence of serum, 5 µM Rh-R8 was localised to vesicular structures in HeLa cells but as the concentration increased, the localisation changed significantly. At 10 µM, the cell population is heterogeneous: some cells have only punctate cytosolic vesicles while others exhibit additional diffuse cytosolic labelling. At 20 µM, Rh-R8 labelled the entire cell cytoplasm and nucleus; nucleolar labelling was also observed (Figure 4-6). Enlarged sections of single section images from Figure 4-6 are shown in Appendix D (Figure D-1).

Figure 4-6: Uptake of Rh-R8 peptide into HeLa cells at 5-20 µM in SFM. Cells were incubated with 5-20 µM Rh-R8 in SFM for 1h at 37ºC, washed and imaged by confocal microscopy. Representative images (N=3) show either a single section through the cell at the mid-point of the nucleus or maximum projection of the whole cell. Nuclei were labelled blue with Hoechst. White arrows indicate nucleolar labelling. Scale bars = 20 µm.

Rh-EJP-18 was shown to label punctate vesicles, many of which were accumulating in a distinct perinuclear region (Figure 4-7). At 5 µM peptide concentration, these were very clearly seen and the fluorescence increased in these structures as the concentration was increased to 20 µM. Unlike Rh-R8 at 20 µM which labelled the entire cell, Rh-EJP-18 at this concentration was predominantly located in vesicular structures but in approximately 25% of the cell population, the fluorescence was observed throughout the cytoplasm and nucleus. Enlarged sections of images from Figure 4-7 are shown in Appendix D (Figure D-2). Experiments were also performed at 1 µM Rh-EJP-18 concentration but the fluorescence signal was below that which could be easily detected above cellular background autofluorescence (Data not shown).

Figure 4-7: Uptake of Rh-EJP-18 peptide into HeLa cells at 5-20 µM in SFM. Cells were incubated with 5-20 µM Rh-EJP-18 in SFM for 1h at 37ºC, washed and imaged by confocal microscopy. Representative images (N=3) showing either a single section through the cell at the mid-point of the nucleus or maximum projection of the whole cell. Nuclei were labelled blue with Hoechst. *White arrows indicate distinct perinuclear labelling. Scale bars = 20 µm.*

To detect whether the cytoplasmic labelling observed at 20 µM was due to general plasma membrane leakage, noting that this concentration reduced cell viability (Figure 4-3), cells were initially incubated with the peptide and at the end of the experiment, the medium was removed and the cells were incubated in imaging medium containing the fluorescent probe DRAQ7. This will only enter cells and nucleus of those with a damaged plasma membrane and Figure 4-8 shows some DRAQ7-stained nuclei suggesting that cytosolic labelling may be due to either cell death or permeabilization. In other cells, there was

evidence of cytosolic peptide (pseudocolour green) but no clear DRAQ7 labelling.
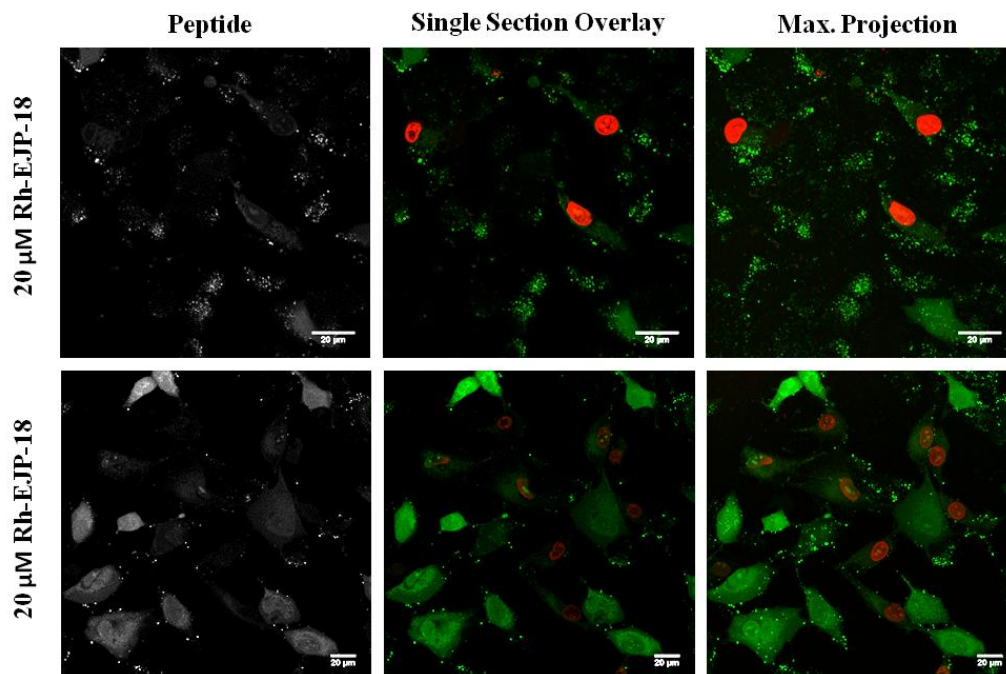
Figure 4-8: Uptake of 20 μM Rh-EJP-18 peptides into HeLa cells in SFM. Cells were incubated with 20 μM Rh-EJP-18 in SFM for 1h at 37ºC, washed and imaged in imaging medium containing DRAQ7 by confocal microscopy. Representative images (N=2) showing either a single section through the cell at the mid-point of the nucleus or maximum projection of the whole cell (top row: experiment 1, bottom row: experiment 2). Dead or permeabilized nuclei were labelled red with DRAQ7 and the rhodamine peptide labelled green. *Scale bars = 20 μm.*

The uptake of cationic CPPs can be affected by the presence of serum; for example, serum albumin can bind a significant amount of peptide thus reducing the concentration of 'active' peptide in the solution (Kosuge *et al.*, 2008, Jones and Sayers, 2012). To study the effect of serum on the internalisation and subcellular localisation of the peptides, uptake experiments described in the earlier section were repeated in the presence of serum. Figure 4-9 shows that incubation of HeLa cells with Rh-R8 in presence of serum reduced the uptake of the peptide (compared to uptake in Figure 4-6). At 20 μM Rh-R8, there was again evidence of cells labelled with rhodamine in punctate structures or

diffusely through the cytoplasm. The extent of cytosolic labelling was much lower than in the absence of serum. Reduced fluorescence was observed at 10 µM and 5 µM when compared to 20 µM. The uptake of Rh-EJP-18 also decreased in the presence of serum and was predominantly labelled in vesicles at 10 µM but at 20 µM, the peptide had in some cells entered into the cytosol as diffuse labelling. Very little fluorescence was detected in cells treated with 5 µM extracellular peptide concentration (Figure 4-10).
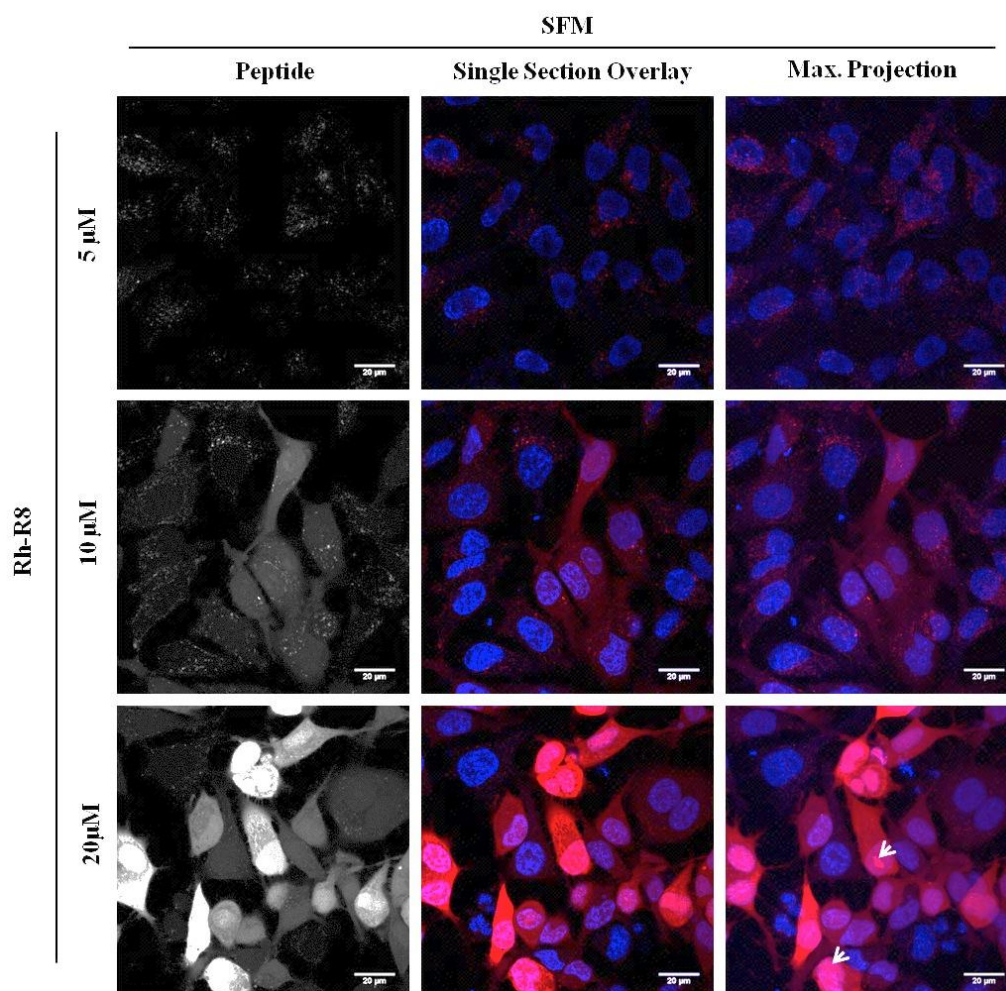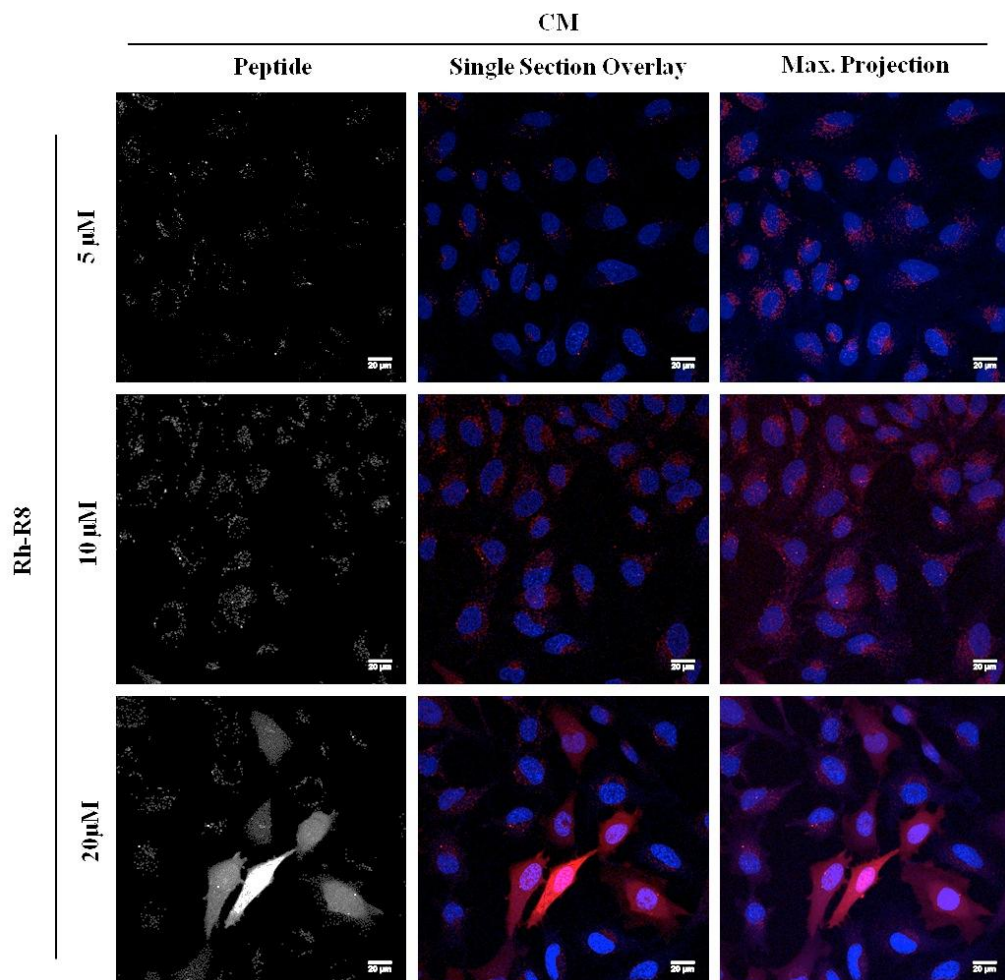

Figure 4-9: Uptake of Rh-R8 peptide into HeLa cells at 5-20 µM in CM. Cells were incubated with 5-20 µM Rh-R8 in CM for 1h at 37ºC, washed and imaged by confocal microscopy. Representative images (N=2) showing either a single section through the cell at the mid-point of the nucleus or maximum projection of the whole cell. Nuclei were labelled blue with Hoechst. *Scale bars = 20 µm*
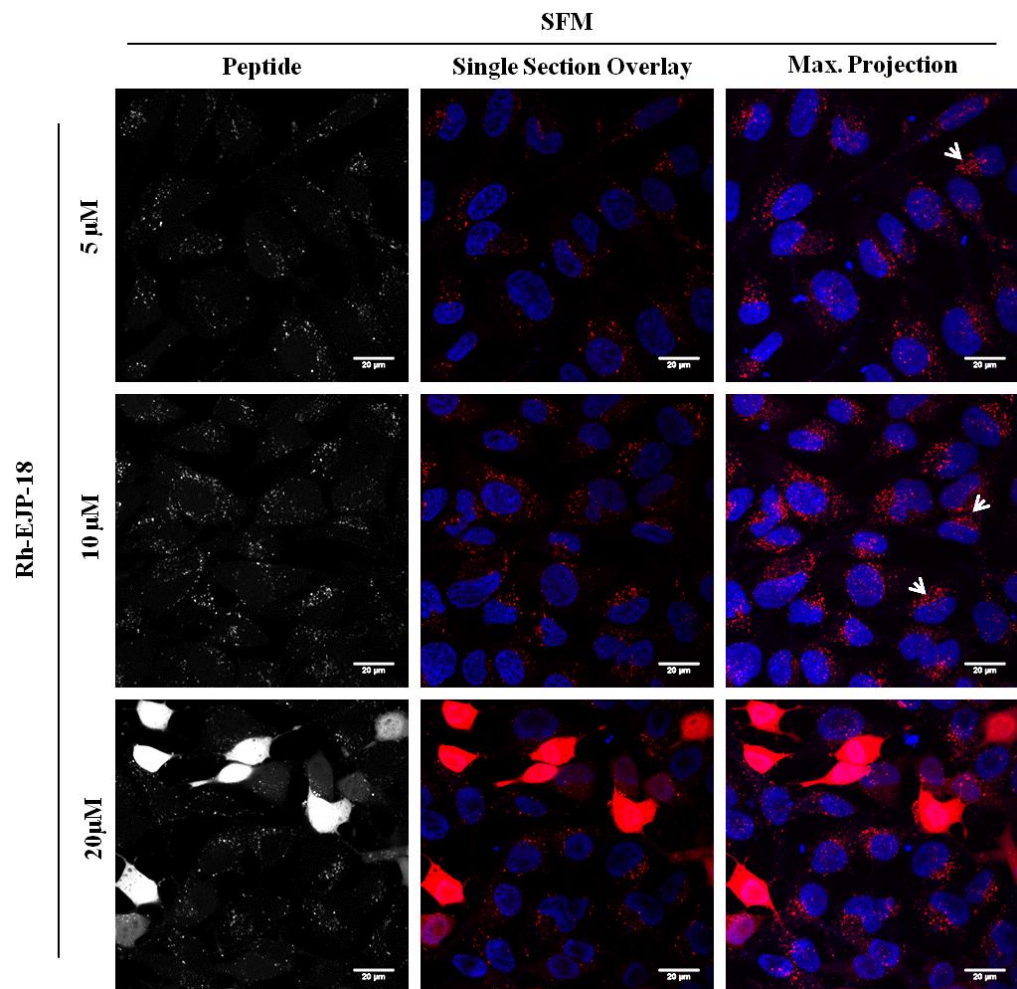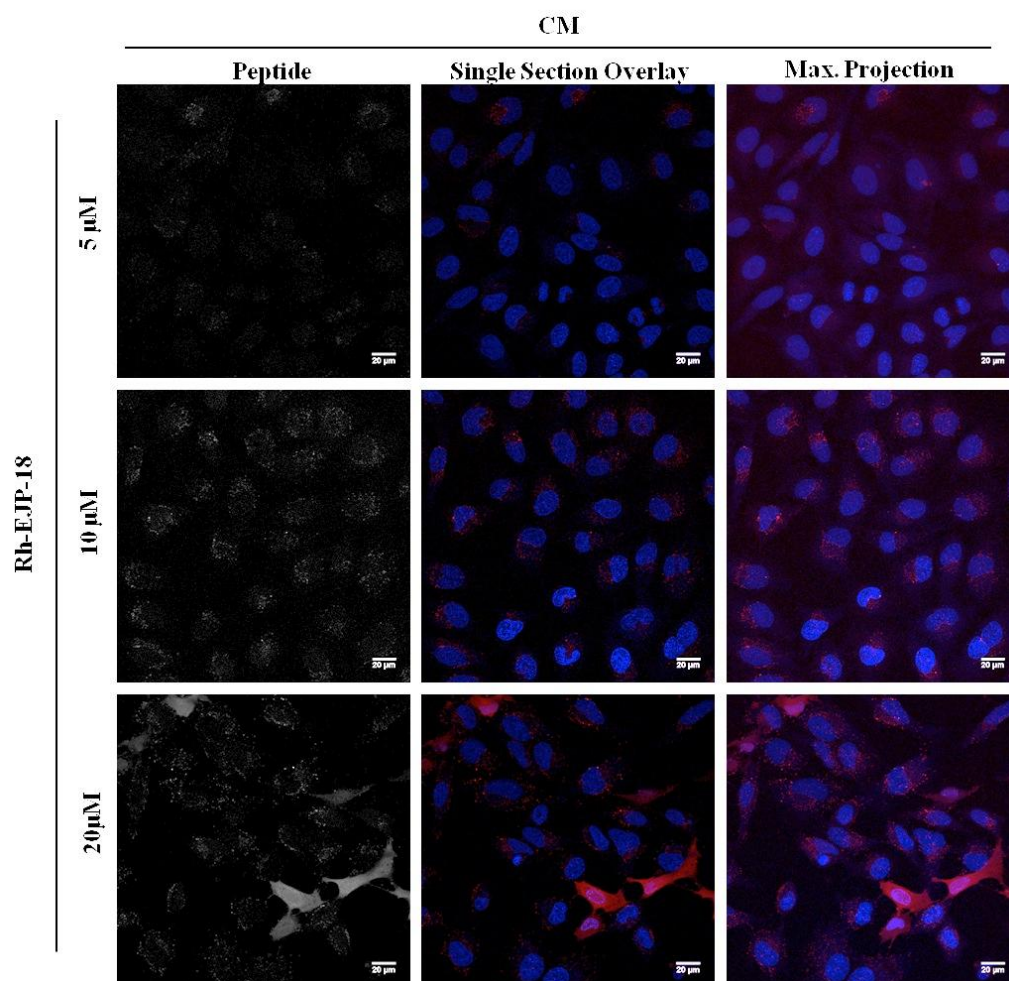
Figure 4-10: Uptake of Rh-EJP-18 peptide into HeLa cells at 5-20 μM in CM. Cells were incubated with 5-20 μM Rh-EJP-18 in CM for 1h at 37ºC, washed and imaged by confocal microscopy. Representative images (N=2) showing either a single section through the cell at the mid-point of the nucleus or maximum projection of the whole cell. Nuclei were labelled blue with Hoechst. *Scale bars = 20 μm*

4.3.4 Cellular uptake of 10 μM Rh-EJP-18 and Rh-R8 in HeLa cells at 4 and 37ºC

Temperature has been shown to affect both the uptake and subcellular distribution of CPPs (Fretz *et al.*, 2007, Watkins *et al.*, 2009a, Watkins *et al.*, 2009b). To test this on Rh-EJP-18 uptake, HeLa cells were incubated for 1 h with 10 μM peptide at 4 and 37ºC and the cells were examined by confocal microscopy as described in section 2.4.1.2. Here, experiments were also performed with Rh-R8. Figure 4-11A reveals that Rh-EJP-18 labelled vesicular

structures in HeLa cells at 37 ºC and the uptake was inhibited at 4ºC (Figure 4-11B). As expected, R8 effectively internalised the fluorescent cargo to cells incubated at 37 and 4ºC, but giving different subcellular localisation. At 37ºC, Rh-R8 labelled vesicular structures and exhibited diffuse cytoplasmic, cytosolic and nuclear distribution (Figure 4-11A). However, when cells were incubated with Rh-R8 at 4ºC, the peptide also strongly labelled the nucleolus (Figure 4-11B). At this temperature, some of the cells had very little fluorescence inside them and the figure clearly demonstrates high heterogeneity of peptide labelling within a single cell population.
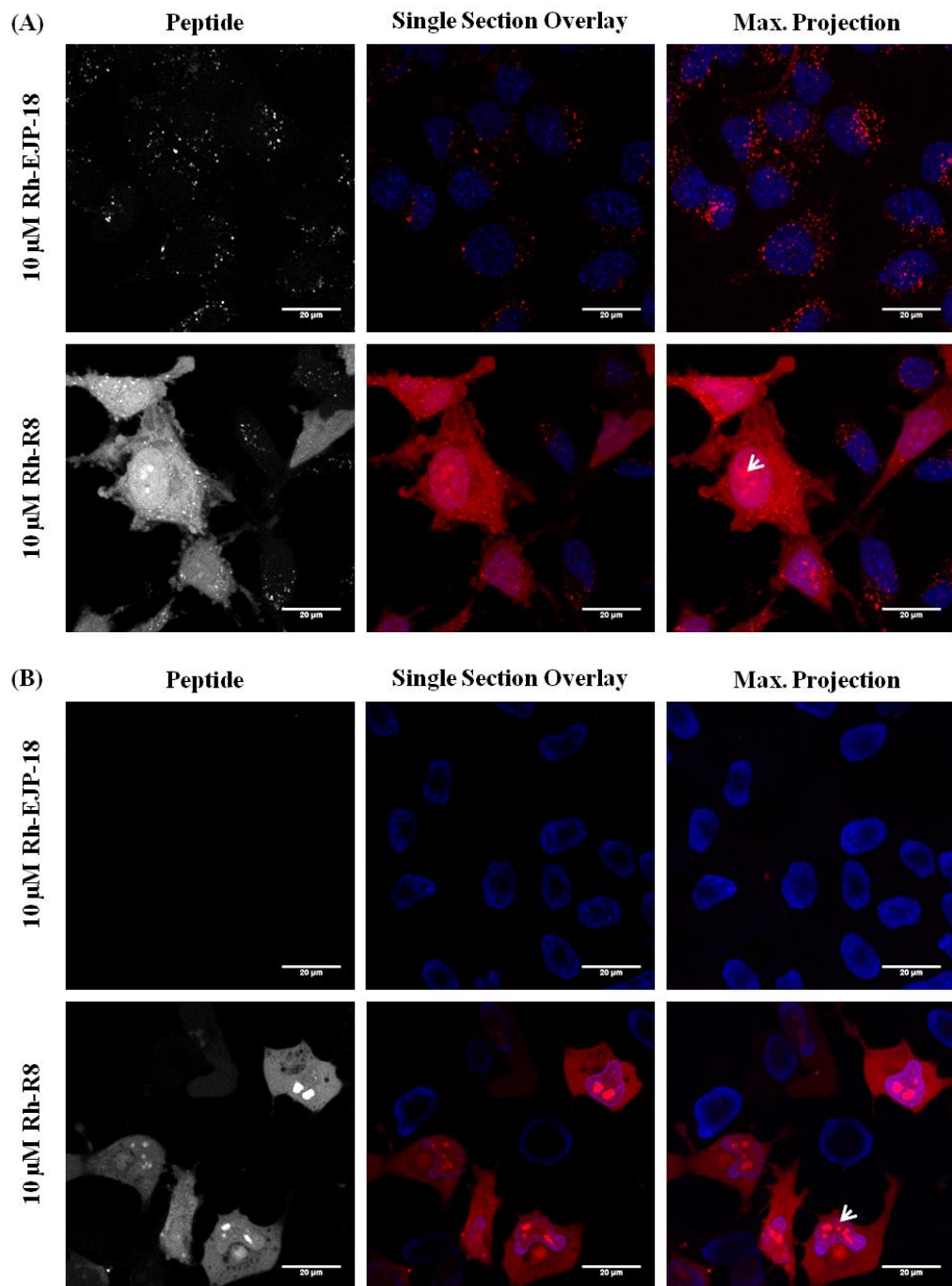
Figure 4-11: Uptake of Rh-EJP-18 and Rh-R8 into HeLa cells at 10 µM in SFM at (A) 37ºC or (B) 4ºC. Cells were incubated with 10 µM Rh-EJP-21 or Rh-E-64562 in SFM for 1h at (A) 37ºC or (B) 4ºC, washed and imaged by confocal microscopy. Representative images (N=3) showing either a single section through the cell at the mid-point of the nucleus or maximum projection of the whole cell. Nuclei were labelled blue with Hoechst. *Scale bars = 20 µm.*

4.4 Discussion

The primary aim of this chapter was to test the cellular uptake, subcellular distribution and cytotoxicity of a peptide sequence termed EJP-18 that was obtained after close scrutiny of the JM region of EGFR. The sequence has three hydrophobic and three hydrophilic regions suggesting it could behave as an amphipathic CPP. Within the CPP world, amphipathic variants include MPG, TP10 and Transportan (Pooga *et al.*, 1998, Soomets *et al.*, 2000, Deshayes *et al*., 2011, Madani *et al*., 2011). Their amphipathicity can in part be attributed to the sequential running of hydrophobic and hydrophilic residues along the sequence and the fact that when they interact with lipids they change their structures to form ß-sheets or alpha helices. EJP-18 is a relatively short peptide and has very clearly defined hydrophobic and hydrophilic regions to suggest that it may also do the same.

Initial cell uptake analysis performed on Rh-EJP-18 by Dr Edward Sayers suggested it was effectively endocytosed into cells but that at extracellular concentrations > 10 µM it was causing plasma membrane perturbation. This was particularly noticeable in the leukaemia cell line KG1a (Fig 4-1). It was then decided to test if this membrane effect was having any effects on cell viability. For this a number of cell lines were tested in this thesis.

These assays revealed that neither EJP-18 nor Rh-EJP-18 affected cell viability up to 10 µM in any of the cell lines tested; however, clear cytotoxicity was seen above 20 µM in some cell lines. Of interest from this data was the finding that sensitivity of the cells was dependent on expression of EGFR that was also

measured in this thesis. A431 and MDA-MB-231 are well known high expressors of EGFR and were the most resistant to the effects of this peptide. Of note is that they are not derived from the same tissue, as A431 and MDA-MB-231 are derived from skin and breast respectively. There are a number of explanations for this apparent dependency on EGFR expression. First, the more sensitive cell lines may have plasma membranes that are more susceptible to EJP-18-mediated damage causing cell lysis (necrosis). This could be by forming pores or the peptide acting as a detergent. Interestingly, the plasma membrane of KG1a, the most sensitive cell line, was relatively porous, compared to other cell lines, to allow direct translocation of cationic CPPs such as Tat and R8 at relatively low concentrations (Al-Taei *et al.*, 2006, Watkins *et al.*, 2009a). A more complex explanation derives from the origin of this sequence in the JM domain of EGFR. EJP-18 when located in the cytosol could sequester endogenous interactors of the corresponding EGFR domain. This could potentially interfere with downstream EGFR signalling for cell growth and survival. Because A431 and MDA-MB-231 have more EGFR, they may also have a corresponding increase in the expression of EGFR interacting proteins. This would mean a higher dose of EJP-18 would potentially be required to sequester the partner proteins and impinge on EGFR signalling. The evidence for this comes from the fact that the previously described EGFR JM derived peptide T654 was able to affect nuclear localisation and EGFR degradation in response to irradiation (Dittmann *et al.*, 2010). The T residue common to T654 and EJP-18 was phosphorylated in T654 and it remains to be

determined whether a phosphorylated EJP-18 would also influence EGFR biology in the same way.

Based on a similar strategy to T645, peptides targeting other cytosolic domains of EGFR have been described including those involved in autophosphorylation (Kuroda *et al*., 2013). Here, the peptides are attached to CPPs such as Tat that is required for cytosolic delivery. Recently and during the course of this studentship, a peptide with a very similar sequence to EJP-18 termed E-64562 (RRRHIVRKRTLRRLLQER) was attached to the C-terminus of Tat to give TE-64562 (RKKRRQRRRGRRRHIVRKRTLRRLLQER) and found to have strong anti-cancer activity that was dependent on EGFR expression. The model presented was that Tat was aiding E-64562 internalization to the cytosol where it was then interfering with EGFR signaling (Boran *et al*., 2012). TE-64562 also had *in vivo* activity in nude mice bearing MDA-MB-231 tumors. Further mention and discussion of this peptide will be provided in Chapter 6 when data are presented on analysis of derivatives of EJP-18.

For Low EGFR expressing KG1a, MCF-7 and HeLa cells, that are more sensitive to EJP-18, a smaller amount of peptide would be needed to sequester interactors, inhibit signalling and induce toxicity.

An alternative scenario to explain our findings is that because EGFR promotes growth and survival, even if EJP-18-induced toxicity is independent of EGFR, there might be a protective effect of the receptor in overexpressing cells. This could be further investigated by testing the peptide in cells transiently overexpressing EGFR or by stably transfected, inducible cell lines.

Rh-EJP-18, at all studied concentrations, labelled vesicular structures in HeLa cells which suggests an endocytic uptake mechanism. Some cells with cytosolic labelling were observed with 20 μM Rh-EJP-18 but this could be due to increased cell porosity or even cell death as illustrated by red staining of nuclei by DRAQ7 (Figure 4-8). R8 is a well characterised cationic CPP and was used during this study as a benchmark to the new peptide. Rh-R8, as expected (Duchardt *et al.*, 2007, Fretz *et al.*, 2007, Watkins *et al.*, 2009a), was predominantly localised to vesicular structures at low concentrations but at 20 μM, was directly translocated across the plasma membrane without showing any evidence of membrane damage (Appendix D- Figure D-3). It was noticeable that in several of these microscopy experiments, within the same cell population, that not all cells contained the same amounts of peptide. This heterogeneity in pattern of uptake and distribution of R8 resembles data published by Duchardt *et al.* who showed increasingly heterogeneous uptake and nucleo-cytoplasmic enrichment of two arginine-rich CPPs (R9 and Tat) as the peptide concentration was increased (Duchardt *et al.*, 2007). The authors concluded that above a critical threshold, internalization of R9 and Tat occurs through a highly efficient nonendocytic pathway originating from spatially confined areas of the plasma membrane (nucleation zones) and leads to rapid release of the peptides into the cytosol without affecting the overall integrity of this structure. Similar results have been reported by Kosuge *et al.* in the uptake of an Alexa488-labelled oligoarginine; R12. Time-course imaging of HeLa cells revealed that initial translocation of R12 peptide occurred at defined

locations before diffusing through the cytosol and nucleus (Kosuge *et al*., 2008).

A different fluorescent conjugate of R8; R8-Alexa488, was shown to be efficiently internalised into HeLa and KG1a cells at a range of concentrations. In HeLa cells, concentrations of up to 20 μM R8-Alexa488 localised to vesicular structures but cytosolic labelling was observed at higher concentration (Watkins *et al*., 2009a). No evidence of R8-Alexa488 localisation in the nuclei was described in the report by Watkins *et al*. which contrasts with the nuclear Rh-R8 observed in Figure 4-6. Together these data indicate that the nature of the cargo (the fluorophore in this case) may affect the subcellular distribution of the peptide conjugate. It has been previously reported that fluorophore tagging of a CPP can affect transport pathway and its subcellular localisation (Palm-Apergi *et al*., 2012). The localisation of luminescent complexes of ruthenium (metal complexes to examine cellular uptake) attached to octaarginine (Ru-D-R8) has been shown to be altered by the presence of a fluorophore. The addition of fluorescein to Ru-D-R8 changes the peptide conjugates' distribution in HeLa cells from punctate structures in the cytosol (Ru-D-R8 alone) to diffuse cytosolic and nuclear labelling, strong nucleolar staining and some punctate cytosolic staining (Ru-D-R8 conjugated to fluorescein) (Puckett and Barton, 2009). The authors suggested that the greater lipophilicity of fluorescein versus the Ru moiety caused an increased interaction with the plasma membrane and this high concentration at the cell surface aided nonendocytic uptake. All this needs to be taken into

consideration when interpreting results from CPP studies involving fluorescently-labelled peptides.

The uptake of Rh-EJP-18 and Rh-R8 was reduced in the presence of serum (Figures 4-9 and 4-10). At 10 μM, serum altered the distribution pattern of Rh-R8 from a mixture of punctate vesicles and cytosolic labelling into punctate vesicles only (Figures 4-6 and 4-9). The same figures show that at 20 μM Rh-R8, the presence of serum reduced the number of cells with nucleocytoplasmic labelling. This could be due to an interaction of both the peptides here with serum proteins such as albumin. Serum bound CPPs could have reduced cellular uptake as their interaction with serum proteins impairs their ability to engage with the cell membrane. The effective concentration of peptide in serum containing medium is therefore reduced as there is less free/active peptide to interact with the cell (Kosuge *et al*., 2008, Jones and Sayers, 2012). It has also recently been reported that presence of serum reduced the uptake of a Voltage-dependent L-type calcium channel subunit alpha-1D protein-derived arginine-rich CPP; P8 (RRWRRWNRFNRRRCR) into HeLa cells which could be due to non-specific electrostatic interaction of the peptide with serum proteins (Gautam *et al*., 2015).

EJP-18 entered cells in a temperature-dependent manner (Figures 4-11). The peptide was internalised at 37ºC and its uptake was abolished at 4ºC which strongly suggests the involvement of an active process, most likely endocytosis. Rh-R8 as expected was able to freely diffuse through the plasma membrane and at the highest 20 μM concentration, labelled the entire cell

including the nucleolus. In contrast, there was no evidence that Rh-EJP-18 was able to label the nucleolus and the reason behind this is unknown.

Nucleolar labelling as presented here with Rh-R8 has previously been observed when leukaemia cells were treated with CPPs including D-R8-Alexa488 (Fretz *et al*., 2007) and CPPs have even been mentioned as being candidate probes for labelling these structures in the nucleus (Martin *et al*., 2007). In this chapter, HeLa cells incubated with Rh-R8 at 4ºC showed a very heterogeneous labelling pattern with some cells showing very little uptake. The reason for this is unknown. Nucleolar labelling was observed when cells were incubated with Rh-R8 at 4ºC and also at 37˚C, though to a much lesser extent. One possibility is that intracellular proteolysis is a contributing factor, reducing the fraction of peptide that is able to migrate to the nucleus and nucleolus. However, protease effects should be significantly diminished at 4ºC and this allows more peptide to translocate to the nucleus (Fretz *et al*., 2007).

4.5   Conclusions

The hypothesis underlying the study of EJP-18 was based on its sequence, its origin in the JM region of EGFR and the possibility that it could have bioportide properties to influence EGFR biology. Cell viability experiments in a panel of cancer cell lines revealed toxicity, the extent of which was EGFR dependent. Of concern before assigning the term bioportide to EJP-18 is the possibility that it could also be classed as a lytic/necrotic peptide. This warranted more detailed analysis of its interaction with cells as a fluorescent conjugate.

The first Rh-EJP-18 microscopy analysis at relatively low peptide concentration highlighted vesicular labelling, strongly suggesting it was entering cells by endocytosis. As the concentration of EJP-18 increased, there was evidence that it was localised to the cytosol but it is difficult to determine whether this is due to translocation across the plasma membrane or membrane damage. The impressive capacity of EJP-18 to enter cells by endocytosis without showing extensive plasma membrane labelling led to questions regarding the possibility that it could deliver cargo much larger than rhodamine to cells at concentrations that does not cause cell death.

4.6   References

AHSAN, A., RAY, D., RAMANAND, S. G., HEGDE, A., WHITEHEAD, C., REHEMTULLA, A., MORISHIMA, Y., PRATT, W. B., OSAWA, Y., LAWRENCE, T. S. & NYATI, M. K. 2013. Destabilization of the epidermal growth factor receptor (EGFR) by a peptide that inhibits EGFR binding to heat shock protein 90 and receptor dimerization. *J Biol Chem,* 288**,** 26879-26886.

AL SORAJ, M., HE, L., PEYNSHAERT, K., COUSAERT, J., VERCAUTEREN, D., BRAECKMANS, K., DE SMEDT, S. C. & JONES, A. T. 2012. siRNA and pharmacological inhibition of endocytic pathways to characterize the differential role of macropinocytosis and the actin cytoskeleton on cellular uptake of dextran and cationic cell penetrating peptides octaarginine (R8) and HIV-Tat. *J Control Release,* 161**,** 132-141.

AL-TAEI, S., PENNING, N. A., SIMPSON, J. C., FUTAKI, S., TAKEUCHI, T., NAKASE, I. & JONES, A. T. 2006. Intracellular traffic and fate of protein transduction domains HIV-1 TAT peptide and octaarginine. Implications for their utilization as drug delivery vectors. *Bioconjugate chemistry,* 17**,** 90-100.

ARAKI, N., EGAMI, Y., WATANABE, Y. & HATAE, T. 2007. Phosphoinositide metabolism during membrane ruffling and macropinosome formation in EGF-stimulated A431 cells. *Experimental cell research,* 313**,** 1496-1507.

BENNASROUNE, A., FICKOVA, M., GARDIN, A., DIRRIG-GROSCH, S., AUNIS, D., CRÉMEL, G. & HUBERT, P. 2004. Transmembrane peptides as inhibitors of ErbB receptor signaling. *Molecular biology of the cell,* 15**,** 3464-3474.

BORAN, A. D., SECO, J., JAYARAMAN, V., JAYARAMAN, G., ZHAO, S., REDDY, S., CHEN, Y. & IYENGAR, R. 2012. A potential peptide therapeutic derived from the juxtamembrane domain of the epidermal growth factor receptor. *PLoS One,* 7**,** e49702.

CHEN, Y.-F. & FU, L.-W. 2011. Mechanisms of acquired resistance to tyrosine kinase inhibitors. *Acta Pharmaceutica Sinica B,* 1**,** 197-207.

DEFAZIO, A., CHIEW, Y. E., SINI, R. L., JANES, P. W. & SUTHERLAND, R. L. 2000. Expression of c-erbB receptors, heregulin and oestrogen receptor in human breast cell lines. *International journal of cancer,* 87**,** 487-498.

DESHAYES, S., KONATE, K., ALDRIAN, G., HEITZ, F. & DIVITA, G. 2011. Interactions of amphipathic CPPs with model membranes. *Cell-Penetrating Peptides.* Springer, 683, 41-56

DITTMANN, K., MAYER, C., FEHRENBACHER, B., SCHALLER, M., KEHLBACH, R. & RODEMANN, H. P. 2010. Nuclear EGFR shuttling induced by ionizing radiation is regulated by phosphorylation at residue Thr654. *FEBS letters,* 584**,** 3878-3884.

DUCHARDT, F., FOTIN-MLECZEK, M., SCHWARZ, H., FISCHER, R. & BROCK, R. 2007. A comprehensive model for the cellular uptake of cationic cell-penetrating peptides. *Traffic,* 8**,** 848-866.

FRETZ, M. M., PENNING, N. A., AL-TAEI, S., FUTAKI, S., TAKEUCHI, T., NAKASE, I., STORM, G. & JONES, A. T. 2007. Temperature-, concentration- and cholesterol-dependent translocation of L- and D-octa-arginine across the plasma and nuclear membrane of CD34+ leukaemia cells. *Biochem J,* 403**,** 335-342.

GAUTAM, A., SHARMA, M., VIR, P., CHAUDHARY, K., KAPOOR, P., KUMAR, R., NATH, S. K. & RAGHAVA, G. P. 2015. Identification and characterization of novel protein-derived arginine-rich cell-penetrating peptides. *European Journal of Pharmaceutics and Biopharmaceutics,* 89**,** 93-106.

HSU, S.-C. & HUNG, M.-C. 2007. Characterization of a novel tripartite nuclear localization sequence in the EGFR family. *Journal of Biological Chemistry,* 282**,** 10432-10440.

HUBBARD, S. R. 2009. The juxtamembrane region of EGFR takes center stage. *Cell,* 137**,** 1181-1183.

HYNES, N. E. & MACDONALD, G. 2009. ErbB receptors and signaling pathways in cancer. *Current opinion in cell biology,* 21**,** 177-184.

JONES, A. T. & SAYERS, E. J. 2012. Cell entry of cell penetrating peptides: tales of tails wagging dogs. *Journal of Controlled Release,* 161**,** 582-591.

JURA, N., ENDRES, N. F., ENGEL, K., DEINDL, S., DAS, R., LAMERS, M. H., WEMMER, D. E., ZHANG, X. & KURIYAN, J. 2009. Mechanism for activation of the EGF receptor catalytic domain by the juxtamembrane segment. *Cell,* 137**,** 1293-1307.

KOSUGE, M., TAKEUCHI, T., NAKASE, I., JONES, A. T. & FUTAKI, S. 2008. Cellular internalization and distribution of arginine-rich peptides as a function of extracellular peptide concentration, serum, and plasma membrane associated proteoglycans. *Bioconjug Chem,* 19**,** 656-664.

KURODA, Y., KATO-KOGOE, N., TASAKI, E., MURATA, E., UEDA, K., ABE, M., MIYAMOTO, K., NAKASE, I., FUTAKI, S. & TOHYAMA, Y. 2013. Oligopeptides derived from autophosphorylation sites of EGF receptor suppress EGF-stimulated responses in human lung carcinoma A549 cells. *European journal of pharmacology,* 698**,** 87-94.

MADANI, F., LINDBERG, S., LANGEL, U., FUTAKI, S. & GRASLUND, A. 2011. Mechanisms of cellular uptake of cell-penetrating peptides. *J Biophys,* 2011**,** 414729.

MARTIN, R. M., TÜNNEMANN, G., LEONHARDT, H. & CARDOSO, M. C. 2007. Nucleolar marker for living cells. *Histochemistry and cell biology,* 127**,** 243-251.

PALM-APERGI, C., LONN, P. & DOWDY, S. F. 2012. Do cell-penetrating peptides actually "penetrate" cellular membranes? *Mol Ther,* 20**,** 695-697.

POOGA, M., HÄLLBRINK, M. & ZORKO, M. 1998. Cell penetration by transportan. *The FASEB journal,* 12**,** 67-77.

PUCKETT, C. A. & BARTON, J. K. 2009. Fluorescein redirects a ruthenium−octaarginine conjugate to the nucleus. *Journal of the American Chemical Society,* 131**,** 8738-8739.

SEBASTIAN, S., SETTLEMAN, J., RESHKIN, S. J., AZZARITI, A., BELLIZZI, A. & PARADISO, A. 2006. The complexity of targeting EGFR signalling in cancer: from expression to turnover. *Biochimica et Biophysica Acta (BBA)-Reviews on Cancer,* 1766**,** 120-139.

SOOMETS, U., LINDGREN, M., GALLET, X., HÄLLBRINK, M., ELMQUIST, A., BALASPIRI, L., ZORKO, M., POOGA, M., BRASSEUR, R. & LANGEL, Ü. 2000. Deletion analogues of transportan. *Biochim. Biophys. Acta,* 1467, 165-176.

TANNER, K. G. & KYTE, J. 1999. Dimerization of the extracellular domain of the receptor for epidermal growth factor containing the membrane-spanning segment in response to treatment with epidermal growth factor. *Journal of Biological Chemistry,* 274**,** 35985-35990.

TARTARONE, A., LAZZARI, C., LEROSE, R., CONTEDUCA, V., IMPROTA, G., ZUPA, A., BULOTTA, A., AIETA, M. & GREGORC, V. 2013. Mechanisms of resistance to EGFR tyrosine kinase inhibitors gefitinib/erlotinib and to ALK inhibitor crizotinib. *Lung Cancer,* 81**,** 328-336.

WATKINS, C., SCHMALJOHANN, D., FUTAKI, S. & JONES, A. 2009a. Low concentration thresholds of plasma membranes for rapid energy-independent translocation of a cell-penetrating peptide. *Biochem. J,* 420**,** 179-189.

WATKINS, C. L., BRENNAN, P., FEGAN, C., TAKAYAMA, K., NAKASE, I., FUTAKI, S. & JONES, A. T. 2009b. Cellular uptake, distribution and cytotoxicity of the hydrophobic cell penetrating peptide sequence PFVYLI linked to the proapoptotic domain peptide PAD. *Journal of Controlled Release,* 140**,** 237-244.

WATKINS, C. L., SAYERS, E. J., ALLENDER, C., BARROW, D., FEGAN, C., BRENNAN, P. & JONES, A. T. 2011. Co-operative membrane disruption between cell-penetrating peptide and cargo: implications for the therapeutic use of the Bcl-2 converter peptide D-NuBCP-9-r8. *Mol Ther,* 19**,** 2124-2132.

Chapter 5: Complexation and Cellular Delivery of Macromolecular cargo by EJP-18

5.1   Introduction

5.1.1   CPPs and endosomal escape

CPPs have significant potential as vectors to facilitate the intracellular delivery of various cargos including those with therapeutic capacity. Access to the inside of the cell is not a simple criterion for successful delivery especially if this is via endocytosis. For example, endosomal entrapment is believed to be a rate-limiting step in efficient intracellular delivery of different cargos by CPPs (El-Sayed *et al*., 2009, Lee *et al*., 2013). Poor nuclear delivery is also a major limitation for CPP and other vector based DNA-based therapies but CPPs containing an NLS can be used to improve nuclear delivery (Cartier and Reszka, 2002, Kerkis *et al*., 2006). In most cases, for a cargo to exert its cellular effects, it needs to escape the endolysosomal network and enter the cytosol, or the nucleus if the cargo is DNA-based (Mäe *et al*., 2009). A number of different approaches have been reported that enhance the endosomal escape of CPP/cargo conjugates. Treatment of cells with lysosomotropic agents such as chloroquine is one such approach (Caron *et al*., 2004). Chloroquine is a weak base that raises the pH of endocytotic compartments thereby preventing endosome acidification and maturation. At high concentrations, chloroquine can cause accumulation of counter ions to protons in endosomes resulting in endosomal swelling and rupture (El-Sayed *et al*., 2009). Elevating the pH of endocytotic vesicles provides a suboptimal pH environment for lysosomal

enzymes (Ciftci and Levy, 2001). Chloroquine has been found to significantly increase TP-10-mediated splice correction of 2′ -OMe RNA oligonucleotides (Mäe *et al*., 2009). Alternatively, addition of peptides with certain sequences such as penetration-accelerating sequence (Pas; FFLIPKG) to CPPs has been found to enhance the intracellular delivery of peptides by promoting endosomal escape. Pas is a short peptide segment derived from the cleavable sequence (GKPILFF) of the lysosomal protease cathepsin D. When linked to R8, Pas has been shown to greatly enhance the uptake of the CPP (Takayama *et al*., 2009). A CPP comprised of R9 and Pas also enhanced the delivery of non-covalently attached quantum dots into A549 cells (Liu *et al*., 2013). Other approaches to enhance endosomal escape include the use of endosome-disruptive peptides (fusogenic peptides) such as the influenza hemagglutinin derived peptide; HA2 and GALA peptide. HA2 is a subunit of hemagglutinin (HA); an envelope glycoprotein of human influenza virus, responsible for endosomal escape. A 23 amino acid sequence taken from the N-terminus of the HA2 subunit (GLFGAIAGFIENGWEGMIDGWYG) is relatively hydrophobic and is referred to as fusion peptide. At reduced endosomal pH, conformational changes in HA2 take place that promote its fusion with the endosomal membrane leading to pore formation. This mechanism has been exploited through using HA2 peptide to enhance CPP-mediated endosomal escape of cargos (Cross *et al*., 2009, Liou *et al*., 2012). R9 tagged with HA2 significantly enhanced the cytosolic delivery of a red fluorescent protein (mcherry) at concentration much lower than that observed for R9 alone (Liou *et al*., 2012). GALA is a pH-sensitive synthetic peptide that has seven glutamic acid residues

(Glu) in its sequence (Table 1-1) and is negatively charged at neutral pH. The reduced endosomal pH decreases the negative charge of Glu residues and leads to the conversion of the structure from random coil to an amphipathic α-helical structure. The α-helix conformation promotes its interaction with and disruption of endosomal membranes thereby promoting endosomal escape (Li *et al*., 2004, Li *et al*., 2012). GALA enabled cytosolic delivery of proteins (EGFP and avidin) and nanoparticles (QDs) into HeLa cells when administered in presence of cationic liposomes (Kobayashi *et al*., 2009).

Development of histidine-containing CPP has also been used to enhance endosomal escape. For example, Tat peptide covalently fused with 10 histidines provided much higher levels of transgene expression (7000 fold higher than Tat alone) in human U251 glioma cells (Lo and Wang, 2008). The imidazole group of histidine has a pKa of 6.0 and in the acidic environment of endosomes (pH 5-6.5), facilitates proton influx (proton sponge effect) leading to endosomal swelling, bursting and thus escape.

EB1 (LIRLWSHLIHIWFQNRRLKWKKK); is an endosomolytic peptide and a penetratin variant in which selected residues are replaced with histidines to yield, in theory, an α-helical structure upon protonation in acidic early-late endosomal compartments and thus aids endosomal escape. EB1 has demonstrated the ability to complex and deliver siRNA and reduce luciferase expression in HeLa cells transiently transfected with the pGL3 luciferase plasmid (Lundberg *et al*., 2007). Penetratin and HA2-penetratin were also tested alongside EB1 for their ability to deliver functional siRNA and reduced

luciferase expression was observed for the HA2-CPP but not for penetratin alone. The study highlights the importance of endosomal escape for obtaining biological effects.

Although endosomal entrapment and downstream delivery to lysosomes is considered a major limitation for CPP-mediated delivery of cargo such as siRNA and plasmids, it provides a potential advantage in the treatment of lysosomal storage diseases (LSDs) (Urbanelli *et al.*, 2011). Lysosomes are specialised degradative compartments in the cells known to be involved in many cellular processes such as digestion of intra- and extracellular material, plasma membrane repair, cholesterol homeostasis and cell death and are considered crucial regulators of cell homeostasis (Appelqvist *et al.*, 2013). LSDs are a group of rare genetic disorders caused by specific mutations in genes encoding lysosomal enzymes that result in deficient lysosomal activity. The loss in enzymatic activity leads to the progressive accumulation of a wide variety of substrates such as glycolipids, glycoprotein, oligosaccharides and proteins in lysosomes and ultimately lead to cellular and organ dysfunctions (Ortolano *et al.*, 2014). LSDs share some cellular changes with protein accumulation diseases such as Alzheimer's, Parkinson's and Huntington's diseases and increasing evidence indicates that lysosomes are also involved in more widespread diseases, such as cancer, Alzheimer's disease and amyotrophic lateral sclerosis (Appelqvist *et al.*, 2013). Recently, approaches have been developed to improve targeting of lysosomal enzymes in LSDs using CPPs. The therapeutic strategy is based on, for example, using chimeric polypeptides consisting of a CPP (DPV3-RKKRRRESRKKRRRES or DPV15-

LRRERQSRLRRERQSR) to facilitate cellular uptake of a lysosomal enzyme, beta-glucuronidase, to replace the missing/mutated enzyme (Arranz, 2007, Urbanelli *et al*., 2011).

Examples of CPP delivering small molecules, proteins, peptides and nanoparticles were listed in sections 1.5.1-1.5.4. Some selective examples of CPPs delivering nucleic acids of various forms are given below and here, endosomal escape is a major requirement for effective delivery.

CADY, a secondary amphipathic peptide (Table 1-1), has been shown to deliver functional siRNA that induced significant depletion of the target mRNA and protein (GAPDH) in a range of cell lines. CADY also delivered an siRNA-targeting p53 and induced 97% knockdown after 48 and 72 h that was maintained at 60% inhibition for 5 days (Crombez *et al*., 2009).

PepFect6, a CPP comprising a proton-accepting moiety (chloroquine analog) covalently linked to a stearylated-TP10, delivered siRNA into a range of cells and caused siRNA-mediated gene silencing *in vitro* and *in vivo* models (Andaloussi *et al*., 2011). C6 (Ac-RLLRLLLRLWRRLLRLLR-NH$_2$), an amphipathic CPP, is claimed to deliver siRNA into the cytosol of CHO-K1 cells (Jafari *et al*., 2012) but despite achieving siRNA delivery the knockdown efficiency of the complex was low and this was attributed to endosomal entrapment (Xu *et al*., 2014). A related peptide, C6M1, was able to deliver non-covalently linked siRNA into CHO-K1 cells and cause a decrease in GAPDH mRNA levels. C6M1 (Ac-RLWRLLWRLWRRLWRLLR-NH$_2$) contains three tryptophan residues in place of the C6 leucines (underlined).

C6M1 was successfully used *in vivo* (in a mouse model) to deliver Bcl-2 siRNA and suppressed tumour cell proliferation and tumour volumes (Xu *et al*., 2014).

ppTG1 (GLFKALLKLLKSLWKLLLKA), a basic amphipathic peptide, efficiently transfected HeLa cells with a luciferase expression plasmid pTG11236 and was found superior to other CPPs used in the same study: KALA (Table 1-1) and JTS1-K13 (GLFEALLELLESLWELLLEACCWKAKKKKKKKKWKKKKQS) (Rittner *et al*., 2002). In a murine model, IV injection of the plasmid complexed with ppTG1 and ppTG20 (GLFRALLRLLRSLWRLLLRA), an amphipathic peptide, led to significant luciferase expression in the lung 24 h after injection.

MPG (Table 1-1), a chimeric peptide derived from the fusion of the HIV glycoprotein 41 peptide and the NLS sequence of SV40 T-antigen, has a documented ability to form stable non-covalent complexes with single- and double-stranded DNA and promote their delivery into fibroblastic HS-68 and NIH-3T3 cells (Morris *et al*., 1997). A later study by Simeoni *et al.* has also showed that MPG can deliver both DNA and siRNA however, siRNA transfection was increased when a mutant of MPG (MPGΔ^{NLS}) was used, in which the second lysine residue in NLS motif was substituted with serine (Simeoni *et al*., 2003).

5.1.2 *Methods of complexation between CPPs and cargos*

Cargos can be associated with CPPs covalently (Lundberg *et al*., 2007, Keller *et al*., 2013), or by formation of non-covalent complexes, mainly through

hydrophobic and electrostatic interactions (Morris *et al*., 2008, Carter *et al*., 2013, Keller *et al*., 2013). Covalent based strategies offer several advantages such as reproducibility and peptide quantity rationalisation, using lower amounts of peptide to achieve biological effects (Heitz *et al*., 2009). The limitation of CPP-cargo covalent linkage is the possible reduction or cleavage of chemical bonds before the complex reaches the target cells (Lundberg *et al*., 2007). On the other hand, non-covalent strategies provide an easy procedure for generating a drug delivery formulation that may only require mixing the CPP and the cargo (Boisguérin *et al*., 2015). Non-covalent complexation also provides the benefit of protecting nucleic acid oligomers against digestion by intra- and extracellular nucleases (Margus *et al*., 2012). However, a limitation to the application of this strategy *in vivo* may be the difference in the pharmacokinetics and biodistribution profiles of both highly charged molecules. This may alter their efficiency to co-localise in sufficient doses at the target site and restrict their application to local administration (Lee *et al*., 2013).

The introduction presented for this chapter provide a brief description of the types of CPPs-delivery strategies that have been investigated to deliver nucleotides to the insides of cells. Noting that, descriptions of CPPs delivering proteins have been discussed in sections 1.5.4 and 1.6. There are clear opportunities for the design of new CPPs to deliver macromolecules to the insides of cells and this is the subject of this chapter using EJP-18 that was initially described in Chapter 4.

5.2   Summary, Aims and Objectives

In chapter 4, EJP-18, as a rhodamine conjugate, was effectively internalised into HeLa cells. The aims of this chapter were to investigate the ability of this peptide to deliver larger and more therapeutically relevant cargos to ascertain whether it had any potential as a delivery vector and to determine whether it could be referred to as a CPP.

The objectives of this chapter were to:

1- Investigate the ability of EJP-18 to form non-covalent complexes with different cargos (protein, siRNA and plasmid DNA) using agarose gel shift assays and/or non-denaturing PAGE.

2- Investigate the uptake of these non-covalent complexes into HeLa cells using live cell confocal microscopy.

3- Investigating the endocytic traffic and subcellular localisation of EJP-18/albumin complexes, in lysosome labelled cells, following their internalisation by endocytosis using live cell confocal microscopy.

4- Investigate the biological effects of cargos delivered by EJP-18 with respect to silencing protein expression using siRNA or transfecting cells with plasmid DNA.

5.3   Results

5.3.1   *EJP-18 mediated cellular delivery of Bovine Serum Albumin (BSA-Alexa647)*

5.3.1.1   EJP-18/BSA complexation

Gel shift assays are routinely performed to assess the complexation of CPPs with nucleotides such as siRNA and plasmids (Rittner *et al*., 2002, Hyndman *et al*., 2004, Liu *et al*., 2005, Lundberg *et al*., 2007, Crombez *et al*., 2009, Jafari *et al*., 2012, Xu *et al*., 2014). Despite studies showing that intact proteins can be complexed with CPPs and delivered to cells, there is very little documentation of the characterisation of these complexes using similar or alternative methods.

In this thesis, a CPP-protein gel shift procedure was developed to examine whether EJP-18 efficiently complexes BSA-Alexa647. Initially this was performed by simple mixing of the peptide and fluorescent protein as described in section 2.7.2.1 and then loading on to agarose gels as described in section 2.7.3. The Typhoon variable mode scanner allows for direct visualisation of fluorescent molecules on gels and immediately after running, the gel was scanned using an excitation wavelength of 633 nm as described in section 2.7.3. BSA-Alexa647 as an uncomplexed protein gave a single band (Figure 5-1A) whose mobility was slightly retarded at molar peptide:protein ratios above 10:1. Despite the fact that the EJP-18 peptide used in this reaction was unlabelled, a faint band was observed in the EJP-18 alone lane. This had barely migrated into the gel and was also observed in all lanes of $\geq$ 20:1 molar ratios.

The BSA band became increasingly faint as the ratio increased and also smearing was observed suggesting the formation of high molecular weight complexes that were retarding migration of the protein.

To further investigate the complexes, samples from identical experiments were loaded and separated on a native PAGE gel as described in section 2.6 and initially analysed using the Typhoon scanner but then subjected to Coomassie blue staining. The gel profile was very different from that obtained from the agarose gel (Figure 5-1B & C). EJP-18 was shown to retard the mobility of BSA-Alexa647 at a lower molar ratio (5:1) than that observed in the agarose gel. At molar ratio of 20:1, only a very faint band corresponding to BSA-Alexa647 was detected that disappeared at higher molar ratios. Similar results were obtained from Coomassie staining that also allowed for the visualisation of molecular weight markers in lane 1.

(A)

(B) **(C)**
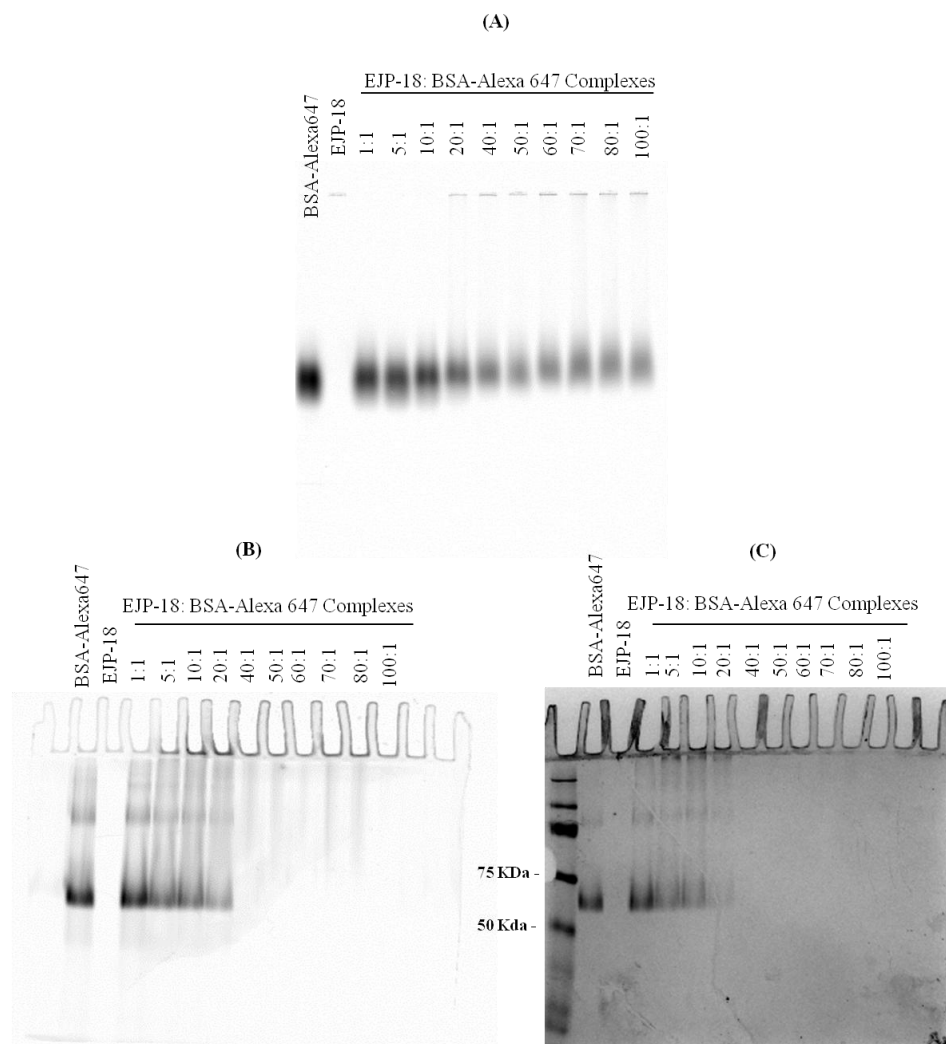
Figure 5-1: Agarose gel shift assay (A) and Native-PAGE (B-C) analysis of the ability of EJP-18 to form complexes with BSA-Alexa647. EJP-18/BSA-Alexa647 complexes were prepared by mixing 1 μg BSA-Alexa647 with increasing concentrations of EJP-18 giving rise to molar ratios of peptide/siRNA ranging from 1-100:1. The complexes were analysed using (A) agarose gel electrophoresis and imaging on the Typhoon scanner or (B) Native-PAGE and imaging on the Typhoon scanner or (C) staining with Coomassie Brilliant Blue. Images shown are representative from (A) three independent experiments or (B) two independent experiments.

5.3.1.2 Cellular uptake (Internalisation) of EJP-18/BSA-Alexa647 complexes in HeLa cells.

The capacity of EJP-18 to deliver BSA-Alexa647 was examined in HeLa cells by confocal microscopy. Complexes were prepared and incubated with cells as described in section 2.4.1.3. For these experiments, a concentration of 10μg/ml BSA-Alexa647 was initially incubated with the cells and after 1 h, no cell associated fluorescence was observed suggesting none or very little had gained access to the cells (Figure 5-2 bottom row). Complexation of BSA-Alexa647 with 2 μM EJP-18 enhanced the internalisation BSA-Alexa647 (Figure 5-2 top row), and this was further increased by raising the concentration of the peptide to 10 μM (Figure 5-2 middle row). EJP-18/BSA-Alexa647 complexes were localised in vesicular structures that were predominantly concentrated in a distinct perinuclear region. This localisation was strongly suggestive of uptake by endocytic pathways.
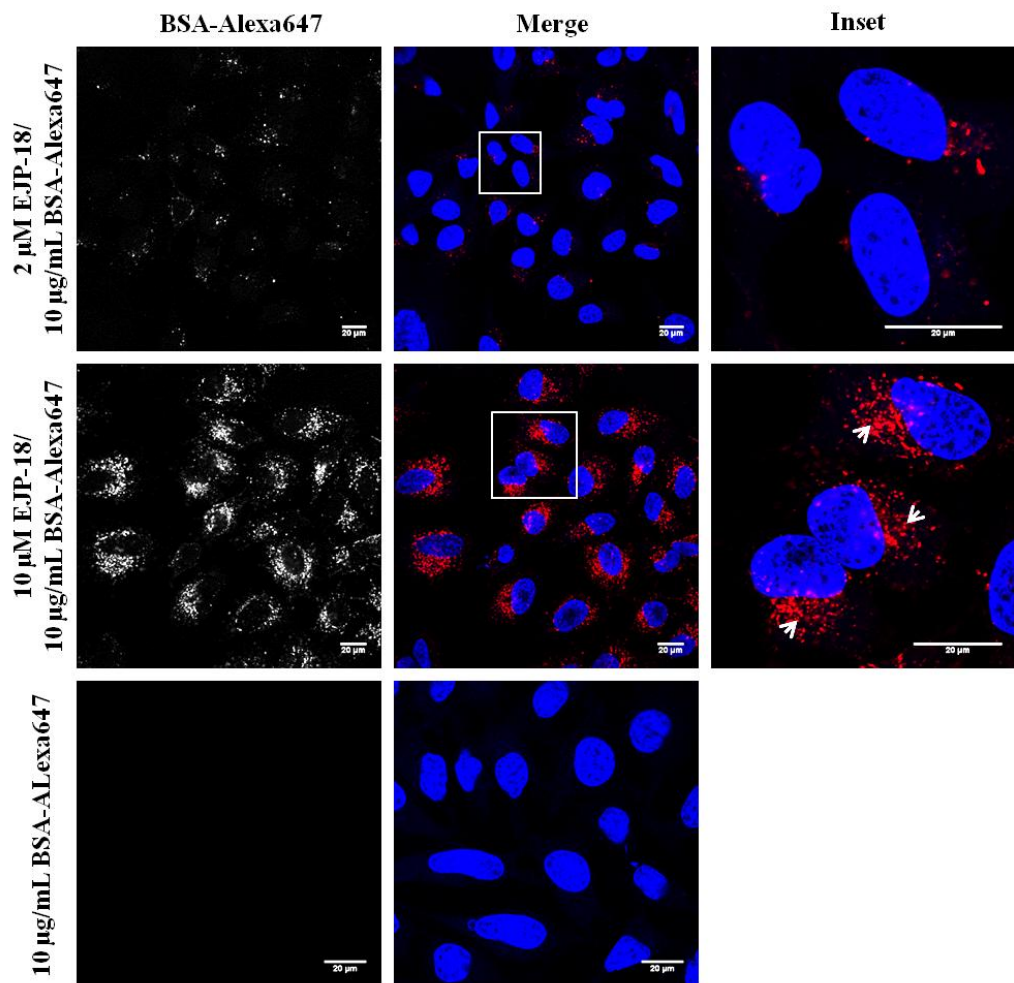
Figure 5-2: Internalisation of EJP-18/BSA-Alexa647 complexes into HeLa cells in SFM. EJP-18 (2 or 10 μM) was complexed with BSA-Alexa647 and subsequently added to cells that were then incubated for 1 h at 37ºC, washed and imaged by confocal microscopy. Bottom row shows cells incubated with BSA-Alexa647 (10 μg/mL) alone. Representative images (N=2) show a single section through the cell at the mid-point of the nucleus, labelled in blue with Hoechst. Inset represents selected regions from the merged images. *White arrows indicate distinct perinuclear fluorescence. Scale bars = 20 μm.*

5.3.1.3 Cellular uptake (internalisation) of labelled BSA complexed with EJP-18, penetratin, R8 and R8-GC in HeLa cells in SFM or CM

The efficiency of EJP-18 to deliver labelled BSA was compared with that of two well characterised CPPs, penetratin and R8, including an R8-GC peptide that is used for labelling with fluorophores.

5.3.1.3.1 EJP-18 mediated internalisation of BSA-Alexa647

The 10 μM peptide/BSA-Alexa647 complexes were prepared and incubated with HeLa cells as described in section 2.4.1.3. Figure 5-3A illustrates that EJP-18 effectively delivered BSA-Alexa647 to label punctate structures in these cells. Only very weak fluorescence signal was detected for penetratin/BSA-Alexa647 and interestingly, R8-GC exhibited a higher delivery efficiency compared with R8 alone; again clear labelling in vesicular structures was observed.

EJP-18, R8 and R8-GC were then assessed for their ability to deliver the labelled albumin at a lower concentration (5 μM). Figure 5-3B demonstrated that only R8-GC and EJP-18 were able to deliver this protein to give consistent fluorescence readout above that of background noise.
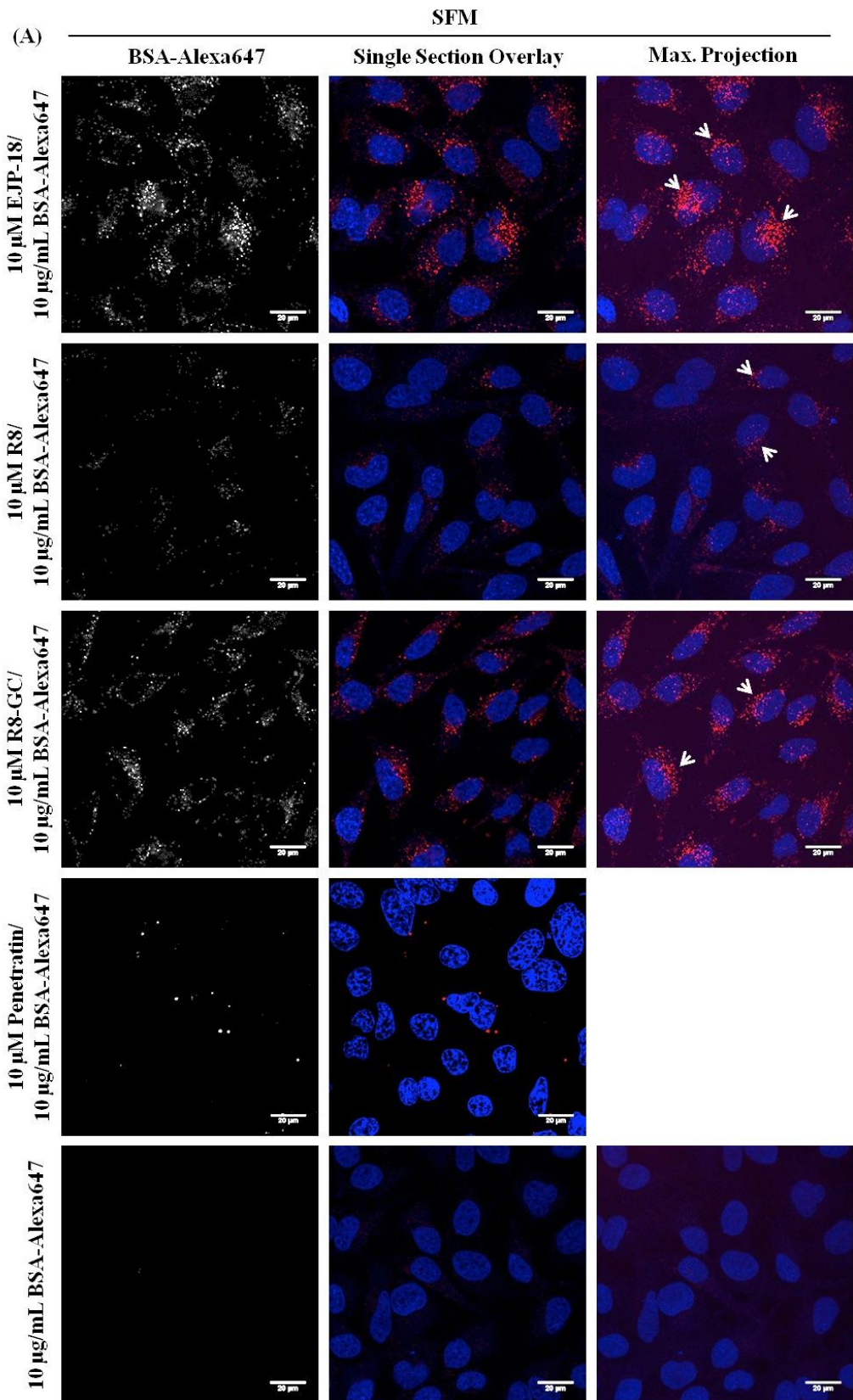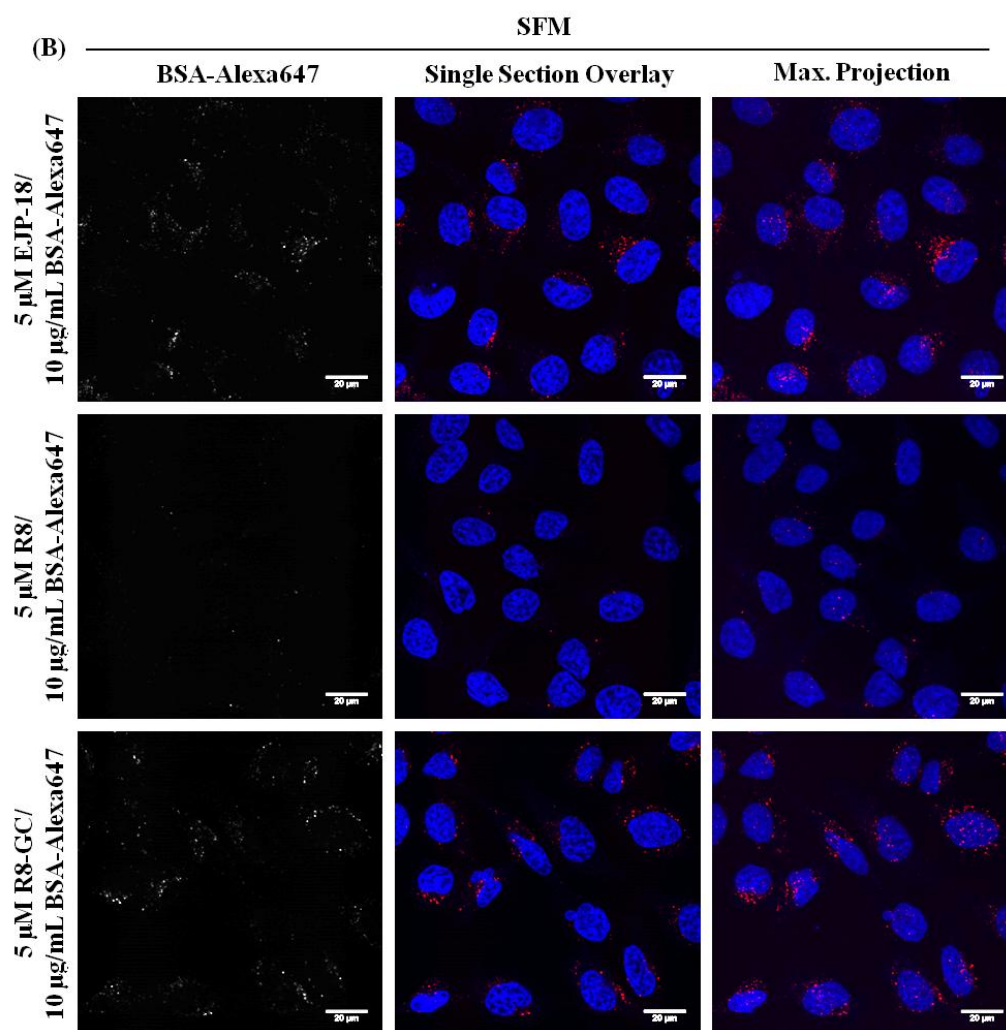
Figure 5-3: Internalisation of peptide/BSA-Alexa647 complexes into HeLa cells in SFM. EJP-18, R8, penetratin and R8-GC peptides: (A) 10 μM or (B) 5 μM was incubated with BSA-Alexa647 and subsequently added to cells that were then incubated for 1 h at 37ºC, washed and imaged by confocal microscopy. Bottom row in (A) shows cells incubated with BSA-Alexa647 (10 μg/mL) alone. Representative images (N=3) showing either a single section through the cell at the mid-point of the nucleus or maximum projection of the whole cell. Nuclei were labelled blue with Hoechst. *White arrows indicate distinct perinuclear labelling. Scale bars = 20 μm.*

To test the effect of serum on the uptake of the complexes, experiments shown in Figure 5-3 employing EJP-18 and R8-GC were then repeated but here the complexes were diluted in serum containing medium (complete medium) rather than serum free medium and then incubated with cells. In complete medium, both CPPs were still able to deliver the labelled albumin into cells as

shown in Figure 5-4. This suggests that the precomplexing stage gives stable

complexes that can withstand possible degradation by serum proteins.
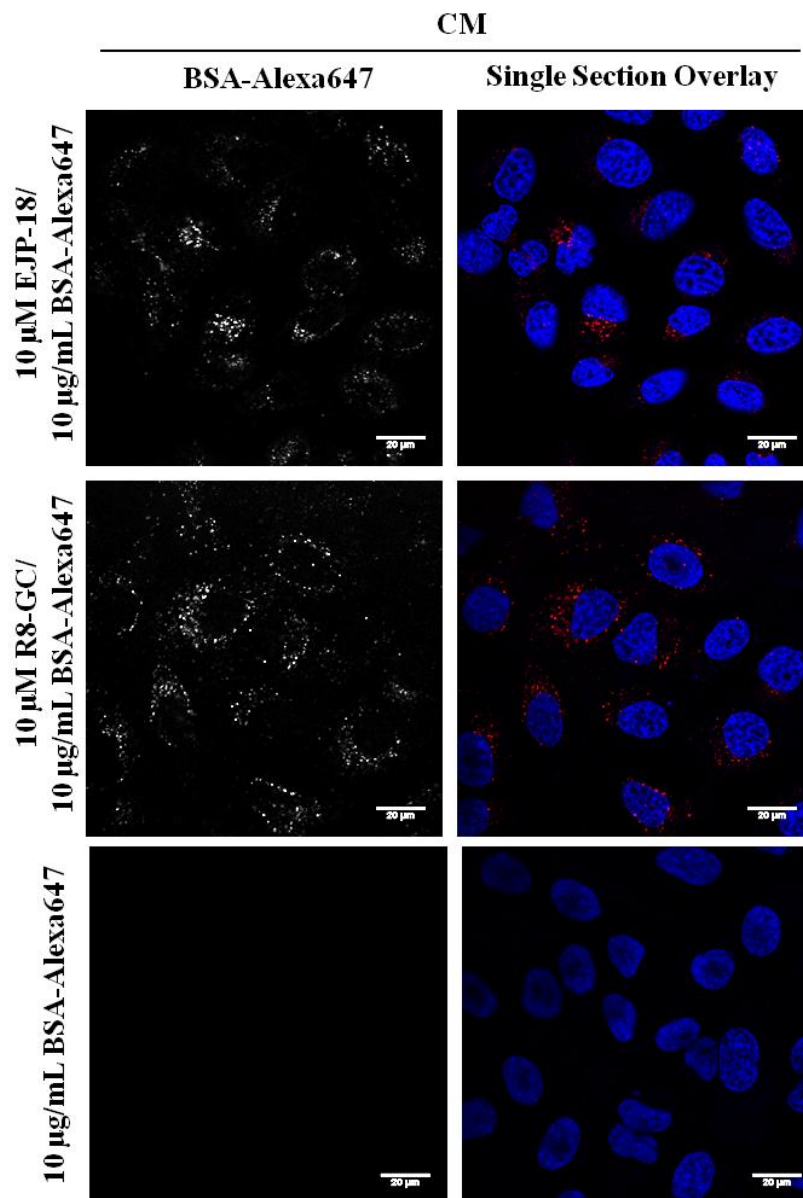
Figure 5-4: Internalisation of peptide/BSA-Alexa647 complexes into HeLa cells in CM.
EJP-18 and R8-GC (10 μM) were incubated with BSA-Alexa647 and subsequently added to
cells that were then incubated for 1 h at 37ºC, washed and imaged by confocal microscopy.
Bottom row shows cells incubated with BSA-Alexa647 (10 μg/mL) alone. Representative
images (N=2) showing a single section through the cell at the mid-point of the nucleus,
labelled in blue with Hoechst. *Scale bars = 20 μm.*

5.3.1.3.2 EJP-18 mediated internalisation of BSA-Alexa488

As reported in the literature and discussed in section 4.4, fluorophores can influence the cellular distribution of CPP and CPP/cargo complexes. For this reason, the BSA delivery experiments were repeated using BSA-Alexa488 rather than Alexa647 noting that these two fluorophores, despite bearing the prefix Alexa, have very different structures (Jones and Sayers, 2012). EJP-18/BSA-Alexa488 complex was prepared and incubated with HeLa in SFM as described above and in section 2.4.1.3. Figure 5-5 illustrates that EJP-18 effectively delivered BSA-Alexa488 to label distinct perinuclear regions of cells as was previously observed with EJP-18/BSA-Alexa647 complexes. Once again no cell-associated fluorescence was observed when the same amount of uncomplexed BSA-Alexa488 was incubated with these cells.
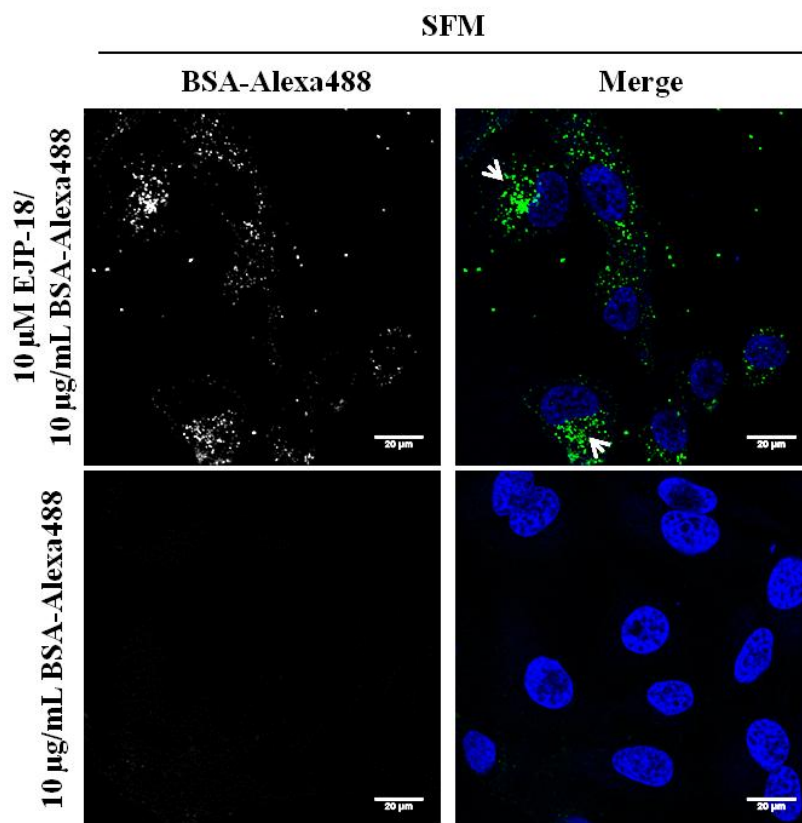
Figure 5-5: Internalisation of EJP-18/BSA-Alexa488 complexes into HeLa cells in SFM. EJP-18 (10 μM) was complexed with BSA-Alexa488 and subsequently added to cells that were then incubated for 1 h at 37°C, washed and imaged by confocal microscopy. Bottom row shows cells incubated with BSA-Alexa488 (10 μg/mL) alone. Representative images (N=2) showing a single section through the cell at the mid-point of the nucleus, labelled in blue with Hoechst. *White arrows indicate distinct perinuclear labelling. Scale bars = 20 μm.*

5.3.1.4 Analysis of the subcellular distribution of Peptide/BSA-Alexa647 complexes

The localisation of the EJP-18/BSA-Alexa647 complexes in a distinct perinuclear region suggested they were internalised by endocytosis and delivered to lysosomes that in the HeLa cell line are often located in this region (Al-Taei *et al.*, 2006). Endocytosis of dextran is well characterised in terms of initial fluid phase uptake into early endosomes, and traffic through late endosomes to lysosomes. To specifically label lysosomes, cells were incubated with dextran-Alexa488 for 2 h followed by an overnight chase into lysosomes that can be achieved via a further incubation in dextran-free complete medium

(Bright *et al*., 2005). The next day, the cells were washed and incubated for 1 h with EJP-18/BSA-Alexa647 or R8/BSA-Alexa647 complexes formed as described above and in section 2.4.1.6. Figure 5-6 demonstrates that BSA-Alexa647 delivered during this 1 h period by EJP-18 and by R8 colocalised with dextran labelled lysosomes to the same extent (Pearson's coefficient = 0.38 ± 0.09 and 0.38 ± 0.04 respectively). A higher degree of colocalisation between the labelled peptides and lysosomes was observed after the complexes were similarly incubated with the cells for 1 h and then chased for a further hour in complex free medium: EJP-18/BSA-Alexa647 and R8/BSA-Alexa647 giving Pearson's coefficient of 0.57 ± 0.03 and 0.49 ± 0.07 respectively. The difference between groups was statistically significant by one-way ANOVA $F_{(3, 10)}$ = 7.040, p = 0.0079. Tukey post-hoc tests revealed that increased colocalisation was only significant between 1 h pulse with EJP-18/BSA complexes and 1 h chase with the same complex (p < 0.05).
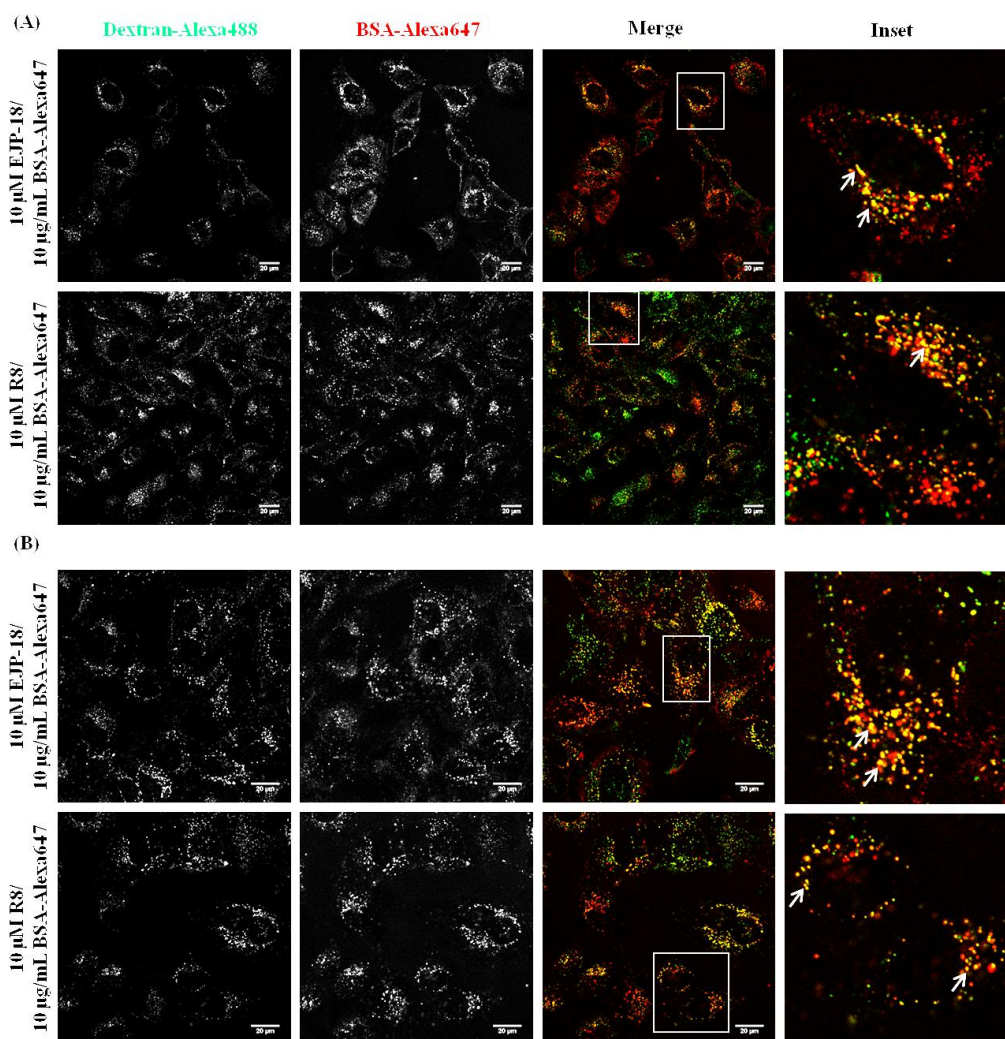
Figure 5-6: Traffic of EJP-18/BSA-Alexa647 or R8/BSA-Alexa647 to lysosomes in HeLa cells. Cells were incubated at 37°C with dextran-Alexa488 for 2 h followed by an overnight chase and were then incubated with EJP-18/BSA-Alexa647 or R8/BSA-Alexa647 complexes for (A) 1 h or (B) 1 h followed by 1 h chase. The cells were then washed and imaged by confocal microscopy. Representative images (N=4) showing a single section through the cells and the right panel in (A) and (B) shows a zoomed image of an identified cell in merge panel. *Colocalisation is marked by white arrows. Scale bars = 20 μm.*

5.3.1.5 Cytotoxicity of Peptides/BSA-Alexa647 complexes

EJP-18, R8 and penetratin were found to be nontoxic at 10 μM (Figures 4-2, 4-4 and 3-3 respectively); the concentration used to deliver labelled albumin. To ensure that the peptide/BSA-Alexa647 complexes were also nontoxic, HeLa cells were incubated with the complexes (10 μM peptide/10 μg/mL BSA) under tissue culture conditions for 24 or 72 h. Cell viability was then

185

determined using CellTiter-Blue assay as described in section 2.3.2. Figure 5-7 shows that none of these complexes were toxic to cells at the concentrations used here and this was confirmed using one-way ANOVA analysis ($p < 0.05$).
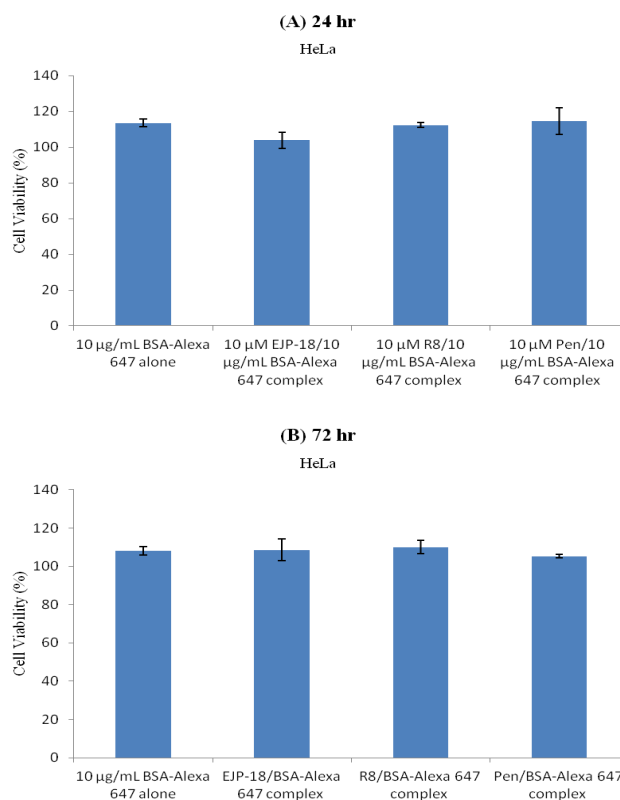
Figure 5-7: Viability of HeLa cells incubated with peptide/BSA-Alexa647 complexes. Viability of cells was evaluated using CellTiter-Blue assay following (A) 24 h or (B) 72 h incubation with CPP/BSA-Alexa647 complexes in HeLa cells. Results represent means ± SD for (A) three independent experiments or (B) two independent experiments, performed in duplicate.

5.3.2 EJP-18 mediated complexing and delivery of siRNA

In section 5.3.1.3.1, EJP-18 was found able to complex and promote the cellular uptake of BSA-Alexa647. It was then decided to investigate the efficacy of EJP-18 to complex and deliver siRNA to inhibit the expression of proteins.

5.3.2.1 Agarose gel shift assay for investigating EJP-18/siRNA complexation

An agarose gel shift assay was developed to detect the interaction between EJP-18 and siRNA targeting Cav-1 and PAK-1. EJP-18/siRNA complexes at increasing molar ratios were prepared as described in section 2.7.2.2. siRNA alone and oligofectamine/siRNA complex were used as controls. Oligofectamine is a commercial cationic polymer based transfection reagent that is routinely used in the laboratory for siRNA delivery and inhibiting the expression of proteins including Cav-1 and PAK-1 (Al Soraj *et al.*, 2012). These specific siRNAs were selected here as examples of validated laboratory sequences. Complexes were prepared and analysed by agarose gel electrophoresis and ethidium bromide staining as described in section 2.7.3. Figure 5-8 (A & B) shows that EJP-18 clearly retarded the migration of both siRNAs at a molar ratio of 20:1. The siRNA retardation efficacy of EJP-18 increased at molar ratios above 20:1 and at 160:1, the retardation of siRNA was complete as no ethidium bromide signal was detected in the gel itself. Interestingly, at molar ratios above 80:1, a faint shadow of ethidium bromide staining was observed above the loading well suggesting that the siRNA had migrated towards the cathode. For both siRNAs, oligofectamine gave two regions of ethidium bromide staining: one at the expected (unhindered) migration point and one in the loading well.
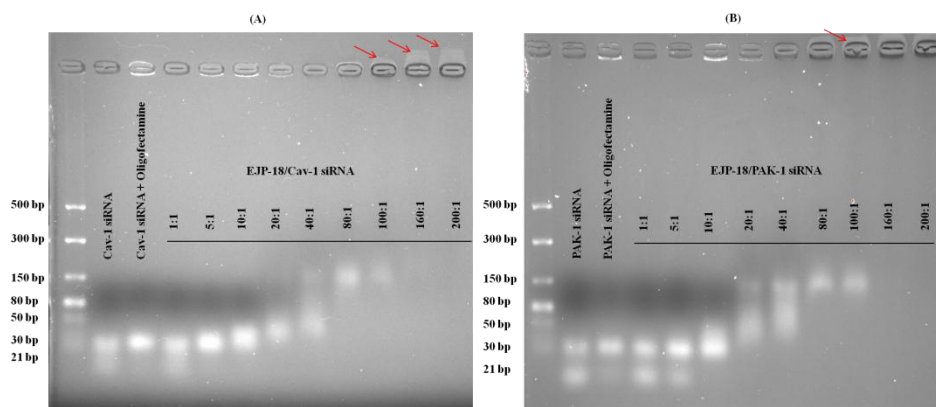
Figure 5-8: Agarose gel shift assay analysis of EJP-18 and oligofectamine/siRNA complexes (A) Cav-1 siRNA and (B) PAK-1 siRNA. EJP-18/siRNA complexes were prepared by mixing 0.5 µg siRNA with increasing concentrations of EJP-18 giving rise to molar ratios of peptide/siRNA ranging from 1 to 200:1. The complexes were analysed using gel shift assay and imaged using a BioRad ChemiDoc system. Images (A & B) shown are representative from two independent experiments. *Red arrows point to migration of siRNA towards the cathode.*

5.3.2.2 Cell uptake of Cy5-Cav-1 siRNA complexed with EJP-18 or oligofectamine in HeLa cells

EJP-18 clearly demonstrated that it could complex siRNA and to analyse, using confocal microscopy, whether it could also deliver siRNA into cells, a custom Cy5 labelled version of the siRNA targeting Cav-1 was purchased. Cy5-Cav-1 siRNA (Cy5-siRNA 50 or 100nM) was then mixed with increasing concentrations of EJP-18 or with oligofectamine as described in section 2.4.1.4. For incubation with 50 nM Cy5-siRNA, molar ratios of up to 200: 1 (EJP-18/siRNA) were used so that the final concentration for EJP-18 was 10 µM (the concentration used to deliver labelled BSA). Lower molar ratios were also evaluated for siRNA delivery. When cells were transfected with 100 nM Cy5-siRNA, the highest molar ratio tested was 100:1 and the final concentration of EJP-18 was maintained at 10 µM. These complexes and

Cy5-siRNA alone were then incubated with HeLa cells for 3 h in Opti-MEM prior to cell washing and analysis by live cell imaging confocal microscopy.

As expected, there was no evidence that Cy5-siRNA alone was able to interact with or enter cells. Figure 5-9 shows that EJP-18/Cy5-siRNA complexes (50 and 100 nM) could be seen in punctate structures in the cell cytoplasm. The fluorescent siRNA was also seen after complexation with oligofectamine. From three independent experiments, a large degree of heterogeneity with respect to subcellular distribution of fluorescence was observed for siRNA (at both concentrations) complexed with EJP-18. This difference was observed within a single cell population and between repeat experiments (Figure 5-9). siRNA internalised by oligofectamine also showed distribution patterns that varied from small vesicles in the cytoplasm of some cells (Figure 5-9 A & B) to large aggregates that were spread throughout the cells (Figure 5-9 C & D). Experiments were also performed at lower molar ratios: 20:1 and 10:1 but the fluorescence signal was below the detection level of this microscopy method (Data not shown).

The ring structures appearing on the overlay in Figure 5-9 are due to a fault on the confocal system. Despite numerous visits by the Leica engineers, this problem was only (partly) resolved at the later stages of the writing of this thesis.

(A)

siRNA	Single Section Overlay	DIC + Overlay

(B)

(C)
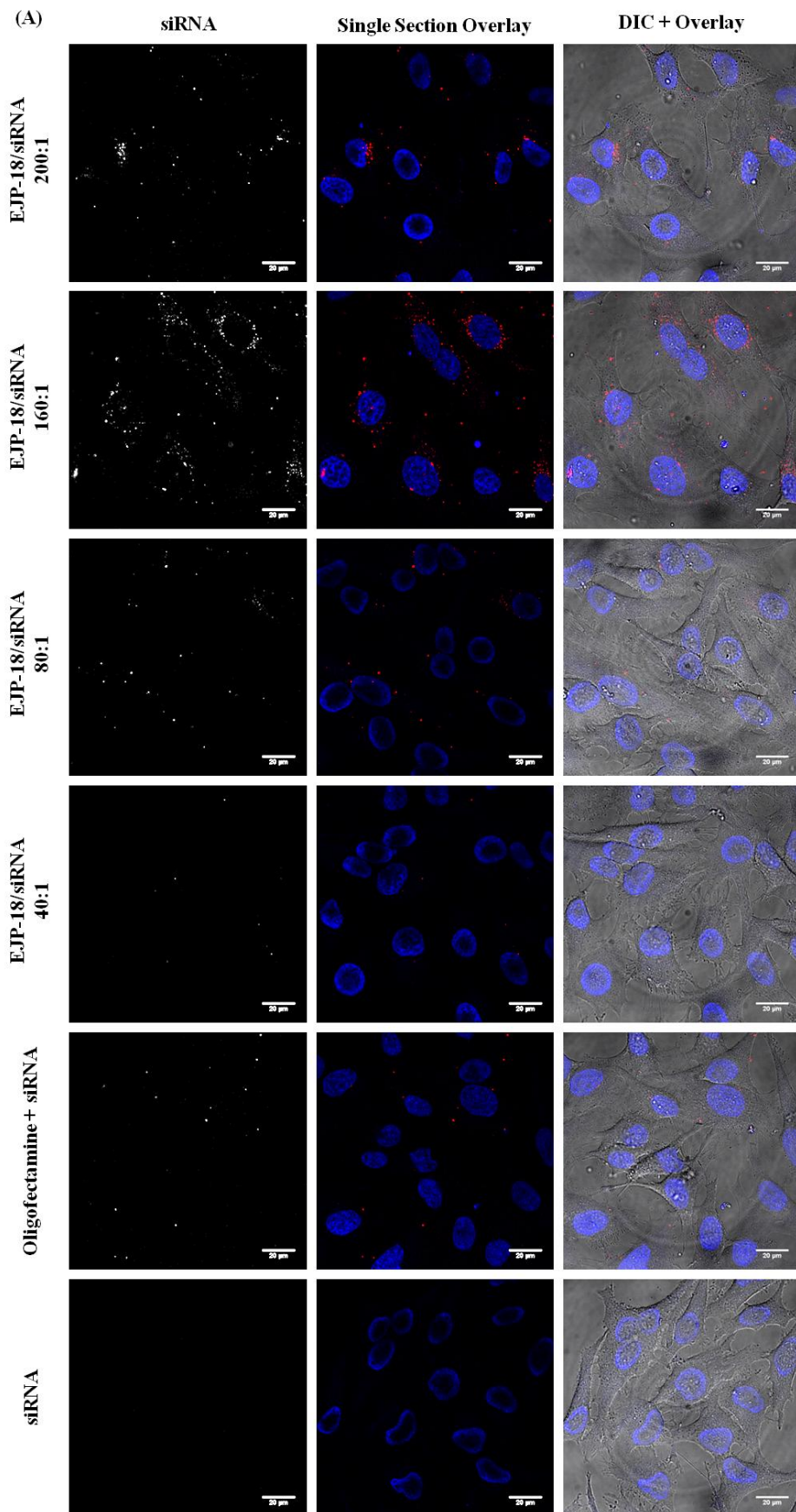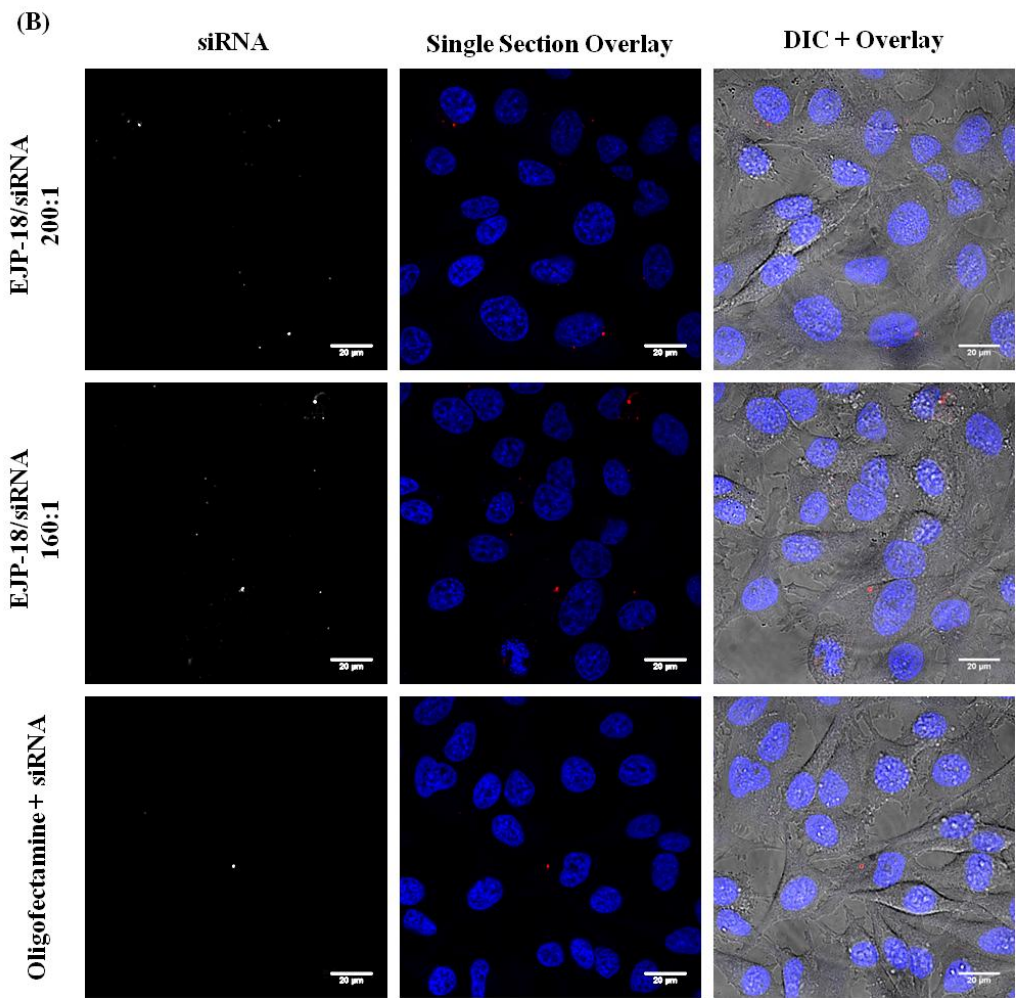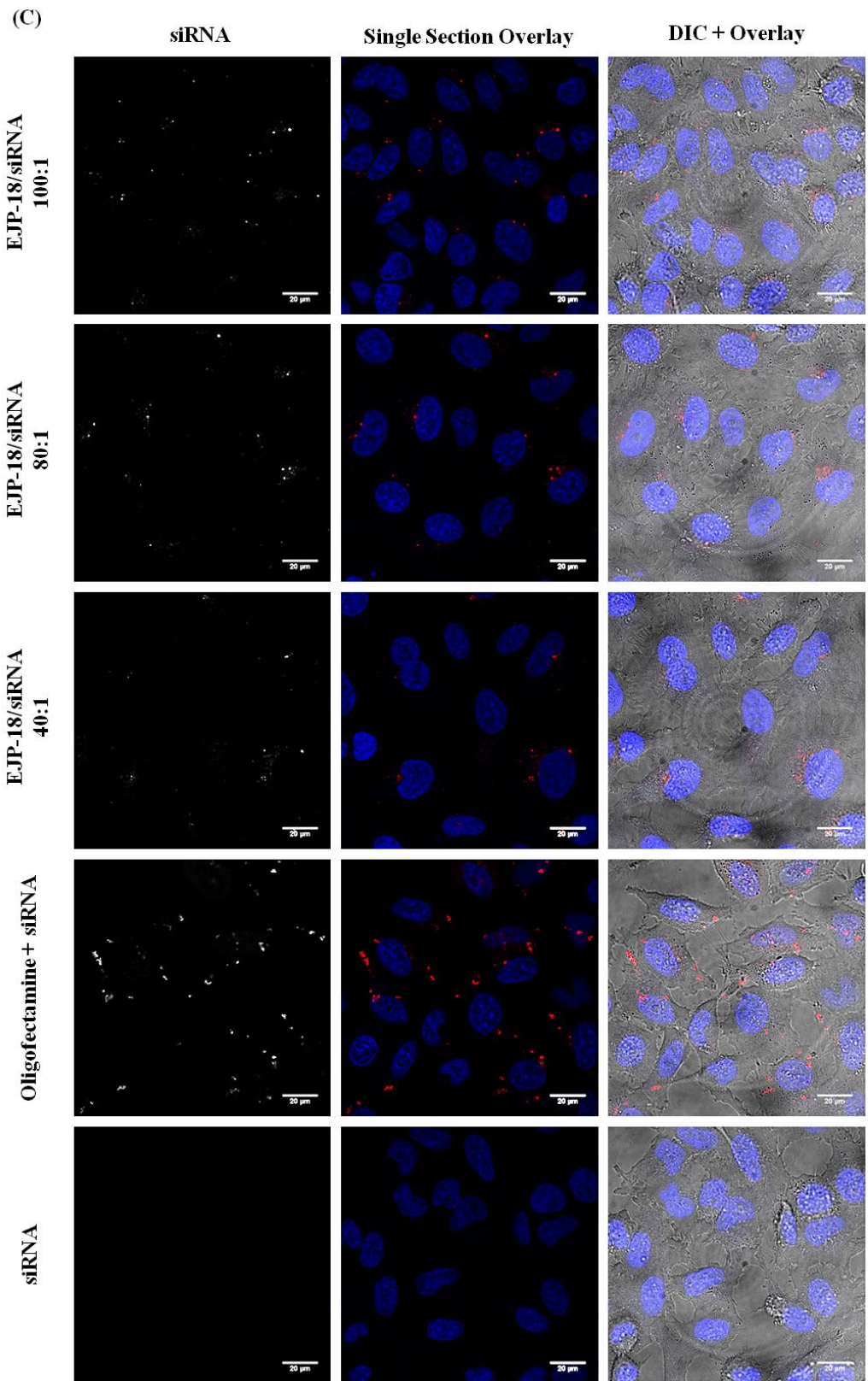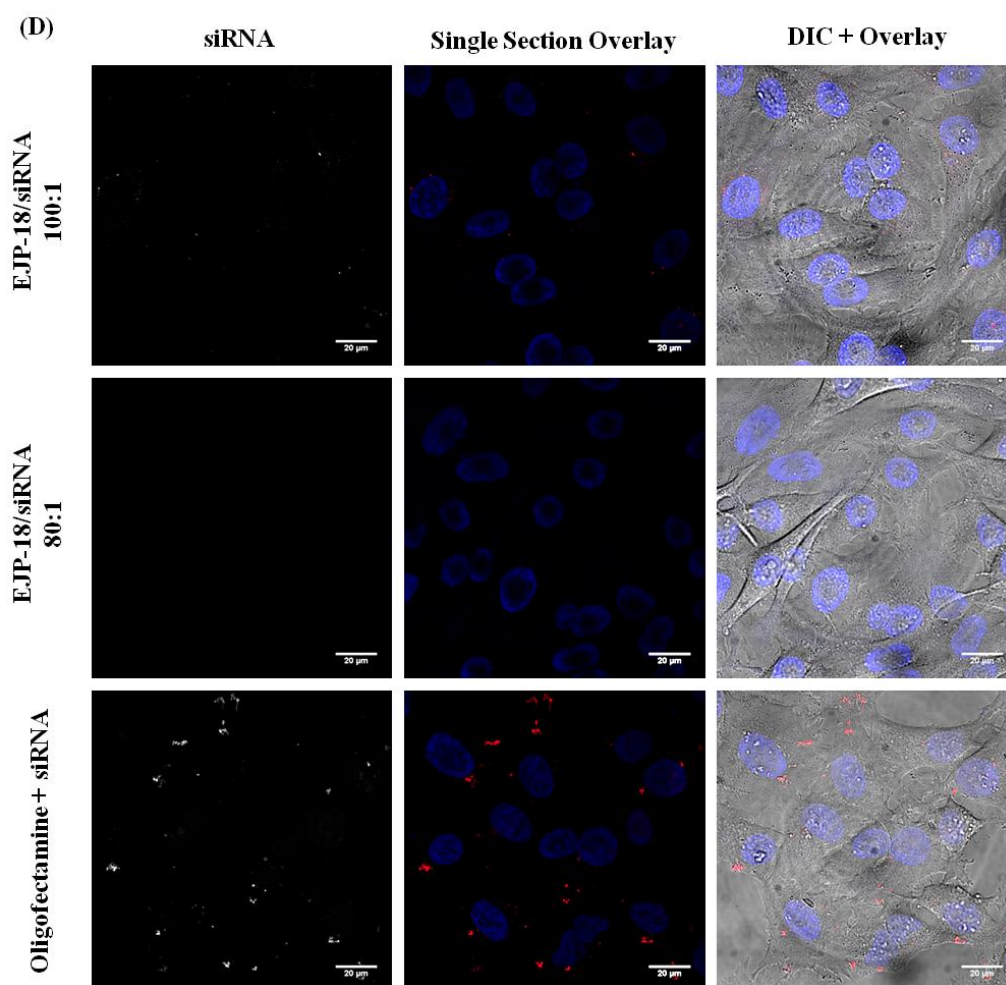
Figure 5-9: Internalisation of EJP-18/Cy5-siRNA complexes into HeLa cells. EJP-18/Cy5-siRNA or oligofectamine/Cy5-siRNA complexes (A & B) 50 nM siRNA and (C& D) 100 nM siRNA were incubated with cells for 3 h at 37ºC prior to analysis by confocal microscopy. Bottom row in A & C shows cells incubated with 50 and 100 nM Cy5-siRNA alone respectively. Images represent a single section through the cell at the mid-point of the nucleus, labelled in blue with Hoechst. Three separate experiments were performed and images from two of these are shown for 50 nM (A & B) and 100 nM (C & D). *Scale bars = 20 μm.*

5.3.2.3 Transfection experiments with EJP-18 or oligofectamine/siRNA complexes

Having achieved promising results from the complexation and cell uptake studies, it was then important to examine whether EJP-18/siRNA complexes were able to deliver siRNA to cells and into the cytosol to deplete protein targets i.e. Cav-1 and PAK-1 as can be performed with oligofectamine (Al Soraj *et al*., 2012).

193

5.3.2.3.1 Transfection experiments with EJP-18/Cav-1 siRNA complexes in HeLa cells

Cav-1 depletion with Cav-1 siRNA (50 nM) was tested in three independent experiments performed in HeLa cells as previously described in section 2.9.1. The molar ratio tested for Cav-1 knockdown was 200:1 (peptide/siRNA) giving a final EJP-18 concentration of 10 μM i.e. the concentration found to deliver BSA and siRNA. As a positive control, siRNA transfection was performed with oligofectamine as previously described (Al Soraj *et al.*, 2012). Transfection with a control GFP non-targeting siRNA was also performed with both oligofectamine and EJP-18 at the same molar ratio to assess specificity for Cav-1 depletion. Cav-1 expression in cells treated with 10 μM EJP-18 alone was also investigated to exclude potential non-specific effects of this peptide on Cav-1 expression. Untransfected cells were included as a control for baseline Cav-1 levels. The cells were incubated with the siRNA for 48 h prior to preparing cell lysates as described in section 2.9.1 that were subjected to Western blotting for Cav-1 expression that was quantified using ImageJ software. One-way ANOVA was performed to determine the statistical significance of differences between groups.

As expected, oligofectamine/Cav-1 siRNA complexes consistently reduced Cav-1 expression (Figure 5-10 B, D and F) and the average reduction in protein expression of three experiments was 80% (Figure 5-10G). In cells transfected with EJP-18/Cav-1 siRNA complexes, there was large intra assay variation in Cav-1 expression. Figure 5-10 (B & F) shows 45 and 25% reduction in Cav-1 expression respectively but Figure 5-10D shows an increase of ≈30% under

identical transfection conditions. The average of the three experiments showed ≈ 13% reduction in Cav-1 levels (Figure 5-10G) but this reduction was not statistically different from control cells. The difference between groups was statistically significant by one-way ANOVA $F_{(7, 16)} = 4.424$, $p = 0.0066$. Tukey post-hoc tests revealed that the reduction in Cav-1 expression was only statistically significant between cells transfected with oligofectamine/Cav-1 siRNA and untransfected cells ($p < 0.05$).
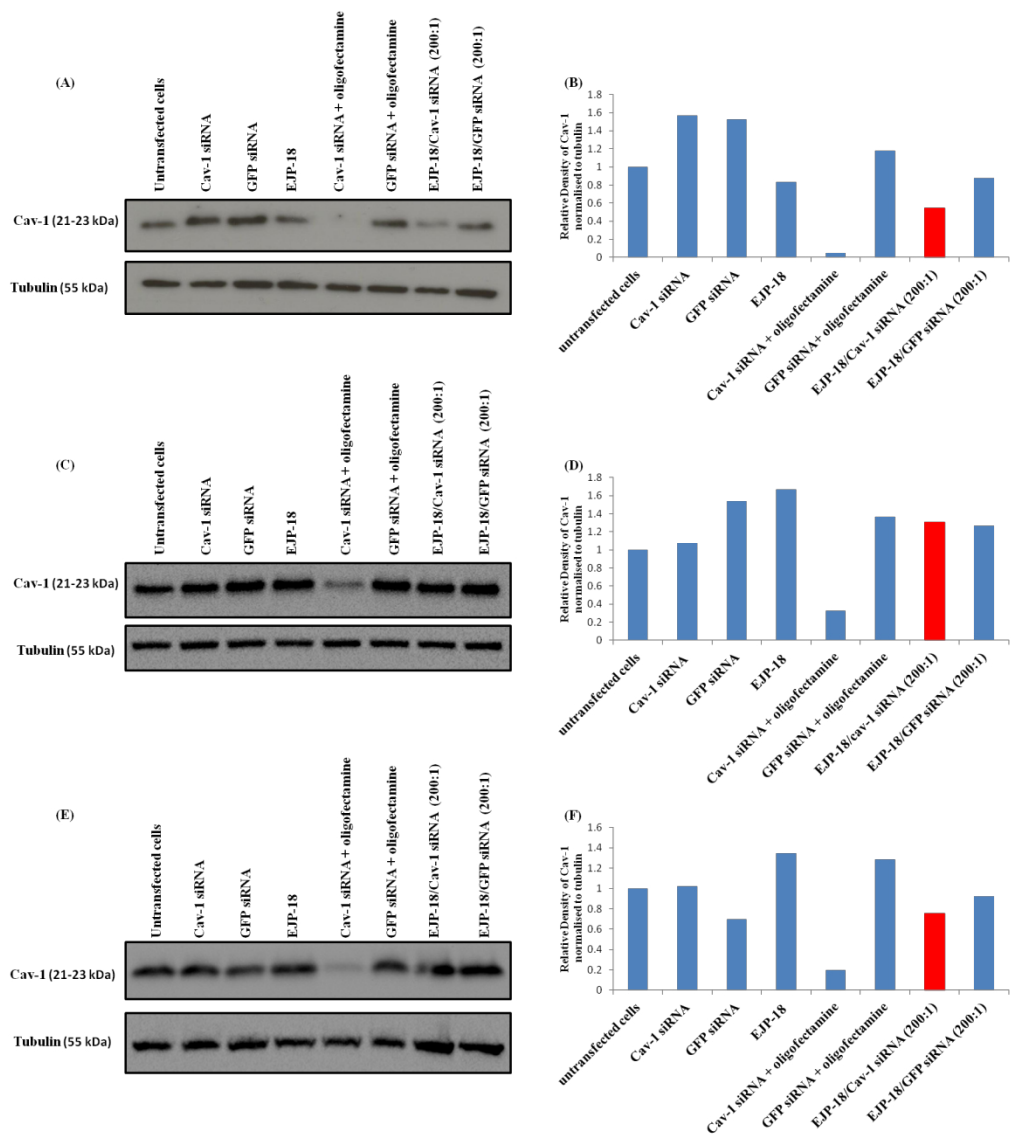
Figure 5-10: Relative levels of Cav-1 in HeLa cells treated with Cav-1 or GFP non-targeting siRNA complexed with oligofectamine or EJP-18. (A, C and E) Immunoblots from three independent experiments. (B, D, F) Relative Cav-1 expression quantified with ImageJ software and normalised to β-tubulin loading control. (G) Relative Cav-1 expression ± SD from three independent experiments (B, D, F). *Cav-1 levels in EJP-18/Cav-1 siRNA transfected cells are highlighted in red. *** Statistical significance p ≤ 0.001.*

5.3.2.3.2 Transfection experiments with EJP-18/PAK-1 siRNA complexes in HeLa cells

Identical experiments and data analysis (5.3.2.3.1) were then performed using 100 nM final siRNA concentration for targeting PAK-1. The molar ratio tested for PAK-1 knockdown was 100:1 (peptide/siRNA) to keep the final concentration of EJP-18 at 10 μM. Figure 5-11G once again demonstrated very efficient protein depletion with oligofectamine giving close to 100% depletion of PAK-1 levels. Reduced levels of PAK-1 were also shown in cells transfected with EJP-18/PAK-1 siRNA complex (Figure 5-11 B, D and F) and the average reduction in PAK-1 expression of three experiments was ≈ 60%.

There was a problem with incorrect loading in the last two lanes of the gel in Figure 5-11E (third experiment). However, since PAK-1 band intensities were quantified relative to GAPDH loading control, this difference in loading was accounted for in the data analysis. The difference between groups was statistically significant by one-way ANOVA $F(7, 16) = 11.77$, $p < 0.0001$. Tukey post-hoc tests revealed that the reduction in PAK-1 expression was statistically significant between cells transfected with oligofectamine/PAK-1 siRNA and untransfected cells ($p < 0.001$), cells transfected with EJP-18/PAK-1 siRNA and untransfected cells ($p < 0.01$). It was also found that oligofectamine/GFP non-targeting siRNA also reduced PAK-1 levels and the reduction was statistically significant ($p < 0.05$). EJP-18 alone, consistently reduced PAK-1 levels but this was not statistically significant.
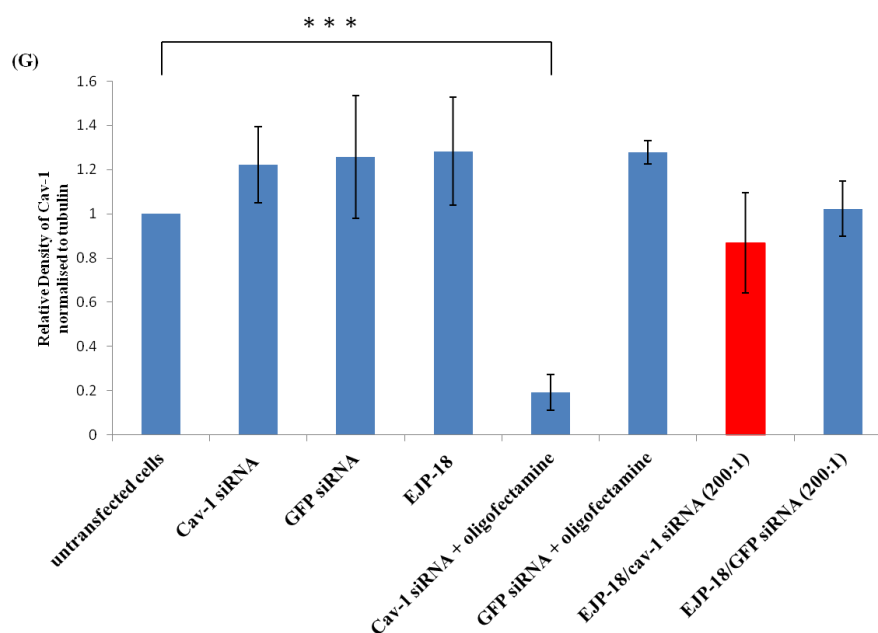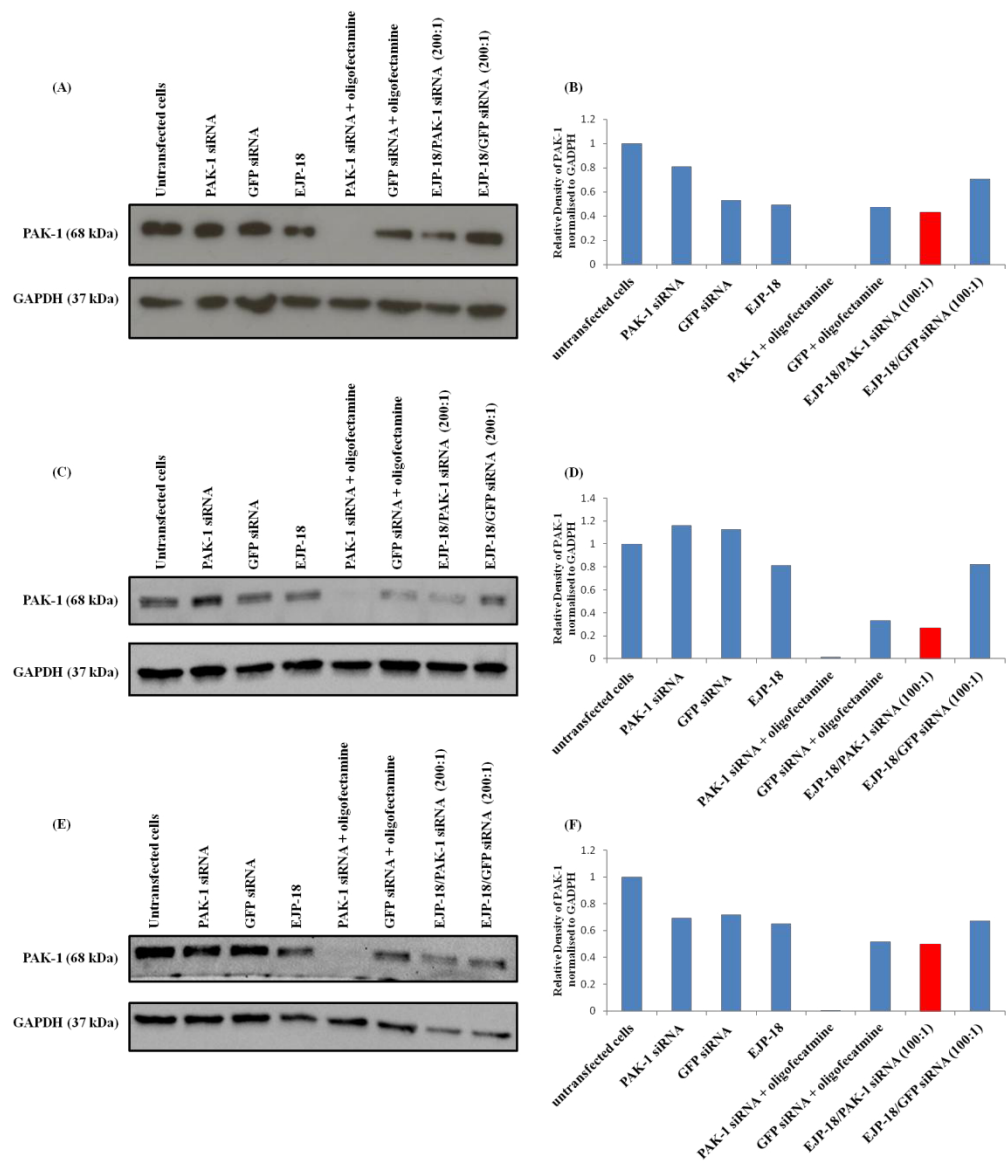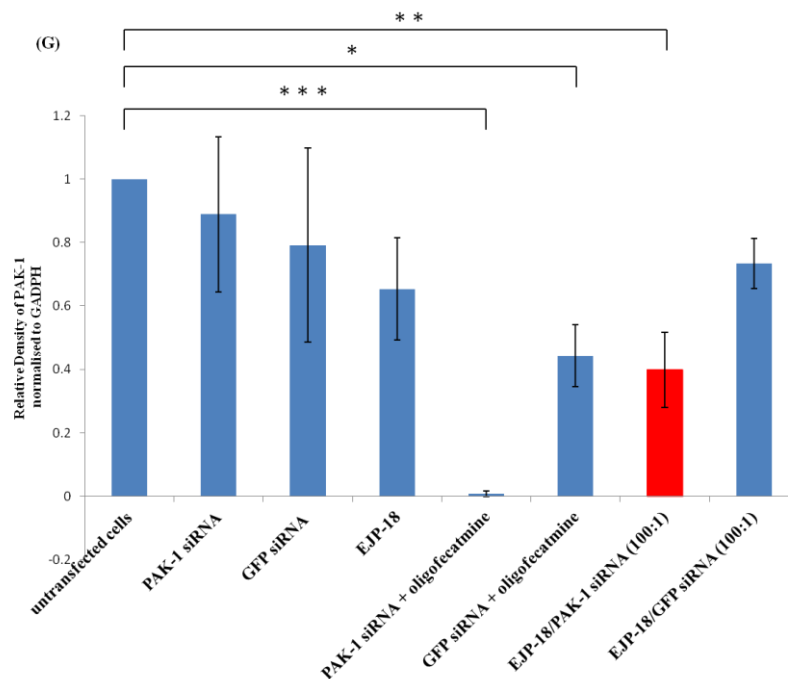
Figure 5-11: Relative levels of PAK-1 in HeLa cells treated with PAK-1 or GFP non-targeting siRNA complexed with oligofectamine or EJP-18. (A, C and E) Immunoblots from three independent experiments. (B, D, E) Relative PAK-1 expression quantified with ImageJ software and normalised to GAPDH loading control. (G) Relative PAK-1 expression ± SD of three independent experiments (B, D, E). *PAK-1 levels in EJP-18/PAK-1 siRNA transfected cells are highlighted in red. *** Statistical significance $p \leq 0.001$. ** Statistical significance $p \leq 0.01$. * Statistical significance $p \leq 0.05$.*

5.3.3 Assessing the capacity of EJP-18 to complex and deliver plasmid DNA

Finally, EJP-18 was tested for its ability to complex and deliver plasmid DNA to the cell nucleus. Here pEGFP-N1; a vector encoding enhanced green fluorescent protein (EGFP), was used as cargo (Liu *et al*., 2012), and the cells were visualised using wide field fluorescence microscopy.

5.3.3.1 Agarose gel shift assay for investigating EJP-18/plasmid DNA complexation

Agarose gel shift assay were initially performed to assess the DNA complexing capacity of EJP-18 for pEGFP-N1. The complexes were prepared by gently mixing 1 µg pEGFP-N1 with increasing concentrations of EJP-18 to give

peptide/plasmid DNA charge ratios between 1:1 and 50:1 as described in section 2.7.2.3. Complexes were analysed by agarose gel electrophoresis and imaged as described in section 2.7.3. EJP-18 showed clear retardation of the plasmid at the lowest charge ratio of 1:1 (Figure 5-12). At higher ratios, a smear of DNA was visible from the loading wells and at 20:1 charge ratio, only a faint smear of DNA was visible and at higher ratios, the plasmid DNA could not be detected.
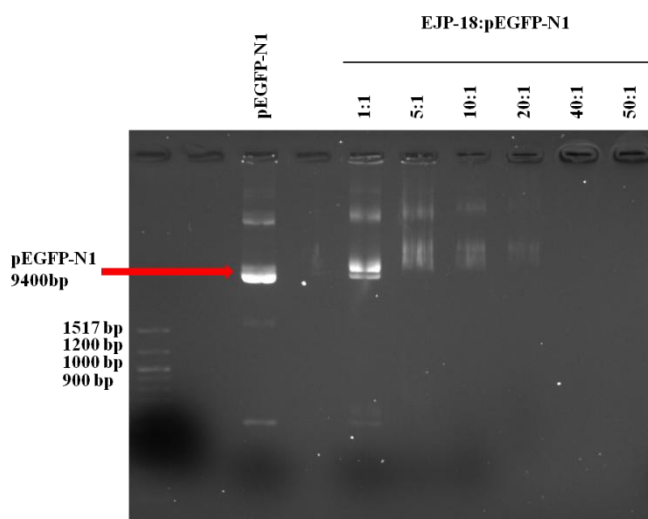
Figure 5-12: Agarose gel shift assay analysis plasmid complexing ability of EJP-18 for pEGFP-N1. EJP-18/pEGFP-N1 complexes were prepared by mixing 1 μg p-EGFP-N1 with increasing concentrations of EJP-18 giving rise to charge ratios of peptide/plasmid DNA ranging from 1 to 50:1. Image shown is representative from two independent experiments. The gels were imaged on the BioRad ChemiDoc system. *Red arrow denoting pEGFP-N1 bands.*

5.3.3.2 Transfection of HeLa with EJP-18/pEGFP-N1 vs FuGENE 6

As EJP-18 effectively complexed plasmid DNA, experiments were performed to assess its capacity to deliver DNA to transfect cells. Here the same pEGFP-N1 plasmid was employed. HeLa cells were incubated with EJP-18/pEGFP-N1 complexes as described in section 2.9.2 to give a highest charge ratio of 50:1 (the final peptide concentration was 20.8 μM). Cells

transfected with commercial transfection agent, FuGENE 6, served as a positive control. This is a cationic polymer formulation and widely used in the laboratory. Post complex addition (48 h), the cells on coverslips were washed, fixed and mounted on coverslides as described in section 2.10 and analysed by wide field microscopy. As expected (Figure 5-13), FuGENE 6 provided high transfection efficiency ($\approx$ 70%) but no EGFP expressing cells were observed following incubation with EJP-18/pEGFP-N1 complexes.
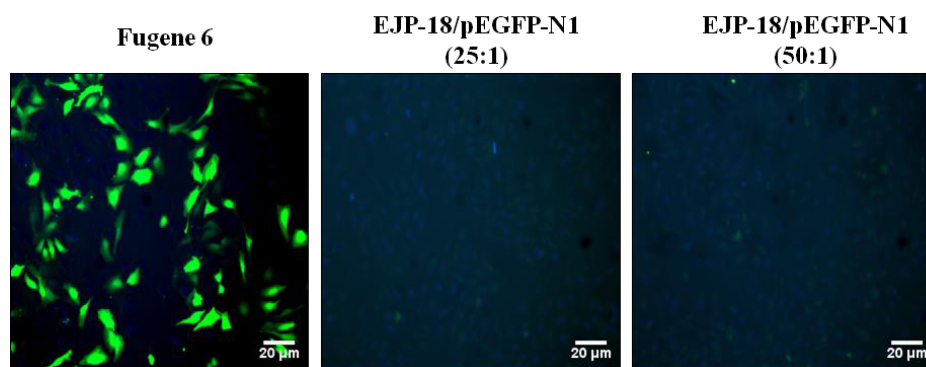
Figure 5-13: Transfection experiments in HeLa cells incubated with pEGFP-N1/ FuGENE 6 or pEGFP-N1/EJP-18 complexes. Cells on coverslips were incubated with the complexes, fixed and analysed by fluorescence microscopy. Cell nuclei were labelled with Hoechst 33342. Shown are representative images from three independent experiments. Nuclei were labelled blue with Hoechst. *Scale bars = 20 μm.*

5.4 Discussion

The aim of this chapter was to investigate the capacity of a novel membrane active peptide, termed EJP-18, to deliver different cargos to cells. For each of these cargos, the initial experiments focused on assessing complex formation. The assays developed are, with the exception of analysing peptide/protein complexes, routine in many laboratories. As they represent new characterisation procedures for the Jones laboratory, some time was required to develop and optimise the methods.

Initially an agarose gel shift assay was utilised to assess EJP-18s ability to complex BSA. These gels are very straightforward to prepare and run. There are, however, only a few examples in the literature of characterisation of CPP/ protein complexes as much of the research focuses on experiments employing CPPs that are covalently (peptide bond) linked to the protein cargo i.e. as CPP-protein conjugates. BSA has an isoelectric point of 4.7 so has a net negative charge in water (Peng *et al*., 2005) and EJP-18 has an isoelectric point of 14 (pepcalc.com) making it positively charged in the same solution allowing for the possibility of electrostatic interaction between the two components. Two different electrophoresis systems were employed to assess whether any complexes had been formed. The agarose gel methods highlighted some retardation in BSA mobility and also clear evidence that some of the complexes were being retained on the loading wells. The data at between 20:1 and 100:1 molar ratio were similar suggesting that maximum complexation was occurring at 20:1 ratios. Native gel electrophoresis gave very different profiles clearly showing a reduction in the expected band at 67 KDa at 20:1 ratios and then complete disappearance of the band at higher ratios. Methods employing direct analysis of the gel on the Typhoon analyser followed by Coomassie staining were developed to gain this information and this represents a robust method to detect complexes of this nature. During the course of these studies, an undergraduate student was supervised in the laboratory by me to conduct similar experiments with the CPP R8. Similar to findings with EJP-18 and BSA interactions, the native gel method provided a better characterisation,

compared with agarose gels, of peptide-BSA complex formation (data not shown).

Non-denaturing PAGE of the type used in this thesis has been previously used to analyse peptide/protein complexation but only one example of this could be found in the literature. Here, Gramicidin A based membrane active peptide vector (VGAIAvVvWIWIWIWβAGSGPKKKRKVC) was shown to complex and deliver β-gal into HeLa cells (Stoilova *et al*., 2008). Despite numerous examples of CPP mediated delivery of proteins, including BSA, as non covalent complexes there is very little information on complex formation of the type shown in this thesis.

BSA has been shown to be internalised into cells via receptor mediated endocytosis and fluid phase endocytosis (Synnes *et al*., 1999, Ikehata *et al*., 2008) but in this chapter, no uptake could be detected by confocal microscopy at 10μg/mL (0.15 μM) in HeLa cells. However as an EJP-18 complex, at the same concentration, BSA was effectively internalised into punctate structures strongly suggesting the involvement of endocytosis. Increasing the concentration of EJP-18 but keeping the BSA concentration the same significantly enhanced cell uptake (Figure 5-2). In these experiments, the labelled BSA was confined to punctate structures and there was no evidence that any significant fraction was localised to the cytosol. The ability of 10 μM EJP-18 to deliver labelled albumin was compared with well characterised CPPs, penetratin, R8 and also R8-GC. Toxicity studies were conducted

(EJP-18, penetratin, R8) at this point showing that none of these complexes were toxic to HeLa cells after 24 and 72 h incubation.

From these analysis, the extent of cell uptake was EJP-18 >R8 > penetratin (Figure 5-3). The data for penetratin are in agreement with Mussbach *et al.* who reported that no detectable amount of ATTO488-BSA in HeLa cells when it was non-covalently complexed with penetratin (Mussbach *et al.*, 2011). In a seperate study, penetratin was able to deliver rhodamine tagged BSA (as non-covalent complexes) but this was in different epithelial cell lines; A431 (skin), A549 (lung) and Caco-2 (gut) and at a higher 20 µM peptide concentrations (Carter *et al.*, 2013). In the latter study, fixed cells were analysed for the detection of labelled albumin uptake with penetratin and two other CPPs; Tat and transportan. It should be noted however that fixation of CPPs is known to give different results relative to live cells due to artefactual localisation induced by the fixation process (Richard *et al.*, 2003). This apparent difference in penetratin's ability to deliver albumin may be due an artefact of fixation, to the differences in cell lines used, the effect of the different fluorophores attached to BSA or combinations of these (Fischer *et al.*, 2004, Jones and Sayers, 2012).

In this thesis, R8 showed moderate BSA delivery capacity and interestingly, the addition of GC to the C-terminus significantly increased uptake. This could have been due to the presence of the reactive cysteine amino acid at the C-terminus which could have caused disulphide bond formation on the peptides or with the peptide and BSA but much more likely is the possibility that the reactive thiol groups on the cysteine were interacting with plasma

membrane components. In support of this, cysteine-containing CPPs were shown to react with thiol membrane proteins, resulting in significantly higher uptake compared to that observed with cysteine free equivalent sequences (Aubry *et al*., 2009). It has also been reported that introducing a single cysteine residue to penetratin and PenArg (RQIRIWFQNRRMRWRR) enhanced the transfection capacity for plasmid DNA (pDNA) in human embryonic kidney cells (HEK293T). The peptides alone were poor at delivering pDNA but transfection capacity increased when transfection was performed in the presence of chloroquine that is known to aid endosomal escape. The influence of the cysteine was thought to be via enhanced stabilisation of the complex (Amand *et al*., 2012). In the same study, addition of cysteine residue to the penetratin analogue EB1 enhanced transfection in the absence of chloroquine suggesting that dimerization can also improve endosomal escape properties.

The distinct perinuclear and vesicular distribution of EJP-18 and R8/BSA-Alexa647 complexes suggested these were being delivered to endo-lysosomal compartments. Colocalisation analysis demonstrated that 38% of both complexes colocalised with lysosomal dextran after 1 h pulse period. Here, a portion of the complexes would be localised in early and late endosomes and also in lysosomes. The degree of colocalisation increased to 57% and 49% for EJP-18/BSA-Alexa 647 and R8/BSA-Alexa 647 complexes respectively confirming that more of the complexes had trafficked to lysosomes. It has been shown that uncomplexed BSA labelled with a fluorophore can be used as a marker for endolysosomal system (Hanaki *et al*., 2003, Shi *et al*., 2010). It is clear here that the peptide significantly enhanced BSA uptake and that it did

not modify the trafficking of the protein. This suggests that CPPs could still have a therapeutic role in delivering proteins such as therapeutic enzymes or albumin conjugated to drugs to the lysosomes of cells. Although endosomal entrapment is believed to be a rate-limiting step in efficient intracellular delivery of cargos by CPPs (El-Sayed *et al*., 2009), lysosomes represent important therapeutic targets (Ortolano *et al*., 2014, Moody *et al*., 2015). The methodology developed for analysing BSA uptake was subsequently used for generating new data on cell uptake of novel CPPs associated with labelled albumin and also quantum dots. This was recently published with acknowledgement of my contribution in the author list (Sayers *et al*., 2014).

There is considerable interest in delivering siRNA as a therapeutic targeting a range of different diseases. The fact that so many CPPs are positively charged makes them attractive candidates as tools for both complexing negatively charged nucleotides (siRNA, pDNA) and delivering them to the cytosol of cells (Hassane *et al*., 2010, Boisguérin *et al*., 2015). Non-covalent complexing between CPPs and siRNA has been well described in literature as have reports showing CPP mediated delivery of siRNA to cells to reduce protein expression (Lundberg *et al*., 2007, Crombez *et al*., 2009, Youn *et al*., 2014). Translation of *in vitro* data to *in vivo* models and the clinic has however not progressed as hoped and the search continues for more effective CPPs. As EJP-18 represented a novel sequence, it merited further study as a delivery vector for nucleotides.

Experiments were therefore undertaken to investigate whether EJP-18 could also act as a delivery vector for nucleotides. Initially, agarose gel shift assays demonstrated that the peptide efficiently complexes two different siRNA sequences. This was not surprising based on the number of positive charges (K, R) in the peptide and that it has an isoelectric point of 14 and a net charge of 8.1 at pH 7 (pepcalc.com).

Effective retardation of siRNA was observed at 20:1 molar ratio peptide: siRNA. The observation of reversed mobility of complexes at molar ratios above 80:1 (Figure 5-8) suggests that as observed with other CPPs, there is a threshold above which increasing the concentration of EJP-18 completely neutralises the charge on the siRNA and causes retardation of mobility (Xu *et al*., 2014). In this thesis, reverse mobility was observed as the siRNA moved towards the cathode rather than the anode. The retardation of siRNA mobility when complexed with EJP-18 could therefore be attributed to the formation of high molecular weight complexes (Crombez *et al*., 2009) and also exclusion of ethidium bromide from siRNA (Lundberg *et al*., 2007, Ramakrishna *et al*., 2014).

EJP-18 was able to deliver Cy5-labelled siRNA (50 and 100 nM) into distinct perinuclear region of HeLa cells within 3 h incubation. Of note from these experiments was a very heterogeneous labelling pattern within separate experiments and within a single field of view. This heterogeneity was observed with EJP-18 mediated delivery of siRNA and also for oligofectamine complexes that were very effective at delivering functional siRNA into the

cytosol. The data with both delivery vectors did not give clear evidence of siRNA localisation in the cytosol, but using the microscopy approaches used here makes analysing the cytosolic siRNA fraction very difficult. It is much easier to identify it in punctate structures that can only be assigned to being in the cytoplasm. Different subcellular distribution of siRNA in similar punctate structures was observed in CHO-K1 cells incubated with oligofectamine/siRNA complexes and also siRNA complexed with the CPP, C6 (Jafari *et al*., 2012). The subcellular labelling pattern of siRNA delivered by C6 was also heterogeneous and in comparison with oligofectamine, C6 was a poor transfection agent for siRNA. Another study using a modified analogue of C6, named C6M1, gave higher transfection but also resulted in heterogeneous siRNA labelling in CHO-K1 cells (Xu *et al*., 2014). It should be noted that in both studies, the cells were fixed before imaging while in this thesis, only live cell imaging was performed. Tat was also shown to deliver Cy3-labelled siRNA into HeLa cells and here the siRNA was localised to distinct perinuclear regions in the cytoplasm (Chiu *et al*., 2004). At 400 nM siRNA, Tat effectively reduced the expression of CDK9 protein comparable with incubating the cells with lipofectamine/siRNA (150 nM) complexes. Perinuclear siRNA distribution was also observed in the lipofectamine transfection suggesting that delivery to this region aids in endosomal escape and siRNA activity. Heterogeneity of labelling was not mentioned in this study as the microscopy images were of single fixed cells only rather than a group of live cells as shown in this thesis.

Although EJP-18 was able to deliver Cy5-labelled Cav-1 siRNA, EJP-18/siRNA complexes at the molar ratio of 200:1 (EJP-18 concentration 10 μM) were unable to reproducibly reduce Cav-1 expression in HeLa cells compared with oligofectamine (Figure 5-10). This could be due to endosomal entrapment of the complexes and/or the possibility that EJP-18 binding to siRNA is very strong giving little opportunity for disassociation and release towards dicer and the RISC loading complex. Further investigations using chloroquine could be performed to examine whether endosomal entrapment is the limiting step in knockdown efficiency. As there was some evidence of EJP-18 mediated siRNA delivery, experiments were performed with another siRNA targeting PAK-1. An experiment using 50 nM PAK-1 siRNA once again gave disappointing results (data not shown) but at 100 nM siRNA concentration, EJP-18 reproducibly delivered PAK-1 siRNA giving an average reduction in PAK-1 levels of 60% (Figure 5-11). However, it should be noted that transfection with GFP non-targeting siRNA with oligofectamine also caused a significant reduction in PAK-1 expression which raises some concern regarding the use of this siRNA and/or oligofectamine as a control. It should be noted that both expression of Cav-1 and PAK-1 was sensitive to some of the controls in here. EJP-18 alone could conceivably have an effect on EGFR biology that could then have indirectly influenced the expression of Cav-1 and PAK-1. This was one of the reasons why this peptide was initially studied. Studies are underway assessing any influence the peptide has on EGFR signalling and a cell line constitutively expressing eGFP is now available in the laboratory to further assess the capacity of EJP-18 to deliver siRNA (eGFP).

EJP-18 was able to complex pEGFP-N1 plasmid (Figure 5-12) however; it failed to transfect HeLa cells, despite it like Tat having a NLS. Time did not allow for similar experiments investigating the uptake of fluorescent plasmid DNA or alternative plasmids. Endosomal entrapment and strong peptide-pDNA association are again factors that cannot be overlooked. Experiments involving the addition of chloroquine could again highlight whether endosomal entrapment is the major hurdle as addition of chloroquine increased the transfection efficiency of Tat-oligomers/plasmid complexes (Rudolph *et al*., 2003).

5.5   Conclusions

The aim of this chapter was to develop techniques to assess the capacity of the previously uncharacterised EJP-18 to deliver three types of cargos into cells. The data from these developed methods including gel shift assays and non-denaturing gels confirmed that the peptide could effectively complex both nucleotides and a protein. In the case of protein and siRNA, EJP-18 demonstrated that it could respectively deliver cargo into cells with higher efficiency compared with two established CPPs and a commercial siRNA transfection reagent. The peptide showed no transfection capacity for plasmid DNA but was able to deliver fluorescent siRNA to cells and it remains to be determined whether it can also deliver functional siRNA to silence expression of proteins. All this suggests that EJP-18 or variants of could be further studied as bioportides and/or delivery vectors and some of these are described in the next chapter.

5.6 References

AL SORAJ, M., HE, L., PEYNSHAERT, K., COUSAERT, J., VERCAUTEREN, D., BRAECKMANS, K., DE SMEDT, S. C. & JONES, A. T. 2012. siRNA and pharmacological inhibition of endocytic pathways to characterize the differential role of macropinocytosis and the actin cytoskeleton on cellular uptake of dextran and cationic cell penetrating peptides octaarginine (R8) and HIV-Tat. *J Control Release,* 161**,** 132-141.

AL-TAEI, S., PENNING, N. A., SIMPSON, J. C., FUTAKI, S., TAKEUCHI, T., NAKASE, I. & JONES, A. T. 2006. Intracellular traffic and fate of protein transduction domains HIV-1 TAT peptide and octaarginine. Implications for their utilization as drug delivery vectors. *Bioconjugate chemistry,* 17**,** 90-100.

AMAND, H. L., NORDEN, B. & FANT, K. 2012. Functionalization with C-terminal cysteine enhances transfection efficiency of cell-penetrating peptides through dimer formation. *Biochem Biophys Res Commun,* 418**,** 469-474.

ANDALOUSSI, S. E., LEHTO, T., MÄGER, I., ROSENTHAL-AIZMAN, K., OPREA, I. I., SIMONSON, O. E., SORK, H., EZZAT, K., COPOLOVICI, D. M. & KURRIKOFF, K. 2011. Design of a peptide-based vector, PepFect6, for efficient delivery of siRNA in cell culture and systemically in vivo. *Nucleic acids research,* 39**,** 3972-3987.

APPELQVIST, H., WÄSTER, P., KÅGEDAL, K. & ÖLLINGER, K. 2013. The lysosome: from waste bag to potential therapeutic target. *Journal of molecular cell biology,* 5**,** 214-226.

ARRANZ, V. 2007. Compositions and methods for treating lysosomal storage diseases. Google Patents. US20100221235 A1

AUBRY, S., BURLINA, F., DUPONT, E., DELAROCHE, D., JOLIOT, A., LAVIELLE, S., CHASSAING, G. & SAGAN, S. 2009. Cell-surface thiols affect cell entry of disulfide-conjugated peptides. *The FASEB Journal,* 23**,** 2956-2967.

BOISGUÉRIN, P., DESHAYES, S., GAIT, M. J., O'DONOVAN, L., GODFREY, C., BETTS, C. A., WOOD, M. J. & LEBLEU, B. 2015. Delivery of therapeutic oligonucleotides with cell penetrating peptides. *Advanced drug delivery reviews,* 87**,** 52-67.

BRIGHT, N. A., GRATIAN, M. J. & LUZIO, J. P. 2005. Endocytic delivery to lysosomes mediated by concurrent fusion and kissing events in living cells. *Curr Biol,* 15**,** 360-365.

CARON, N. J., QUENNEVILLE, S. P. & TREMBLAY, J. P. 2004. Endosome disruption enhances the functional nuclear delivery of Tat-fusion proteins. *Biochemical and biophysical research communications,* 319**,** 12-20.

CARTER, E., LAU, C. Y., TOSH, D., WARD, S. G. & MRSNY, R. J. 2013. Cell penetrating peptides fail to induce an innate immune response in epithelial cells in vitro: implications for continued therapeutic use. *Eur J Pharm Biopharm,* 85**,** 12-19.

CARTIER, R. & RESZKA, R. 2002. Utilization of synthetic peptides containing nuclear localization signals for nonviral gene transfer systems. *Gene therapy,* 9**,** 157-167.

CHIU, Y. L., ALI, A., CHU, C. Y., CAO, H. & RANA, T. M. 2004. Visualizing a correlation between siRNA localization, cellular uptake, and RNAi in living cells. *Chem Biol,* 11**,** 1165-1175.

CIFTCI, K. & LEVY, R. J. 2001. Enhanced plasmid DNA transfection with lysosomotropic agents in cultured fibroblasts. *International journal of pharmaceutics,* 218**,** 81-92.

CROMBEZ, L., ALDRIAN-HERRADA, G., KONATE, K., NGUYEN, Q. N., MCMASTER, G. K., BRASSEUR, R., HEITZ, F. & DIVITA, G. 2009. A new potent secondary amphipathic cell–penetrating peptide for siRNA delivery into mammalian cells. *Molecular therapy,* 17**,** 95-103.

CROSS, K. J., LANGLEY, W. A., RUSSELL, R. J., SKEHEL, J. J. & STEINHAUER, D. A. 2009. Composition and functions of the influenza fusion peptide. *Protein and peptide letters,* 16**,** 766-778.

EL-SAYED, A., FUTAKI, S. & HARASHIMA, H. 2009. Delivery of macromolecules using arginine-rich cell-penetrating peptides: ways to overcome endosomal entrapment. *AAPS J,* 11**,** 13-22.

FISCHER, R., KOHLER, K., FOTIN-MLECZEK, M. & BROCK, R. 2004. A stepwise dissection of the intracellular fate of cationic cell-penetrating peptides. *J Biol Chem,* 279**,** 12625-12635.

HANAKI, K.-I., MOMO, A., OKU, T., KOMOTO, A., MAENOSONO, S., YAMAGUCHI, Y. & YAMAMOTO, K. 2003. Semiconductor quantum dot/albumin complex is a long-life and highly photostable endosome marker. *Biochemical and biophysical research communications,* 302**,** 496-501.

HASSANE, F. S., SALEH, A., ABES, R., GAIT, M. & LEBLEU, B. 2010. Cell penetrating peptides: overview and applications to the delivery of oligonucleotides. *Cellular and molecular life sciences,* 67**,** 715-726.

HEITZ, F., MORRIS, M. C. & DIVITA, G. 2009. Twenty years of cell-penetrating peptides: from molecular mechanisms to therapeutics. *Br J Pharmacol,* 157**,** 195-206.

HYNDMAN, L., LEMOINE, J. L., HUANG, L., PORTEOUS, D. J., BOYD, A. C. & NAN, X. 2004. HIV-1 Tat protein transduction domain peptide facilitates gene transfer in combination with cationic liposomes. *Journal of controlled release,* 99**,** 435-444.

IKEHATA, M., YUMOTO, R., NAKAMURA, K., NAGAI, J. & TAKANO, M. 2008. Comparison of albumin uptake in rat alveolar type II and type I-like epithelial cells in primary culture. *Pharmaceutical research,* 25**,** 913-922.

JAFARI, M., XU, W., NAAHIDI, S., CHEN, B. & CHEN, P. 2012. A new amphipathic, amino-acid-pairing (AAP) peptide as siRNA delivery carrier: physicochemical characterization and in vitro uptake. *The Journal of Physical Chemistry B,* 116**,** 13183-13191.

JONES, A. T. & SAYERS, E. J. 2012. Cell entry of cell penetrating peptides: tales of tails wagging dogs. *J Control Release,* 161**,** 582-591.

KELLER, A.-A., MUSSBACH, F., BREITLING, R., HEMMERICH, P., SCHAEFER, B., LORKOWSKI, S. & REISSMANN, S. 2013. Relationships between cargo, cell penetrating peptides and cell type for uptake of non-covalent complexes into live cells. *Pharmaceuticals,* 6**,** 184-203.

KERKIS, A., HAYASHI, M. A., YAMANE, T. & KERKIS, I. 2006. Properties of cell penetrating peptides (CPPs). *IUBMB Life,* 58**,** 7-13.

KOBAYASHI, S., NAKASE, I., KAWABATA, N., YU, H.-H., PUJALS, S., IMANISHI, M., GIRALT, E. & FUTAKI, S. 2009. Cytosolic targeting of macromolecules using a pH-dependent fusogenic peptide in combination with cationic liposomes. *Bioconjugate chemistry,* 20**,** 953-959.

LEE, S. H., CASTAGNER, B. & LEROUX, J.-C. 2013. Is there a future for cell-penetrating peptides in oligonucleotide delivery? *European Journal of Pharmaceutics and Biopharmaceutics,* 85**,** 5-11.

LI, W., NICOL, F. & SZOKA, F. C. 2004. GALA: a designed synthetic pH-responsive amphipathic peptide with applications in drug and gene delivery. *Advanced drug delivery reviews,* 56**,** 967-985.

LI, Y., WANG, J., WIENTJES, M. G. & AU, J. L.-S. 2012. Delivery of nanomedicines to extracellular and intracellular compartments of a solid tumor. *Advanced drug delivery reviews,* 64**,** 29-39.

LIOU, J.-S., LIU, B. R., MARTIN, A. L., HUANG, Y.-W., CHIANG, H.-J. & LEE, H.-J. 2012. Protein transduction in human cells is enhanced by cell-penetrating peptides fused with an endosomolytic HA2 sequence. *Peptides,* 37**,** 273-284.

LIU, B. R., LIN, M.-D., CHIANG, H.-J. & LEE, H.-J. 2012. Arginine-rich cell-penetrating peptides deliver gene into living human cells. *Gene,* 505**,** 37-45.

LIU, B. R., LO, S.-Y., LIU, C.-C., CHYAN, C.-L., HUANG, Y.-W., ARONSTAM, R. S. & LEE, H.-J. 2013. Endocytic trafficking of nanoparticles delivered by cell-penetrating peptides comprised of nona-arginine and a penetration accelerating sequence. *PloS one,* 8**,** e67100.

LIU, Z., LI, M., CUI, D. & FEI, J. 2005. Macro-branched cell-penetrating peptide design for gene delivery. *Journal of controlled release,* 102**,** 699-710.

LO, S. L. & WANG, S. 2008. An endosomolytic Tat peptide produced by incorporation of histidine and cysteine residues as a nonviral vector for DNA transfection. *Biomaterials,* 29**,** 2408-2414.

LUNDBERG, P., EL-ANDALOUSSI, S., SUTLU, T., JOHANSSON, H. & LANGEL, U. 2007. Delivery of short interfering RNA using endosomolytic cell-penetrating peptides. *FASEB J,* 21**,** 2664-2671.

MARGUS, H., PADARI, K. & POOGA, M. 2012. Cell-penetrating peptides as versatile vehicles for oligonucleotide delivery. *Molecular Therapy,* 20**,** 525-533.

MOODY, P. R., SAYERS, E. J., MAGNUSSON, J. P., ALEXANDER, C., BORRI, P., WATSON, P. & JONES, A. T. 2015. Receptor Crosslinking: A General Method to Trigger Internalization and Lysosomal Targeting of Therapeutic Receptor: Ligand Complexes. *Molecular Therapy*, doi: 10.1038/mt.2015.178

MORRIS, M., VIDAL, P., CHALOIN, L., HEITZ, F. & DIVITA, G. 1997. A new peptide vector for efficient delivery of oligonucleotides into mammalian cells. *Nucleic acids research,* 25**,** 2730-2736.

MORRIS, M. C., DESHAYES, S., HEITZ, F. & DIVITA, G. 2008. Cell-penetrating peptides: from molecular mechanisms to therapeutics. *Biol Cell,* 100**,** 201-217.

MUSSBACH, F., FRANKE, M., ZOCH, A., SCHAEFER, B. & REISSMANN, S. 2011. Transduction of peptides and proteins into live cells by cell penetrating peptides. *J Cell Biochem,* 112**,** 3824-3833.

MÄE, M., ANDALOUSSI, S. E., LUNDIN, P., OSKOLKOV, N., JOHANSSON, H. J., GUTERSTAM, P. & LANGEL, Ü. 2009. A stearylated CPP for delivery of splice correcting oligonucleotides using a non-covalent co-incubation strategy. *Journal of Controlled Release,* 134**,** 221-227.

ORTOLANO, S., VIÉITEZ, I., NAVARRO, C. & SPUCH, C. 2014. Treatment of lysosomal storage diseases: recent patents and future strategies. *Recent patents on endocrine, metabolic & immune drug discovery,* 8**,** 9-25.

PENG, Z., HIDAJAT, K. & UDDIN, M. 2005. Selective and sequential adsorption of bovine serum albumin and lysozyme from a binary mixture on nanosized magnetic particles. *Journal of colloid and interface science,* 281**,** 11-17.

RAMAKRISHNA, S., DAD, A.-B. K., BELOOR, J., GOPALAPPA, R., LEE, S.-K. & KIM, H. 2014. Gene disruption by cell-penetrating peptide-mediated delivery of Cas9 protein and guide RNA. *Genome research,* 24**,** 1020-1027.

RICHARD, J. P., MELIKOV, K., VIVES, E., RAMOS, C., VERBEURE, B., GAIT, M. J., CHERNOMORDIK, L. V. & LEBLEU, B. 2003. Cell-penetrating peptides. A reevaluation of the mechanism of cellular uptake. *J Biol Chem,* 278**,** 585-590.

RITTNER, K., BENAVENTE, A., BOMPARD-SORLET, A., HEITZ, F., DIVITA, G., BRASSEUR, R. & JACOBS, E. 2002. New basic membrane-destabilizing peptides for plasmid-based gene delivery in vitro and in vivo. *Molecular Therapy,* 5**,** 104-114.

RUDOLPH, C., PLANK, C., LAUSIER, J., SCHILLINGER, U., MÜLLER, R. H. & ROSENECKER, J. 2003. Oligomers of the arginine-rich motif of the HIV-1 TAT protein are capable of transferring plasmid DNA into cells. *Journal of Biological Chemistry,* 278**,** 11411-11418.

SAYERS, E. J., CLEAL, K., EISSA, N. G., WATSON, P. & JONES, A. T. 2014. Distal phenylalanine modification for enhancing cellular delivery of fluorophores, proteins and quantum dots by cell penetrating peptides. *Journal of Controlled Release,* 195**,** 55-62.

SHI, H., HE, X., YUAN, Y., WANG, K. & LIU, D. 2010. Nanoparticle-based biocompatible and long-life marker for lysosome labeling and tracking. *Analytical chemistry,* 82**,** 2213-2220.

SIMEONI, F., MORRIS, M. C., HEITZ, F. & DIVITA, G. 2003. Insight into the mechanism of the peptide-based gene delivery system MPG: implications for delivery of siRNA into mammalian cells. *Nucleic acids research,* 31**,** 2717-2724.

STOILOVA, T. B., KOVALCHUK, S. I., EGOROVA, N. S., SUROVOY, A. Y. & IVANOV, V. T. 2008. Gramicidin A-based peptide vector for intracellular protein delivery. *Biochimica et Biophysica Acta (BBA)-Biomembranes,* 1778**,** 2026-2031.

SYNNES, M., PRYDZ, K., LØVDAL, T., BRECH, A. & BERG, T. 1999. Fluid phase endocytosis and galactosyl receptor-mediated endocytosis employ different early endosomes. *Biochimica et Biophysica Acta (BBA)-Biomembranes,* 1421**,** 317-328.

TAKAYAMA, K., NAKASE, I., MICHIUE, H., TAKEUCHI, T., TOMIZAWA, K., MATSUI, H. & FUTAKI, S. 2009. Enhanced intracellular delivery using arginine-rich peptides by the addition of penetration accelerating sequences (Pas). *Journal of Controlled Release,* 138**,** 128-133.

URBANELLI, L., MAGINI, A., POLCHI, A., POLIDORO, M. & EMILIANI, C. 2011. Recent developments in therapeutic approaches for lysosomal storage diseases. *Recent patents on CNS drug discovery,* 6**,** 1-19.

XU, W., JAFARI, M., YUAN, F., PAN, R., CHEN, B., DING, Y., SHEININ, T., CHU, D., LU, S. & YUAN, Y. 2014. In vitro and in vivo therapeutic siRNA delivery induced by a tryptophan-rich endosomolytic peptide. *Journal of Materials Chemistry B,* 2**,** 6010-6019.

YOUN, P., CHEN, Y. & FURGESON, D. Y. 2014. A Myristoylated Cell-Penetrating Peptide Bearing a Transferrin Receptor-Targeting Sequence for Neuro-Targeted siRNA Delivery. *Molecular pharmaceutics,* 11**,** 486-495.

Chapter 6: Cellular Uptake and Protein Delivery of EJP-21 and E-64562

6.1   Introduction

During studies investigating the capacity of EJP-18 to bind to cells and deliver cargo to cells, a study was published where a peptide sequence termed E-64562 (RRRHIVRKRTLRRLLQER) was conjugated to the Tat sequence to give TE-64562 (RKKRRQRRRG-RRRHIVRKRTLRRLLQER (Boran *et al.*, 2012). The cargo here is, like EJP-18, derived from the EGFR juxtamembrane region but is missing the N-terminal LFM sequence and gaining a QER at the C-terminus (Table 2-1). In breast cancer MDA-MB-231 cells, E-64562 was non toxic up to 100 µM but TE-64562 was 100% toxic at the same concentration and displayed an EC_{50} of 12.6 µM. TE-64562 also had *in vivo* activity in nude mice bearing MDA-MB-231 tumors.

The other main findings from the Boran *et al.* manuscript are summarized here:

1. In cancer cell lines, the effect of TE-64562 on cell viability varied according to cancer cell type, relative ErbB levels and the presence of serum. TE-64562 was more toxic to cells with medium and high expression of these receptors. NR6 (NIH/3T3 fibroblasts) which is an EGFR-null cell line was relatively resistant to the effect of TE-64562 (EC_{50}= 104.2 µM). The effect of TE-64562 appeared to be specific to cancer cells as normal lung fibroblasts (IMR-90) were very resistant to TE-64562 treatment although these fibroblasts express EGFR. The activity of TE-64562 was reduced ($EC50$= 38.4 µM) in normal breast

(human mammary epithelial cell, HMEC) compared to EGFR/Her2 overexpressing breast cancer cells.

2. A fluorescein derivative of TE-64562 was shown at only 1.25 μM extracellular concentration to label the entire cytoplasm of cells after 50 min incubation and clearly demonstrating that it was entering the cytosol. 5-carboxyfluorescein (FAM)-E-64562 alone also labelled cells but the staining suggested it was aggregating and there was no evidence of cytosolic labeling. Further microscopy and cell uptake analysis were not performed, but there was also evidence of significant aggregation of FAM-TE-64562.

3. In an *in vivo* model of nude mice bearing MDA-MB-231 tumors, IP injection of TE-64562 reduced tumor growth and increased the survival rate of the treated-mice.

4. Evidence was provided that TE-64562 (12.5 μM) inhibited EGFR signaling and dimerization and caused a dose-dependent reduction in EGFR levels in MDA-MB-231 cells.

Of the 28 residues in the TE-64562 chimera, 17 are either lysines or arginines and thus this represents a highly basic peptide and of interest from a delivery perspective was the contribution made by the cargo to cell uptake.

Data presented on EJP-18 in Chapter 4 showed that it was able to enter cells to an extent comparable to R8. Interestingly, it showed toxicity in a manner that appeared to be dependent on EGFR expression; this was also noted for TE-64562 i.e. high EGFR expressing cell lines were more resistant. EJP-18

was also able to complex and deliver different cargos other than a fluorophore. One of the initial criteria for investigating EJP-18 was the fact that it had a hydrophobic N- and C-terminus that was hypothesised to influence cell interaction and uptake. Noting here that previous studies on a Bcl-2 targeting peptide had demonstrated that single hydrophobic residues several residues away from the CPP sequence can influence uptake and affect cell toxicity profiles (Watkins *et al*., 2011).

6.2   Summary, Aims and Objectives

In view of the data presented in chapters 4 and 5 and new published information, a new sequence termed EJP-21 (642-LFMRRRHIVRKRTLRRLLQER-662) was purchased to investigate the role of N- and C-terminal modifications and in view of the Boran *et al.* study, the E-64562 peptide i.e. lacking the Tat extension was also investigated. As unmodified peptides, E-64562 and EJP-21 have masses of 2442.92, and 2834.45 respectively but the same isoelectric point of 12.58 and net charge of 8.1 at pH 7.0 (pepcalc.com). The specific aims of this chapter were to study the cellular uptake and toxicity of sequences- EJP-21 and E-64562, and to investigate their ability to deliver fluorescent albumin to HeLa cells.

The objectives of this chapter were then to:

1- Analyse the effect of EJP-21, E-64562 and their rhodamine conjugates on viability of cancer cell lines using CellTiter-Blue assay.

2- Analyse the cellular uptake of fluorescent conjugates of EJP-21 and E-64562 under different experimental conditions using live cell confocal microscopy.

3- Study the colocalisation of rhodamine conjugates of EJP-18, EJP-21 and E-64562 with dextran that was pre-loaded into the endolysosomal system.

4- Analyse the cellular delivery capacity of EJP-21 and E-64562 for BSA-Alexa647.

6.3 Results

6.3.1 Cell Viability assays for EJP-21, E-64562 and their rhodamine conjugates

6.3.1.1 Effect of EJP-21 and E-64562 on the cell viability in a panel of cancer cell lines

In order to assess the cytotoxicity of EJP-21 and E-64562, cell viability was examined in a panel of cancer cells as used in EJP-18 experiments from Chapter 4. Cells seeded in 96-well plates were incubated with 0-100 μM EJP-21 or E-64562 for 24 h under tissue culture conditions. Viability was then determined using the CellTiter-Blue assay. Figure 6-1 shows that EJP-21 and E-64562 had a different cell viability profile from EJP-18 (Figure 4-2). E-64562 had no effect on viability in any of the tested cell lines at all studied concentrations. EJP-21 was also non toxic to all cell lines at the studied concentrations except for KG1a where 100 μM of the peptide induced 25% loss in cell viability.
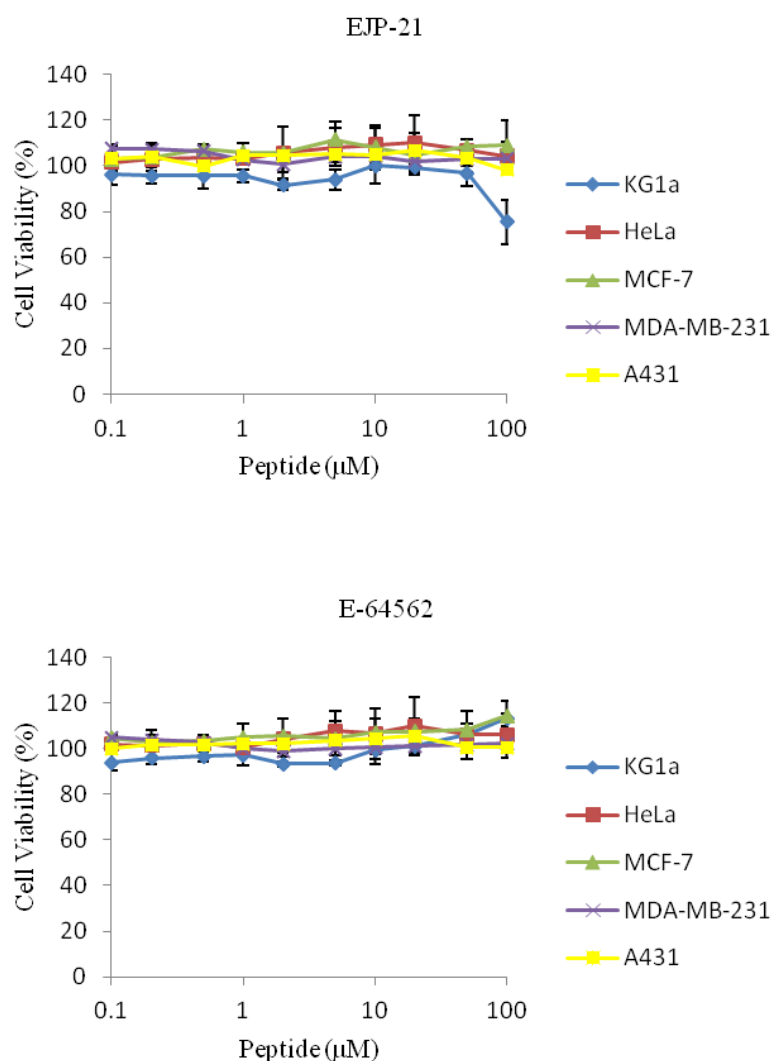
Figure 6-1: Viability of different cell lines incubated with EJP-21 and E-64562. Viability of cells was evaluated using CellTiter-Blue assay following 24 h incubation with 0-100 µM EJP-21 or E-64562 and is expressed as the percentage of viable cells relative to untreated controls. Results represent means ± SD for three independent experiments performed in duplicate.

6.3.1.2 Effect of Rh-EJP-21 and Rh-E-64562 on the cell viability in HeLa cell line

Cell viability experiments were also performed for the rhodamine labelled peptides (Rh-EJP-21 and Rh-E-64562) on HeLa cells that were then going to

be used for cell uptake studies. Rhodamine correction was performed as described in section 4.3.1.2. Figure 6-2 shows that up to 20 µM, Rh-EJP-21 had no significant effect on viability but at 100 µM there was complete cell death. Cells treated with Rh-E-64562 were > 85 % viable up to 100 µM peptide concentration.
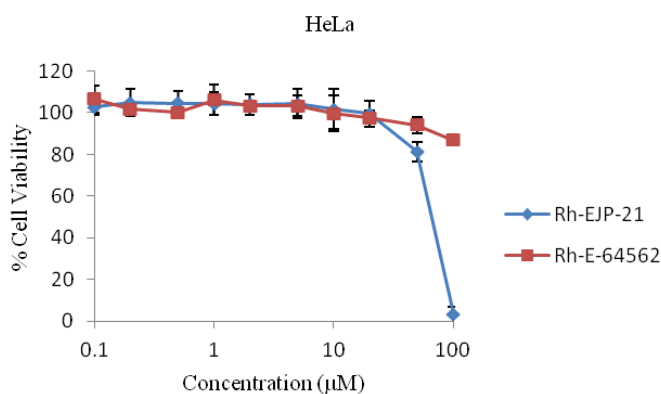
Figure 6-2: Viability of HeLa cells incubated with Rh-EJP-21 and Rh-E-64562. Rhodamine corrected viability of cells was evaluated using CellTiter-Blue assay following 24 h incubation with 0-100 µM Rh-EJP-21 or Rh-E-64562. Cell viability is expressed as the percentage of viable cells relative to untreated controls. Results represent means ± SD for three independent experiments performed in duplicate.

6.3.2 Cellular uptake (subcellular distribution) of Rh-EJP-21 and Rh-E-64562 in HeLa cells

To evaluate the cellular uptake and distribution of EJP-21 and E-64562, HeLa cells were seeded into 35 mm MatTek dishes and after 24 h incubation, were treated for 1 h with 5-20 µM Rh-EJP-21 or 5-20 µM Rh-E-64562. The cells were washed then imaged as live cells by confocal microscopy. Figure 6-3 shows clear uptake of 5 µM Rh-EJP-21 into punctate vesicles whose intensity increased at 10 µM. At 20 µM, the localisation changed significantly: some cells have only punctate cytosolic vesicles while others exhibit additional

diffuse cytosolic labelling and nucleolar labelling was also observed (Figure 6-3).

Figure 6-3: Uptake of Rh-EJP-21 peptide into HeLa cells at 5-20 μM in SFM. Cells were incubated with 5-20 μM Rh-EJP-21 in SFM for 1 h at 37ºC, washed and imaged by confocal microscopy. Representative images (N=3) showing either a single section through the cell at the mid-point of the nucleus or maximum projection of the whole cell. Nuclei were labelled blue with Hoechst. *White arrows indicate nucleolar labelling. Scale bars = 20 μm.*

Rh-E-64562 (10 μM) also labelled punctate vesicles but only very weak fluorescence was observed at 5 μM (Figure 6-4). Again at 20 μM and similar to Rh-EJP-21, some cytosolic distribution of Rh-E64562 was observed but there was no evidence of nucleolar labelling.
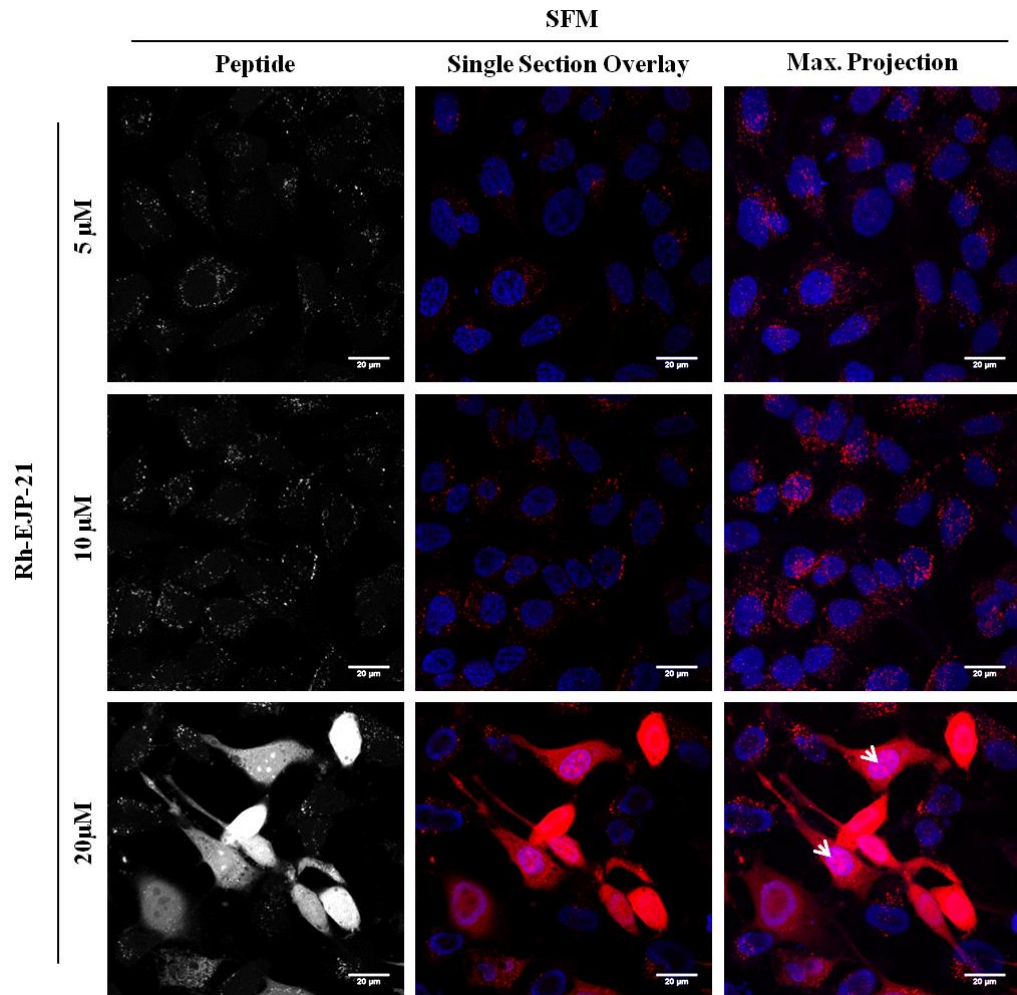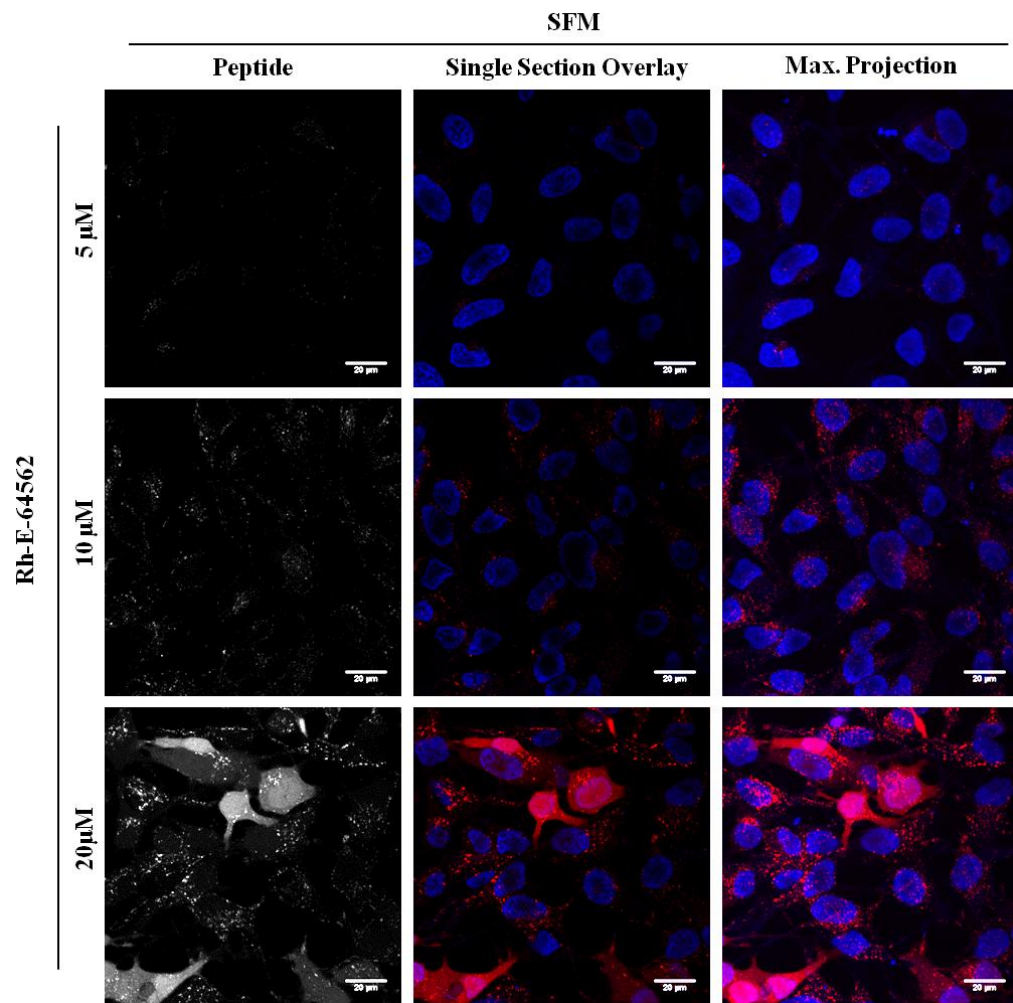
Figure 6-4: Uptake of Rh-E-64562 peptide into HeLa cells at 5-20 µM in SFM. Cells were incubated with 5-20 µM Rh-E-64562 in SFM for 1 h at 37ºC, washed and imaged by confocal microscopy. Representative images (N=3) showing either a single section through the cell at the mid-point of the nucleus or maximum projection of the whole cell. Nuclei were labelled blue with Hoechst. *Scale bars = 20 µm.*

To detect whether the cytoplasmic labelling observed at 20 µM for both peptides was due to general plasma membrane leakage, the cells following incubation with peptides were further incubated for 5 minutes with imaging medium containing the fluorescent probe DRAQ7. Figure 6-5 shows the distribution of the peptides (pseudocolour green) and also some orange DRAQ7-stained nuclei in cells treated with 20 µM Rh-EJP-21. All cells that had clear cytosolic peptide labelling were not also DRAQ positive. All cells treated with 20 µM Rh-E-64562 were free from DRAQ7 (Figure 6-5). The data

here further highlight the higher capacity of Rh-EJP21 to enter cells compared with Rh-E-64562 but viability data (Figure 6-1 and 6-2) suggest that rhodamine may have significant influence on membrane binding and integrity and also potentially on cell uptake.
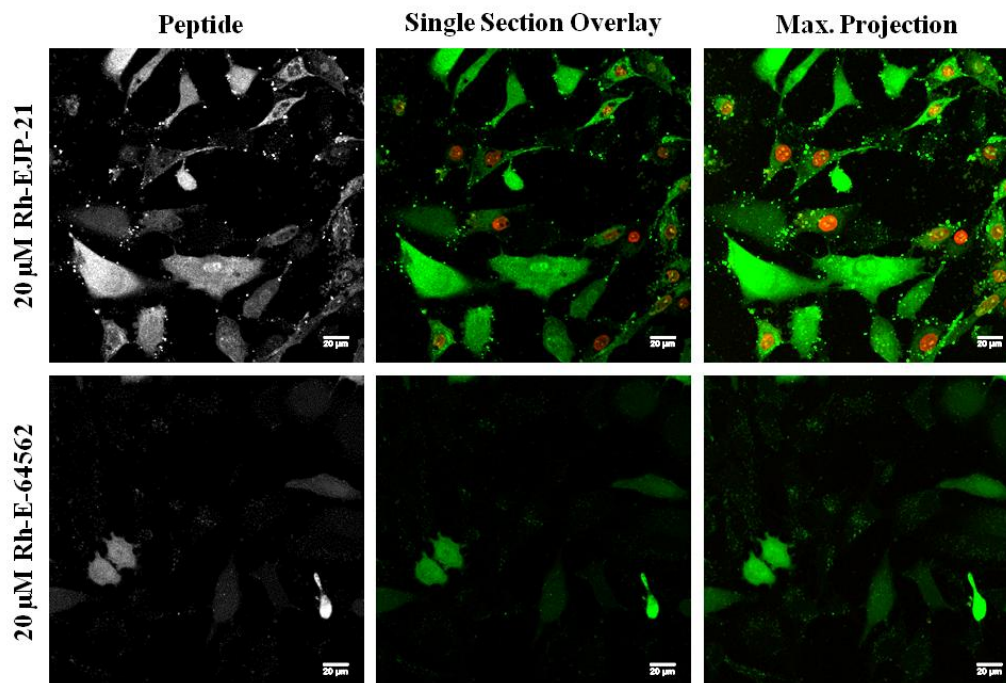
Figure 6-5: Uptake of 20 μM Rh-EJP-21 and Rh-E-64562 peptides into HeLa cells in SFM. Cells were incubated with 20 μM Rh-EJP-21 or Rh-E-64562 in SFM for 1 h at 37ºC, washed and imaged by confocal microscopy. Representative images (N=2) showing either a single section through the cell at the mid-point of the nucleus or maximum projection of the whole cell. Dead or permeabilized nuclei were labelled red with DRAQ7 and the rhodamine peptide labelled green. *Scale bars = 20 μm.*

6.3.3 Cellular uptake of 10 μM Rh-EJP-21 and Rh-E-64562 in HeLa cells at 4 and 37ºC

To test the effect of temperature on Rh-EJP-21 and Rh-E-64562 uptake, HeLa cells were incubated for 1 h with 10 μM of both peptides at 4 or 37ºC. The cells were then examined by live cell confocal microscopy. As expected,

vesicular peptide was observed for both peptides at 37ºC but there was no evidence of cell uptake at 4˚C (Figure 6-6).
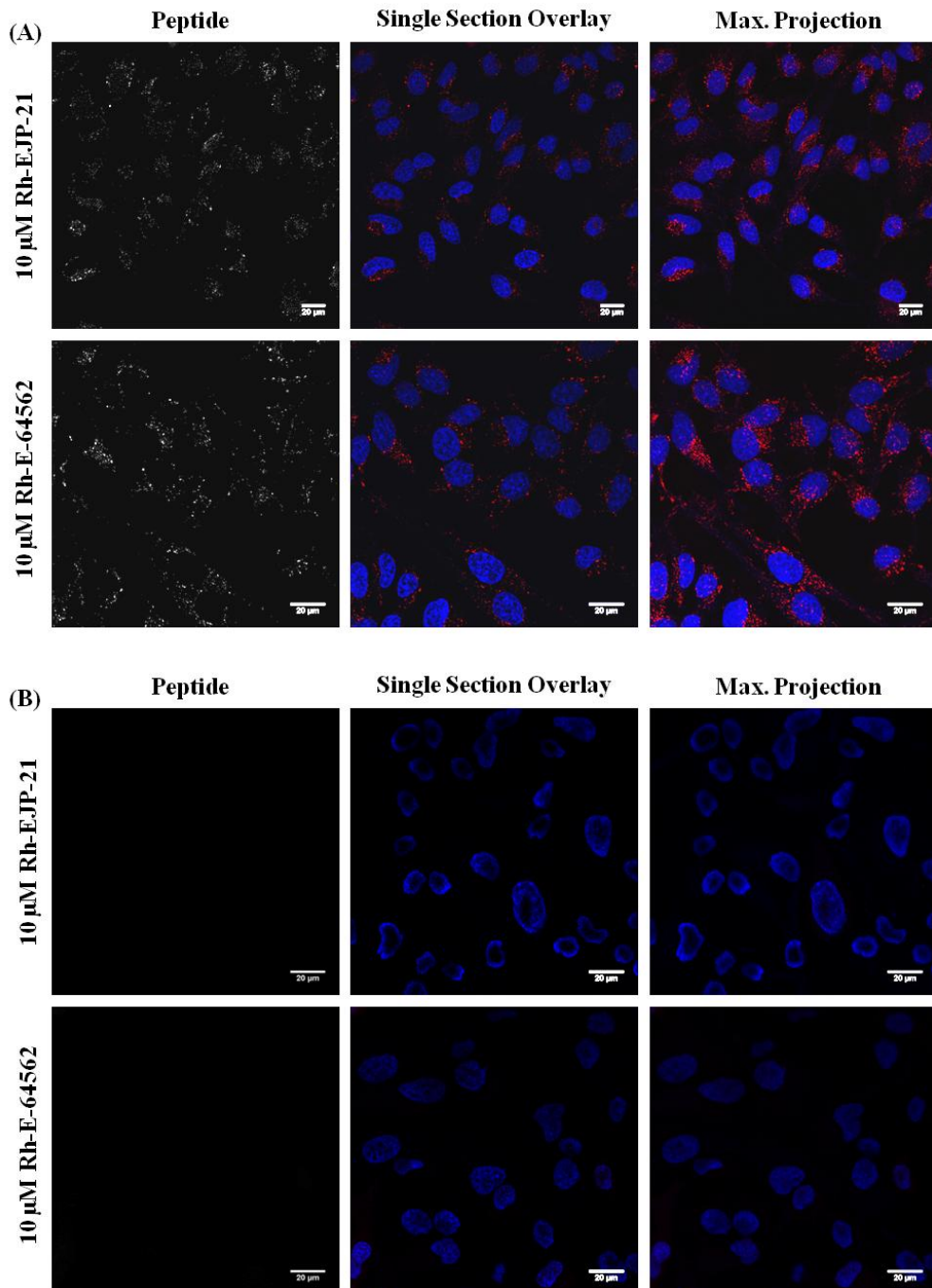
Figure 6-6: Uptake of Rh-EJP-21 and Rh-E-64562 into HeLa cells at 10 μM in SFM at (A) 37ºC or (B) 4ºC. Cells were incubated with 10 μM Rh-EJP-21 or Rh-E-64562 in SFM for 1 h at (A) 37ºC or (B) 4ºC, washed and imaged by confocal microscopy. Representative images (N=3) showing either a single section through the cell at the mid-point of the nucleus or maximum projection of the whole cell. Nuclei were labelled blue with Hoechst. *Scale bars = 20 μm.*

6.3.4 Analysis of the subcellular distribution of Rhodamine conjugates of EJP-18, EJP-21 and E-64562

The observation that the rhodamine conjugates of EJP-18 (Figure 4-7), EJP-21 and E-64562 at 10 μM labelled vesicular structures when incubated at 37ºC suggested the involvement of endocytosis in cell uptake. To investigate this, fluorescent dextran was utilised as an endocytic probe to specifically label lysosomes. For this, cells were incubated with dextran-Alexa488 for 2 h followed by an overnight chase in dextran-free medium as described in section 2.4.1.5. The next day the cells were washed and incubated for 1 h with the Rh-peptides or for 1 h followed by a 1 h chase in peptide free medium. Figure 6-7A shows low colocalisation between lysosomes and Rh-EJP-18 (Pearson's coefficient = 0.28 ± 0.04). A higher degree of traffic to these organelles was noted for Rh-EJP-21 and Rh-E-64562 (Pearson's coefficient = 0.37 ± 0.02 and 0.39 ± 0.03 respectively). Increasing the time of incubation with the peptides (1 h pulse- 1 h chase) increased the degree of colocalisation between the two fluorophores with Rh-EJP-18, Rh-EJP-21 and Rh-E-64562 giving Pearson's coefficients of 0.42 ± 0.05, 0.56 ± 0.05 and 0.45 ± 0.02 respectively. The difference in lysosomal dextran colocalisation was statistically significant between the different peptides by one-way ANOVA $F(5, 12) = 18.72$, $p < 0.0001$ and Tukey post-hoc tests was performed to reveal the statistical significance between groups (Figure 6-7C).
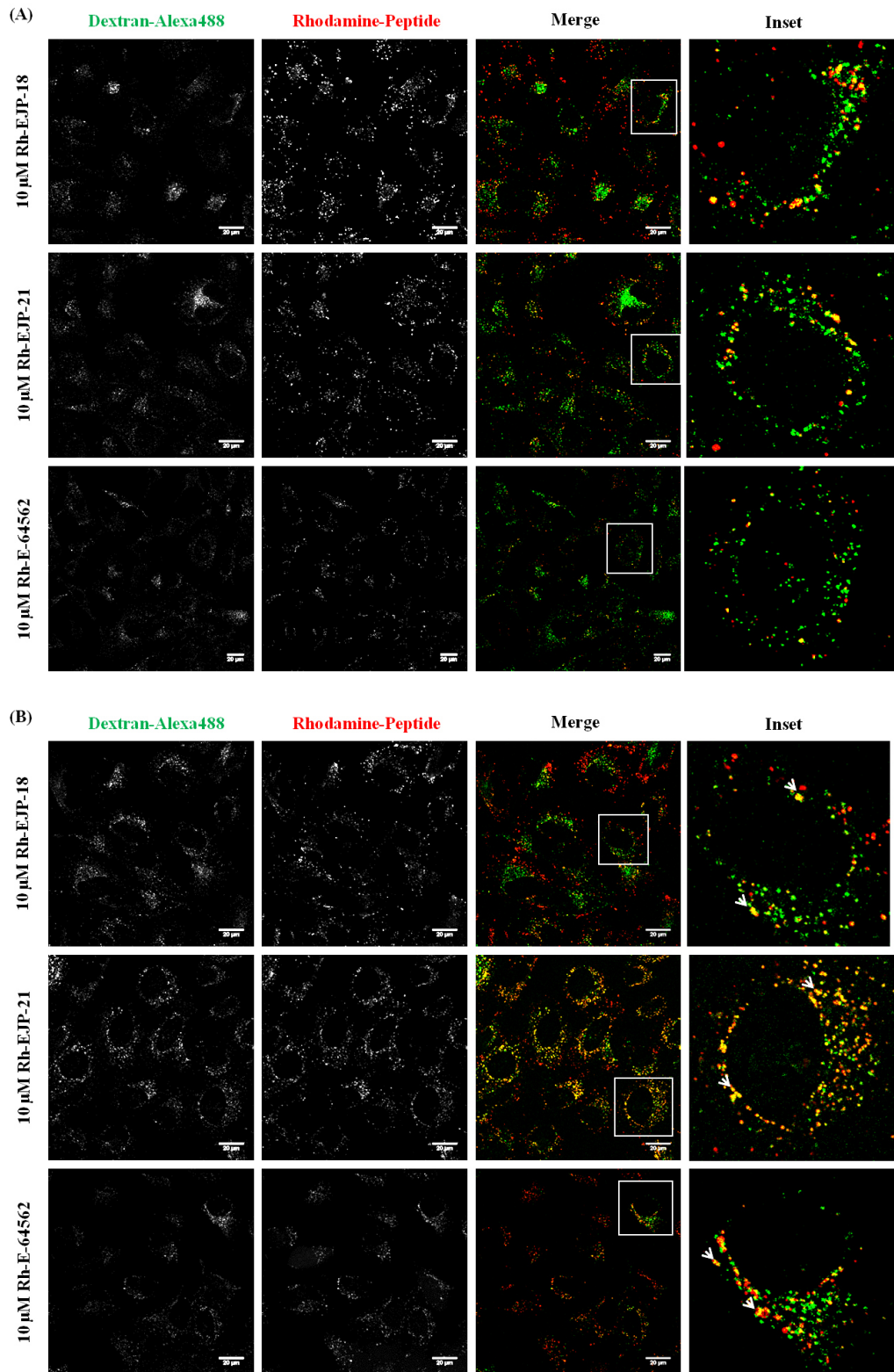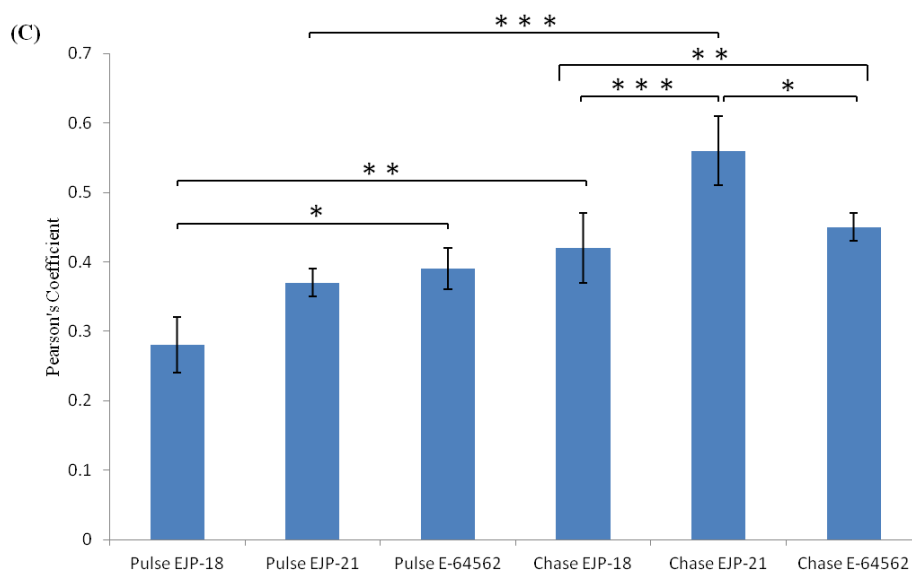
Figure 6-7: Traffic of Rh- EJP-18, Rh-EJP-21 and Rh-E-64562 to lysosomes in HeLa cells. Cells were incubated with dextran-Alexa488 for 2 h followed by an overnight chase and were then incubated with 10 μM Rh-peptides for (A) 1 h or (B) 1 h followed by a 1 h chase. The cells were then washed and imaged by confocal microscopy. Representative images (N=3) showing a single section through the cells and the right panel in (A) and (B) shows a zoomed image of an identified cell in merge panel. (C) plot for Pearson's coefficient values and statistical significance between groups. *Statistical Significance *** p ≤ 0.001, ** p ≤ 0.01 and * p ≤ 0.05. White arrows denote colocalisation. Scale bars = 20 μm.*

6.3.5 *Cellular uptake (Internalisation) of labelled BSA complexed with EJP-21 and E-64562 in HeLa cells in SFM*

To examine the capacity of EJP-21 and E-64562, for protein delivery they, like EJP-18 in Chapter 5, were mixed with BSA-Alexa647 and then incubated with HeLa cells. Here, 5 and 10 μM peptide/BSA-Alexa647 complexes were prepared and incubated with HeLa cells as described in section 2.4.1.3. At 10 μM, there was no evidence that E-64562 delivered the cargo (Figure 6-8A). Upon mixing with EJP-21, BSA-Alexa647 was clearly identified in vesicular structures in the distinct perinuclear region of the cell at 10 μM (Figure 6-8A) and to a lesser extent at 5 μM (Figure 6-8B).
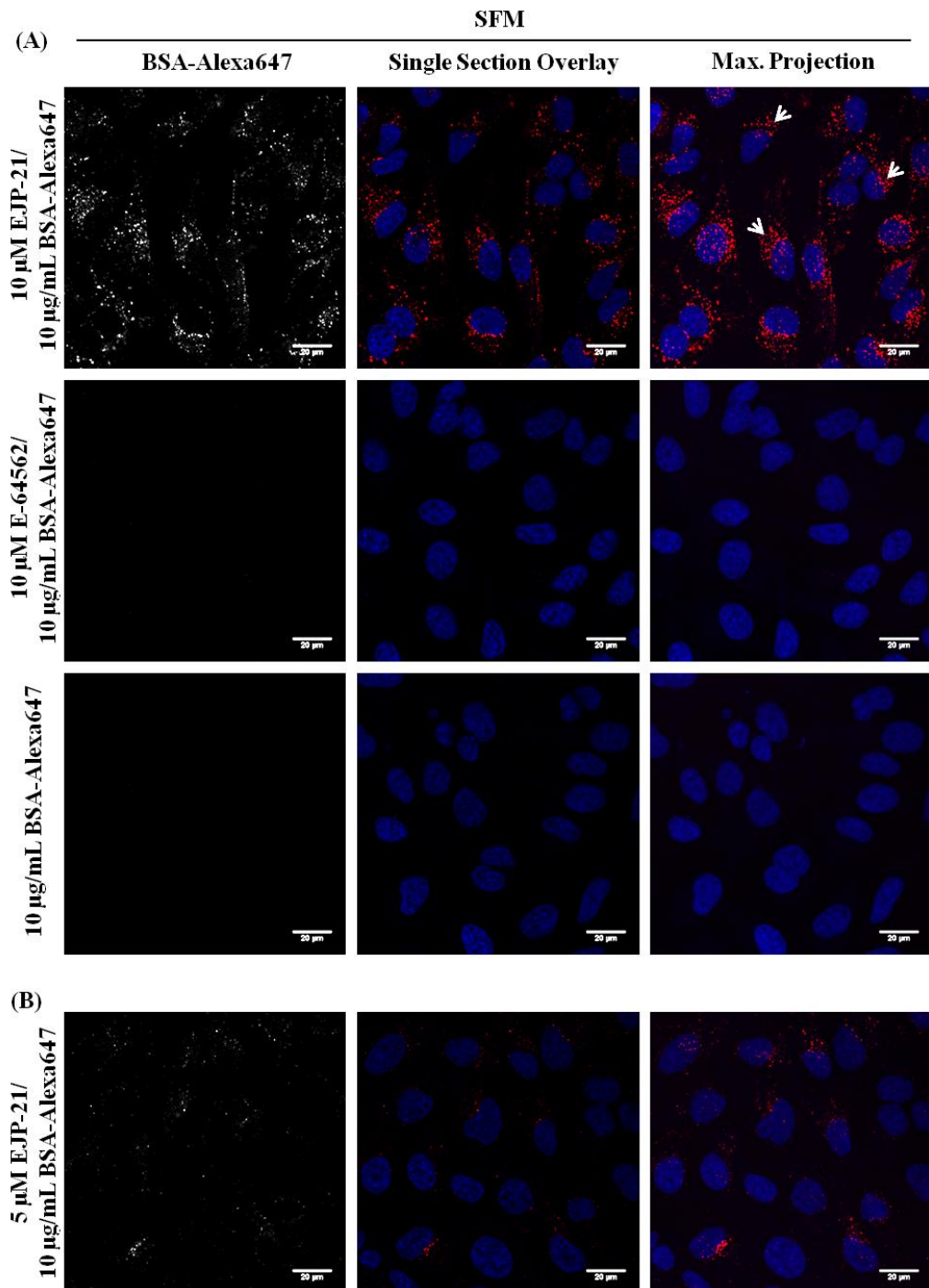
Figure 6-8: Internalisation of peptides/BSA-Alexa647 complexes into HeLa cells in SFM. (A) 10 μM EJP-21 or E-64562 or (B) 5 μM EJP-21 were incubated with BSA-Alexa647 and subsequently added to HeLa cells that were then incubated for 1 h at 37ºC, washed and imaged by confocal microscopy. Bottom row in (A) shows cells incubated with BSA-Alexa647 (10 μg/mL) alone. Representative images (N=3) showing either a single section through the cell at the mid-point of the nucleus or maximum projection of the whole cell. Nuclei were labelled blue with Hoechst. *White arrows indicate distinct perinuclear labelling. Scale bars = 20 μm.*

6.3.6   *Cytotoxicity of peptides/BSA-Alexa647 mixtures*

EJP-21 and E-64562 were found to be nontoxic at 10 μM (Figure 6-1); the concentration used to deliver labelled albumin. To ensure that peptide/BSA-Alexa647 complexes were also nontoxic, HeLa cells were incubated with the complexes (10 μM peptide/10 μg/mL BSA) under tissue culture conditions for 24 or 72 h. Cell viability was then determined using CellTiter-Blue assay as described in section 2.3.2. Figure 6-9 shows that none of these complexes were toxic to cells at the concentrations used here and this was confirmed using one-way ANOVA analysis.

Figure 6-9: Viability of HeLa cells incubated with peptide/BSA-Alexa647 complexes. Viability of cells was evaluated using CellTiter-Blue assay following (A) 24 h or (B) 72 h incubation with peptides/BSA-Alexa647 complexes in HeLa cells. Results represent means ± SD for (A) three independent experiments or (B) two independent experiments performed in duplicate.

6.4 Discussion

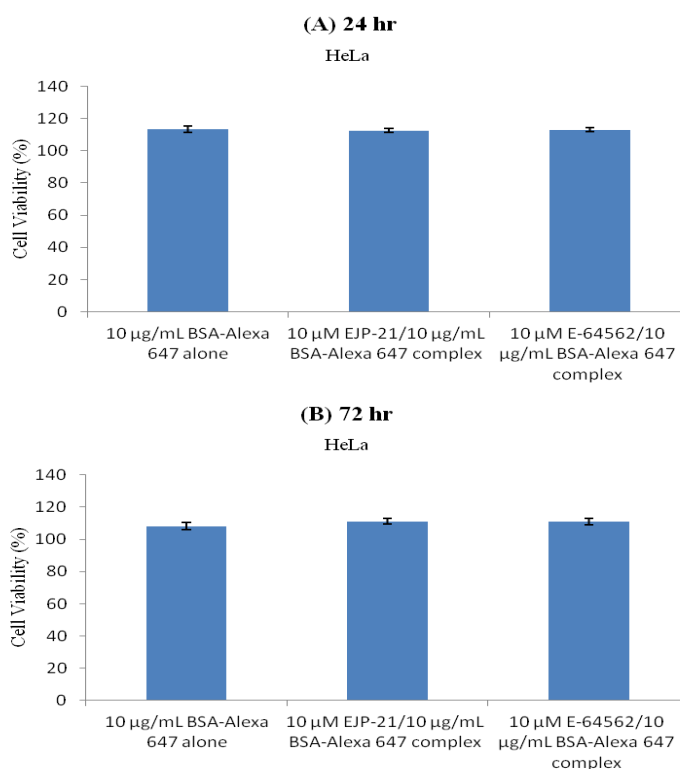The primary aim of this final section of the project was to test the cellular uptake, subcellular distribution and cytotoxicity of two peptide sequences related to EJP-18. E-64562 was a peptide that was reported, as a Tat-chimera, to have, in an EGFR dependent manner, anti-cancer activity (Boran *et al*., 2012). Also of significant interest is that a peptide termed EGFR-13 corresponding to amino acids 645-657 (RRR<u>E</u>IVRKRTLRR) of the EGFR JM domain was found to increase the tyrosine kinase activity and autophosphorylation of EGFR (Poppleton *et al*., 1999). EGFR-13 resembles the sequence of E-64562 with five missing residues at the C-terminus and the fourth residue (underlined) is glutamic acid rather than histidine that is present in the original sequence. This H-E change was not discussed and may in fact represent a typographical error. Peptide T654 (RKRT(PO3H2)LRRLK, with a phosphorylated T, has some overlap with EJP-18 and E-64652 and in a separate study, was able to enter cells in the absence of a CPP and affect EGFR biology (Dittmann *et al*., 2010). This linked with previous studies in our laboratory showing the effects of hydrophobicity on the terminus of bioactive peptides, with respects to cell interaction and uptake, in part led to the investigations in this thesis using two other peptides based on EJP-18.

Viability assays revealed that E-64562 was not toxic in any of the cell lines tested up to 100 μM. This is in line with data published by Boran *et al.* (2012) using several other cell lines with only the MDA-MB-231 line overlapping between this study and presented thesis. EJP-21 had no effect on cell viability up to 100 μM in any of the cell lines tested except for KG1a were minimal

toxicity ($\approx$15%) was noted at 100 μM. A study of a sequence from the JM region of EGFR (643-FMRRRHIVRKRTLRRLLQERE-663) that is very close to the EJP-21 sequence conjugated to the CPP PTD-4 (YARAAARQARA), termed EJ1, was toxic to two breast cancer cells: MDA-MB-468 and T47D at 20 μM, however, MDA-MB-231 cells were less sensitive to EJ1 peptide at the same concentration (Hart *et al*., 2013). The difference was attributed to K-ras mutations that protected the cells from EJ1.

E-64562, EJP-18 and EJP-21 are all peptides from the JM region of EGFR and the later two have an additional LFM at the N-terminus and this triplet resides within the membrane. Toxicity profiles of E-64562 and EJP-21 differed considerably from EJP-18 (Figure 4-2). Noted here is that EJP-18 has two hydrophobic termini (LF and LL), E-64562 has two very hydrophilic termini (RR and ER) and EJP-21 has the N-terminus of EJP-18 and the C-terminus of E-64562. This difference in the terminal hydrophobicity of the peptides may have altered peptide-membrane interaction and possible downstream effects including plasma membrane perturbation or influx of the peptides into the cells to exert some other effect. It would now be interesting to study the interaction of these peptides with artificial membrane models (Di Pisa *et al*., 2014).

In this study, Rh-E-64562 was clearly shown to enter HeLa cells, in a concentration dependant manner, i.e. in the absence of a CPP. At 5 μM, fluorescence was observed at very low levels in the cytoplasm within 1 h (Figure 6-4). The Boran *et al*. study (2012) showed that FAM-E-64562 at 5 μM was unable to enter MDA-MB-231 cells even after an overnight incubation

however, the uptake of higher concentrations (as in our study) was not included. Conjugation of Tat to E-64562 was shown to be essential for internalisation of the FAM conjugated peptide and for this Tat conjugate, strong cytosolic labelling was observed at 5 μM (Boran *et al.*, 2012). The reason for the difference between results presented in this thesis and Boran *et al.* could have been due to differences in the cell lines used in the studies or potentially due to the use of different peptide concentrations. It may also be that the differences in uptake (at 5 μM) were due to the use of different fluorophores, FAM vs rhodamine. As described, the incorporation of a fluorescent label can change the cellular uptake and intracellular localisation of CPPs (Puckett and Barton, 2009, Madani *et al.*, 2011, Palm-Apergi *et al.*, 2012, Bechara and Sagan, 2013). Further to the discussion in chapter 4, the CPP-Dmt-D-R-F-K (Dmt, 2′,6′-dimethyltyrosine) attached to relatively small, amino acid-based fluorophores ß-dansyl-L-α,ß-diaminopropionic acid (dns) or ßanthraniloyl-L-α,ß-diaminopropionic acid (atn) had different subcellular localisation patterns in Caco-2 cells. The dns form showed diffuse cytoplasmic distribution and caused mitochondrial swelling and cell death while the atn form exhibited a mitochondrial localisation and served as a mitoprotective agent (Szeto *et al.*, 2005). Additionally, conjugation of fluorescein isothiocyanate (FITC) to the N-terminus of ^{19}F-octaarginine using a ɣ-aminobutyric acid (GABA) spacer, has been shown by in-cell fluorine-19 nuclear magnetic resonance (NMR) spectroscopy to increase uptake. This was attributed to the hydrophobic nature of the fluorophore which was thought to increase the peptide's affinity for cell membranes (Okamura *et al.*, 2005).

The mixed pattern of distribution (punctate vesicles and cytosolic labelling) observed when HeLa cells were incubated with 20 µM Rh-E-64562 (Figure 6-4) was similar to that seen in the Boran *et al.* study for MDA-MB-231 cells following incubation with FAM-TE-64562 at 1.25 µM (Boran *et al.*, 2012). This may suggest that E-64562 can enter cells at relatively high concentrations, but as expected, Tat promotes cell uptake at lower concentration that may be aided by the cargo.

Figures 6-3, 6-7A and data from chapter 4 (Figure 4-7) reveal that the uptake of Rh-EJP-21 at 5-10 µM exhibited similar distribution to Rh-EJP-18 in vesicular structures of HeLa cells. Rh-EJP-21 fluorescence intensity was, however, higher and at 20 µM, cytosolic labelling was more prominent and some cells incubated with Rh-EJP-21 had fluorescent nucleoli. Cytosolic labelling at this concentration was associated with plasma membrane permeabilization illustrated by red staining of nuclei by DRAQ7. However, there was also clear evidence of cytosolic peptide localisation in DRAQ7 negative cells suggesting that the peptide entry was not solely due to plasma membrane disruption. Viability assays showed that 20 µM Rh-EJP-21 was non-toxic to HeLa cells but this could be due to the difference in the duration of incubation with the peptide and the possibility that the DRAQ7 positive cells recover from the initial damage. Alternatively, this could be due to serum effects. Cell viability assays were performed in the presence of serum while in the uptake experiment; the cells were incubated with Rh-EJP-21 in absence of serum. The absence of serum may have increased the cell sensitivity to the peptide's effect. In the study of Boran *et al.* (2012), the presence of serum

reduced the sensitivity of MDA-MB-231 to TE-64562-induced toxicity. A separate study showed that increasing serum concentrations in the medium decreased the toxicity induced by phosphorodiamidate morpholino oligomers-R_9F_2C (PMO-R_9F_2C) conjugates (Moulton *et al*., 2004). Further comparative analysis investigating the cytotoxic and delivery capacity of these peptides in the absence and presence of serum are required.

Rh-E-64562 and Rh-EJP-21 entered cells in a temperature-dependent manner (Figure 6-6). Both peptides, as with Rh-EJP-18, were internalised at 37ºC and their uptake was abolished at 4ºC which confirms the involvement of an active process and endocytosis being prominent at concentrations $\leq$ 10 µM. At 20 µM, there was strong evidence that direct translocation was occurring manifest as strong cytosolic labelling. Colocalisation studies at 10 µM showed that after 1 h incubation with the Rh-peptides followed by 1 h chase, a significant fraction had been delivered to lysosomes. This further confirms the involvement of endocytosis in the uptake of these peptides.

EJP-21 (10 µM), efficiently delivered labelled BSA into HeLa cells (Figure 6-8) and the protein was found localised in a distinct perinuclear region, showing similar uptake and distribution to that by EJP-18 (Figure 5-3). Somewhat surprisingly, E-64562 was unable at the same concentration to deliver BSA although it effectively delivered rhodamine. Due to time constraints, the ability of E-64562 to complex BSA was not assessed by native PAGE in this thesis but subsequent studies using a Zetasizer Nano ZS instrument that was only recently purchased by the department showed similar

BSA complexation ability for this EJP-18 and EJP-21 (Dr Edward Sayers). It may be that the N-terminal LFM in EJP-18 and EJP-21 is critical for enhancing cell entry of the peptide as a fluorescent entity but also when it is attached to much larger cargo such as BSA. Placing hydrophobic residues at either the N- or C-terminus of CPPs has been found in a number of studies to enhance membrane interaction and uptake of CPPs (Jones and Sayers, 2012). For example the addition of a distal phenyl alanine to different CPPs (penetratin, R8 and TP10) has been found to enhance the delivery capacity of range of macromolecules (Sayers *et al*., 2014). pVEC (Table 1-1), a CPP derived from the murine vascular endothelial-cadherin protein, has an extremely hydrophobic N-terminus (LLIIL) (Elmquist *et al*., 2001). The deletion of the three amino acids from the N-terminus or replacement of the entire N-terminal hydrophobic domain by alanine completely abolished the uptake in human bowes melanoma cells (Elmquist *et al*., 2006). In another study, the addition of two phenylalanine residues to the C-terminus of nonaarginine (R9) improved the delivery of phosphorodiamidate morpholino oligomers (PMO) and R_9F_2C-PMO conjugates corrected splicing more effectively than PMO conjugated with Tat, penetratin or PTD4 (Moulton *et al*., 2004). A single hydrophobic residue mutation (Alanine-Phenylalanine) at the N-terminus of the Nur77 derived D-Nu-BCP-9-r8 (fsrslhsll) was shown to significantly enhance membrane interaction and cellular uptake of the peptide and to mediate rapid cell death via a Bcl-2 independent mechanism. Mutating the first and last residue of D-NuBCP-9-r8 cargo to an alanine led to loss of activity of the peptide (Watkins *et al*., 2011). In conclusion, it is apparent that the

hydrophobic (LFM) N-terminus in EJP-21 is essential for the delivery properties of the peptide.

There are also important issues here regarding the different cargos used to show delivery capacity for the EGFR derived peptides; rhodamine vs BSA and their influence on CPP uptake. In the case of E-64562, the hydrophobicity of rhodamine at the N-terminus may have aided cell association and entry, but BSA that would interact very differently with the peptide, may serve as a hindrance to cell entry either via endocytosis or especially via direct plasma membrane translocation.

6.5   Conclusions

The initial aims of this chapter were to study the cellular uptake, subcellular distribution and cytotoxicity of two peptides related to EJP-18 that also originated in the JM region of EGFR. Although having closely related sequences, they gave distinct cell cytotoxicity profiles compared with EJP-18. Both EJP-21 and E-64562 as rhodamine conjugates were internalised by HeLa but only the former delivered BSA. Key identified factors that influenced cell uptake were the hydrophobicity at the N- or C-terminus and the nature of the cargo.

6.6 References

BECHARA, C. & SAGAN, S. 2013. Cell-penetrating peptides: 20years later, where do we stand? *FEBS letters,* 587**,** 1693-1702.

BORAN, A. D., SECO, J., JAYARAMAN, V., JAYARAMAN, G., ZHAO, S., REDDY, S., CHEN, Y. & IYENGAR, R. 2012. A potential peptide therapeutic derived from the juxtamembrane domain of the epidermal growth factor receptor. *PLoS One,* 7**,** e49702.

DI PISA, M., CHASSAING, G. & SWIECICKI, J.-M. 2014. Translocation mechanism (s) of cell-penetrating peptides: biophysical studies using artificial membrane bilayers. *Biochemistry,* 54**,** 194-207.

DITTMANN, K., MAYER, C., FEHRENBACHER, B., SCHALLER, M., KEHLBACH, R. & RODEMANN, H. P. 2010. Nuclear EGFR shuttling induced by ionizing radiation is regulated by phosphorylation at residue Thr654. *FEBS letters,* 584**,** 3878-3884.

ELMQUIST, A., HANSEN, M. & LANGEL, Ü. 2006. Structure–activity relationship study of the cell-penetrating peptide pVEC. *Biochimica et Biophysica Acta (BBA)-Biomembranes,* 1758**,** 721-729.

ELMQUIST, A., LINDGREN, M., BARTFAI, T. & LANGEL, Ü. 2001. VE-cadherin-derived cell-penetrating peptide, pVEC, with carrier functions. *Experimental cell research,* 269**,** 237-244.

HART, M. R., SU, H.-Y., BROKA, D., GOVERDHAN, A. & SCHROEDER, J. A. 2013. Inactive ERBB Receptors Cooperate With Reactive Oxygen Species To Suppress Cancer Progression. *Molecular Therapy,* 21**,** 1996-2007.

JONES, A. T. & SAYERS, E. J. 2012. Cell entry of cell penetrating peptides: tales of tails wagging dogs. *Journal of Controlled Release,* 161**,** 582-591.

MADANI, F., LINDBERG, S., LANGEL, U., FUTAKI, S. & GRASLUND, A. 2011. Mechanisms of cellular uptake of cell-penetrating peptides. *J Biophys,* 2011**,** 414729.

MOULTON, H. M., NELSON, M. H., HATLEVIG, S. A., REDDY, M. T. & IVERSEN, P. L. 2004. Cellular uptake of antisense morpholino oligomers conjugated to arginine-rich peptides. *Bioconjug Chem,* 15**,** 290-299.

OKAMURA, E., NINOMIYA, K., FUTAKI, S., NAGAI, Y., KIMURA, T., WAKAI, C., MATUBAYASI, N., SUGIURA, Y. & NAKAHARA, M. 2005. Real-time in-cell 19F NMR study on uptake of fluorescent and

nonfluorescent 19F-octaarginines into human Jurkat cells. *Chemistry Letters,* 34**,** 1064-1065.

PALM-APERGI, C., LONN, P. & DOWDY, S. F. 2012. Do cell-penetrating peptides actually "penetrate" cellular membranes? *Mol Ther,* 20**,** 695-697.

POPPLETON, H. M., WIEPZ, G. J., BERTICS, P. J. & PATEL, T. B. 1999. Modulation of the protein tyrosine kinase activity and autophosphorylation of the epidermal growth factor receptor by its juxtamembrane region. *Arch Biochem Biophys,* 363**,** 227-236.

PUCKETT, C. A. & BARTON, J. K. 2009. Fluorescein redirects a ruthenium−octaarginine conjugate to the nucleus. *Journal of the American Chemical Society,* 131**,** 8738-8739.

SAYERS, E. J., CLEAL, K., EISSA, N. G., WATSON, P. & JONES, A. T. 2014. Distal phenylalanine modification for enhancing cellular delivery of fluorophores, proteins and quantum dots by cell penetrating peptides. *Journal of Controlled Release,* 195**,** 55-62.

SZETO, H. H., SCHILLER, P. W., ZHAO, K. & LUO, G. 2005. Fluorescent dyes alter intracellular targeting and function of cell-penetrating tetrapeptides. *The FASEB journal,* 19**,** 118-120.

WATKINS, C. L., SAYERS, E. J., ALLENDER, C., BARROW, D., FEGAN, C., BRENNAN, P. & JONES, A. T. 2011. Co-operative membrane disruption between cell-penetrating peptide and cargo: implications for the therapeutic use of the Bcl-2 converter peptide D-NuBCP-9-r8. *Mol Ther,* 19**,** 2124-2132.

Chapter 7: General Discussion

Cell penetrating peptides (CPPs) have received significant research interest in the last two decades as potential delivery vectors for a range of therapeutic cargo. Studies have generally focused on areas such as: (1) using CPPs as delivery vectors for a variety of macromolecules including peptides, proteins, plasmid DNA and siRNA *in vitro* and *in vivo*, (2)   elucidating the mechanisms of cell entry of CPPs and the numerous factors that influence uptake and also subcellular distribution- attached cargo or fluorophore, cell line, temperature and serum (3) defining the structural basis of internalisation capacity in order to develop new CPPs with improved activity. Hundreds of CPP sequences have now been described that are covalently or non-covalently associated with cargo not forgetting bioportides that serve as single entity delivery vectors and modifiers of cell physiology (Howl *et al*., 2012). However, despite this huge effort spent to study and cover the above research areas, the translation of CPP based delivery systems from preclinical research to human subjects and clinical trials has been disappointing.

One of the aims of this project working in conjunction with Newcastle University was to extend the research about an existing CPP; penetratin, and its capacity to deliver the NBD targeting the NF-κB pathway. Pen-NBD peptide (commercially available) is well described in the literature to influence NF-κB activity; albeit at high concentrations. To achieve this aim, there was a need to develop reliable in house *in vitro* models for analysing activation or attenuation of NF-κB signalling. In these respect, the project was successful and two

assays were developed and are now available in the laboratory for subsequent studies: (1) Western blotting and immunodetection of IκB-α degradation in lysates of cells treated with the NF-κB activator TNF-α and (2) luciferase assay in a HeLa cell line that expresses luciferase in response to NF-κB activation.

Extending from previous reports, the ability of Pen-NBD peptide to interfere with NF-κB signalling via inhibition of TNF-α-induced NF-κB activation using the developed assays was assessed before designing and studying new peptide sequences. Surprisingly, Pen-NBD peptide was unable to reduce TNF-α-induced IκB-α degradation however, the results for the NF-κB reporter HeLa cell line showed a significant reduction in TNF-α-induced luciferase activity when cells were pre-treated with the peptide. Interestingly, the reduction in TNF-α-induced luciferase activity was not limited to the effect of Pen-NBD chimera and reduced luciferase activity was also observed in the stable HeLa cells pre-treated with penetratin or DMSO (the diluent). This reduction in luciferase activity was not observed when the same experiment was performed using R8 instead of penetratin. In line with published findings, penetratin was considered to have intrinsic biological activity rather than just being an inert delivery vector (Bolton *et al*., 2000, Fotin-Mleczek *et al*., 2005, Letoha *et al*., 2006). The results presented in Chapter 3 highlighted some potentially significant issues involving a number of factors that could influence the CPP studies including: the influence of the CPP alone, the specifics of the assays with respects to when and how long the reagents are incubated with cells and the choice of cell lines. Another critical factor that was explored in

this chapter was the influence of diluents on the conducted studies. A major factor hampering studies employing NF-κB targeting peptides was their insolubility in aqueous solutions. This significantly hindered progress towards designing new peptide based systems for targeting this pathway. Because of this and the availability of EJP-18 as a novel membrane active peptide, the work on targeting NF-κB was halted but we continued to interact with collaborators and our work with them was presented as a poster in two international conferences (see publications on page xviii).

Some very preliminary work had been performed on EJP-18 before this PhD studentship commenced. EJP-18 represented a novel peptide, appeared to be membrane active and had an interesting sequence of alternating hydrophilic/cationic and hydrophobic residues. From initial data and published work that appeared during the course of this thesis (Boran *et al*., 2012), other peptides based on the EJP-18 sequence were also studied- EJP-21 and E-64562. The difference in the N- and C-terminus between the three peptides resulted in very interesting observations regarding their cytotoxicity, cell uptake and capacity to deliver cargo. The hydrophobic N-terminus was clearly important for cell interaction and delivery capacity. EJP-21, sharing the hydrophobic N-terminus with EJP-18, was able to deliver labelled albumin as efficient as EJP-18, however, E-64562 that lacks the hydrophobic N-terminus was unable to deliver albumin at the same concentration. This is in line with publications and previous observations in Jones laboratory and others that highlighted the significant effect of placing hydrophobic residues to either termini of CPPs or associated cargo on CPP-membrane binding and uptake

(Elmquist *et al*., 2006, Watkins *et al*., 2011, Jones and Sayers, 2012, Sayers *et al*., 2014).

The effects of the three peptides on cell viability were unexpected and although the three peptides were from the same origin, a significant difference in viability profiles was observed with EJP-18 being the most toxic and in a seemingly EGFR-dependent manner. Studies are now underway to investigate the effects of these peptides on EGFR signalling. EJP-18 and EJP-21 were able to deliver BSA into the cells by endocytosis and in the case of EJP-18 to deliver it to lysosomes. Again confirming endocytosis as the mechanism, all three peptides, as fluorescent conjugates, were localised to this organelle after 1 h incubation at ≤ 10 μM. In the thesis, a non denaturing PAGE based assay was developed to assess the capacity of EJP-18 to complex BSA and this will be a useful tool for subsequent studies looking at protein complexation by CPPs for cell delivery. Studies in the laboratory are now comparing protein complexing ability of the three EGFR derived peptides using this new assay and also the newly acquired Zetasizer that will provide additional information with respects to charge and size of the complexes. The work presented on BSA delivery here was instrumental for studies investigating uptake by other novel CPP-based system differing only in single residue hydrophobic changes at the N-terminus of a cell impermeable cargo $-(SG)_4$ (Sayers *et al*., 2014).

Although endolysosomal entrapment and degradation has always been considered as a rate-limiting step in efficient cytosolic delivery of cargos by CPPs (El-Sayed *et al*., 2009), delivery to lysosomes is required for targeting

lysosomal storage diseases (LSDs) with enzymes (Urbanelli *et al*., 2011). The ability of EJP-18 to deliver therapeutic cargos targeting LSDs could be further explored but its effects on cell viability and potentially EGFR signalling cannot be ignored. It would be interesting to obtain an all D-form of this peptide to investigate whether it is still cytotoxic in an EGFR dependant manner. This could also highlight the possibility that EJP-18 is able to enter cells and specifically interfere with the JM domain of the receptor. The D-form would also be less sensitive outside and inside cells to degradation by proteases. Single amino acid substitutions in EJP-18 (or EJP-21) could also be introduced with a view to further enhancing cell uptake and/or avoid interaction with EGFR.

As expected, based on charge, EJP-18 proved to be an efficient complexing reagent for both siRNA and plasmid DNA. Unfortunately, the results regarding its capacity to deliver siRNA to the right location in cells was inconclusive. Additional experiments using lysosomotropic agents such as chloroquine could be performed to examine whether endosomal entrapment is the limiting step in transfection efficiency. The same is true for plasmid DNA and here there was no evidence that it could deliver to the cytosol and nucleus. It is interesting that like Tat, EJP-18 has an NLS but based on microscopy there was no real evidence that this was functioning to enrich the peptide in the nucleus. Nuclear labelling was observed at high peptide concentrations that revealed cytosolic staining; this fraction is likely to have come from direct translocation across the plasma membrane and through nuclear pores that also occurs with R8 that is able to do this at higher efficiency and, importantly also in the absence of

energy that abolished cell labelling of all studied EGFR JM peptides. Figure 7-1 summarizes the findings and hypothesis regarding EJP-18.

Although many questions remain to be answered, this project has provided new information on *in vitro* activity of some well explored CPPs and CPP-chimeras. Additionally new CPP(s) derived from a human protein of significant medical interest has been discovered that may in fact interfere with its biology. Can we now label EJP-18 as a new CPP? Its membrane activity and ability to complex biological cargo and also deliver them and fluorophores to cells suggest the answer is YES. Whether it has any future, as it stands or as a modified sequence, as a single entity bioportide-delivery vector remains to be determined.
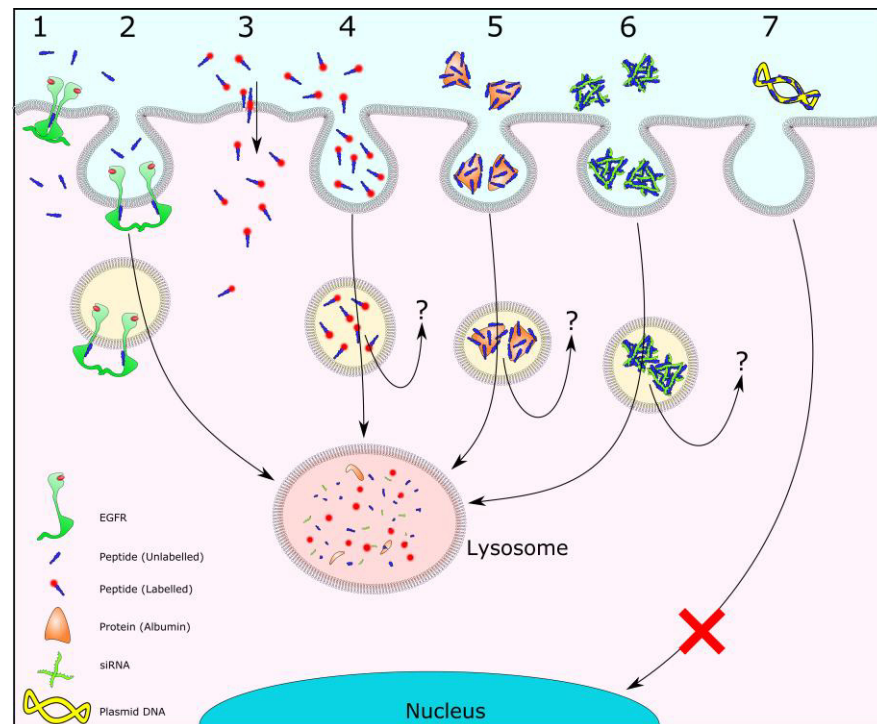
Figure 7-1: Summary of EJP-18-mediated delivery of macromolecules and possible membrane interactions. (1) EJP-18-EGFR interaction in the JM region following translocation of the peptide across the plasma membrane or following endosomal escape, (2) EJP-18-EGFR interaction via mechanisms described in 1, in the JM region inhibiting receptor dimerization at the plasma membrane causing internalisation of the receptor to the endolysosomal pathway, (3) direct translocation of EJP-18, as a fluoroscent conjugate, across the plasma membrane, (4) receptor-mediated or fluid phase uptake of EJP-18, as a fluorescent conjugate, (5) intracellular delivery of EJP-18/BSA complexes by endocytosis, (6) intracellular delivery of EJP-18/siRNA complexes by endocytosis, (7) EJP-18/plasmid complexes were formed but studies showed no evidence of delivery to transfect cells (?) denotes the unknown capacity of the peptide and associated cargo to escape from endosomes.

7.1 References

BOLTON, S. J., JONES, D. N., DARKER, J. G., EGGLESTON, D. S., HUNTER, A. J. & WALSH, F. S. 2000. Cellular uptake and spread of the cell-permeable peptide penetratin in adult rat brain. *European Journal of Neuroscience,* 12**,** 2847-2855.

BORAN, A. D., SECO, J., JAYARAMAN, V., JAYARAMAN, G., ZHAO, S., REDDY, S., CHEN, Y. & IYENGAR, R. 2012. A potential peptide therapeutic derived from the juxtamembrane domain of the epidermal growth factor receptor. *PLoS One,* 7**,** e49702.

EL-SAYED, A., FUTAKI, S. & HARASHIMA, H. 2009. Delivery of macromolecules using arginine-rich cell-penetrating peptides: ways to overcome endosomal entrapment. *AAPS J,* 11**,** 13-22.

ELMQUIST, A., HANSEN, M. & LANGEL, Ü. 2006. Structure–activity relationship study of the cell-penetrating peptide pVEC. *Biochimica et Biophysica Acta (BBA)-Biomembranes,* 1758**,** 721-729.

FOTIN-MLECZEK, M., WELTE, S., MADER, O., DUCHARDT, F., FISCHER, R., HUFNAGEL, H., SCHEURICH, P. & BROCK, R. 2005. Cationic cell-penetrating peptides interfere with TNF signalling by induction of TNF receptor internalization. *J Cell Sci,* 118**,** 3339-3351.

HOWL, J., MATOU-NASRI, S., WEST, D. C., FARQUHAR, M., SLANINOVA, J., OSTENSON, C. G., ZORKO, M., OSTLUND, P., KUMAR, S., LANGEL, U., MCKEATING, J. & JONES, S. 2012. Bioportide: an emergent concept of bioactive cell-penetrating peptides. *Cell Mol Life Sci,* 69**,** 2951-2966.

JONES, A. T. & SAYERS, E. J. 2012. Cell entry of cell penetrating peptides: tales of tails wagging dogs. *Journal of Controlled Release,* 161**,** 582-591.

LETOHA, T., KUSZ, E., PAPAI, G., SZABOLCS, A., KASZAKI, J., VARGA, I., TAKACS, T., PENKE, B. & DUDA, E. 2006. In vitro and in vivo nuclear factor-κB inhibitory effects of the cell-penetrating penetratin peptide. *Molecular pharmacology,* 69**,** 2027-2036.

SAYERS, E. J., CLEAL, K., EISSA, N. G., WATSON, P. & JONES, A. T. 2014. Distal phenylalanine modification for enhancing cellular delivery of fluorophores, proteins and quantum dots by cell penetrating peptides. *Journal of Controlled Release,* 195**,** 55-62.

URBANELLI, L., MAGINI, A., POLCHI, A., POLIDORO, M. & EMILIANI, C. 2011. Recent developments in therapeutic approaches for lysosomal storage diseases. *Recent patents on CNS drug discovery,* 6**,** 1-19.

WATKINS, C. L., SAYERS, E. J., ALLENDER, C., BARROW, D., FEGAN, C., BRENNAN, P. & JONES, A. T. 2011. Co-operative membrane disruption between cell-penetrating peptide and cargo: implications for the therapeutic use of the Bcl-2 converter peptide D-NuBCP-9-r8. *Mol Ther,* 19**,** 2124-2132.

Appendix A

List of reagents used in the project, manufacturer and catalogue number:

Biorad (Hemel Hempstead, UK):

- Precision plus protein dual colour standards (#161-0374)
- Clarity, Western ECL substrate (#170-5060)
- Agarose (#161-3100)
- SDS (#161-0301)
- Mini-PROTEAN$^®$ TGX^{TM} Gels 10% (#456-1033)
- Mini-PROTEAN$^®$ TGX^{TM} Gels 12% (#456-1043)

Biostatus (Leicestershire, UK):

- DRAQ7^{TM} (DR71000)

DAKO (Ely, UK):

- Fluorescence mounting medium "Dako oil" / (#S3023)

Fisher Scientific (Loughborough, UK):

- Coverslips No. 1 circle 16mm diameter (#12313138)
- 40% acrylamide/Bis (#10376643)
- PVDF membrane (#10344661)
- SuperSignal West Femto Chemiluminescent Substrate (#34094)

Life Technologies (Paisley, UK):

- DMEM (#21885)
- RPMI 1640 (#21875)
- FBS (#16000-044)
- 0.05% Trypsin EDTA (#25300062)
- Hoechst 33342 (#H3570)
- Oligofectamine transfection reagent (#12252-011)
- Dextran, Alexa fluor$^®$ 488 (#D22910)
- BSA-Alexa fluor$^®$ 488 (#A13100)
- BSA-Alexa fluor$^®$ 647 (#A34785)

New England Biolabs (Hitchin, UK):

- 100 bp DNA Ladder (#N3231S)
- dsRNA ladder (#N0363S)

Promega (Loughborough, UK):

- Fugene 6 transfection reagent (#E2691)
- CellTiter Blue viability assay (#G8080)
- Luciferase Assay system (#E1500)

Roche Diagnostics (Burgess Hill, UK):

- Complete Protease Inhibitor Cocktail Tablets (#11836153001)
- Hygromycin (#10843555001)

Sigma Aldrich (Poole, UK):

- Triton X-100 (#X100)
- BSA (#A7906)
- Saponin (#47036)
- Bicinchoninic Acid solution (#B9643)
- Copper (II) Sulphate solution (#C2284)
- TEMED (#T9281)
- Ponceau S solution (#P7170)
- Tween 20 (#P1379)
- Ethidium bromide (#E1510)
- Trypan Blue solution (0.4%) (#T8154)
- LookOut® Mycoplasma PCR Detection Kit (#MP0035)

VWR (Lutterworth, UK):

- Coomassie brilliant blue (#44329)

Appendix B

Table B-1: Confocal microscope settings

Hardware/Software	Settings
Objective magnification	63X
Numerical aperture (NA) of objective	1.4
Objective type	Oil immersion λBlue HCX PL APO
Thickness of cover slip	No. 1.5 (0.16-0.19 mm)
Lasers	405 (Diode), 488 (Argon), 543 and 633 (HeNe) nm
Immersion oil	Leica type F (refractive index = 1.518)
Pinhole size	95.5 μm (1 Airy unit)
Imaging speed	400 or 700 Hz
Imaging direction	Bidirectional (offset -30.5)
Line average	3
Rastor size	1024 x 1024
Zoom	1 (Figure BSA) and 1.5 (Rh-peptides)
Pixel size	240 nm x 240 nm
Resolution	8 bit

Table B-2: Wide field microscope settings

Hardware/Software	Settings
Objective magnification	10X
Numerical aperture (NA) of objective	0.25
Objective type	Air
Thickness of cover slip	No. 1.5 (0.16-0.19 mm)
Illumination	Mercury lamp
Filter cubes	Leica code A BP 340-380 nm (UV excitation) Leica code I3 BP 450-490 nm (Blue excitation)
Immersion oil	Leica type F (refractive index = 1.518)
Rastor size	1280 x 1024
Binning	1
Pixel size	640 x 640 nm
Resolution	12 bit

Appendix C

Table C-1: 50 nM Cy-5-siRNA and increasing concentration of peptide to achieve increasing molar ratios

Molar ratio of EJP-18/Cy5-siRNA complexes	Cy5-siRNA (10 μM stock)	EJP-18 (50 μM stock)	Opti-MEM (to 50 μL)	EJP-18 final working concentration
200:1	1 μL	40 μL	9 μL	10 μM
160:1	1 μL	32 μL	17 μL	8 μM
80:1	1 μL	16 μL	33 μL	4 μM
40:1	1 μL	8 μL	41 μL	2 μM
20:1	1 μL	4 μL	45 μL	1 μM
10:1	1 μL	2 μL	47 μL	0.5 μM
50 nM Cy5-siRNA alone	1 μL	-	49 μL	-

Table C-2: 100 nM Cy5-siRNA and increasing concentration of peptide to achieve increasing molar ratios

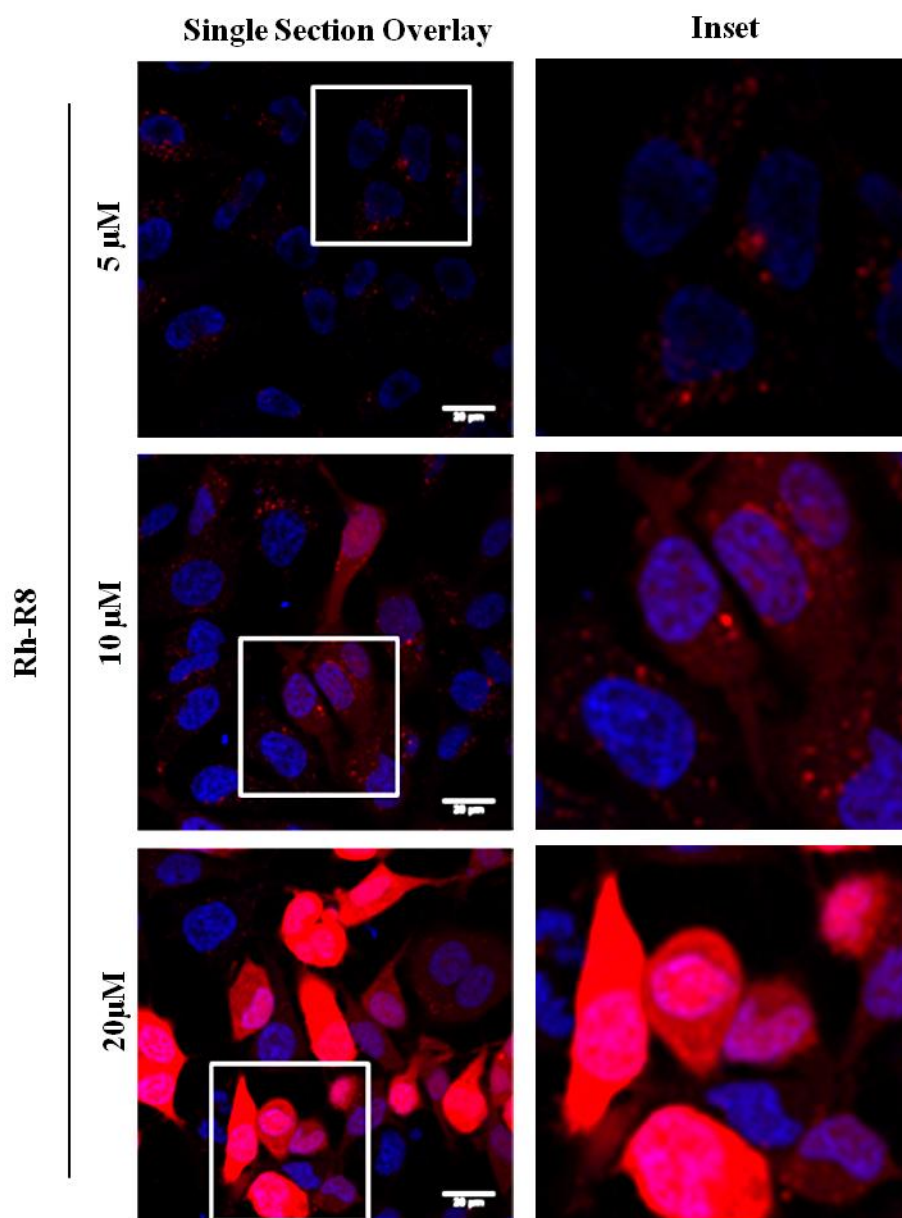| Molar ratio of EJP-18/Cy5-siRNA complexes	Cy5-siRNA (10 μM stock)	EJP-18 (50 μM stock)	Opti-MEM (to 50 μL)	EJP-18 final working concentration
100:1	2 μL	40 μL	8 μL	10 μM
80:1	2 μL	32 μL	16 μL	8 μM
40:1	2 μL	16 μL	32 μL	4 μM
20:1	2 μL	8 μL	40 μL	2 μM
10:1	2 μL	4 μL	44 μL	1 μM
100 nM Cy5-siRNA alone	2 μL	-	48 μL	-

Appendix D

Figure D-1: Enlarged sections of single section images from Figure 4-6.
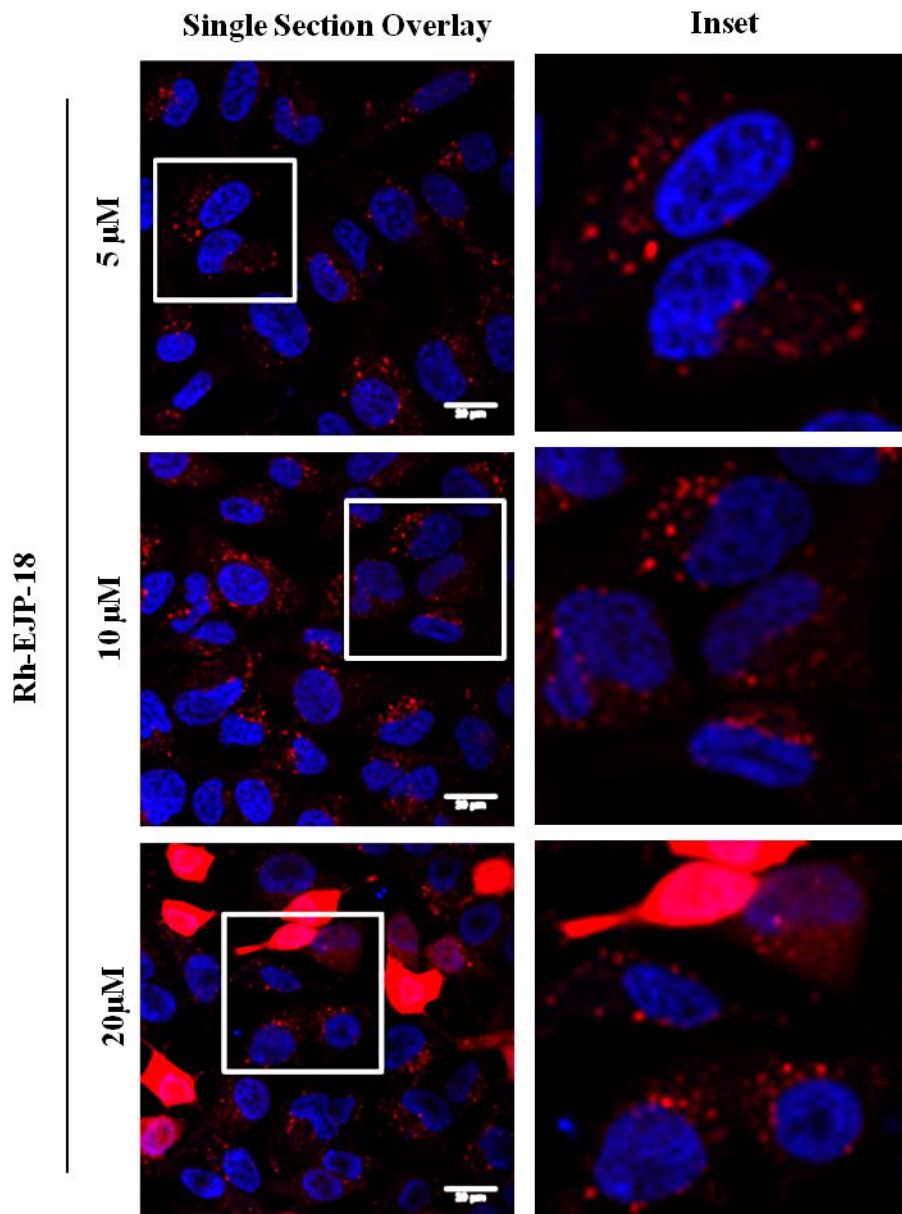
Figure D-2: Enlarged sections of single section images from Figure 4-7.

Uptake of 20 µM Rh-R8 peptides into HeLa cells in SFM for assessment of membrane integrity

HeLa cells were initially incubated with 20 µM Rh-R8 for 1 h. The medium was removed and the cells were incubated in imaging medium containing the fluorescent probe DRAQ7 and imaged by confocal microscopy. The data shown below (Figure D-3) show that none of the cells were labelled with DRAQ7.
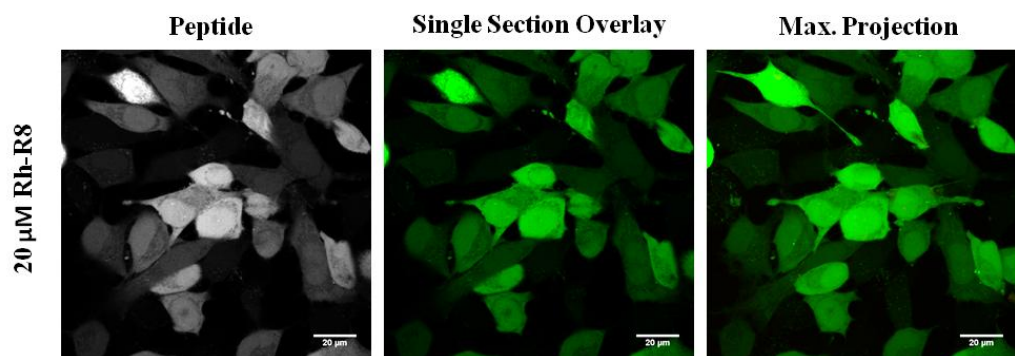

Figure D-3: Uptake of 20 µM Rh-R8 peptides into HeLa cells in SFM. Cells were incubated with 20 µM Rh-R8 (pseudo labelled green) in SFM for 1h at 37ºC, washed and imaged in imaging medium containing DRAQ7 by confocal microscopy. Representative images (N=2) showing either a single section through the cell at the mid-point of the nucleus or maximum projection of the whole cell. *Scale bars = 20 µm.*